RFP-3331/2
UC-60

UTRC 15-kW WIND SYSTEM DEVELOPMENT

Phase I - Design and Analysis

Volume II - Technical Report

December 1981

R. B. Taylor
M. C. Cheney

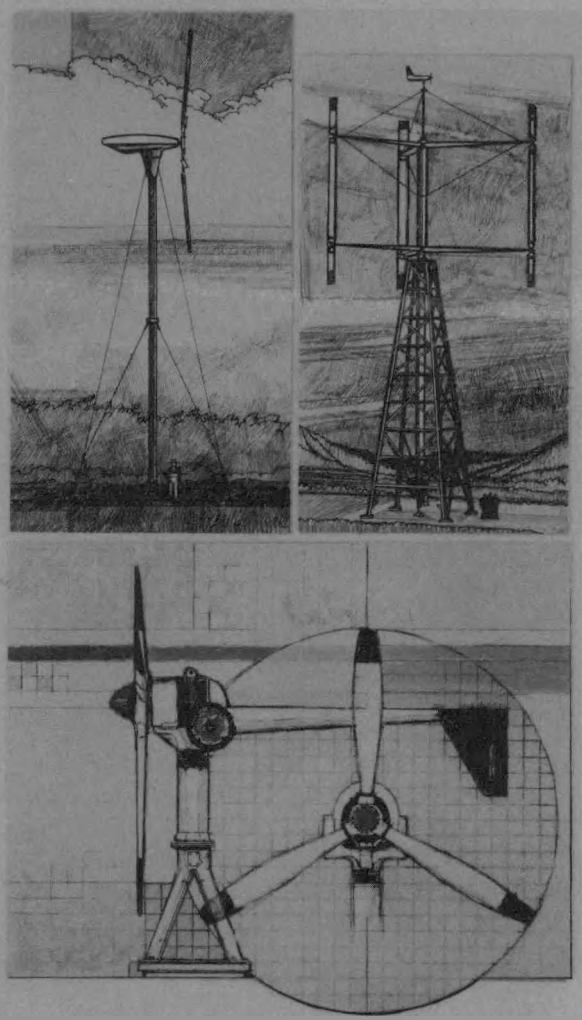

Prepared by
UNITED TECHNOLOGIES RESEARCH CENTER
East Hartford, Connecticut 06108

For
Rockwell International Corporation
Energy Systems Group
Rocky Flats Plant
Wind Systems Program
P.O. Box 464
Golden, Colorado 80402-2464

Subcontract No. PF-93652T

As Part of the
UNITED STATES DEPARTMENT OF ENERGY
WIND ENERGY TECHNOLOGY DIVISION
FEDERAL WIND ENERGY PROGRAM

Contract No. DE-AC04-76DP03533

RFP-3331/2
UC-60

RFP--3331/2

DE82 021710

UTRC 15-kW WIND-SYSTEM DEVELOPMENT

Phase I - Design and Analysis

Volume II - Technical Report

December 1981

R.B. Taylor
M.C. Cheney

Prepared by

(2) United Technologies Research Center
East Hartford, Connecticut 06108

For

(1) Rockwell International Corporation
Energy Systems Group
Rocky Flats Plant
Wind Systems Program
Golden, Colorado 80402-0464

Subcontract No. PF-93652T

As Part of the

UNITED STATES DEPARTMENT OF ENERGY
WIND ENERGY TECHNOLOGY DIVISION
FEDERAL WIND ENERGY PROGRAM

Contract No. DE-AC04-76DP03533

TABLE OF CONTENTS

TABLE OF CONTENTS (Cont'd)

ABSTRACT

This Phase I summary report contains a description of the design of a 15-kW wind turbine developed by United Technologies Research Center (UTRC) for the Department of Energy. The wind turbine employs the UTRC Composite Bearingless Rotor Concept in conjunction with a passive pendulum control system which controls blade pitch for start-up, efficient power generation, and high-speed survivability. Also included in this report is a summary of experimental material and component tests which were performed in support of the wind turbine design. Studies of system reliability, maintainability, availability and safety are reported and an estimate of the cost-of-energy is also made for a production wind system.

ACKNOWLEDGEMENTS

The authors wish to acknowledge the contributions made by the persons listed below for their assistance during the design phase of this program and the preparation of this report. Thanks also go out to the Wind Systems Staff at Rocky Flats for their guidance during the course of this Phase I effort.

D. J. Longtin R. H. Ross	Component design
R. W. Gagnon	Tower design
T. A. Murrin	Electrical design
J. S. Foley	Performance, cost of energy
J. R. Strife	Material characterization
P. W. Ingle	Availability analysis, safety analysis

SUMMARY

This report contains the major results of Phase I of the United Technologies Research Center (UTRC) contract to design, fabricate, and test a 15-kW wind turbine generator (WTG) under the Department of Energy's (DOE) small wind energy conversion system program. The Phase I activity reported on herein consists of several analytical and experimental programs in support of the design. Material and component experimental tests were performed and analytical aeroelastic predictions were made to further understand and support the WTG system design. Studies performed, in addition to the complete description of the design and performance characteristics, include reliability, maintainability, availability and safety analysis of the system,plus a study of the cost-of-energy as a function of design variations and production quantities.

A complete set of detailed engineering drawings has been prepared for the final system design. Microfilms of these drawings can be obtained at cost from Wind Systems, Rockwell International, Rocky Flats Plant, Box 464, Golden, CO, 80401.

NOMENCLATURE

a	rotor height factor used in gust calculations; = 1.2 + 0.05 ln Z_H
AKWH	Annual energy capture in kilowatt-hours
AOM	annualized operation and maintenance cost
b	width of material specimen
C_d	airfoil profile drag coefficient
C_i	cost item
COE	cost of energy
C_P	wind turbine rotor power coefficient
C_Q	wind turbine rotor torque coefficient
D	rotor diameter or aerodynamic drag force
D_{NAC}	nacelle drag
D_{TWR}	tower drag
E	Young's modulus or edgewise blade mode
F	denotes flatwise blade mode or tower foundation
FCR	annual fixed charge (interest) rate
F_g	gust factor
F_s	factor of safety
F_{ty}	tensile yield strength
F_v	rotor vertical force at hub
F_x	horizontal shear force on tower foundation
F_z	vertical shear force on tower foundation
g(v)	velocity intensity function

G	shear modulus
GPa	gigapascal
h	depth of material specimen
H	time factor in Rayleigh wind speed distribution
I	moment of inertia
IC	initial investment cost
ID	inside diameter
J	velocity ratio, rotor tip speed divided by wind speed
kWG	generator kilowatt rating
kWR	rotor kilowatt rating
M	overturning moment on tower foundation or mean value
MPa	megapascal
OD	outside diameter
P	power output or applied load
PF	generator power factor
PM	rotor pitching moment at hub
P_p	passive earth pressure acting on foundation
r	distance from rotor center to a point along blade span
R	rotor radius
rpm	revolutions per minute
S	span dimension of material specimen
S/h	span-to-depth ratio
T	rotor thrust, applied torque or torsion blade mode
V_{ci}	rotor cut-in wind speed normalized to median wind speed

V_{co}	rotor cut-out wind speed normalized to median wind speed
V_R	rotor rated speed normalized to median wind speed
V_w	instantaneous wind speed
$\bar{V}_w$	mean wind speed
V_z	wind speed at elevation z
$\bar{V}_z$	mean wind speed at elevation z
W	weight of component or width measurement
W_i	weight item
Wp	pendulum weight
Z	reference height above ground
Z_H	elevation of rotor hub above ground
Z_o	terrain roughness parameter
βc	rotor coning angle
βp	instantaneous angle of pendulum from rotor disc plane, positive towards disc plane (downwind)
βp_o	initial angle of pendulum from rotor disc plane, positive towards disc plane (downwind)
δ	elastic deflection
θ	twist angle of material specimen or blade pitch angle, positive nose up so that the leading edge is downwind
θ_{75}	blade pitch angle at 75% radius station
λ	past failures per year
λ^*	past failures per million operating hours
ϕ	angle of flexstrap attachment to blade

ρ	air density
σ	stress or standard deviation, or rotor solidity
σ_{11}	tensile stress
σ_{22}	transverse stress
τ	shear stress or gust period
ζ	fraction of gust penetration
ω	natural frequency of mode (subscript number denotes mode)
Ω	angular rotor speed

LIST OF ILLUSTRATIONS

LIST OF ILLUSTRATIONS (Cont'd)

LIST OF ILLUSTRATIONS (Cont'd)

LIST OF TABLES

LIST OF TABLES (Cont'd)

INTRODUCTION

This report summarizes the results of a design study performed under Phase I of a contract with Rockwell International for the Department of Energy to develop a 15-kW wind turbine generator (WTG). The objective of the contract is to develop a WTG capable of yearly energy output between 45,000 and 55,000 kWh at a mean annual wind of 5.4 m/s (12 mph). An additional objective is to achieve an energy cost goal of 3¢/kWh using a high volume production cost estimate.

The Phase I activity consisted of several analytical and experimental programs in support of the design. Material and component experimental tests were performed and analytical aeroelastic predictions were made to further understand and support the WTG system design. Studies performed, in addition to the complete description of the design and performance characteristics, include reliability, maintainability, availability and safety analysis of the system, plus a study of the cost-of-energy as a function of design variations and production quantities.

The key characteristic of the UTRC 15-kW WTG is the use of a Composite Bearingless Rotor (CBR) developed for helicopter applications. The CBR rotor, coupled with a passive pendulum control system, provides a system which is simple and is potentially low in manufacturing costs. The rotor is comprised of two distinct parts: a) the blade, or aerodynamic, portion which is fabricated from E fiberglass; and b) the inner portion of the rotor, called the flexbeam, which is made of S-2 fiberglass. The flexibility of the flexbeam provides freedom for the rotor blade to deflect in bending to relieve aerodynamic bending moments and also to twist so that the blade pitch angle is optimum for aerodynamic efficiency. The mechanism that twists the blades is another important feature of the UTRC WTG concept - a passive control system consisting of movable pendulums sensitive to centrifugal force.

Using the basic CBR concept for the rotor, and the pendulums for the passive pitch control system, a design was developed that is similar in many aspects to the 8-kW WTG that was designed, fabricated, and tested, as reported in Refs. 1 and 2. The 15-kW WTG design that has evolved is basically a scaled-up version of the 8-kW WTG incorporating modifications with the objective of improving the design, and reducing manufacturing and life cycle costs.

SYSTEM DESIGN

Philosophy

The design philosophy behind the 15-kW wind turbine was to apply the experience gained on previous UTRC wind turbine and helicopter programs. The applicable experience reaches back to the development of the Composite Bearingless Rotor (CBR) concept at UTRC for helicopter applications. The CBR rotor design is the key to the UTRC wind turbine concept, and therefore all the design, manufacturing, and operational advantages offered by the CBR design can be realized in the 15-kW wind turbine design.

The second area of valuable experience that has been used to advantage in the 15-kW wind turbine design is the development effort of the UTRC 8-kW wind turbine, documented in Refs. 1 and 2. The 8-kW wind turbine program proceeded in logical stages of design, fabrication of a prototype, and field testing. The 8-kW WTG is presently undergoing field test evaluation at Rocky Flats, Colorado. This wind turbine also utilizes a CBR type rotor, as well as the passive pendulum control system. The 8-kW WTG has performed well and the field testing to date has successfully demonstrated the various features of the UTRC wind turbine concept. The experimental data that are available, plus the experience gained in the design and fabrication of the 8-kW system, are particularly valuable in the development of the larger 15-kW wind turbine.

Based on this past experience with CBR rotors and the 8-kW WTG program, it is logical that the design philosophy used for the present 15-kW wind turbine program was to scale up the existing 8-kW wind turbine to develop a basic design configuration, and then modify the design in those areas where past experience has shown the potential for improvement.

This philosophy is also cost effective since it is easier to scale up and modify an existing design than it is to design from initial concepts. In effect, the philosophy used was to learn from experience, so that the 15-kW design could be considered a scaled-up, second generation of the 8-kW wind turbine.

Overview of System Design

Figure 1 is a schematic of the 15-kW WTG system that has evolved from this design study. The wind system consists of a horizontal-axis, two-bladed, downwind rotor, which is free in yaw and is supported by a cantilevered free standing tower. The rotor diameter is 14.6 m (48 ft) and the rotor height above the ground is 12.5 m (41 ft). The rotor blades consist of an aerodynamic lifting portion, extending from 0.21 R to the full radius, which is made of E fiberglass with a 0.45-m (18-in.) chord, and an inner, non-aerodynamic portion called the

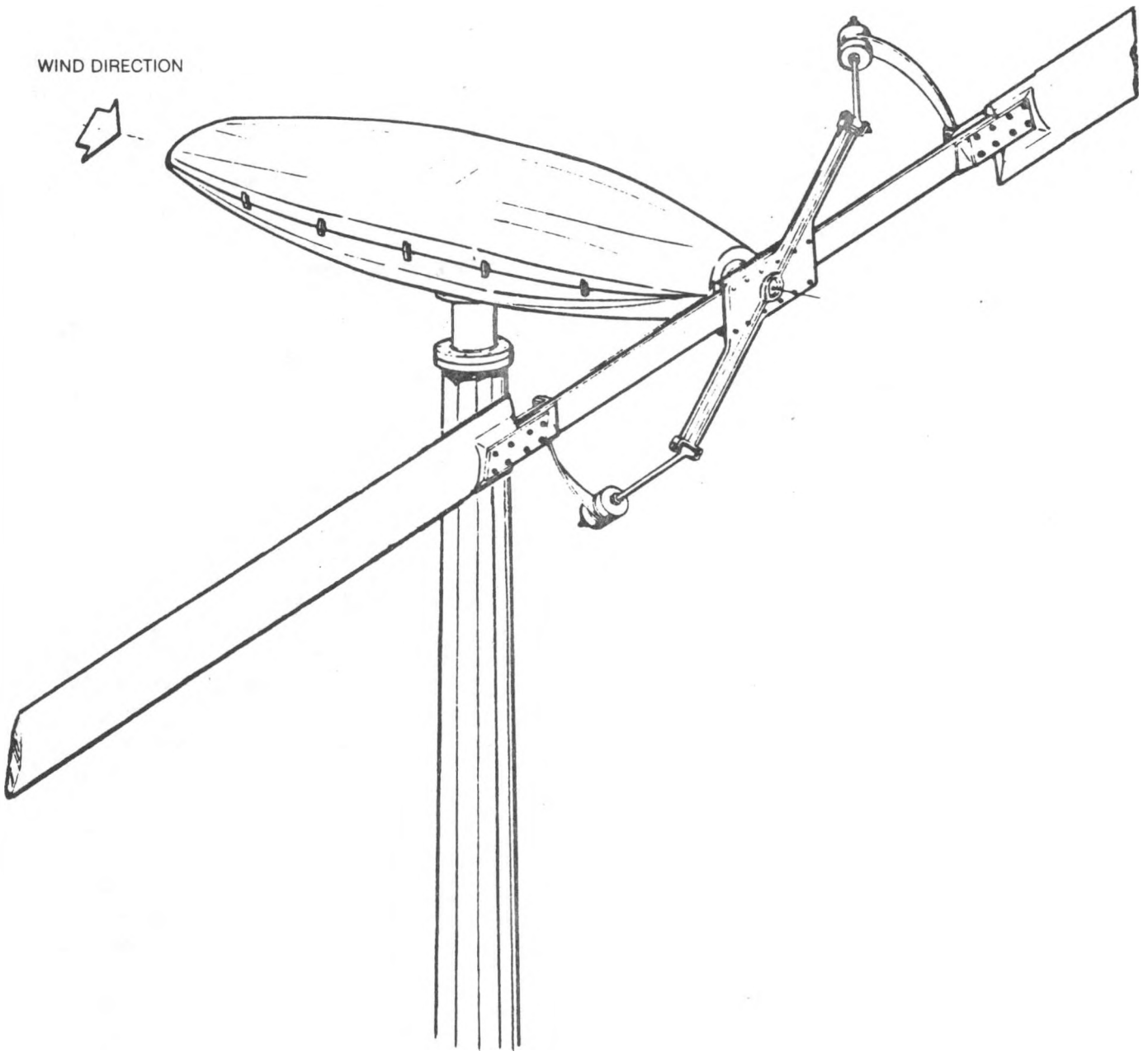

Figure 1. Schematic of 15-kW WTG Design

81-6-164-1

flexbeam, comprised of S-2 fiberglass which provides the flexibility for the rotor blades to deflect under loading. Control of blade pitch is provided by a passive system consisting of pendulums which are sensitive to centrifugal forces created by rotor rotation. As rotor speed increases from start-up, the pendulums progressively twist the blade, acting through a steel flexstrap connection between the pendulums and the flexbeam.

Rotor speed control in high winds is achieved by blade stall and the system is designed to withstand wind gusts up to 56 m/s (125 mph). A special WTG design is also presented for wind gusts up to 74 m/s (165 mph).

The WTG system is free in yaw so that the nacelle, which houses the electromechanical system (transmission-generator, etc.), rotates with little or no resistance. Because of the inherent dynamic characteristics of a CBR type rotor, the rotor will automatically track changes in wind direction. Power sliprings are located at the top of the tower to transfer the generated electricity from the freely yawing head assembly into the fixed system. The tower is a tapered, 10-sided, aluminum pole of stand-alone design; i.e., there are no guy wires to support the tower. A rectangular plate is welded to the base of the tower and the plate is then bolted to a concrete foundation. Table I summarizes the general design characteristics of the 15-kW WTG design.

Design Criteria

The criteria used for the design of the prototype address the allowable stresses for the total wind energy system. Two basic criteria are used, as shown in Table II. The first criterion is directed toward the applied static load; a 1.5 factor of safety based on the material yield stress is used to determine the allowable stress. This criterion is standard for helicopter rotor design and is also used by the Federal Aviation Administration (see Federal Air Regulations, Part 29).

The second criterion addresses the applied cyclic loads and is used to ensure an adequate fatigue stress margin. To establish this criterion, the fatigue endurance limit for each material (e.g., flexbeam composite material) is determined. Referring to the example stress versus cycle curve shown in Table II, the endurance limit is the maximum value of alternate stress that can be applied to the material for an infinite number of cycles without having material failure. Stress versus cycle experimental data are generally available in the open literature or available from the manufacturers of the material. In addition, some fatigue testing has been performed on candidate flexbeam materials to determine the endurance limit, and this will be discussed more fully later.

TABLE I

UTRC 15-kW WIND SYSTEM

ROTOR

Type	Horizontal axis, Downwind
Ground Clearance	5.1 m (17 ft)
Number of Blades	2
Blade Type	Fiberglass composite pultrusion
Diameter	14.6 m (48 ft)
Solidity	4%
Precone	0°
Generating Speed	72-77 rpm
Blade Tip Speed	55 m/s (180 ft/s) (normal operation)
Airfoil Section	NACA 23112
Taper	None
Twist	None
Swept Area	168 m^2, (1810 ft^2)
Cut-in Wind Speed	4 m/s, (9 mph)
Rated Wind Speed	12.5 m/s, (28 mph)
Survival Wind Speed	56 m/s, (125 mph)

GENERATOR

Type	Single-phase Induction
Speed	1800 rpm (synchronous)
Rating	30 hp, 22.4 kW
Full Load Efficiency	77%
Peak Efficiency	84% at 10 kW

TRANSMISSION

Type	Helical Gear, Two Stage, In Line
Max Output Speed	1890 rpm (power on), 3600 rpm (power off)
Input Speed	Up to 77 rpm (normal operation)
Step-Up Ratio	1:25.1
Input Torque	3756 N·m (2770 lbf·ft)
Output Torque	146 N·m (108 lbf·ft)
Efficiency at Rated Torque	96%

TOWER

Type	Free Standing, Tapered Al Pole
Height	12 m (39 ft)
Hub Height	12.5 m (41 ft)
Diameter	0.6 m (24 in.) at base, 0.25 m (10 in.) at top
Erection system	Gin pole and winch
Foundation	Reinforced concrete with embedded anchor bolts

TABLE II

15-kW WTG DESIGN CRITERIA

- Peak loads
  - 1.5 factor of safety for yield stress as per FAR, Part 29
- Fatigue loads
  - Infinite part life
  - Endurance limit based on M-3σ

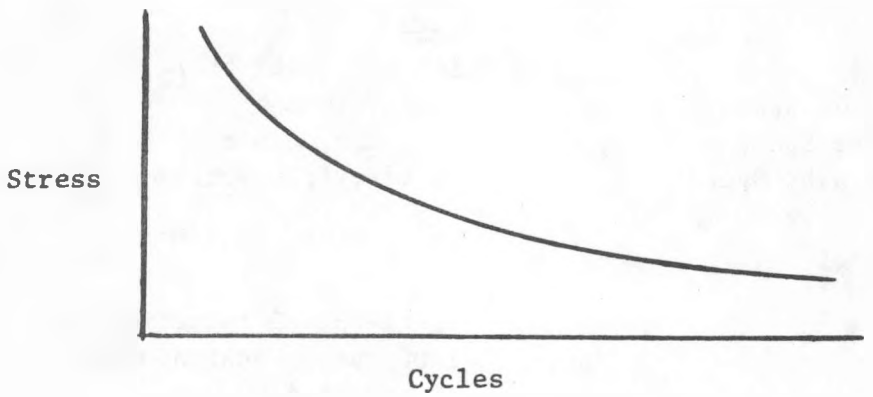

There are a variety of types of endurance limits used for stress analysis, e.g., mean of data, bottom-of-scatter data, etc. For the design of the 15-kW wind energy system, one of the most conservative definitions of endurance limit has been used. The mean minus 3σ value (M-3σ) is used to determine the allowable fatigue stress level. To determine this value, the mean of the test data is used to compute the stress versus cycle curve, and then three standard deviations (3σ), based upon the test data, are subtracted from the mean value. This definition of endurance limit is standard for helicopter rotor design. Generally, this results in an allowable fatigue stress value that is 65-70% of the mean stress. Since an infinite fatigue life is required for all parts subjected to cyclic stress, this means that no fatigue damage is allowed to occur, and therefore the fatigue stress may never be greater than the mean minus 3σ value of the endurance limit fatigue stress.

In summary, two criteria have been used to establish allowable stresses for the wind energy system. The static stress criteria follows Federal Aviation Administration guidelines and the fatigue stress criteria is one of the most conservative criteria used in rotor system design, particularly when infinite part life is required.

Critical Loads and Stresses

For the design of the 15-kW wind turbine, rotor-induced loads were calculated and then used in conjunction with the design criteria previously discussed. High speed wind conditions with the wind turbine disconnected from the electrical grid and also gust conditions over the normal operating range were investigated. The analysis used to predict the rotor-induced loads is the UTRC F762 aeroelastic analysis. This analysis is a comprehensive, multi-blade, moving hub analysis with a detailed description of the pendulum control system and the hub/nacelle degrees of freedom.

This analysis was used to predict the design loads for the 8-kW wind turbine, documented in Ref. 1. A more detailed description of the analysis can be found in Ref. 1.

Two types of loading are calculated by the analysis. First, the rotor blade shears and moments due to aerodynamic, inertial and gravity forces are calculated. These loads are useful in determining the steady and fatigue stresses in the flexbeam. Second, the rotor hub loads in the fixed system are calculated, both steady and harmonic. These loads are useful in designing the mechanical components in the fixed system, e.g., rotor shaft, bearings, yaw shaft, etc. The following sections discuss the predicted loads for a) high steady wind conditions, and b) gust conditions.

High Steady Wind Conditions

The extreme wind condition is a critical design condition for steady hub loads in the fixed system and also for steady flexbeam flatwise (out-of-plane) stresses. In an extreme wind with the wind turbine disconnected from the electrical grid, the rotor is autorotating at about twice its normal operating rotor speed. Because of the high wind and rotor speeds, the rotor produces a large thrust, as shown in Fig. 2. In addition, a steady vertical force and pitching moment on the rotor hub are also created due to gravity and wind shear. These three loads will influence the design of the mechanical components in the nacelle and also the tower and foundation. The high thrust also causes the rotor blades to deflect out-of-plane (steady coning) and, therefore, flexbeam stresses for this condition are a significant design factor.

Two extreme wind conditions were investigated, as shown in Table III.

TABLE III

EXTREME WIND CONDITIONS

Wind Speed m/s (mph)	Rotor Speed m/s (ft/s)
56 (125) (standard design)	107 (350)
74 (165) (special design)	107 (350)

STANDARD DESIGN 56 m/s (125 mph)
SPECIAL DESIGN 74 m/s (165 mph)

		THRUST		VERTICAL FORCE		PITCH MOMENT	
m/s	(mph)	N	(lb)	N	(lb)	N-m	(ft-lb)
56	(125)	34265	(7700)	1113	(250)	1827	(1400)
74	(165)	51175	(11500)	1380	(310)	783	(600)

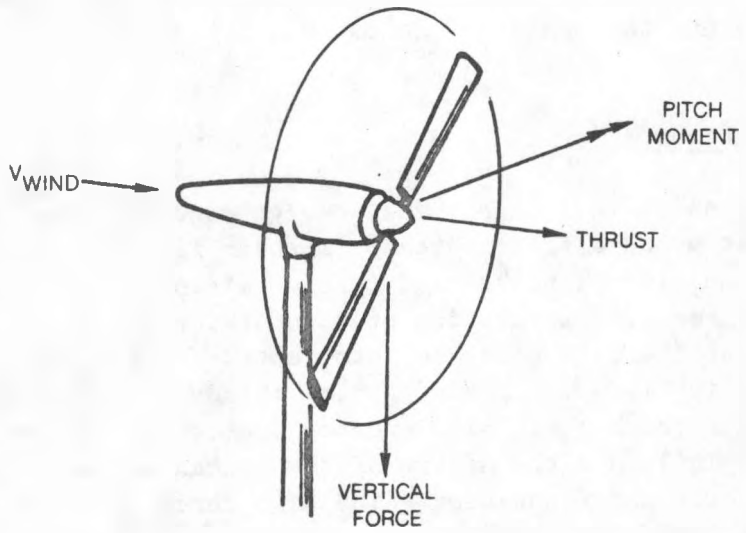

Figure 2. Rotor Hub Steady Loading for Extreme Wind Conditions

81-6-164-2

The wind model used in the aeroelastic analysis (F762) to simulate the extreme wind condition is shown in Fig. 3. Two individual wind profiles are defined and then summed with the basic wind velocity to develop radial and azimuthal variations in wind velocity over the rotor disc.

A vertical shear wind profile, based on the 1/7 power law, is calculated and summed with the basic wind velocity. For the 14.6-m (48-ft)-diameter rotor operating at the 56-m/s (125-mph)-extreme wind condition, the vertical wind shear may vary as much as +4 m/s (+9 mph) at the top of the rotor disc and -7 m/s (-16 mph) at the bottom of the rotor disc from the design wind speed at the rotor center. In addition to the vertical shear, a symmetrical lateral shear is added to the basic wind velocity. The model for the lateral shear is taken from Ref. 3 and is a function of terrain roughness, rotor diameter, and the mean wind velocity. A standard terrain roughness (Z_o = 0.1) has been assumed in the calculations. The formula developed in Ref. 3 for the lateral wind shear is based on statistical evaluation of experimental wind data, and therefore a level of confidence can be applied in the calculations. For the lateral wind shear model used in the F762 analysis, two standard deviations (2σ) have been applied to the calculated lateral wind component. This, of course, increases the magnitude of the calculated lateral shear, but in doing so, a 95% level of confidence is established that the lateral shear will never be exceeded. For the 56-m/s (125-mph)-extreme wind condition, the calculated lateral wind shear (with 2σ applied) is about $\pm$ 7 m/s ($\pm$ 16 mph). Based upon the wind model just described, the rotor loads were calculated by F762 for the two extreme wind conditions. The predicted steady hub loads are shown in Fig. 2.

As previously mentioned, the large rotor thrust at high wind conditions causes the rotor blades to cone, which results in higher steady flatwise stresses for the flexbeam. The stresses along the blade span, from the blade tip inboard to about 10% rotor radius, are quite low because the centrifugal forces acting on the coned rotor blade nearly cancel the applied aerodynamic loading. The rotor blade cones about 16^{o} to achieve this equilibrium position for the 56-m/s (125-mph)-extreme wind condition. For flexbeam type rotors, the coning is a result of flexbeam deflection close to the hub, about 10% radius. Inboard of this position, the hub restraint allows small flexbeam deflections to relieve the applied thrust loading, and this is the area of highest stress on the entire rotor system. In Fig. 4, the flatwise flexbeam stresses resulting from the high thrust are shown for both extreme wind conditions. Based upon these calculated stresses, the factor of safety for the S-2 glass* flexbeam is also shown. For both extreme wind conditions, the 56-m/s (125-mph)-design condition and the 74-m/s (165-mph)-special condition, the factor of safety is well above the 1.5 factor of safety specified in the design criteria.

Gust Conditions

The impact of gust conditions on rotor system loads was predicted by using a time-varying wind model in the F762 analysis. This analysis solves the

* trademark of Owens-Corning Fiberglass Corporation

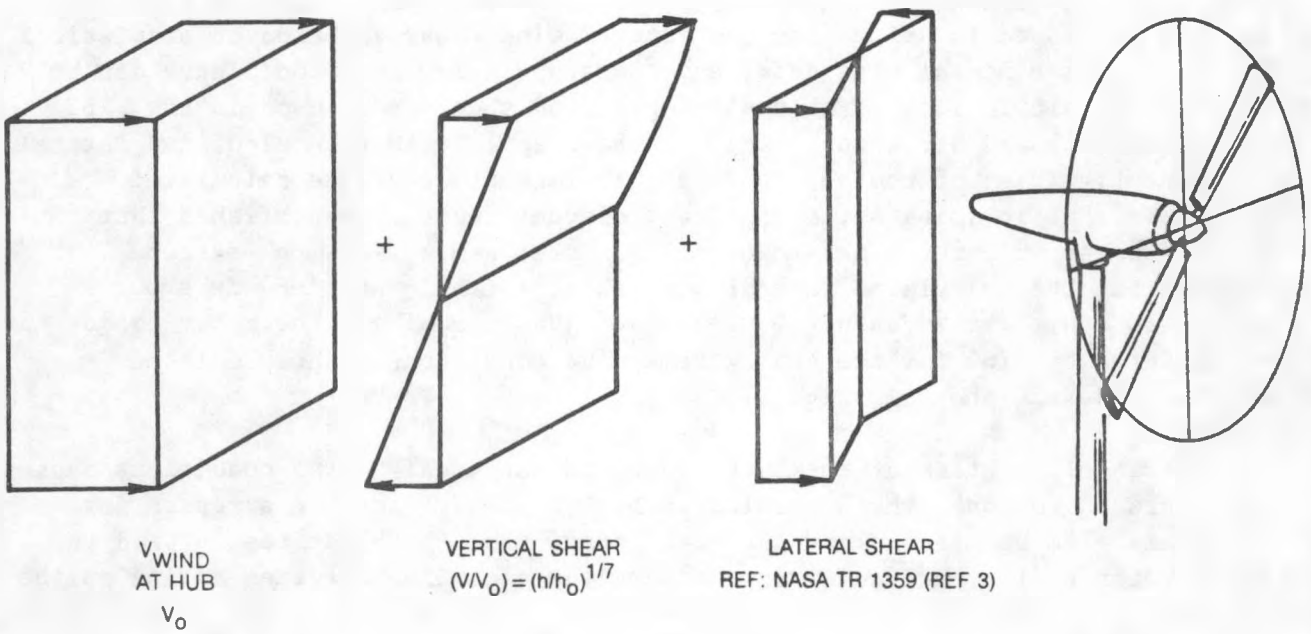

Figure 3. Wind Model for Calculation of Rotor Hub Steady Loading at Extreme Wind Conditions

81-6-164-3

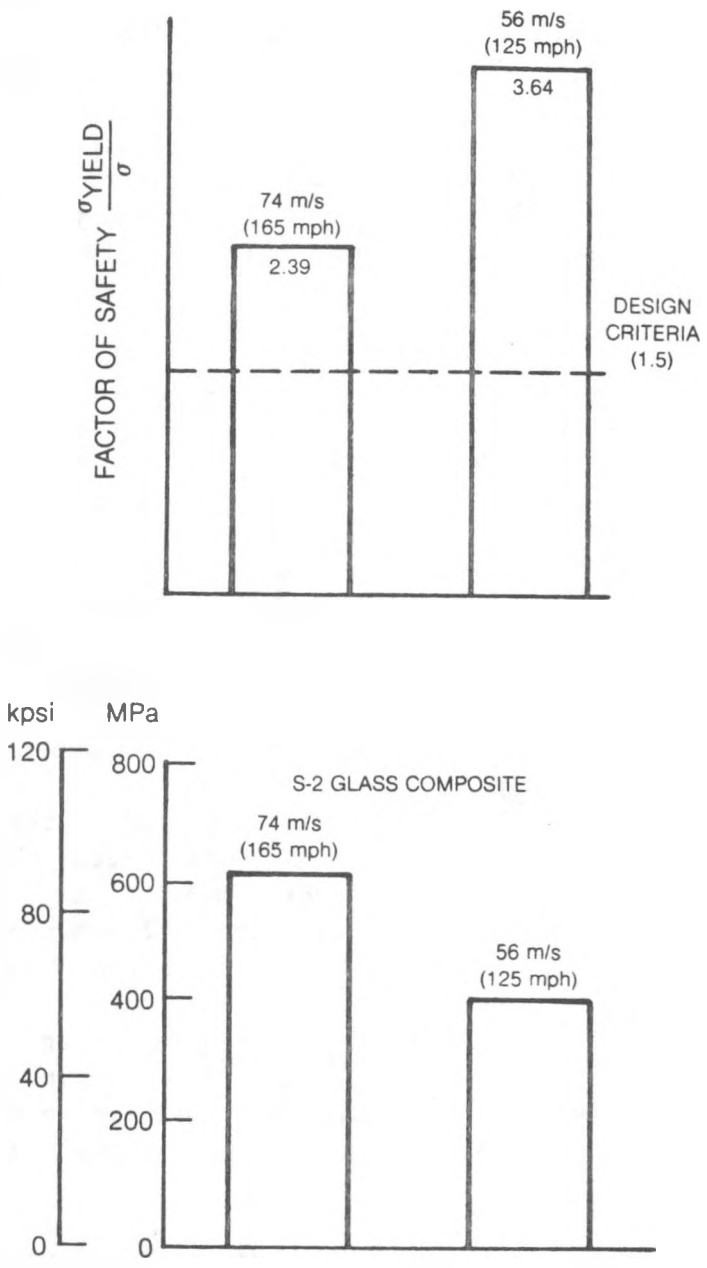

Figure 4. Maximum Flexbeam Stresses for Extreme Wind Conditions

81-6-164-4

aeroelastic equations of rotor/hub motion in the time domain and is, therefore, well suited to simulate wind gusts. The gust model that was used in the F762 analysis is shown in Fig. 5. This gust model was taken from Ref. 3 and describes a time variation in the longitudinal wind speed over the entire rotor disc as a function of mean wind speed, gust factor, gust duration, and gust rise time. In Fig. 5, a sample gust profile is shown for the 15-kW wind turbine for a mean wind speed of 5.4 m/s (12 mph). For this particular gust profile, at time 0^- the wind speed is the mean value, 5.4 m/s (12 mph). At time 0^+ the wind speed rises abruptly as shown and peaks at 25% of gust duration time, as specified. Since the gust duration time is specified nondimensionally, the actual time of duration can be any value specified, but the shape of the gust profile remains constant. At the end of the gust, the wind speed returns to the mean value.

One of the most important parameters in the calculation of the longitudinal gust profile is the gust factor F_g, which is the ratio of the peak wind speed during the gust to the mean wind speed. This is shown in Fig. 5. Various experimental data as well as some semi-empirical data were used to choose the gust factors to be used in the loads calculations. Figure 6 shows experimental and semi-empirical data over a mean wind speed range up to 30 m/s (67 mph). Of particular importance is the Boulder, Colorado area data, taken a few miles away from the Rocky Flats test site. These data show the highest gust factors over a wind speed range that includes the normal operating range of the wind turbine. Also shown in Fig. 6 are the gust factors used in the loads calculations. These gust factors envelop the data shown over the entire wind speed range.

The remaining parameter to be defined is the period of the gust (τ). To ensure maximum response of the wind turbine system to gusts, the gust period was set close to the period of the first natural mode of the wind turbine system, including the tower, in the longitudinal direction. This period is about 1 sec, and more will be said later in regard to the tower natural frequencies.

Table IV summarizes the gust conditions that were investigated using the gust model defined in the F762 aeroelastic analysis. The wind conditions cover the normal operating range with the wind turbine connected to the electrical grid, and also three high speed conditions - two with increasing gusts and one with a decreasing gust.

The predicted rotor and tower gust responses for the 5.4-m/s (12-mph)-design condition are shown in Figs. 7 and 8. The results are shown in the form of a time history during and after the gust, which is also shown in time history form. Before the gust (time 0^-), the wind turbine is operating in a steady state condition at the mean wind speed of 5.4 m/s (12 mph) with little or no transient perturbations. In Fig. 7, the flexbeam stresses at the root of the flexbeam,

TABLE IV

SUMMARY OF GUST CONDITIONS USED FOR LOADS CALCULATIONS

Mean Wind Speed		Rotor Tip Speed		Gust Factor	Gust Period	Max Wind Speed in Gust	
m/s	mph	m/s	ft/s	F_g	Sec	m/s	mph
5.4	12	57	188	3.4	1	21	48
12	26	57	188	3.4	1	44	98
22	50	57	188	2.0	1	49	110
35	78	107	350	1.6	1	56	125
46	103	107	350	1.6	1	74	165
56	125	107	350	1.6	(decreasing gust to 35 m/s (78 mph))		

where stresses are the largest, are shown along with the pendulum motion. As the gust rises, the longitudinal wind component increases and this causes an increase in blade section angle of attack. As a result, the rotor thrust increases transiently and an increase in rotor coning follows. This is reflected in the transient increase in flexbeam flatwise stress, shown in Fig. 7. At the end of 2 sec, or 1 sec after the gust has been completed, the flexbeam flatwise stress has nearly returned to the steady-state level held before the gust was initiated. The rapid recovery is indicative of the beneficial aerodynamic damping available for flatwise motion; the blades act as paddles in the wind. Conversely, the lack of aerodynamic damping for the in-plane blade motion is evident in the flexbeam edgewise stress. In this case, the blade is slicing the air instead of working against it, and the primary damping available is the structural damping due to the flexbeam material. The frequency of the flexbeam edgewise stress response is about 4 Hz, which is the natural frequency of the first rotor in-plane mode. The level of edgewise stress is not large but the periodic response at its natural frequency does continue over the 4 sec time history shown. Both the flexbeam torsion and the pendulum respond transiently and nearly in phase, as expected, since pendulum motion and flexbeam torsional motion are highly coupled through the flexstrap. There is more damping available in blade torsion motion than in edgewise motion, and this is exhibited by the decaying response of the torsional stress and flexbeam motion. All of the flexbeam stresses shown in Fig. 7 are relatively low and their relationship to the fatigue endurance limit stress will be shown later.

In Fig. 8, the response of the tower/nacelle to the gust is shown for the 5.4-m/s (12-mph)-design condition. The most important parameter is the longitudinal motion of the tower, since the period of the gust has been set to the period of the wind turbine system in the longitudinal mode. As the gust rises, rotor thrust increases, as previously described, and this increases the longitudinal

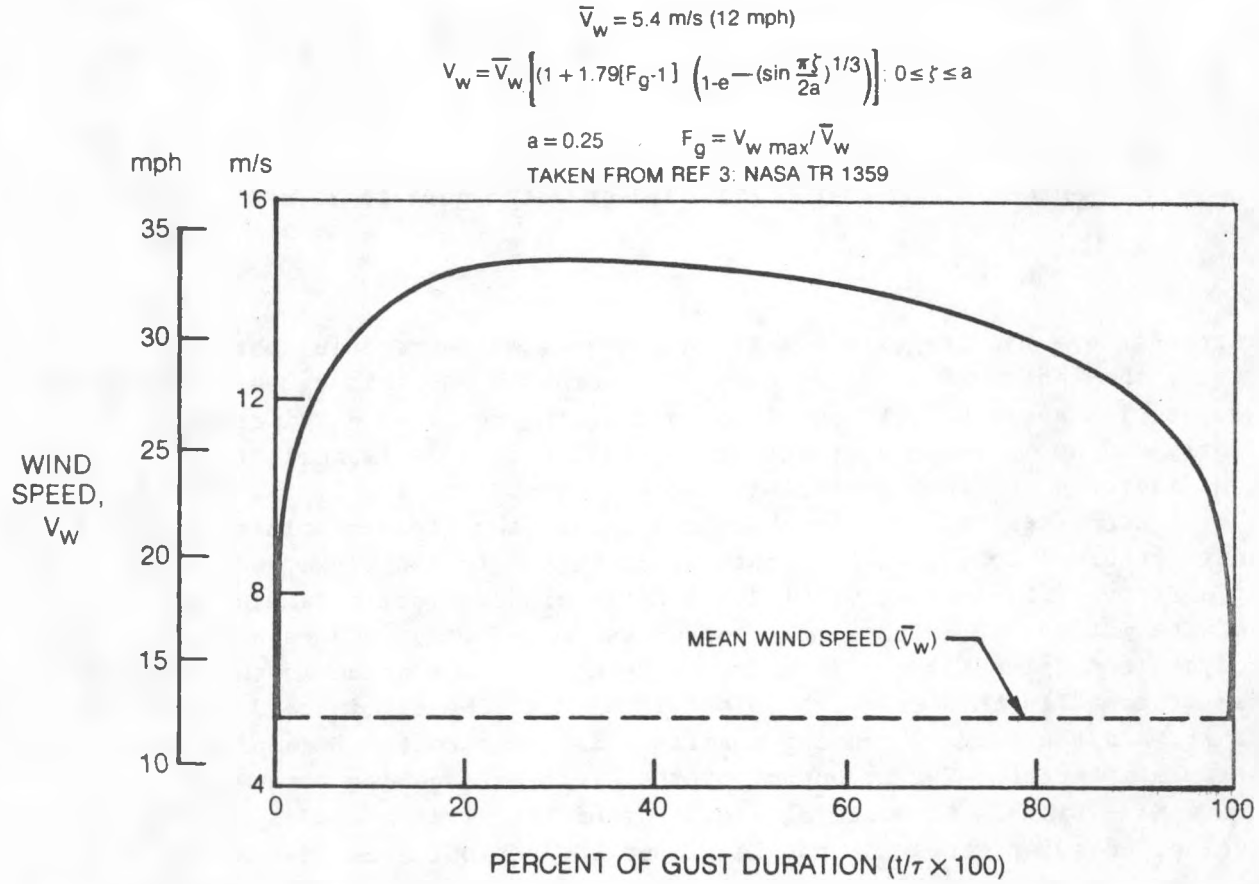

Figure 5. Longitudinal Gust Model for Mean Wind Speed Condition

81-6-164-5

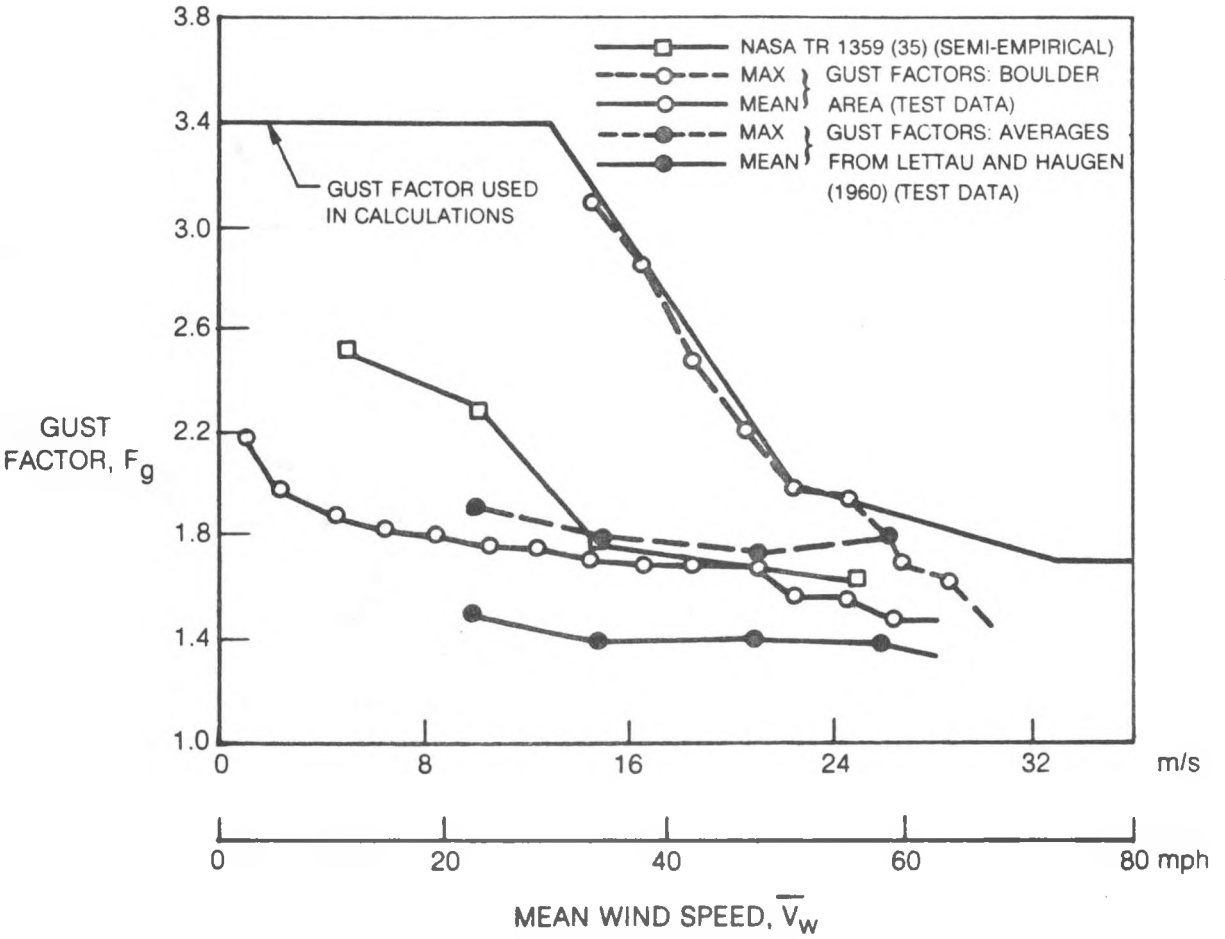

Figure 6. Gust Factors, Comparison of Experimental Data and That Used in Loads Calculations

81-6-164-6

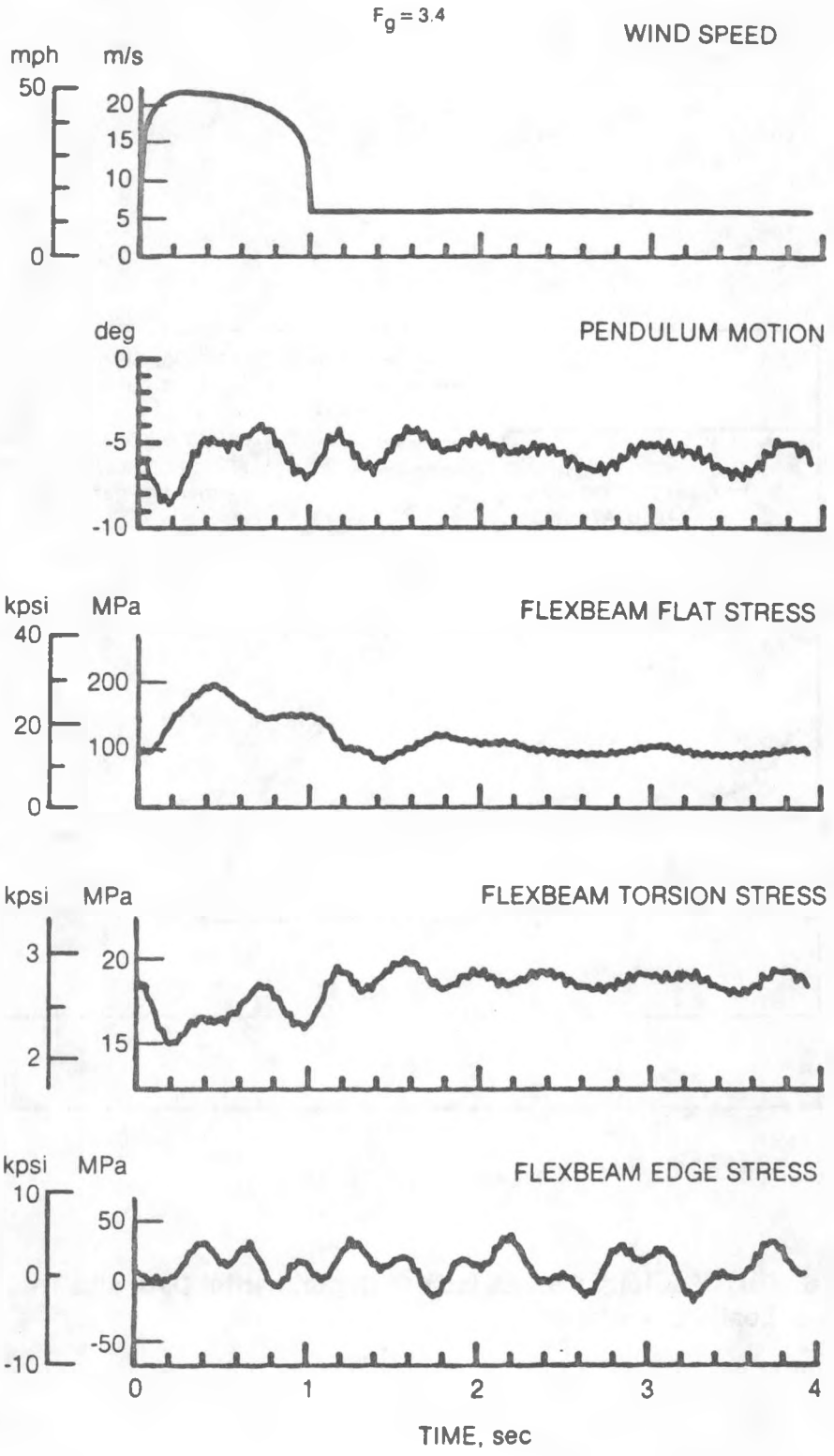

Figure 7. Predicted Rotor Gust Response at 5.4 m/s (12 mph)

81-6-164-7

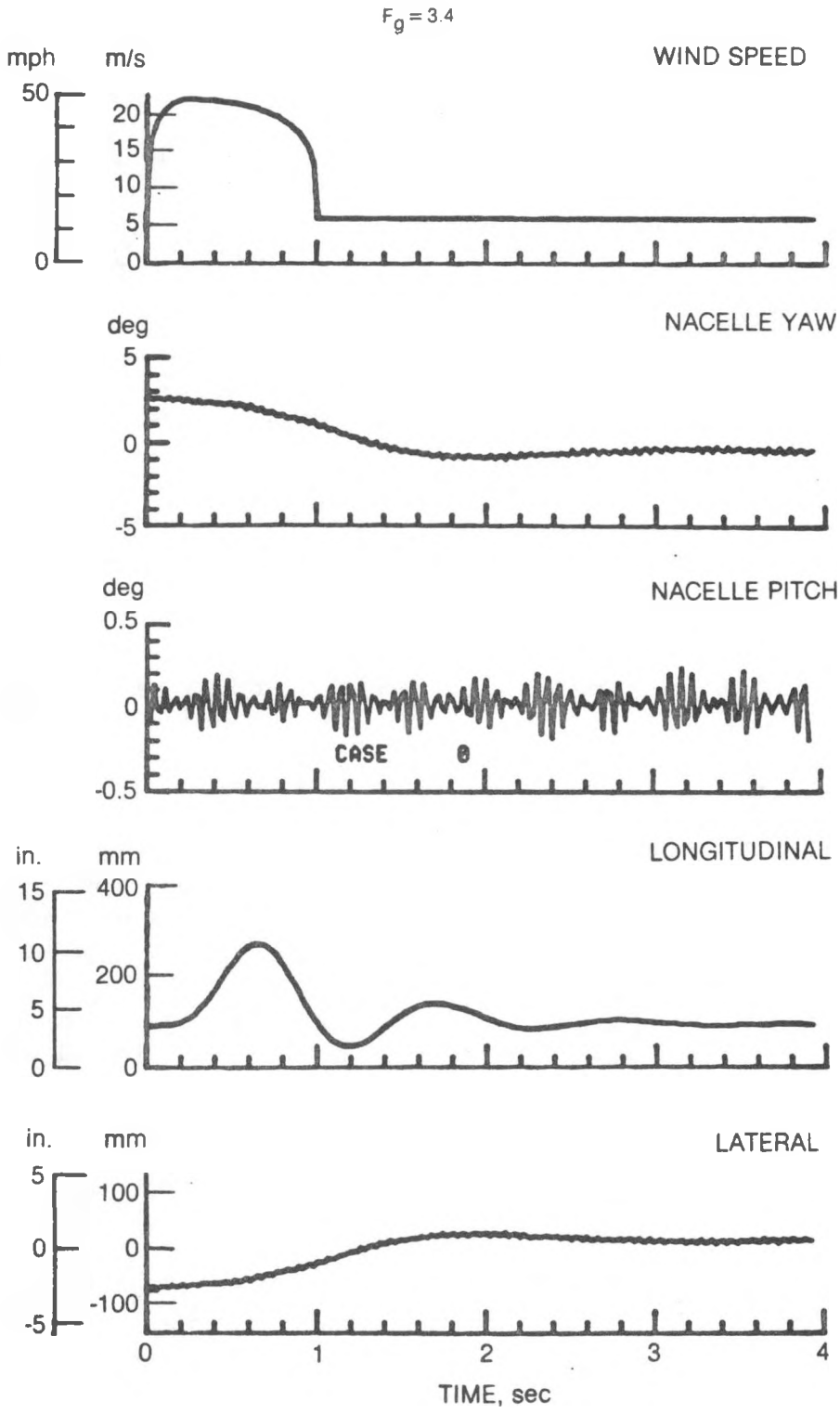

Figure 8. Predicted Tower Gust Response at 5.4 m/s (12 mph)

81-6-164-8

bending moment on the tower. The tower longitudinal motion responds accordingly in a transient fashion, and the period of the response is about 1 Hz, the same as the system longitudinal natural frequency.

The most important characteristic of the tower longitudinal response, shown in Fig. 8, is the high rate of decay exhibited. After 3 sec the tower longitudinal motion is nearly quasi-static. Obviously, there is a significant amount of damping available in this mode, and the damping is nearly all due to the total rotor disc, acting as a paddle in the wind. As long as the rotor disc is aligned perpendicular to the wind direction, this beneficial damping will be available to attenuate the response of the wind turbine system in the direction of the wind. Also shown in Fig. 8 are nacelle yaw motion, which responds as a zero frequency system, and tower lateral motion, which responds in a similar manner.

Neither of these parameters returns to the quasi-static position before the gust was initiated (time 0^-), but should do so after a period of time longer than that shown in Fig. 8. The last parameter shown in Fig. 8 is nacelle pitch motion. This motion is indicative of response of the second longitudinal wind turbine system mode, with a frequency of about 9 Hz. The response of this tower/nacelle mode is low, due to the separation in frequency between the gust and the mode involved.

Figures 9-18 show the gust response results of the rotor and tower/nacelle for the other gust conditions listed in Table IV. These results are basically the same as that shown in Figs. 7 and 8 for the 5.4-m/s (12-mph) condition. The flexbeam flatwise stress and the tower longitudinal motion rise with the gust and decay rapidly, and the flexbeam edgewise stress responds transiently at the first in-plane natural frequency and exhibits little damping to decay the motion. Generally, flexbeam stresses and tower motions rise with increasing mean wind speed, but the level of stress and motion is acceptable from both a peak stress and fatigue stress viewpoint. This is shown in Table V.

In Table V, the flexbeam peak and fatigue bending stresses are compared with the yield stress and endurance limit stress, respectively, for all of the gust conditions investigated. For all of these conditions, both the flatwise and edgewise peak bending stress safety factors are well above the specified 1.5 level. Also the fatigue stresses are well below the specified endurance limit stresses. These predicted results indicate that the flexbeam should accumulate no fatigue or static stress damage, and therefore have an infinite life.

It was mentioned previously that blade stresses on the lifting portion of the blade are much lower than flexbeam stresses. This is demonstrated in Table VI which shows the blade flatwise stresses at the point where the blade joins the flexbeam. Both static and cyclic stresses are well within the specified design criteria.

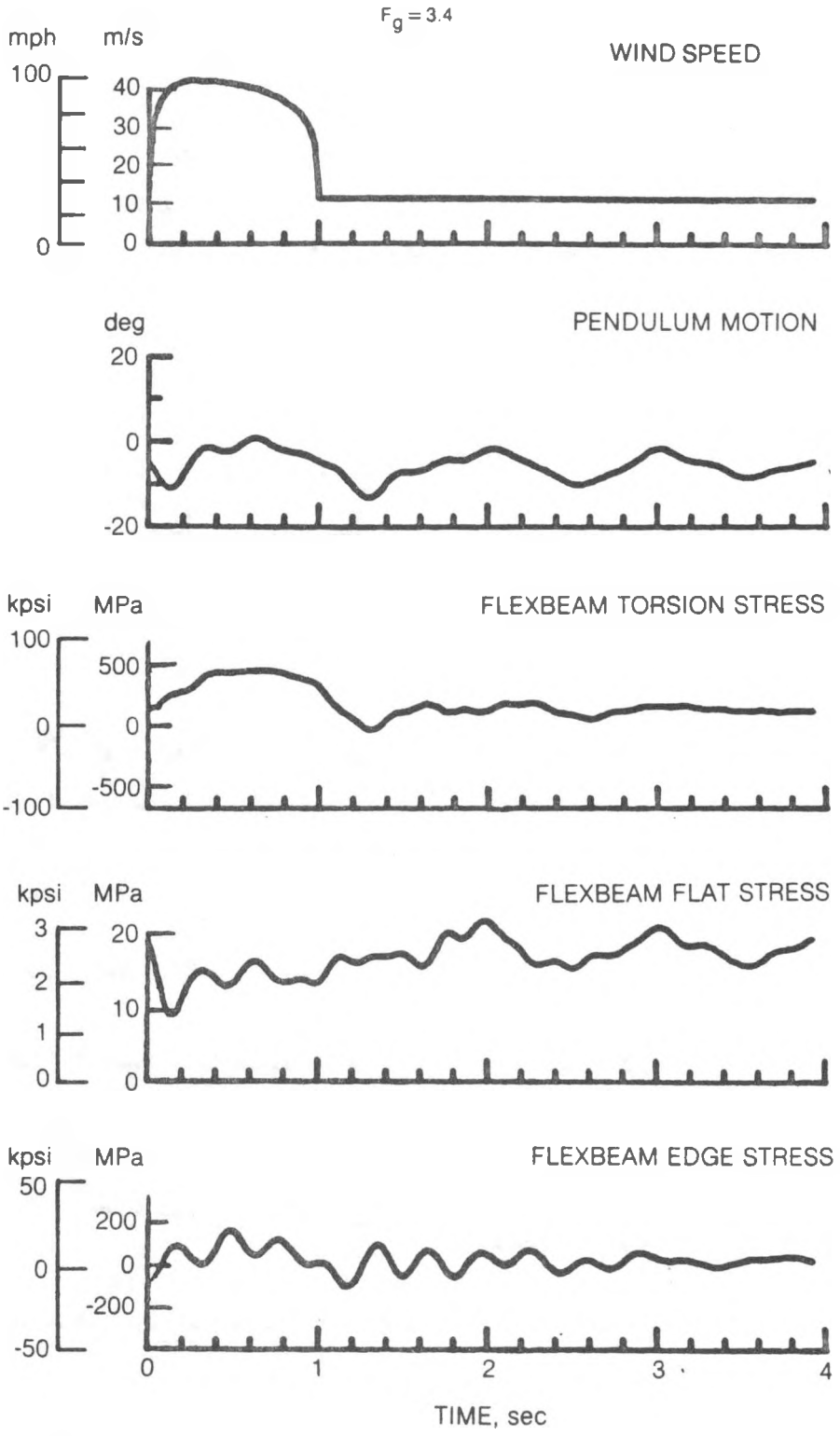

Figure 9. Predicted Rotor Gust Response at 12 m/s (26 mph)

81-6-164-9

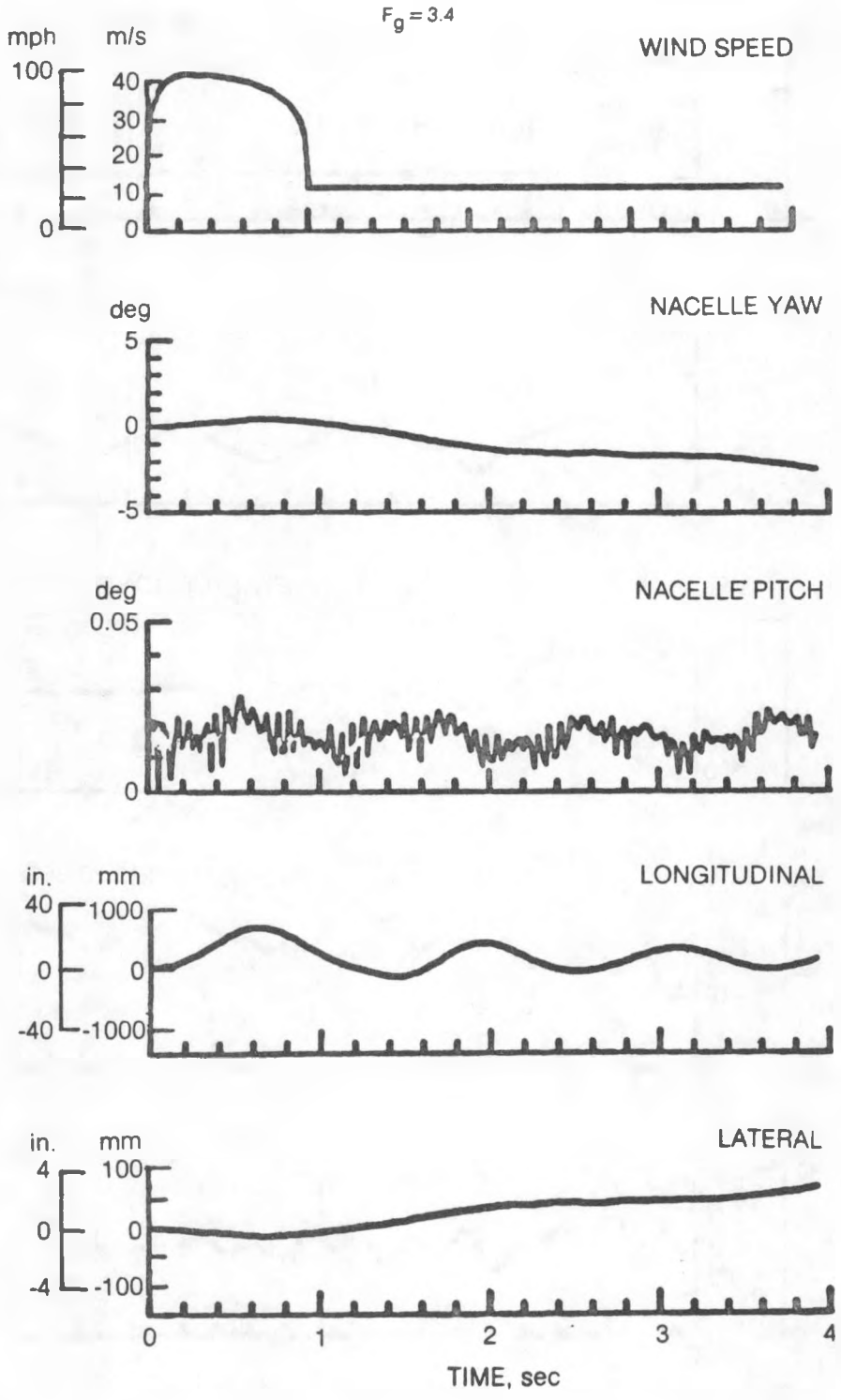

Figure 10. Predicted Tower Gust Response at 12 m/s (26 mph)

81-6-164-10

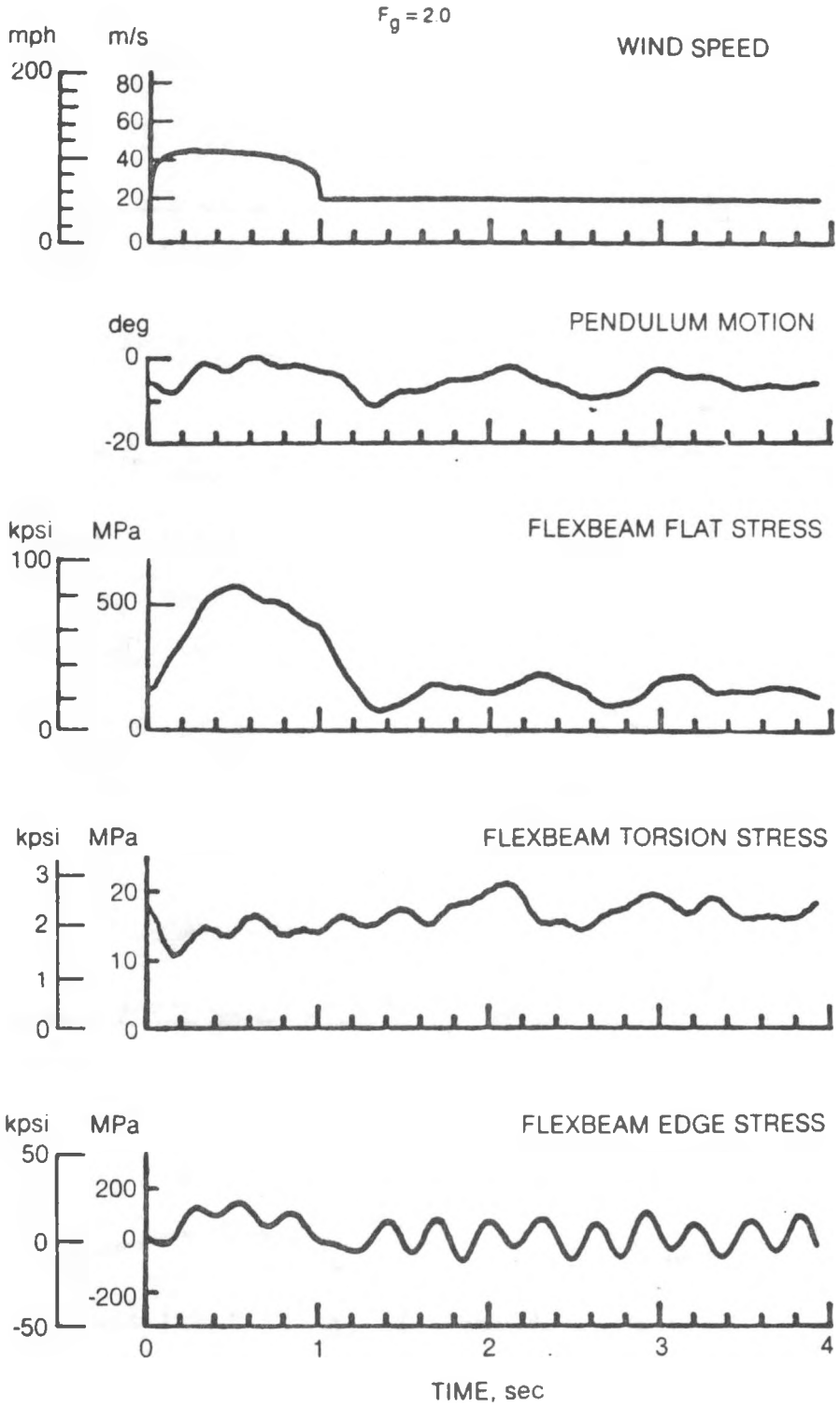

Figure 11. Predicted Rotor Gust Response at 22.5 m/s (50 mph)

81-6-164-11

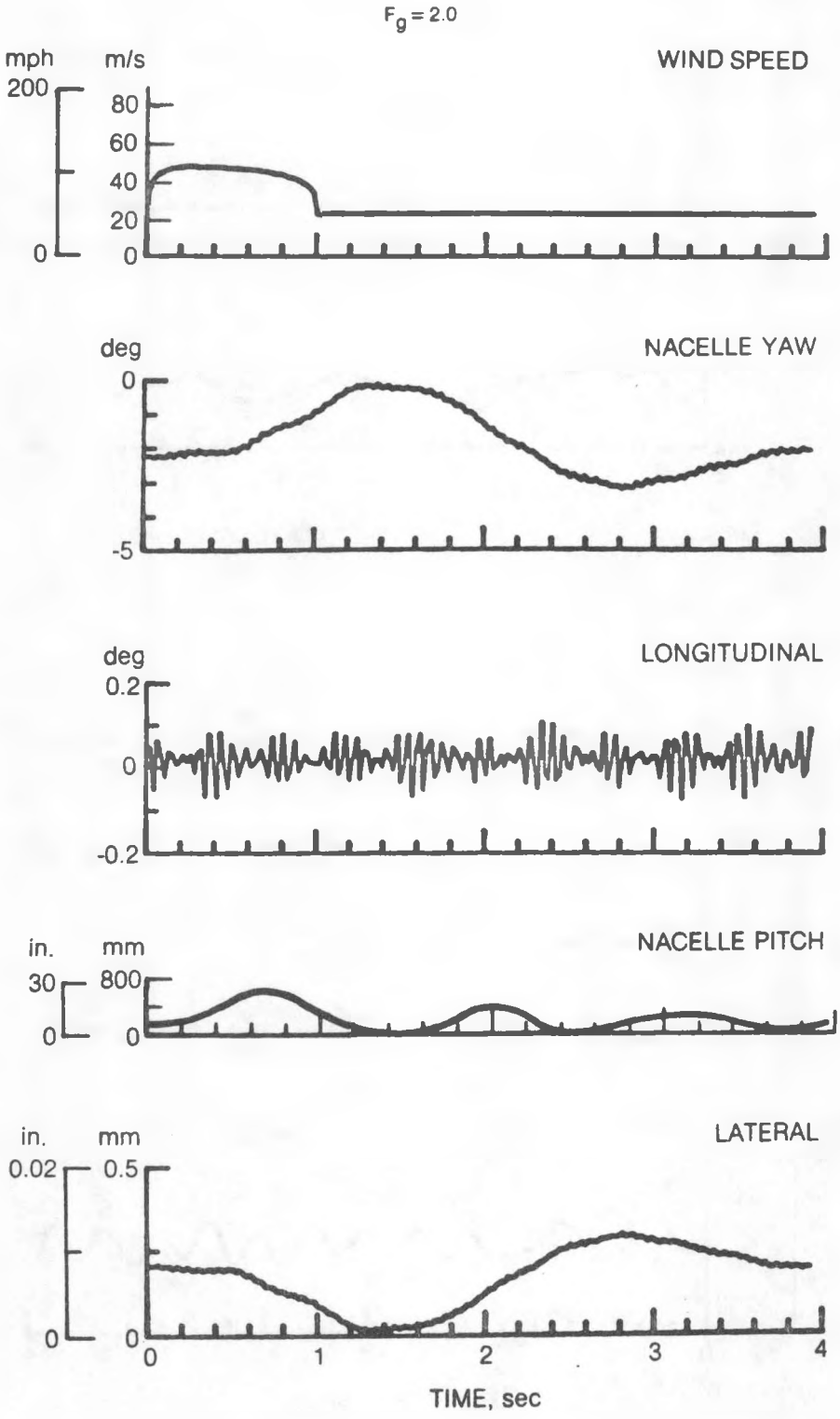

Figure 12. Predicted Tower Gust Response at 22.5 m/s (50 mph)

81-6-164-12

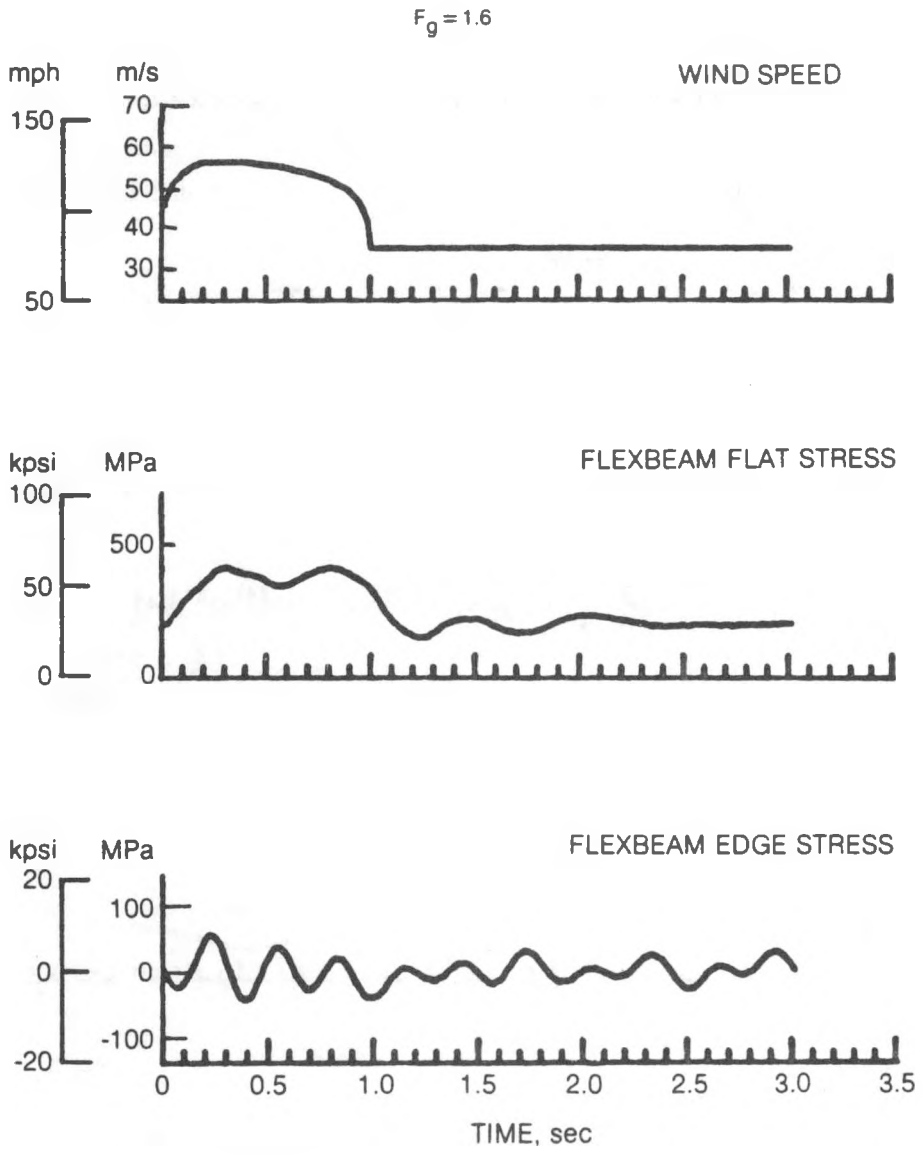

Figure 13. Predicted Rotor Gust Response at 35 m/s (78 mph)

81-6-164-13

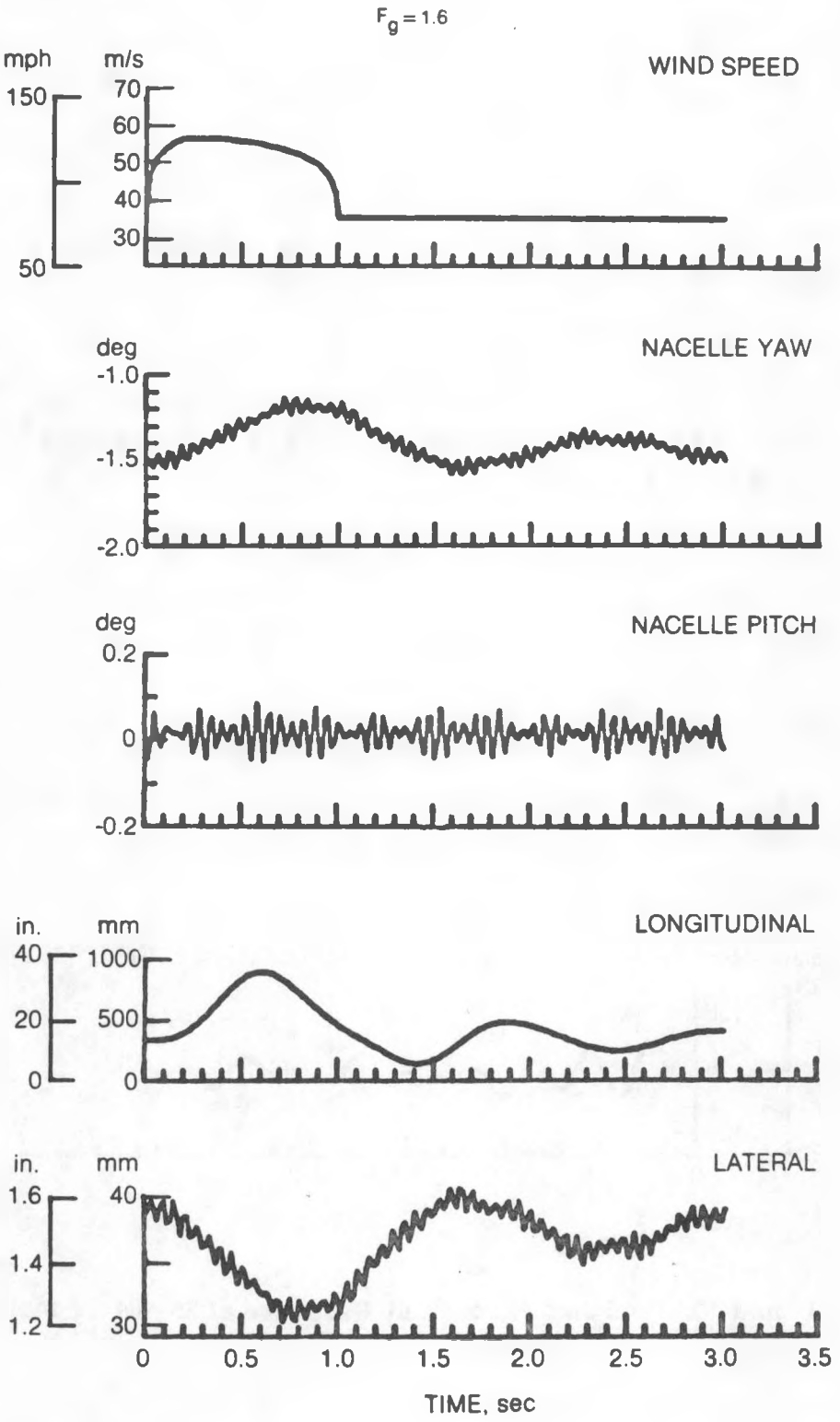

Figure 14. Predicted Tower Gust Response at 35 m/s (78 mph)

81-6-164-14

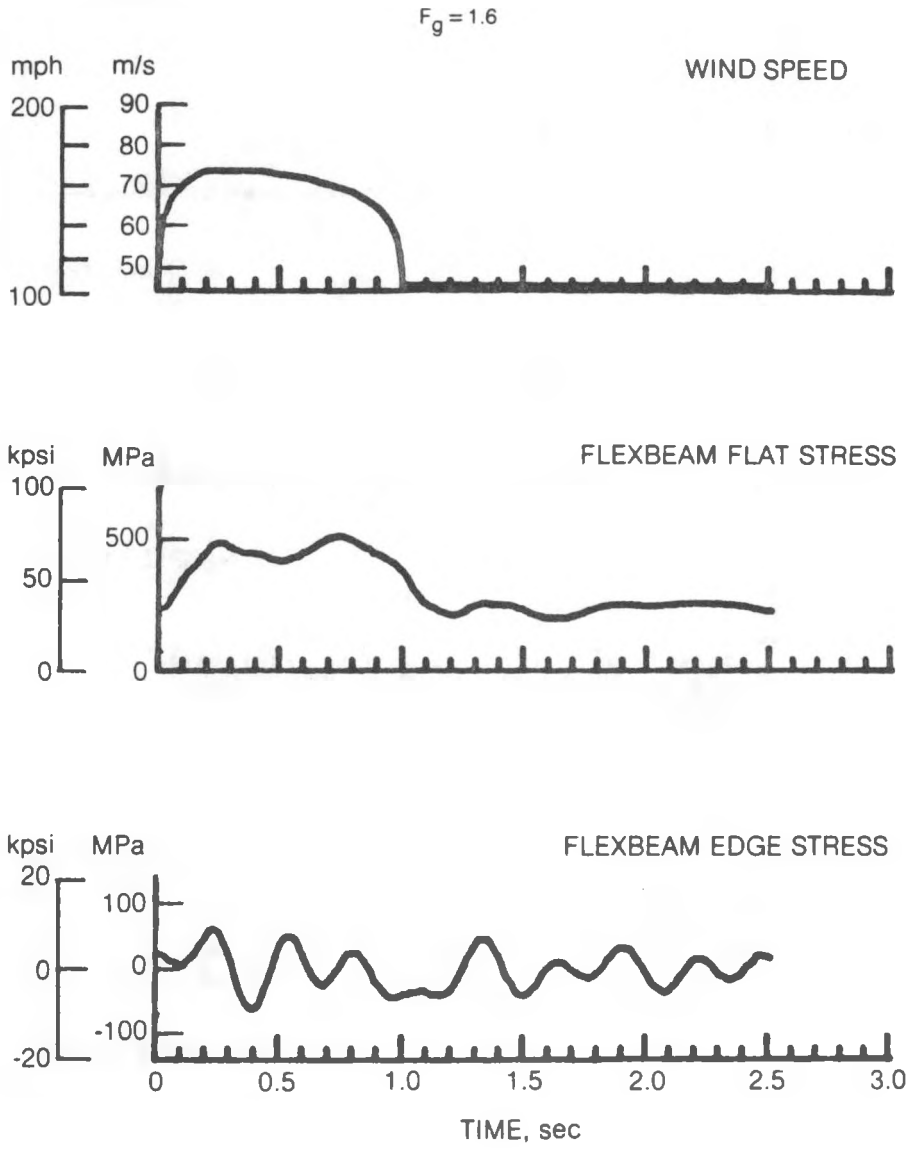

Figure 15. Predicted Rotor Gust Reponse at 46 m/s (103 mph)

81-6-164-15

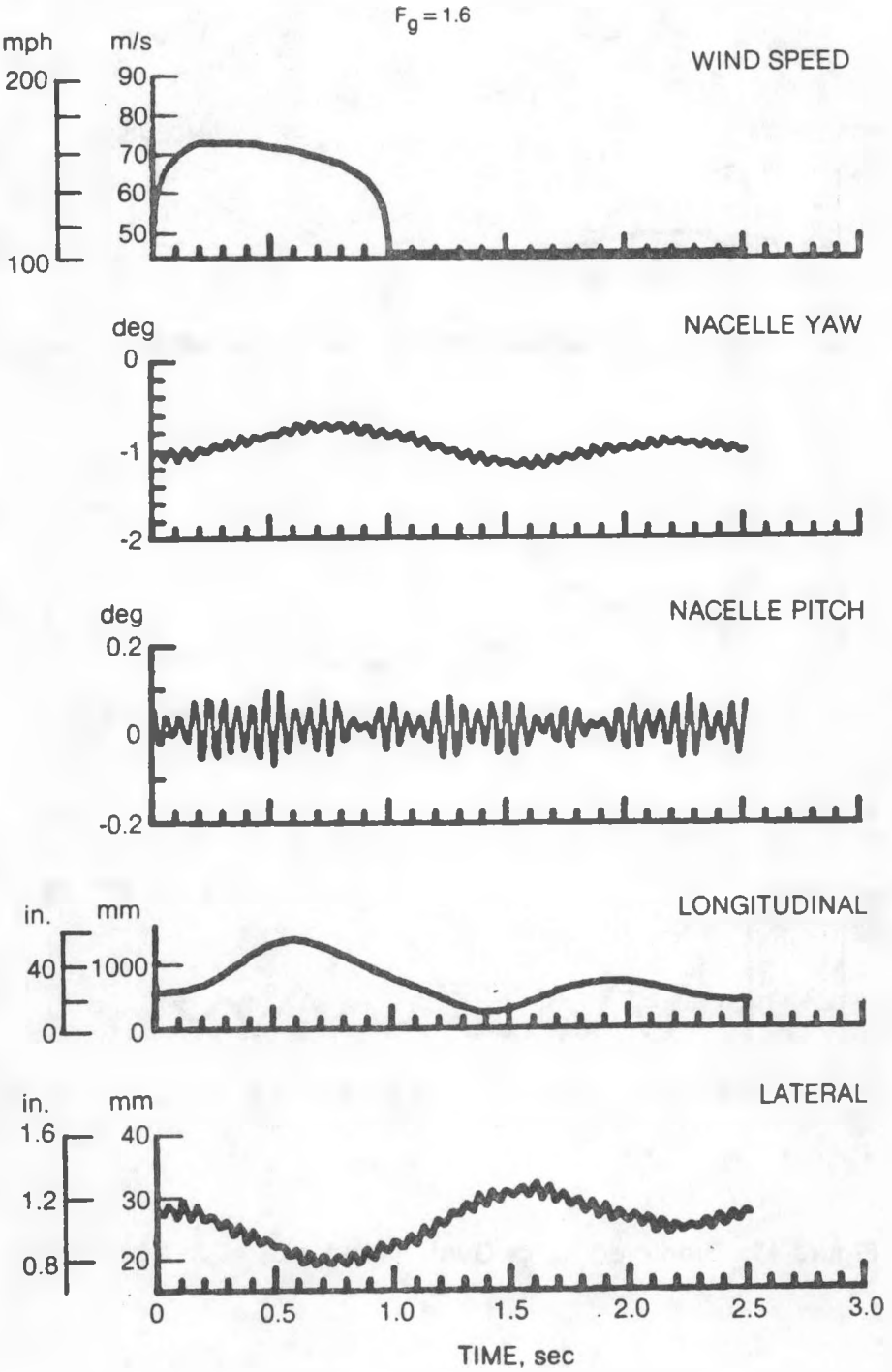

Figure 16. Predicted Tower Gust Response at 46 m/s (103 mph)

81-6-164-16

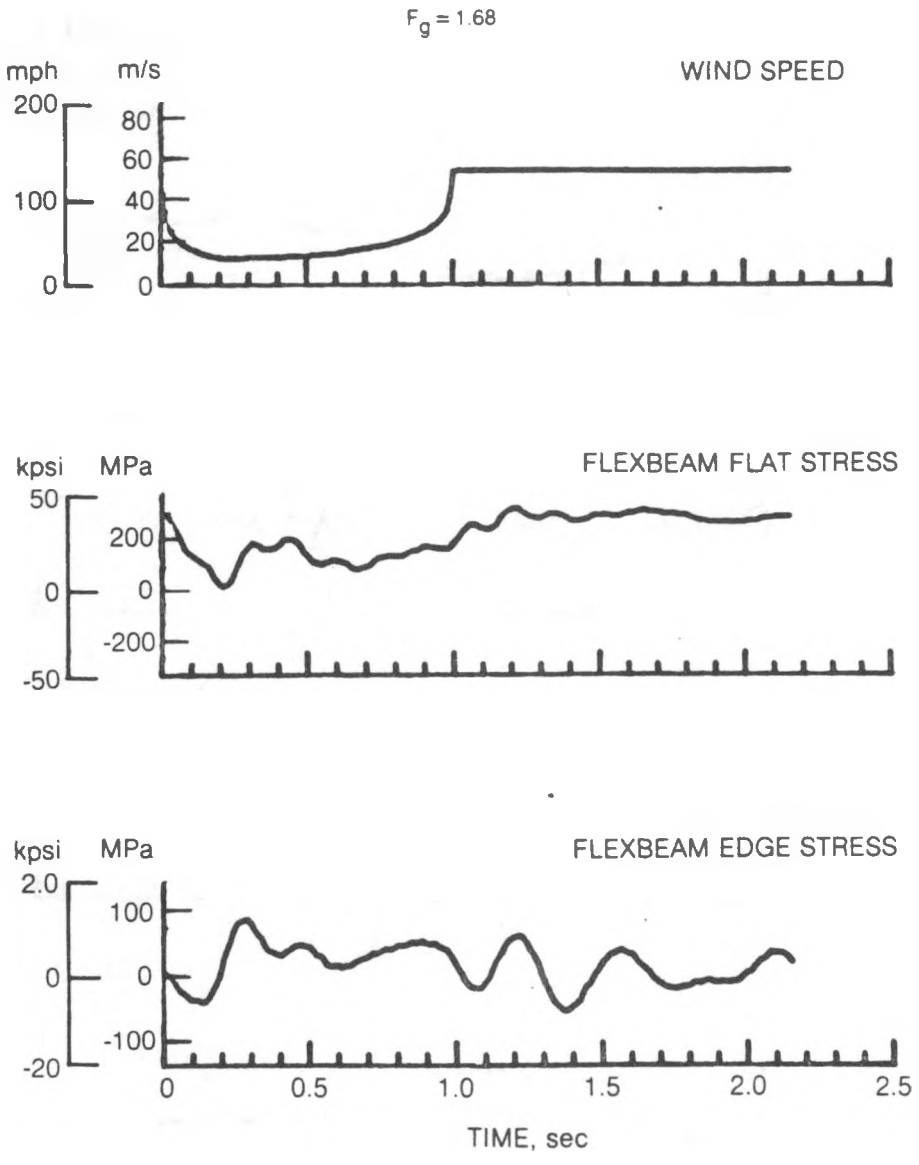

Figure 17. Predicted Rotor Gust Response at 56 m/s (125 mph)

81-6-164-17

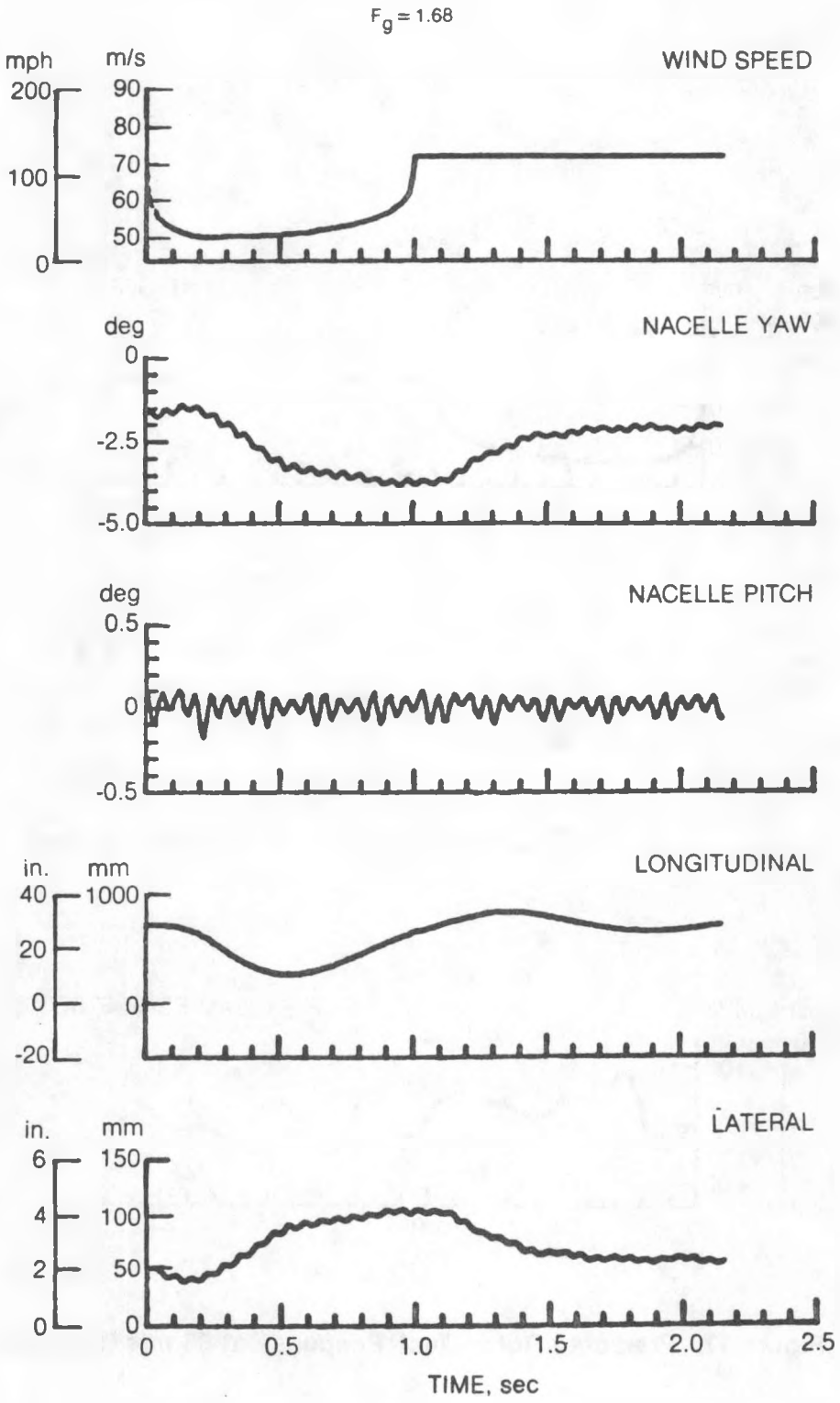

Figure 18. Predicted Tower Gust Response at 56 m/s (125 mph)

81-6-164-18

TABLE V

SUMMARY OF PREDICTED MAXIMUM FLEXBEAM BENDING STRESSES FOR GUST CONDITIONS

Mean Wind Speed m/s	mph	Gust Factor Fg	Peak Wind Speed m/s	mph	Max Flexbeam Stresses Factor of Safety Flatwise	Edgewise	Percent Endurance Limit Flatwise	Edgewise
5.4	12	3.4	21	48	7.4	43.0	22	22
12	26	3.4	44	98	3.3	10.2	50	72
22	50	2.0	49	110	2.5	8.6	44	72
35	78	1.6	56	125	3.6	26.9	33	39
46	103	1.6	74	165	2.9	23.9	28	44
35	78	1.6	56	125*	5.1	17.9	56	44

Note: design criteria are a) 1.5 minimum factor of safety
b) less than 100% of endurance limit

TABLE VI

SUMMARY OF PREDICTED MAXIMUM BLADE BENDING STRESSES FOR GUST CONDITIONS

Mean Wind Speed m/s	mph	Gust Factor Fg	Peak Wind Speed m/s	mph	Max Blade Stresses Factor of Safety Flatwise	Edgewise	Percent Endurance Limit Flatwise	Edgewise
5.4	12	3.4	21	48	44	114	12	4
12	26	3.4	44	98	22	27	14	12
22	50	2.0	49	110	16	27	11	34
35	78	1.6	56	125	24	34	5	21
46	103	1.6	74	165	21	57	7	25
35	78	1.6	56	125*	44	43	14	22

Note: design criteria are a) 1.5 minimum factor of safety
b) less than 100% of endurance limit

*Power off, 100% overspeed condition

A summary of the gust response of the tower in the longitudinal mode is shown in Fig. 19. The motion of the tower is represented in terms of longitudinal deflection at the nacelle, and the motion is converted into equivalent factors of safety for key gust conditions. The critical stress point for the tower is at the base and the factors of safety that are shown and the yield point are for the tower base. These results show that a 1.5 factor of safety is reached for a 49-m/s (110-mph)-peak gust and at 56 m/s (125 mph) for a steady extreme wind condition. For a gust condition with peak wind of 56 m/s (125 mph), the factor of safety is 1.26. This value is below the design criteria but deemed acceptable for a number of reasons. First, the yield point will not be exceeded until a peak gust up to 67 m/s (150 mph) is experienced. Second, the gust factor used (1.68) is quite conservative, based on the data shown in Fig. 6, and may be high by a factor of 2. Third, the time period that is used for the gusts is 1 sec. Gusts at high wind speeds normally have much longer periods, particularly for higher gust factors, whereas the gust simulation for the 56-m/s (125-mph) condition depicts a wind speed rise from 35 m/s (78 mph) to 56 m/s (125 mph) and then a return to 35 m/s (78 mph) within 1 sec. For longer gust periods, the tower response would approach the static deflection value, and this is shown to have a 1.5 factor of safety for the 56-m/s (125-mph)-extreme wind condition.

The maximum fatigue stresses for the tower can be calculated from Fig. 19 as the difference between peak stress and static stress. The results are shown in Table VII. For all gust conditions, the tower fatigue stresses are below the fatigue endurance limit.

TABLE VII

SUMMARY OF MAXIMUM TOWER STRESSES FOR GUST CONDITIONS

Mean Wind Speed		Gust Factor	Peak Wind Speed		Percent Endurance
m/s	mph	F_g	m/s	mph	Limit
5.4	12	3.4	22	48	11
12	26	3.4	44	98	28
22	50	2.0	49	110	28
35	78	1.6	56	125	26
46	103	1.6	74	165	28

In summary, rigorous wind conditions, both gust and extreme wind, have been used in the analytical simulation to predict the critical loads for the wind turbine system. In most cases, the assumptions for the wind conditions are conservative in order to establish confidence in the design from a stress viewpoint. The predicted results indicate that the rotor and tower design are acceptable for stresses, and no stress-related problems should be encountered during normal operation with gust or extreme wind conditions.

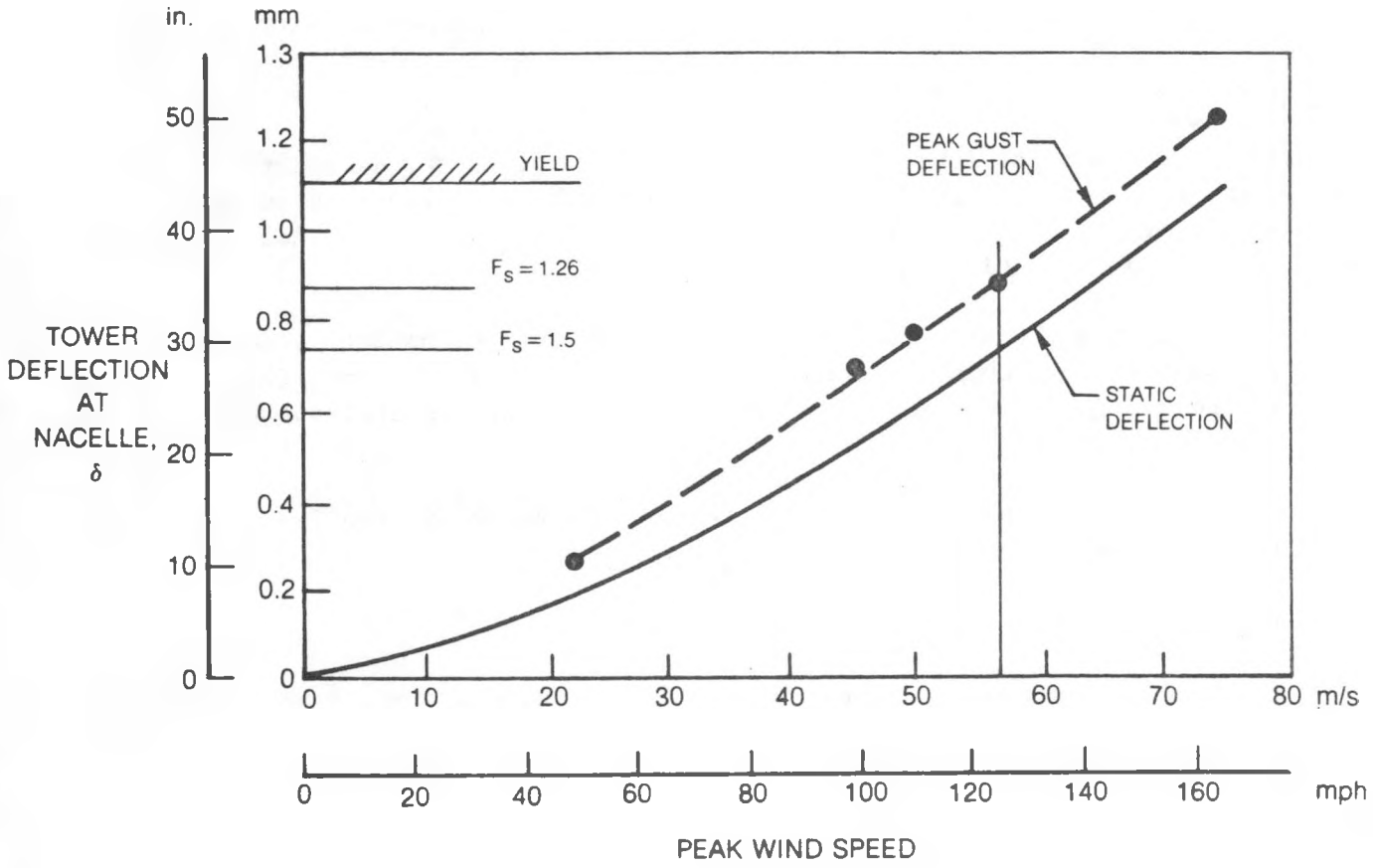

Figure 19. Predicted Tower Deflection in Gusts

81-6-164-21

Trade-Off Studies

To facilitate the selection of the best design parameters for wind energy conversion systems, a computer program has been developed at UTRC to guide the design process. This computer program is useful for evaluating system concepts for the minimization of cost of energy (COE) and sizing of a wind system for maximum performance at a given wind site. The COE Sizing and Rating (COESAR) computer program (described in Ref. 4) is, in reality, a complete preliminary design process which accepts, as independent variables, specifications for a wind system design (rotor diameter, rated power, etc.), and wind site characteristics (mean wind speed and shear profiles). The program calculates all weights, costs, and energy production quantities to arrive at a complete description of the wind system. An important feature of the program is a routine which can optimize one or more of four key variables (rotor rpm, rotor diameter, rated power, and tower height) for minimum COE. Although the primary output of the program is the system COE, the COESAR program is a very powerful analytical tool which is intended to guide the design process by:

- Displaying the sensitivity of COE to subsystem component variations.
- Optimizing on combinations of design variables for minimum COE.
- Providing the required data for sizing and rating selections with full visibility of COE implication.

This program has been used extensively in the trade-off studies to arrive at the UTRC 15-kW system design with the lowest COE.

Wind Site

The trade-off studies for optimization of the wind system assumed a standard density sea level wind site with an annual mean wind speed of 5.4 m/s (12 mph), measured at a 9.1-m (30-ft) height above the ground. The Rayleigh wind speed distribution curve described the wind speed duration profile as:

$$H = 8766 \, \mathrm{Exp}\left[-\frac{\pi}{4}\,\frac{V_z^2}{\bar{V}_z^2}\right] \qquad (1)$$

where V_z = wind speed at elevation z

$\bar{V}_z$ = mean wind speed at elevation z

H = annual time in hours that wind speed is equal to or exceeds the value of V_z

The wind speed variation with height above the ground was assumed to follow the 1/7 power law so that:

$$V_z = V \left(\frac{Z_H}{9.1}\right)^{1/7} \quad (2)$$

where V = wind speed at the reference height of 9.1 m (30 ft)

Z_H = hub height elevation in meters above the ground

The selection of the rated wind speed for the system is made as a compromise between the desire to minimize capital cost and the need to maximize annual energy output. The energy available at a wind site depends on the integration of the wind system's power profile and the wind speed duration distribution, while the wind system costs depend largely on the rated power and rotor size. The total annual energy output from a wind system is based on the rotor power coefficient (C_p), transmission efficiency, and generator efficiency as the wind speed varies over the operating speed range as given by Eq. (3):

$$kWh = 8766 \left[\int_{V_{ci}}^{V_R} P\ g(v)\ dv + \int_{V_R}^{V_{co}} P\ g(v)\ dv \right] \quad (3)$$

where P = wind system power output as a function of wind speed

V_{ci} = rotor/generator cut-in wind speed normalized to the median wind speed

V_R = rotor rated speed normalized to the median wind speed

V_{co} = rotor/generator cut-out wind speed normalized to the median wind speed

g(v) = the velocity intensity, or density function given by the derivative of Eq. (1)

The calculated values of annual energy output are based on an assumed 90% availability of the wind turbine when the wind speed is between the cut-in and cut-out rotor speeds.

Weight and Cost Estimating Relationships

A set of weight and cost estimating relationships for each major component of the wind system, at an annual production rate of 10,000 units, was developed for use in the COESAR program. The final version of these relationships is given in Table VIII. (Refer to the nomenclature section for the meaning of the symbols used.)

TABLE VIII

WEIGHT AND COST ESTIMATING RELATIONSHIPS

Cost Item (Ci)	Assembly	Weight (lb)	Cost* (1980 Dollars)
C_1	Rotor	$0.124(\sigma)^{0.8}\ (D)^{2.64}$	$12.0(\sigma)^{0.8}\ (D)^{1.78}$
C_2	Transmission	$1600\left(\frac{kWR}{rpm}\right)^{0.7}$	$5287\left(\frac{kWR}{rpm}\right)^{0.7}$
C_3	Generator	$19538\left(\frac{kWG}{rpm}\right)^{0.84}$	$104620\left(\frac{kWG}{rpm}\right)^{0.84}$
C_4	Yaw Journal	$619\left(\frac{kWR}{rpm}\right)^{0.64}$	$3682\left(\frac{kWR}{rpm}\right)^{0.64}$
C_5	Tower	$1.98\ (Z_H)^{1.25}\ (\tau)^{0.37}$	$11.65(Z_H)^{1.25}\ (\tau)^{0.37}$
C_6	Foundation		$65.5(Z_H)^{0.324}\ (\tau)^{0.324}$
C_7	Utility Interconnect		$112(kWG)^{0.8}$
C_8	Assembly & Test		$0.0075\sum_{1}^{7} C_i$
C_9	Subtotal	$\sum_{1}^{5} W_i$	$\sum_{1}^{8} C_i$
C_{10}	Indirect Cost		$0.1\ C_9$
C_{11}	Total Cost		$C_9 + C_{10}$

* Cost is the total retail cost of each assembly for an annual production rate of 10,000 units. The total retail cost includes material, labor, G&A, cost of sales and profit. The total installed cost of the system (total investment) is given by Item 11 (Total Cost).

The cost for each component represents the total retail selling price and therefore includes the cost of material, labor, general and accounting costs (G&A) and cost of sales and profit. The cost estimates are based on a G&A cost of 17% of the material cost, a fully burdened labor rate of $16/hour, on a cost of sales of 33% and a net profit of 10%. In addition to the direct costs associated with the wind system, the weight and cost relationships include installation and erection costs, and an indirect cost allowance of 10% of total direct costs to cover contingency/ spare parts cost incurred during installation of the system at a specific site.

Rotor Performance

The wind system rotor aerodynamic performance was estimated using an early version of the UTRC Horizontal Axis Wind Turbine Performance Analysis (WECSPER) computer program described in Ref. 5. The program uses a lifting line, blade element model and assumes a classical, undistorted wake with uniform transport velocity to compute locally induced axial velocities. These induced velocities, along with rotational speed, wind velocity, and two-dimensional airfoil data at each blade element station, are then used in calculating the spanwise forces at each section. These forces are integrated over the rotor span, resulting in overall rotor performance for one combination of geometric and aerodynamic conditions. To generate a performance map the program must be re-run for each new combination of parameters. Input variables in the program include rotor tip speed, number of rotor blades, rotor radius, blade twist angle, blade collective pitch, blade coning angle, blade chord, rotor solidity, wind speeds, and two-dimensional airfoil data. Output data include spanwise circulation, spanwise angles-of-attack, spanwise induced velocities, rotor torque, rotor thrust, rotor power, velocity ratio, power coefficient, thrust coefficient, and mean induced velocity.

Utilizing this version of the UTRC rotor performance code WECSPER, a set of general performance data was generated which covers a wide range of geometric blade pitch angles and velocity ratios. These results are presented, in Figs. 20 to 23, in terms of rotor power coefficient, C_p, and torque coefficient, $C_p/J^3 \times 10^3$, as a function of velocity ratio, J.

The solid symbols in Figs. 20, 21, and 22 are related to the system's rated operating capability. In turn, the operating point is a function of the wind system pitch control system and the type of electrical generator used. The UTRC rotor, as previously described, has a passive pendulum pitch control that changes rotor pitch setting directly with changes in rotor rpm. In addition, the 15-kW WTG uses an induction generator tied into the utility grid, which operates at a near constant rotor speed and, therefore, pitch angle. Therefore, the electrical generating system must be sized to absorb the maximum power that the rotor can develop at the operating pitch angle. The nameplate rating of the generator must be at least as high as the rotor power generated when operating at the velocity ratio for the C_p at maximum

torque (the solid symbols indicated in Figs. 20, 21, and 22). This condition defines the operating point at which the system's rated power, rated wind speed and rotor speed are determined.

Figure 20 shows the predicted rotor performance for a rotor with 4% solidity, and a fixed pitch angle, θ_{75}, of 0°, at two values of linear twist, 0° and 12° respectively. Two sets of curves are presented in Fig. 20 covering the variation in power coefficient or aerodynamic efficiency and torque coefficient with velocity ratio.

The baseline rotor with a solidity of 4% and 0° pitch and twist has a predicted peak C_p of 0.408 at a velocity ratio of 9.6 and a C_p of 0.154 and velocity ratio of 4.75 at maximum torque. Figure 20 shows that incorporating 12° of linear twist into the blade would increase the C_p at maximum torque to 0.209 and reduce the velocity ratio at peak C_p to 8.6. In addition, the twist variation studied indicates a reduction in C_p will occur at high velocity ratios. The impact of these two performance curves on COE was determined by COESAR to show a slightly lower COE (about 0.3%) for the design without twist. Because of the difficulty in manufacturing pultruded blades with twist and the indicated marginal pay-off, an optimum linear twist schedule was not further investigated.

Figure 21 shows the sensitivity of rotor performance (C_p) to an increase in profile drag coefficient of 0.001 over the baseline airfoil. The sensitivity was measured at three values of velocity ratio as indicated by the points marked with an "X". The increased drag coefficient has little effect on rotor efficiency except at the highest velocity ratio tested where rotor efficiency was reduced by about 40%. The impact on wind system performance would be to reduce the power at low wind speed and lower the energy capture of the wind rotor.

Figures 22 and 23 show the variation of rotor performance (C_p vs J) as a function of rotor solidity, σ, and blade fixed pitch angle, θ_{75}. As the rotor solidity decreases from 5% to 3% (Fig. 22), the rotor C_p at high velocity ratio increases, giving the rotor a wider wind speed operating range. Conversely, as the rotor fixed pitch angle increases from -2° to +2° (Fig. 23), the rotor C_p at high velocity ratios decreases, reducing the wind speed operating range of the rotor. The rotor performance in terms of velocity ratio (J), aerodynamic efficiency (C_p) and torque coefficient (C_p/J^3) is summarized in Table IX for the points of maximum aerodynamic efficiency and maximum torque. These data indicate that the maximum rotor efficiency, C_p, varies from a low of 0.372 to a high of 0.408 with an average value for the six cases of 0.392. But the maximum torque coefficient (far right column) shows a strong variation with rotor parameters. Varying the pitch angle angle from -2° to +2° for a rotor solidity of 4% shows a variation of torque of about 39%.

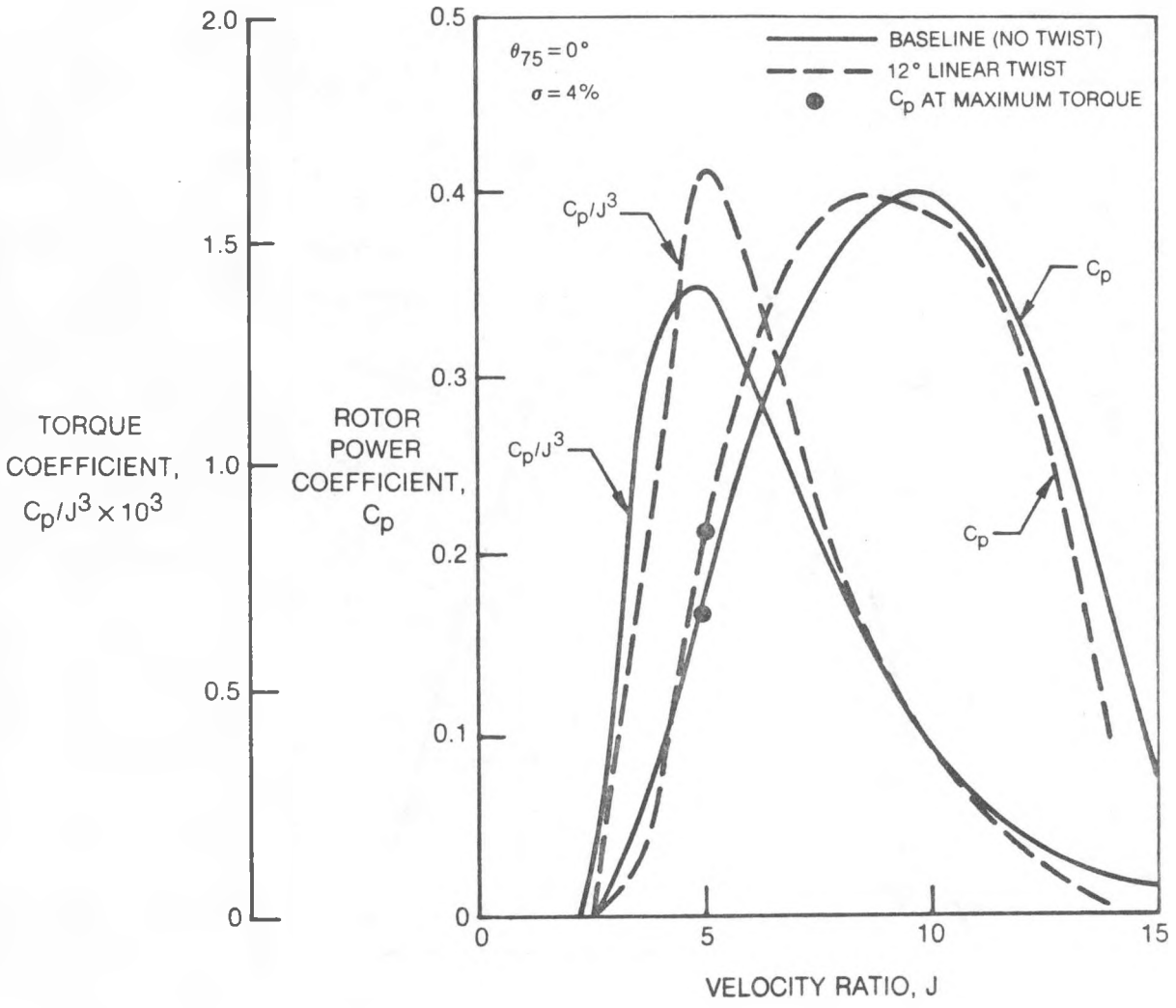

Figure 20. Wind Turbine Performance Predictions

81-6-164-20

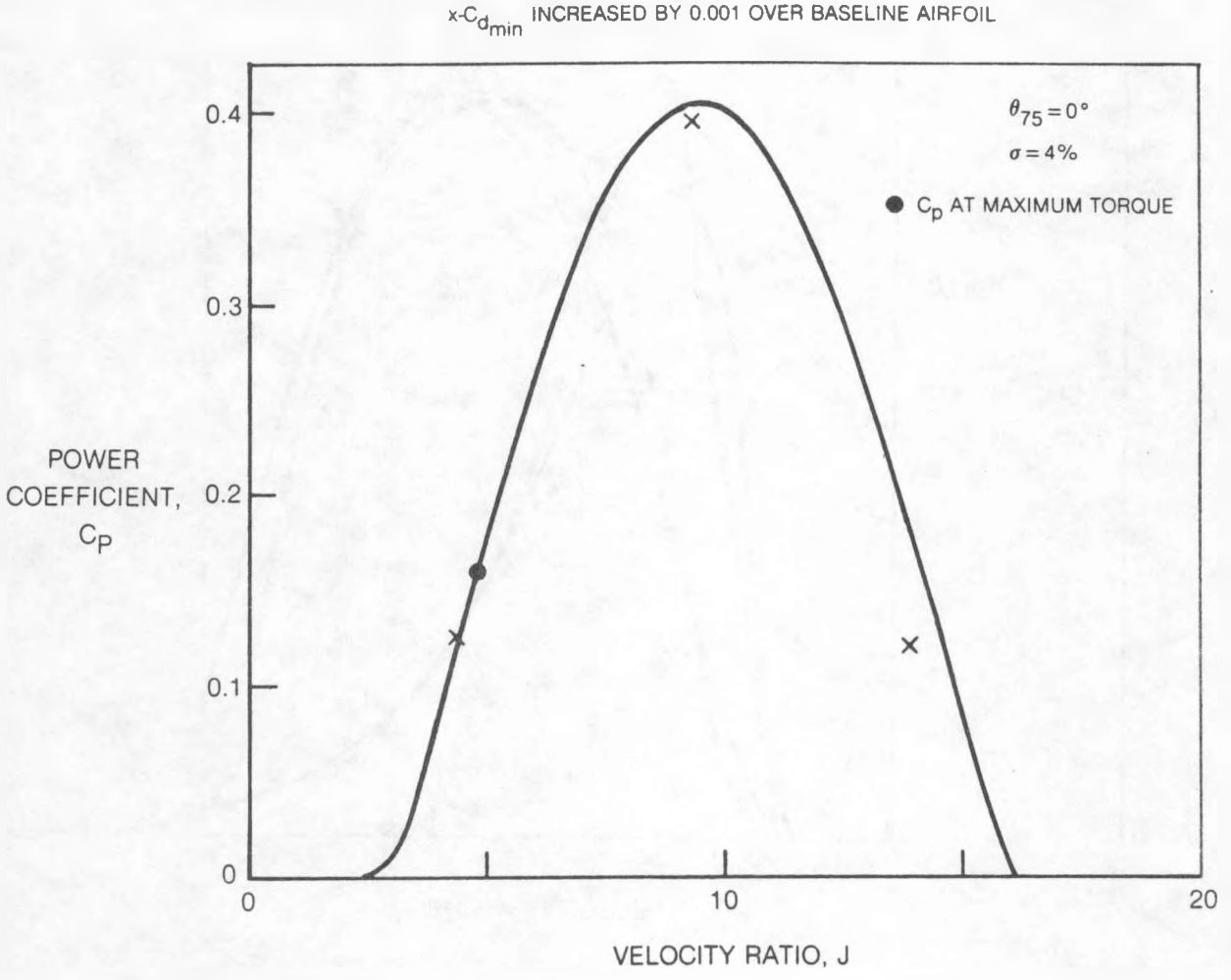

Figure 21. Effect of Airfoil Characteristics on Performance

81-6-164-19

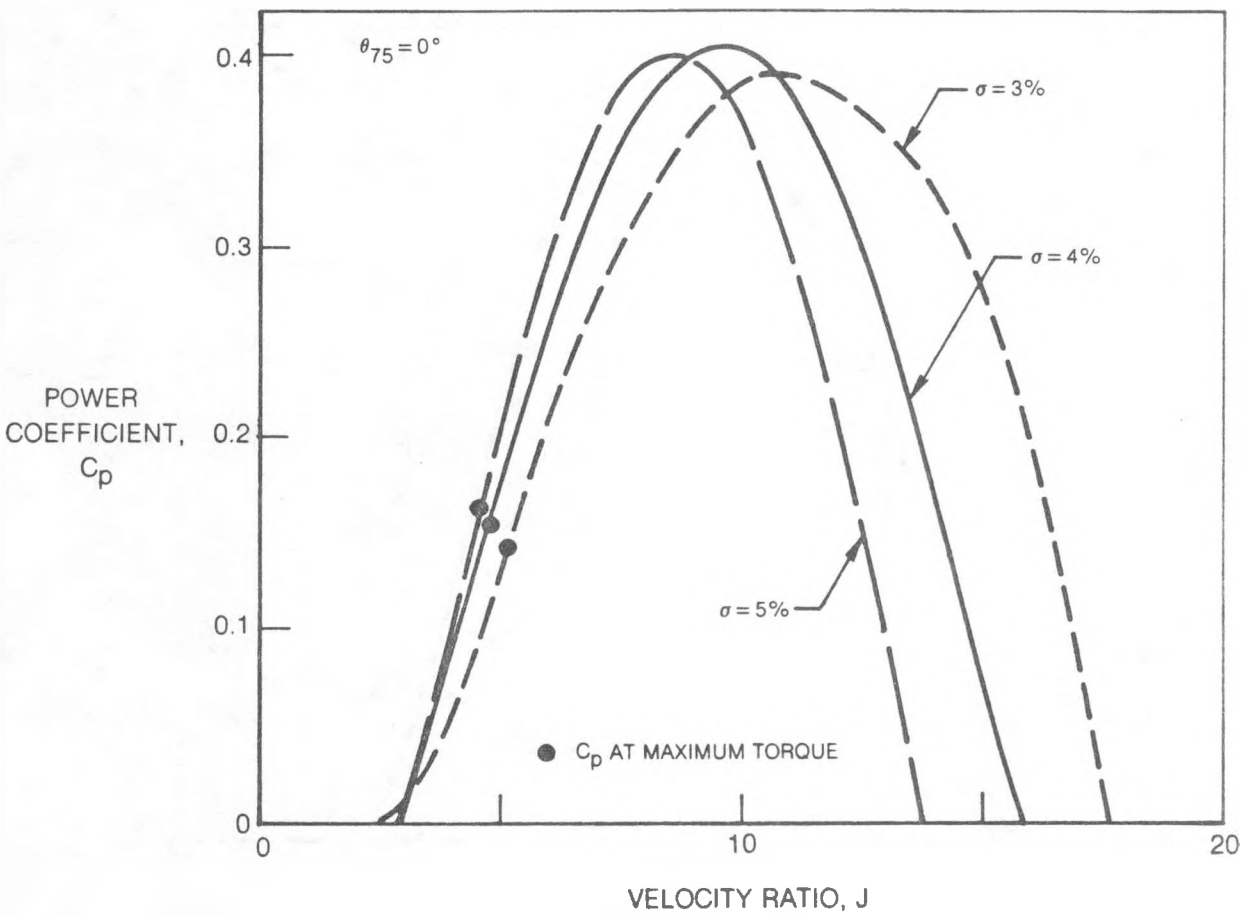

Figure 22. Effect of Rotor Solidity on Predicted Power Coefficient

81-6-164-22

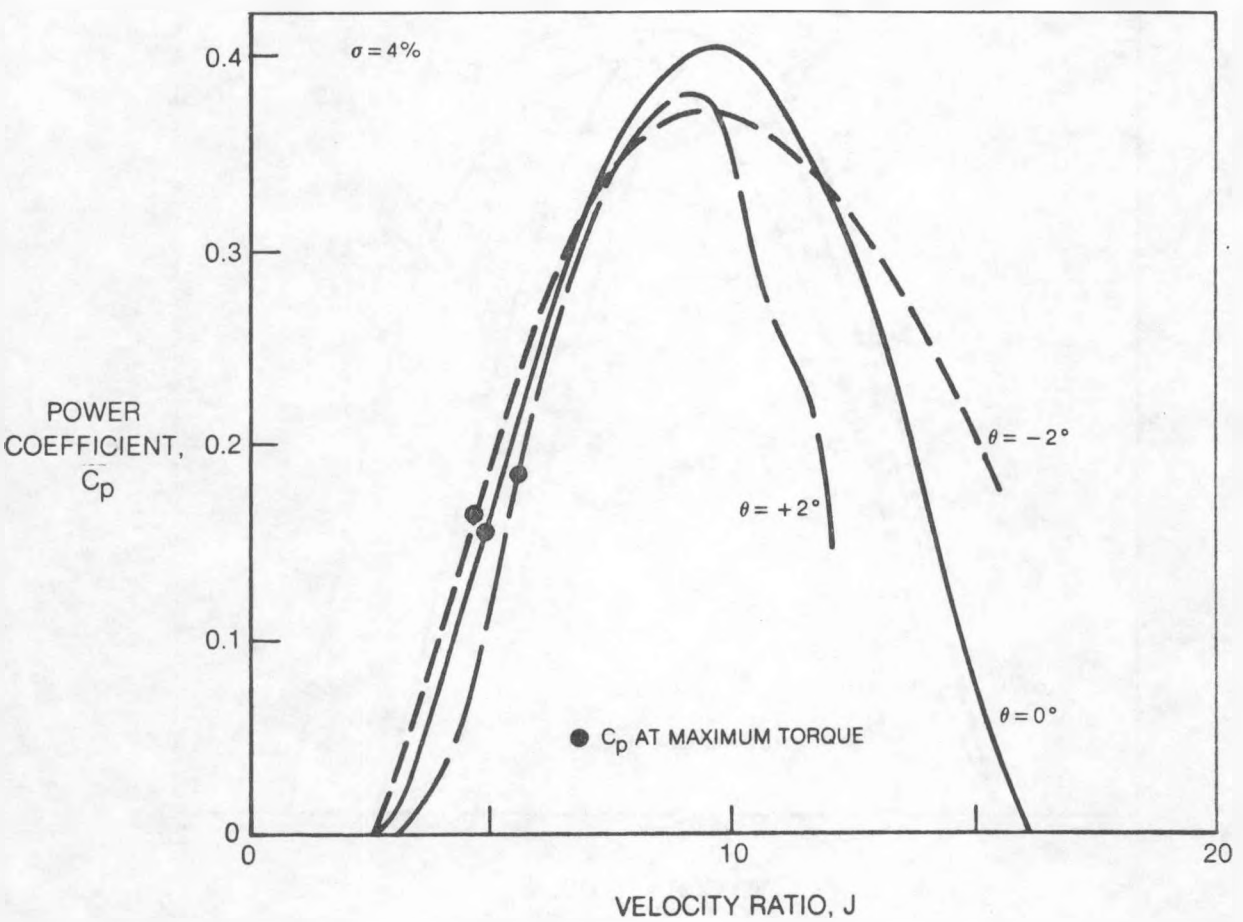

Figure 23. Effect of Collective Pitch on Predicted Power Ratio

81-6-164-23

TABLE IX

ROTOR PERFORMANCE SUMMARY

Solidity	Pitch Angle	Linear Twist	Max Efficiency			Max Torque		
%	Deg.	Deg.	J	C_p	$C_p/J^3 10^3$	J	C_p	$C_p/J^3 10^3$
3	0	0	10.2	0.392	0.37	5.0	0.140	1.12
4	-2	0	9.4	0.372	0.45	4.5	0.160	1.76
4	0	0	9.6	0.408	0.46	4.75	0.154	1.44
4	2	0	9.4	0.381	0.46	5.5	0.180	1.08
4	0	12	8.6	0.401	0.63	5.0	0.209	1.67
5	0	0	8.5	0.400	0.65	4.5	0.165	1.81

The sensitivity of the UTRC 15-kW wind system's COE to the rotor performance characteristics presented in Figs. 22 and 23 is shown in Fig. 24. The left hand portion of Fig. 24 shows the sensitivity of COE to rotor solidity for a 0° fixed pitch angle and the right hand portion shows the COE sensitivity to the fixed pitch angle for a rotor solidity of 4%. The wind system has been sized for an annual energy capture of 55,000 kWh with a hub height of 12.5 m (41 ft). For each value of solidity and fixed pitch angle the system has been optimized by selecting the combination of rotor diameter, rotor speed, and rated power that minimizes the COE. A rotor solidity of 3% gives the wind system design with the lowest COE, but because of reduced edgewise stiffness levels at low solidity (or shorter chord), the design solidity of 4% was selected as the best compromise between minimum COE and possibly high edgewise deflections.

The COE shows a significant sensitivity to the blade pitch angle. A blade pitch angle of 0° gives the lowest COE and this value was selected as the design condition. Reducing the pitch angle to -2° increased the COE by 5% due to the lower peak power coefficient and the lower velocity ratio for maximum torque relative to the design with zero pitch. Designing the rotor to operate at +2° increased the COE by 2.5% because of the lower peak power coefficient and the narrower range of operating velocity ratios relative to 0° pitch.

As a result of the COE sensitivity analysis to rotor blade design characteristics, the final rotor design for the UTRC 15-kW wind system has an untwisted blade operating at a pitch setting of 0° and a solidity of 4%.

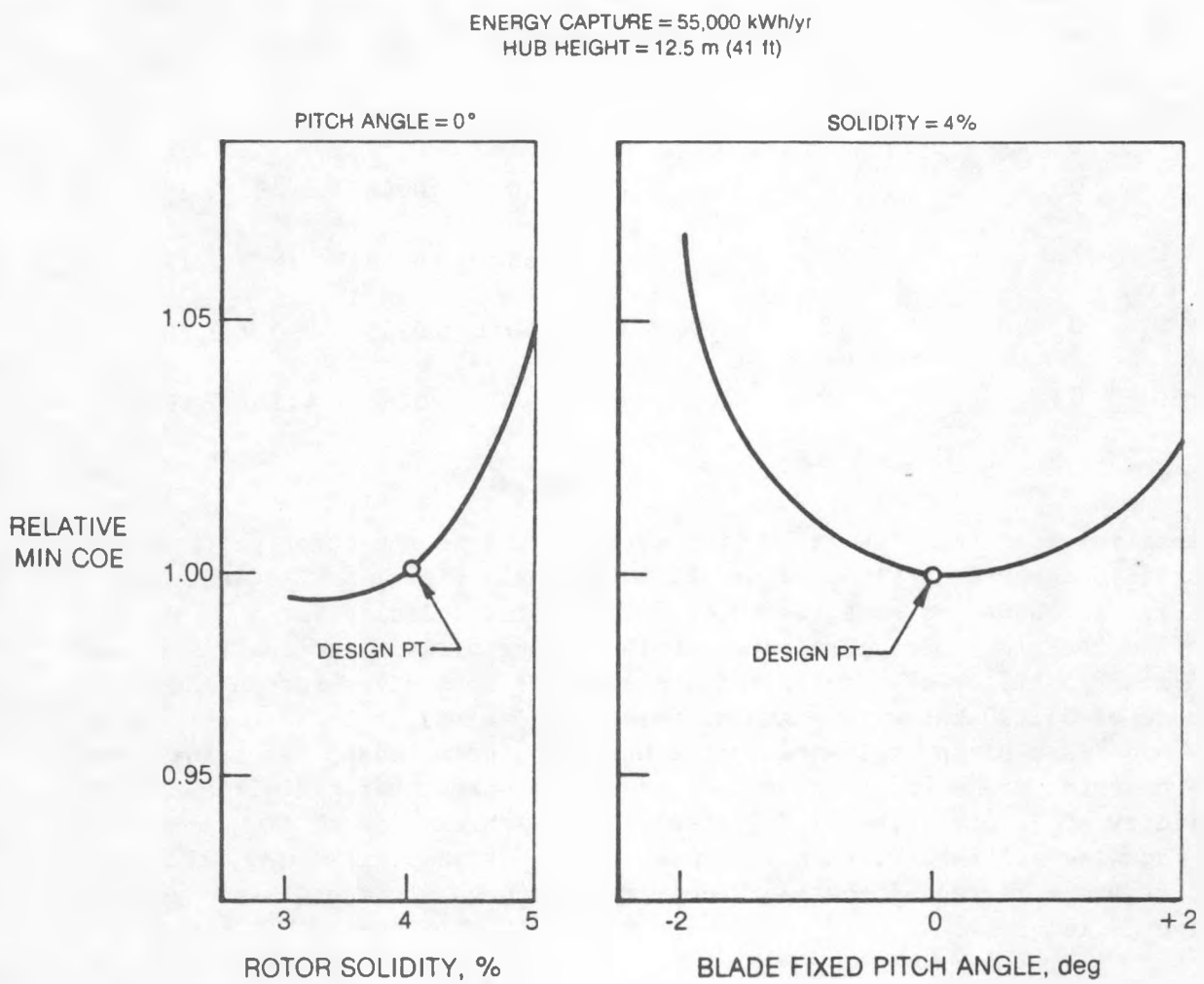

Figure 24. COE Sensitivity to Rotor Blade Design

81-6-164-24

Tower Type

In the selection of the tower configuration, consideration was given to both free standing and guyed tower designs. Of the two systems, the guyed system has potentially lower initial cost. However, the free standing tower system was selected because of four reasons: 1) improved aesthetics; 2) potentially critical cable tensioning problems with guyed systems; 3) improved rotor/blade clearance due to the elimination of the cable attachments; and 4) less interference at ground level near the tower. The aesthetics of the free standing tower were judged to be more acceptable and compatible with land use planning since the absence of the guy cables significantly reduces the dedicated "footprint" area of the tower. The proper tensioning of the guy cables on installation is critical to avoid potentially hazardous vibration problems in both the tower and cables and to ensure that the tower is plumb. Because of the normal vibrations in the system, the cable tension will vary with time, requiring frequent checks and retensioning of the cables. Since this tensioning is potentially a critical maintenance operation, the long term survivability of the system is enhanced if the guy cables are not required for the system.

In addition, the guyed tower system was rejected because the presence of the cables decreased the clearance between rotor blades and tower by at least 0.66 m (2 ft). To recover the lost clearance would involve extending the rotor shaft and support system with an unacceptable increase in the system cost.

Tower Height

Sensitivity of system COE to rotor hub height is shown in Fig. 25. The wind system was designed for an annual energy capture of 55,000 kWh using a single-phase induction generator designed for a NEMA 286TC frame with 120 μF of capacitance in the auxiliary winding. The generator size was fixed at 30 hp to standardize on the available NEMA frame size and ensure that the COE sensitivity would reflect a series of possible design solutions. As the tower height was varied, the rotor diameter, rotor speed, and transmission were optimized for minimum COE to give the 55,000 kWh energy capture. The results of this sensitivity analysis show that the minimum COE occurred at a tower height of 12.5 m (41 ft) and required a rotor diameter of 15.1 m (49.6 ft). Increasing the tower height to 15.2 m (50 ft) increased the COE by about 7.5% but decreased the required rotor diameter to 14.5 m (47.5 ft). The reason for the COE increase with tower height is that the tower is the highest material cost component of the system, being almost three times as expensive per foot as the rotor system. Therefore, it is more cost effective to lower the tower height and increase the rotor diameter than to reduce the required rotor size for the given energy capture. The final tower height was selected at 12.5 m (41 ft) to give adequate ground clearance and is the maximum tower height that could be accommodated in a standard flat bed truck. The tower height is 11.9 m (39 ft) and a 0.61-m (2-ft) long yaw assembly puts the hub height at 12.5 m (41 ft). Other considerations (e.g., aesthetics, site selection, customer preference, higher energy capture) may alter this configuration.

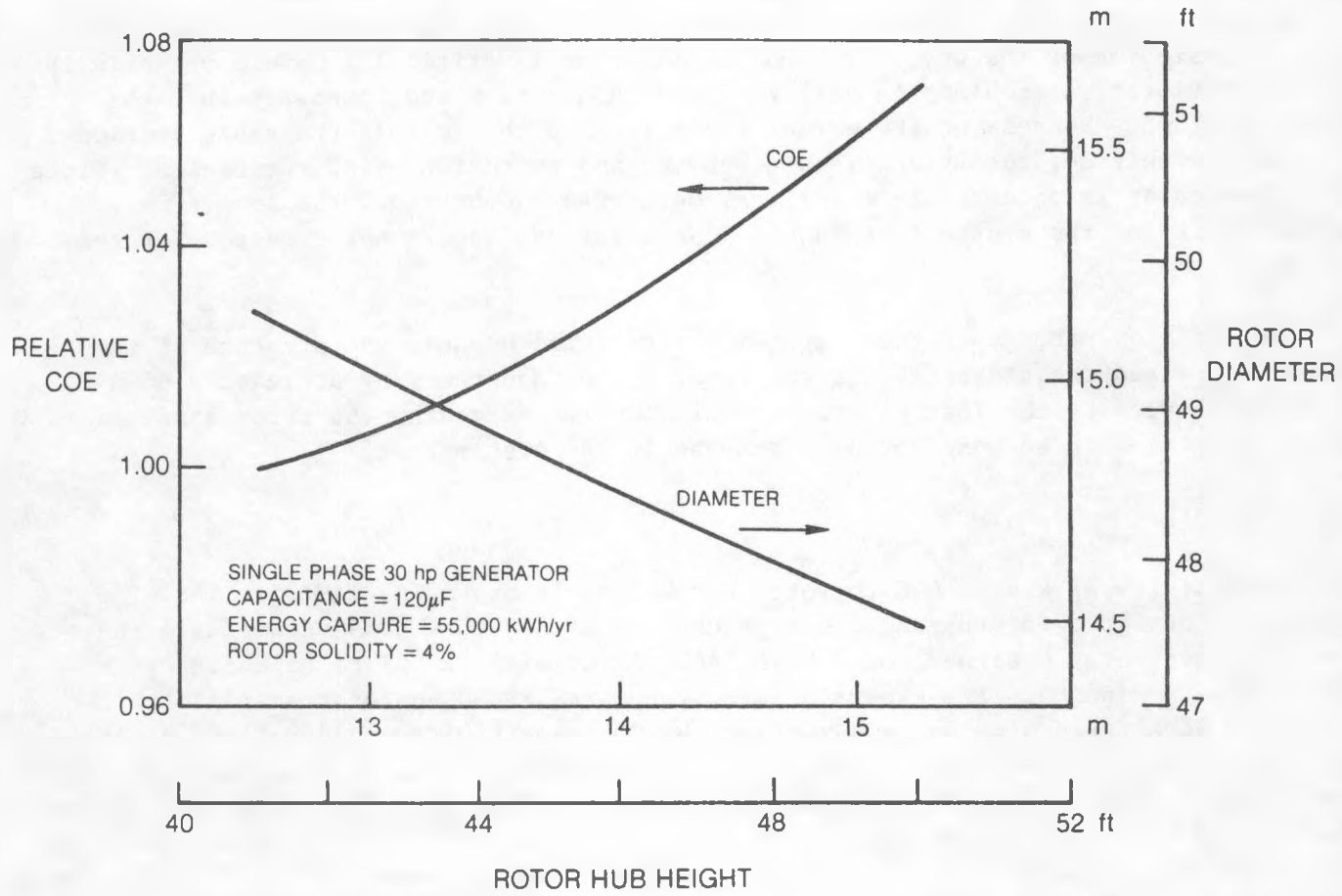

Figure 25. Effect of Tower Height on Wind System Cost and Size

81-6-164-25

Tower Materials and Configuration

Several tower materials and configurations were investigated. The tower height in the initial design stages was 16.7 m (55 ft). A cylindrical 0.5-m (20-in.) OD x 13-mm (1/2-in.) wall pultruded E-glass/vinyl ester pipe was analyzed for possible use, however the composite pipe was rejected for several reasons. At the 56-m/s (125-mph) wind condition, a tower top deflection of approximately 3 m (10 ft) was considered excessive. Furthermore, tests of this material at UTRC indicated that the interlaminar shear strength, discussed in a later section, was not sufficient to withstand maximum calculated shear stresses. Also, for elevated temperatures, the flexural strength and modulus were significantly reduced from room temperature properties. This will be discussed more fully later. Finally, the manufacturability would be complicated by the need for sophisticated methods of interface between the tower and the base.

Several low carbon steel towers were investigated, beginning with straight cylindrical pipes from 273-mm (10-3/4-in.) OD through 609-mm (24-in.) OD and wall thicknesses ranging from 9.5 to 12.2 mm (3/8 to 1/2 in.). Towers of this configuration which were strong enough to meet design loads would be difficult to install using a simple winch and gin pole and also showed high first mode natural frequencies. Tower natural frequencies are a major consideration because of the impact on wind system stresses and stability. To reduce weight and the first tower frequency, a single-step diameter reduction was introduced. While tower weight was able to be sufficiently reduced for erection viability, natural frequencies were still unacceptable in the low carbon and high strength steels.

An aluminum tower was also investigated and most closely met the combined requirements of stress and natural frequency. Several tapered configurations were studied to further reduce weight and frequencies. Since manufacturing techniques for this type of tower are simplified by the use of press brakes, the aluminum tower configuration was altered from tapered cylindrical to tapered polygonal. The optimum number of sides was found to be 10 based on stress and natural frequency requirements, and this geometry was adopted into the final tower design. Table X summarizes the several tower configurations that were considered during the design.

An extensive aluminum material survey was conducted to indicate the optimum base and filler alloy choices with regard to price, manufacturability, corrosion resistance and availability in the strength range required. Alloys 5456-H343 and 5083-H343 were indicated as good choices for production tower base alloys but are unavailable on a prototype basis. Alloy 6061-T6, while slightly less corrosion-resistant, is another good candidate, and because of its general availability, was chosen as the prototype material. The use of 5356 welding filler alloy was considered most suitable for use with alloy 6061. Special localized heat treatment techniques are under development to avoid the need for a full tower post-weld heat treatment, if possible, and still improve on the as-welded strength in the heat affected zone.

TABLE X

TOWER CANDIDATES AND VIBRATION CHARACTERISTICS

Configuration	Material	F_{T_Y}(ksi)	ω_1(Hz)	ω_2(Hz)
20" OD x 1/2" W, Straight	E glass	43	0.9	9.7
24" OD x 1/2" W, Straight	A53 GRB STL	35	2.36	17.80
24" OD x 16" OD x 1/2" W, Stepped	A53 GRB STL	35	2.25	13.42
16" OD x 10-3/4" OD x 1/2" W, Stepped	SA333, GR8 STL	75	1.25	8.39
23" OD x 8" OD x 1/4" W, Tapered	A572 MOD STL	65	1.12	9.09
24" OD x 16" OD x 1/2" W, Stepped	6061-T6 Aluminum	40	1.39	11.21
25" OD x 12" OD x 1/2" W, Tapered, Welded	6061-T6 Aluminum	40,30*	1.19	10.27
28.5" OD x 10" OD x 3/8" W, Tapered, Welded	6061-T6 Aluminum	40,30	1.12	9.77
24" OD x 12" OD x 3/8" W, Tapered, Welded	6061-T6 Aluminum	40	1.00	9.45
39" OD x 12" OD x 1/4" W, Tapered, Welded	6061-T6 Aluminum	40,30	1.41	12.48
27" OD x 10" OD x 3/8" W, Tapered, Welded 10 Sides	6061-T6 Aluminum	40,30	1.07	6.22
**26" OD x 10-1/2" OD x 3/8" W, Tapered, Welded 10 Sides	6061-T6 Aluminum	40,30	1.05	6.21

* The first number refers to the parent material. The second number refers to the welded material.

** Selected

As a check of an alternative tower approach, several multi-tube truss type tower configurations were examined. When area moments of inertia were small enough to move the tower natural frequencies into the proper range, individual tubes in this configuration were exposed to unacceptable compression loading. With bracing spaced sufficiently for compression resistance, the stiffness became too high for proper dynamic response. Increasing the stiffness to exceed 6.0 Hz for the second tower frequency was deemed an inefficient use of material and made tower erection very difficult. A welded plate and concentric pipe approach were also looked at and rejected as impractical.

Single-Phase Generator Performance

The current specification for the 15-kW wind system calls for single-phase generation of power. Initially the contract called for three-phase output, however single phase was substituted following a report from the U.S. Dept. of Agriculture indicating the prevalence of single phase electricity in U.S. farms. This decision required a specially built generator since single-phase induction generators generally were not available in sizes larger than 8 kW. Among the approaches reviewed for this application, two were selected as offering the best opportunity to achieve economical, single-phase power generation. The two approaches are the use of: 1) a permanent-split-capacitor (PSC) single-phase induction generator, and 2) a standard three-phase induction generator used for single-phase power. Of the two approaches, the permanent-split-capacitor (PSC) generator was chosen because of indicated lower cost and higher efficiency. Test data on a Baldor 15-kW, 4-pole single-phase PSC generator (NEMA frame 256TC) is shown in Fig. 26. The generator efficiency and power factor are shown as a function of output power for the generator wired for "standard" and "reverse" rotation. Wiring the generator for reverse rotation increased the efficiency (above 15% power levels) by about 3.5 percentage points and improved the power factor by about 10 percentage points. A peak efficiency of 85% was attained at 45% of rated power. At rated power, the reverse rotation condition has an efficiency of 78% and a power factor of 79%.

Figures 27 and 28 show the variation in efficiency and power factor respectively, as a function of output power for four levels of installed capacitance. Increasing the capacitance decreases the generator efficiency at partial power but increases it at full power. The power factor is strongly influenced by the size of the capacitor tested with the generator. Increasing the capacitance from 80 to 120 μF allowed the generator to reach a power factor of 100% at about 20% of rated output power, and increasing the capacitance still further increased the power level at which unity power factor is reached.

The sensitivity of the COE to the level of capacitance in the generator circuit is shown in Fig. 29. The specifications for the wind system design require a maximum annual energy capture of 55,000 kWh at a wind site with a 5.4-m/s (12-mph) mean wind speed. The rotor hub height is fixed at 12.5 m (41 ft) and generator size is fixed at 30 hp (NEMA frame 286TC). Since the generator size is larger than the size for which test data have been shown, the capacitance levels have been increased in proportion to the rated power (30 hp/20 hp). Increasing the capacitance level from 120 to 300 μF increases both the COE and the rotor diameter required to achieve an annual energy capture of 55,000 kWh. Over the range of

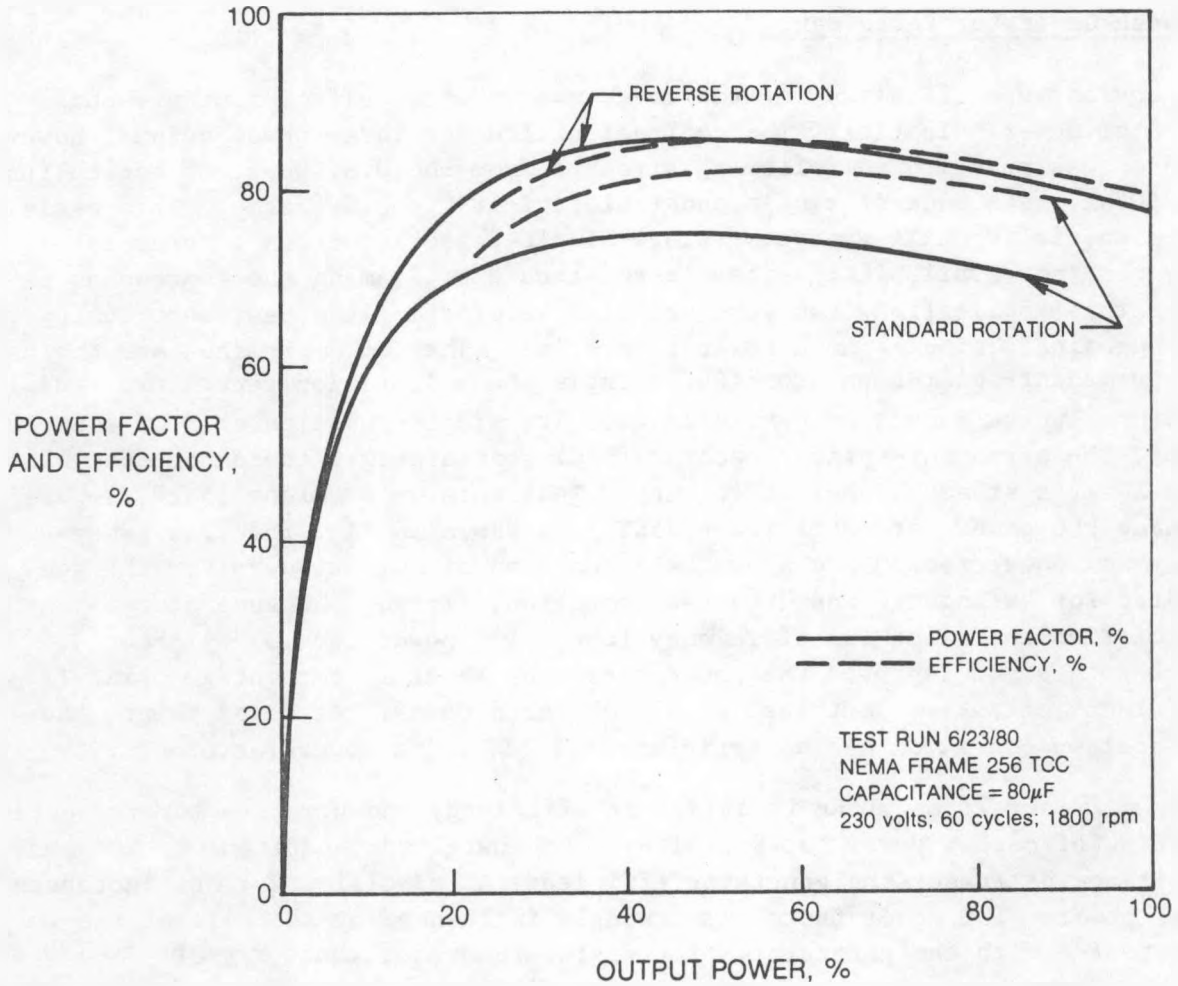

Figure 26. Test Performance of Baldor 15-kW Single Phase Generator

81-6-164-26

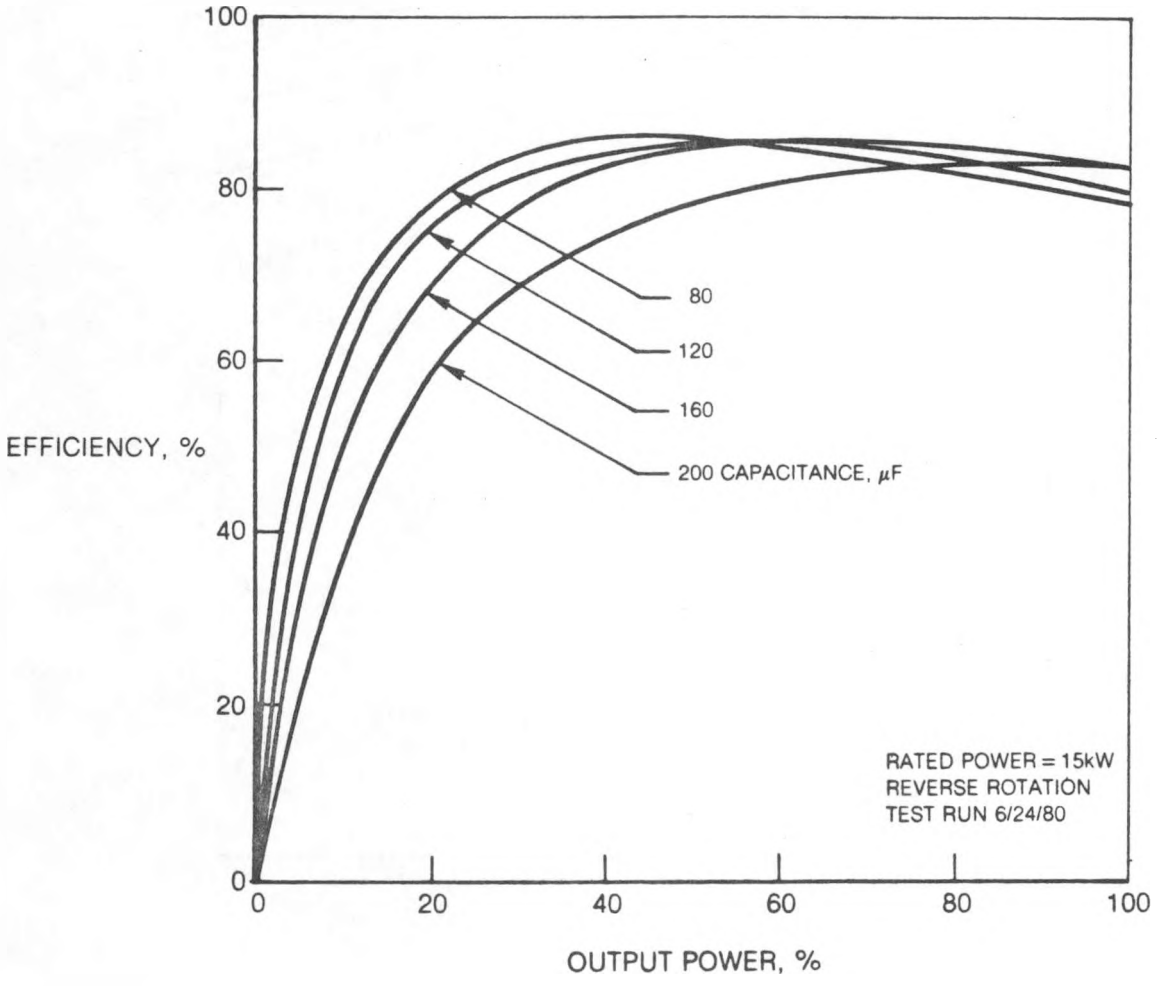

Figure 27. Effect of Capacitance on Single Phase Generator Efficiency

81-6-164-27

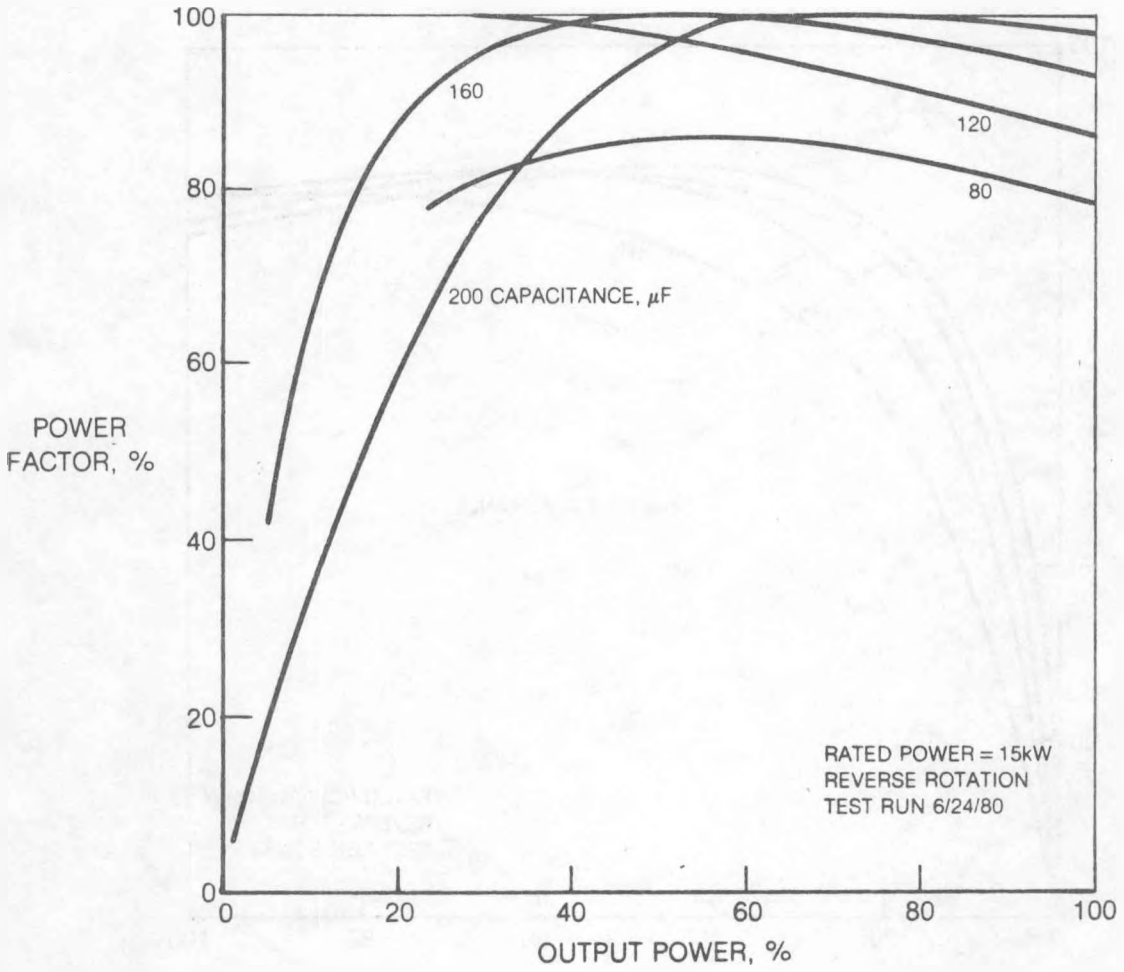

Figure 28. Effect of Capacitance on Single Phase Generator Power Factor

81-6-164-28

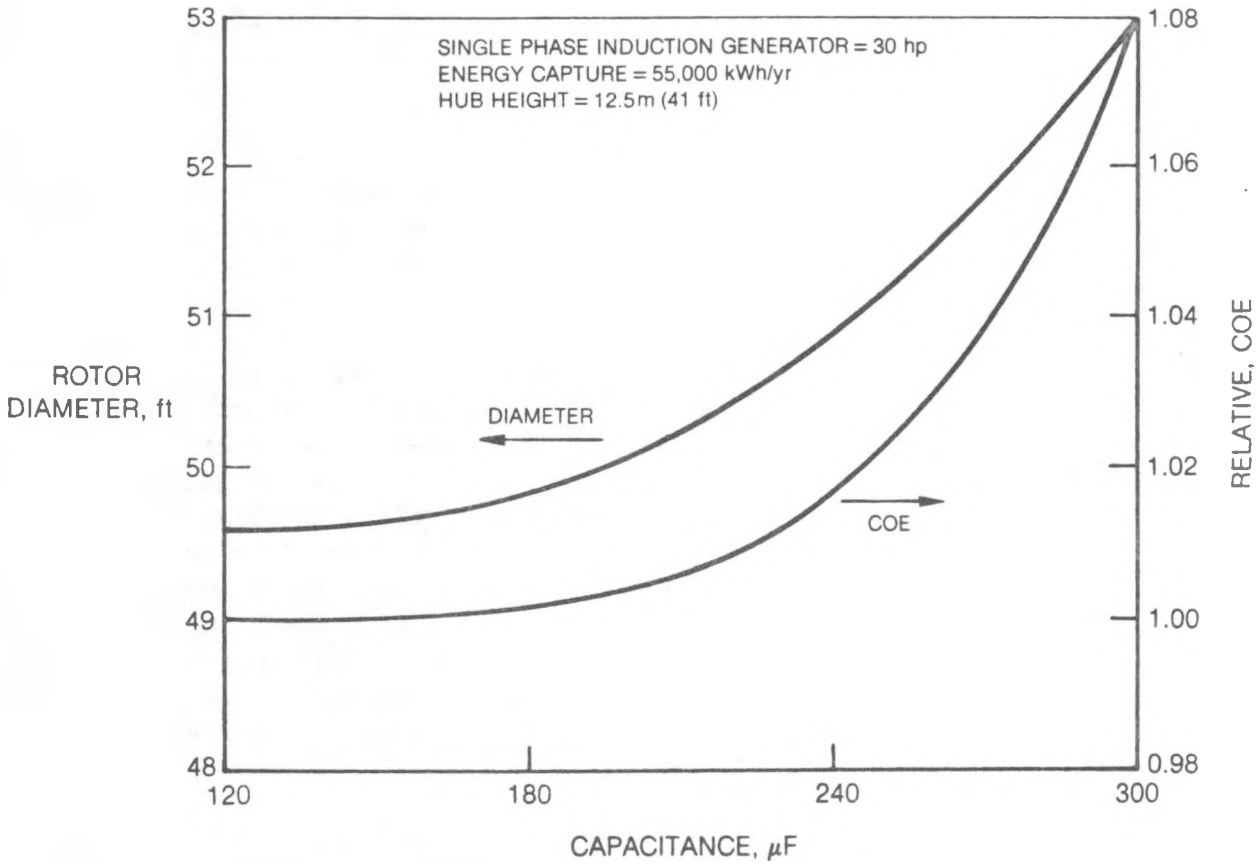

Figure 29. Effect of Capacitance on Wind System COE and Size

B1-6-164-29

capacitance levels studied, the rotor diameter would increase from 15.1 to 16.2 m (49.6 to 53 ft) with an increase in COE of 8% as the capacitance increased from 120 to 300 μF.

The reason for increased COE with increasing capacitance is due primarily to the decrease in efficiency at the low power levels. As shown in Fig. 30, as capacitance increased from 120 to 300 μF the cut-in speed increased from 4.5 to 5 m/s (10 to 11 mph) reducing the time on-line by about 500 h annually. The rated speed, on the other hand, was reduced from 12.1 to 11.6 m/s (27 to 26 mph) because of the increase in efficiency at rated power as capacitance is increased. Therefore, the capacitance level selected for the UTRC 15-kW system is 5.4 μF per rated kW (i.e., 120 μF for a single-phase generator rated at 22.4 kW).

Rotor Diameter and Rated Power

The specifications for the 15-kW wind system call for a design optimized for COE that interfaces with a single-phase utility system and has an annual energy capture between 45,000 and 55,000 kWh at a wind site with a mean wind speed of 5.4 m/s (12 mph). The design characteristics of the wind system that will minimize COE are given in Table XI. Left to be determined are the size of the rotor, generator and transmission system. Relative COE of the 15-kW design, as calculated by COESAR, is shown in Fig. 31 as a function of energy capture for several values of rotor diameter. The variation in energy capture at a fixed value of rotor diameter is achieved by varying generator size and rated speed. Two envelopes of minimum COE are apparent from the chart: the envelope of minimum COE vs energy capture and the envelope of minimum COE vs rotor diameter. If the data had been plotted for constant values of generator nameplate rating, then a third locus of minimum COE would also be apparent. The wind system designs of primary interest are those that not only produce the desired energy, but also produce that energy for minimum COE. Therefore, the design band of interest is bounded in Fig. 31 by the lines of constant energy capture and the lines of constant COE for each energy capture.

Further insight into the rotor and generator selection process can be gained by plotting the loci of minimum COE and constant energy capture on a graph of rotor diameter vs generator rating, as in Fig. 32. The wind system rotor/generator size combinations of interest are bounded on the left by the locus of minimum COE as a function of rated power, on the right by the locus of minimum COE as a function of rotor diameter, and at the bottom and top by the loci for constant energy capture. The locus of minimum COE as a function of energy capture falls between the other two minimum-COE loci and represents the lowest investment cost solution for the required energy capture. That solution represents a good compromise between the low-rated-power and small-rotor-diameter solutions.

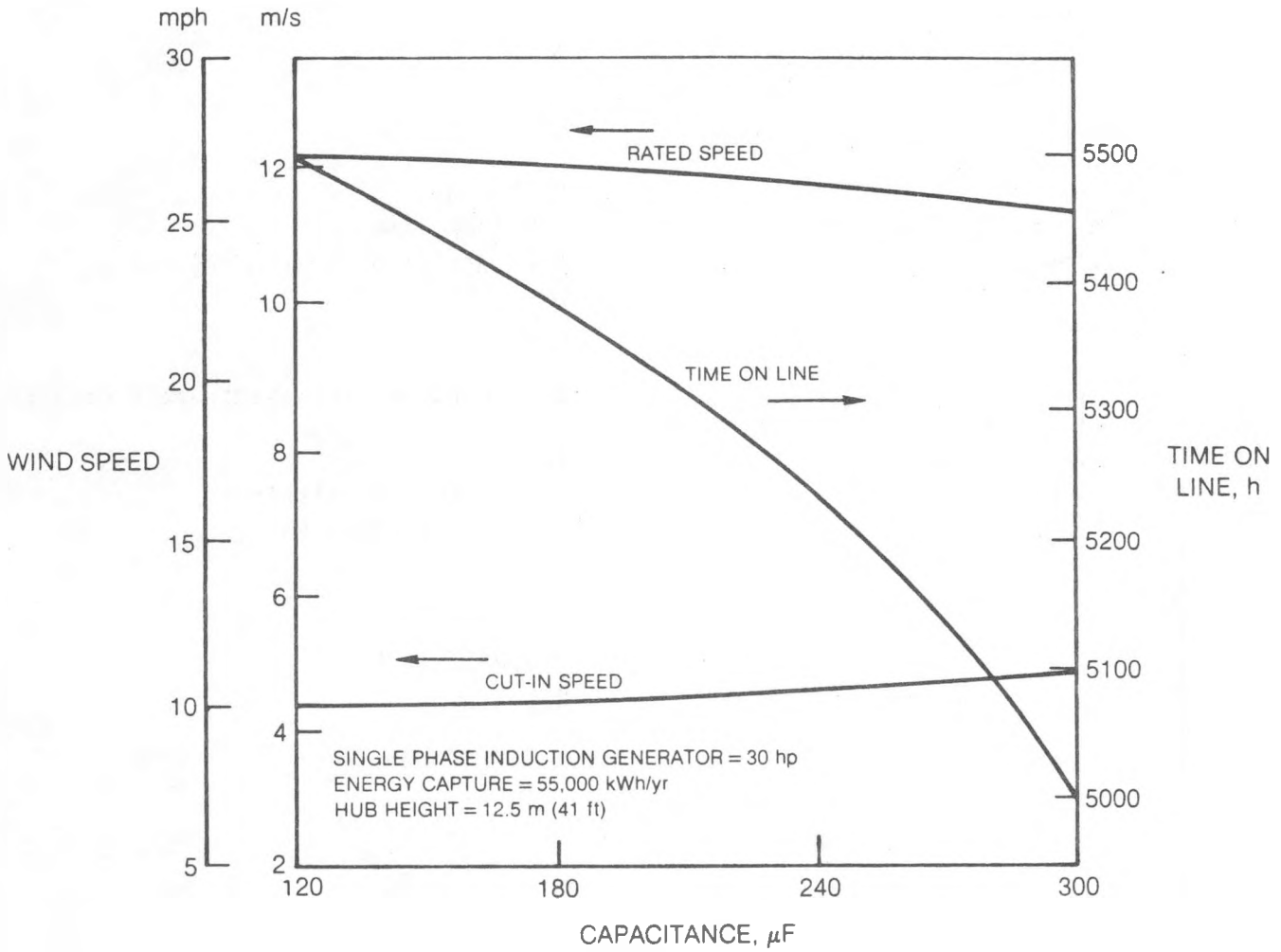

Figure 30. Effect of Capacitance on Wind System Operation

TABLE XI

WIND SYSTEM DESIGN CHARACTERISTICS

Rotor	
Solidity	4%
Operating pitch angle	0°
Tower	
Height	12.5 m (41 ft)
Material	Aluminum Alloy
Type	Free Standing Tapered Pole
Generator	
Type	Single-Phase, Permanent-Split Capacitor
Insulation Class	F
Synchronous Speed	1800 rpm
Mounting	C-face to transmission
Capacitance	5.4 μF per rated kW
Transmission	
Type	Helical, In Line
No. of Stages	2

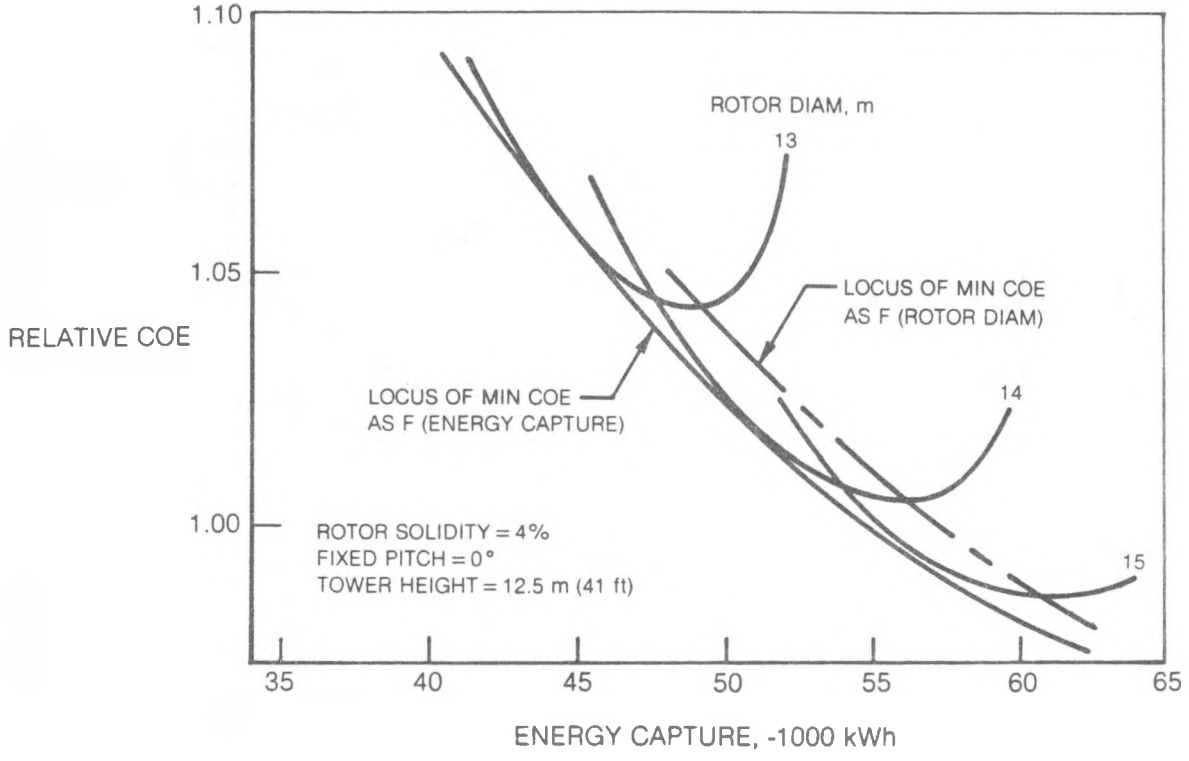

Figure 31. Cost of Energy

81-6-164-31

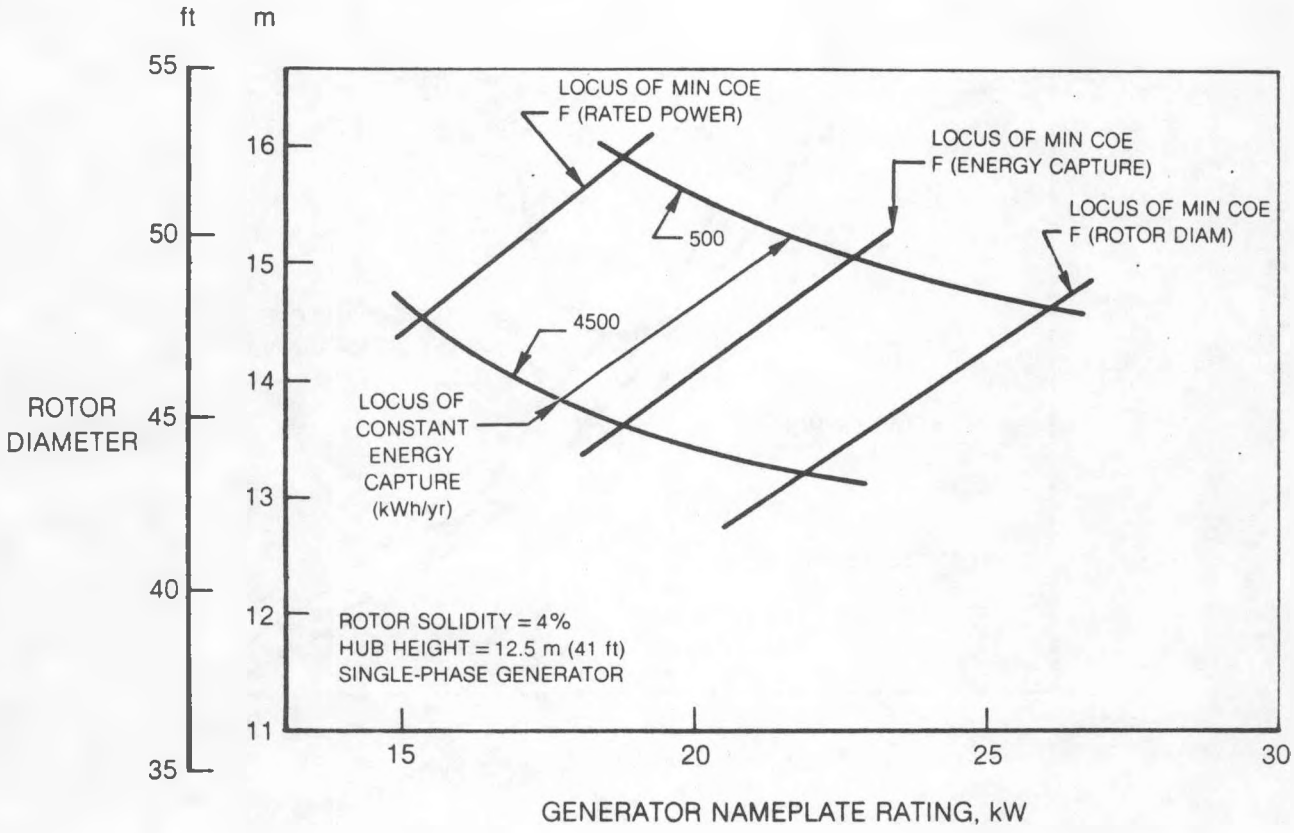

Figure 32. Rotor Diameter and Generator Selection

81-6-164-60

Table XII is a summary of the characteristics of the six design points of interest; i.e., the points of intersection on the five lines of Fig. 32. For each energy capture group, the low-diameter configuration has the highest rated generator power and the highest rotor rpm, cut-in, rated and cut-out speeds. Because of the high cut-in speed, the small-diameter configurations show the lowest time-on-line (hours per year generating electricity). Conversely, because of their low cut-in speed, the designs with the low generator rating show the longest time-on-line.

All the design points for an energy capture of 55,000 kWh/yr show lower COE than those for the 45,000 kWh case. The lowest COE for the six designs is produced by the 55,000 kWh energy capture-constrained configuration. Therefore, the energy capture-constrained design represents the best compromise between the small-rotor-diameter design and the low-rated-power design. But since the variation in COE among the three designs is small, any one could be acceptable. If the accepted design is biased away from minimum COE, it should be biased toward the low-rated-power design because of the increase in time-on-line relative to the small diameter design.

Finally, because generators come in standard sizes set by the industry, the design choice is strongly influenced by the available generator size classes. Available NEMA generator frame sizes of interest for the 15-kW system are NEMA 256T, 284T and 286T (20, 25 and 30 hp respectively). For these available generator sizes three designs were selected for comparison from Fig. 32 and are shown in summary in Table XIII. The wind system designed around the NEMA 286T frame (22.4 kW) with 15.12-m (49.6-ft) rotor diameter shows the lowest COE. Subsequent detailed analysis of this configuration indicated that the large rotor size impacted the tower design requiring a resizing of the rotor. The rotor diameter was reduced to 14.6 m (48 ft) and rotor speed increased to 76.8 rpm giving a tip speed of 59 m/s (193 ft/s). The characteristics of the 15-kW system with the 14.6-m (48-ft) rotor diameter and NEMA 286T generator size are given in the last column of Table XIII. This design has an annual energy capture of 52,600 kWh and a COE 1.5% higher than that estimated for the lowest COE design that would give an energy capture of 55,000 kWh/yr.

Electrical Design

The electrical system components are shown schematically in Fig. 33. The primary active components are the speed switch, the contactor, parking brake, and the self-excitation interlock. The speed switch is a Natural Power, Inc. Model C46 wind trigger which determines generator shaft speed by measuring the frequency of an ac signal produced by a 60-tooth gear and a magnetic pickup. The measured frequency is digitally compared with adjustable setpoints to actuate and release the contactor as required.

TABLE XII

SUMMARY OF WIND SYSTEM DESIGN POINTS

Hub Height = 12.5 m (41 ft)

Annual Energy Capture, → kWh (5.4 m/s mean wind)	55,000			45,000		
Configuration for Min COE vs →	Diameter	Energy Capture	Generator	Diameter	Energy Capture	Generator
Rotor Diameter, m	14.63	15.05	15.85	13.2	13.6	14.53
Rated Power, kW	26.14	22.80	19.02	22.0	19.6	15.40
Rotor Speed, rpm	80.92	73.73	63.68	90.03	81.75	69.50
Cut-in Speed, m/s	4.72	4.92	4.02	4.77	4.42	3.94
Rated Speed, m/s	13.05	12.23	11.03	13.04	12.21	10.88
Time-On-line, h/yr	5070	5420	5910	5070	5470	5950
Relative COE	1.009	1.000	1.020	1.079	1.067	1.084

TABLE XIII

SUMMARY OF CANDIDATE WIND SYSTEM DESIGNS

Rotor Hub Height = 12.5 m (41 ft)

Generator NEMA frame size	256T	284T	286T	
Nameplate rating, kW(hp)	14.9(20)	18.6(25)	22.4(30)	
Synchronous Speed, rpm	1800	1800	1800	
Rotor Diameter, m(ft)	14.66(48.1)	15.95(52.33)	15.12(49.6)	14.63(48.0)
Rotor Torque, N·m (lbf·ft)	2867 (2114)	3824 (2820)	3964 (2923)	3752 (2767)
Rotor Speed, rpm	66.88	62.59	72.73	76.82
Rotor Tip Speed, m/s(ft/s)	51.3(168.4)	52.3(171.5)	57.6(189.0)	58.8(193.0)
Cut-in Speed, m/s	3.91	3.98	4.38	4.48
Rated Speed, m/s	10.81	11.01	12.12	12.39
Time On-line, h/yr	6020	5960	5470	5350
Energy Capture, kWh/yr (5.4 m/s wind)	45,000	55,000	55,000	52,600
Relative COE	1.090	1.024	1.000	1.015

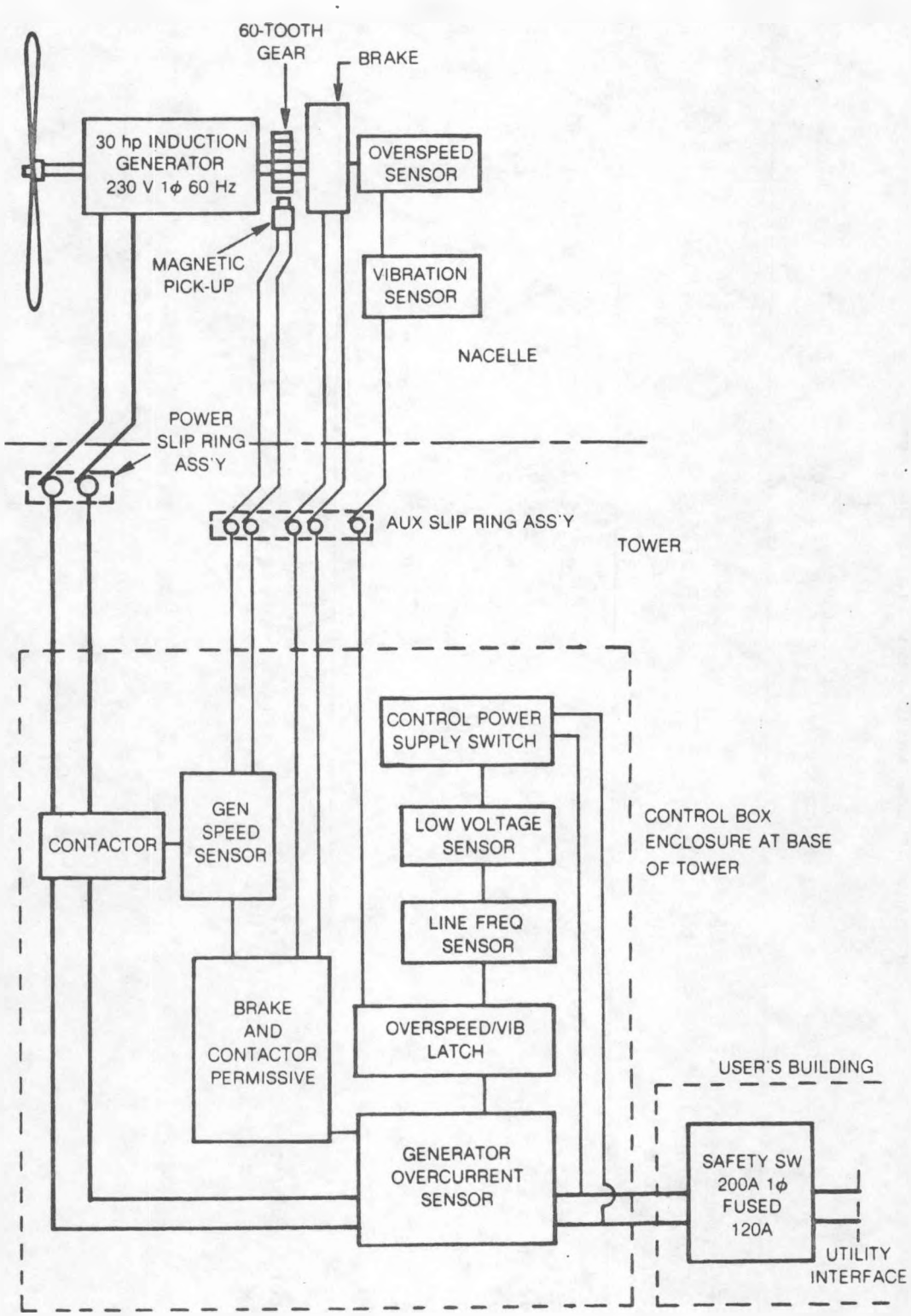

Figure 33. UTRC 15-kW WTG Electrical System

81-9-55-1

In the 15-kW system, the speed switch is programmed to operate in a hysteresis mode, delaying connection of the generator to the utility grid until the generator speed is 1820 rpm, to ensure that sufficient wind for power generation is present. Connection is maintained until the generator speed decreases to less than 1800 rpm for at least 3 sec. The delay of 3 sec is used to avoid excessive contactor operation in marginal wind conditions. The speed switch also incorporates a generator speed display and control status indicators. The self-excitation interlock consists of a frequency-sensing switch which prevents operation of the magnetic contactor unless the line frequency at the WTG is 60 Hz. Since the frequency of power generated by self-excitation (a condition of resonance between an induction generator and connected resistance and capacitance) is likely to be different from 60 Hz, this interlock will prevent "live wire" conditions which might otherwise occur during utility outages if the resonant capacitance and resistance were to remain connected to the WTG. The parking brake is comprised of steel discs which are separated by friction pads driven by the generator shaft. The pads and steel discs are compressed with an ac solenoid.

Mechanical Design

Several designs of the rotor drive and gearbox assembly were studied in an effort to optimize the head assembly. Layouts of various cast or welded frames were evaluated. These configurations, such as the one shown in Fig. 34, formed platforms on which a standard step-up gearbox was mounted. The rotor shaft and bearings were also mounted on its surface. The rotor shaft was attached to the low speed side of the gearbox through a flexible coupling. These designs were hampered by the bulk of the standard gearbox housing and the need for providing adjustment for aligning the components at assembly. The adjustment feature was eliminated on some configurations by finish machining of the components. These all proved to be costly. Because the distance between the yaw shaft and rotor plane was specified as 1.52 m (5 ft), they were all large and heavy machines.

The concept of the extended shaft gearbox design shown in Fig. 35 evolved from these studies. Many advantages were realized from this design:

1. The platform on which the components were supported was eliminated.
2. The distance from the rotor shaft to the attachment base was shortened thus minimizing the load on yaw bearings.
3. The assembly alignment or machining of components was eliminated.
4. The gearbox/rotor shaft coupling was eliminated.
5. The number of bearings required to support the rotor shaft was reduced.
6. Weight was reduced.
7. Cost was reduced.
8. The unit presented a neat, uncluttered appearance.

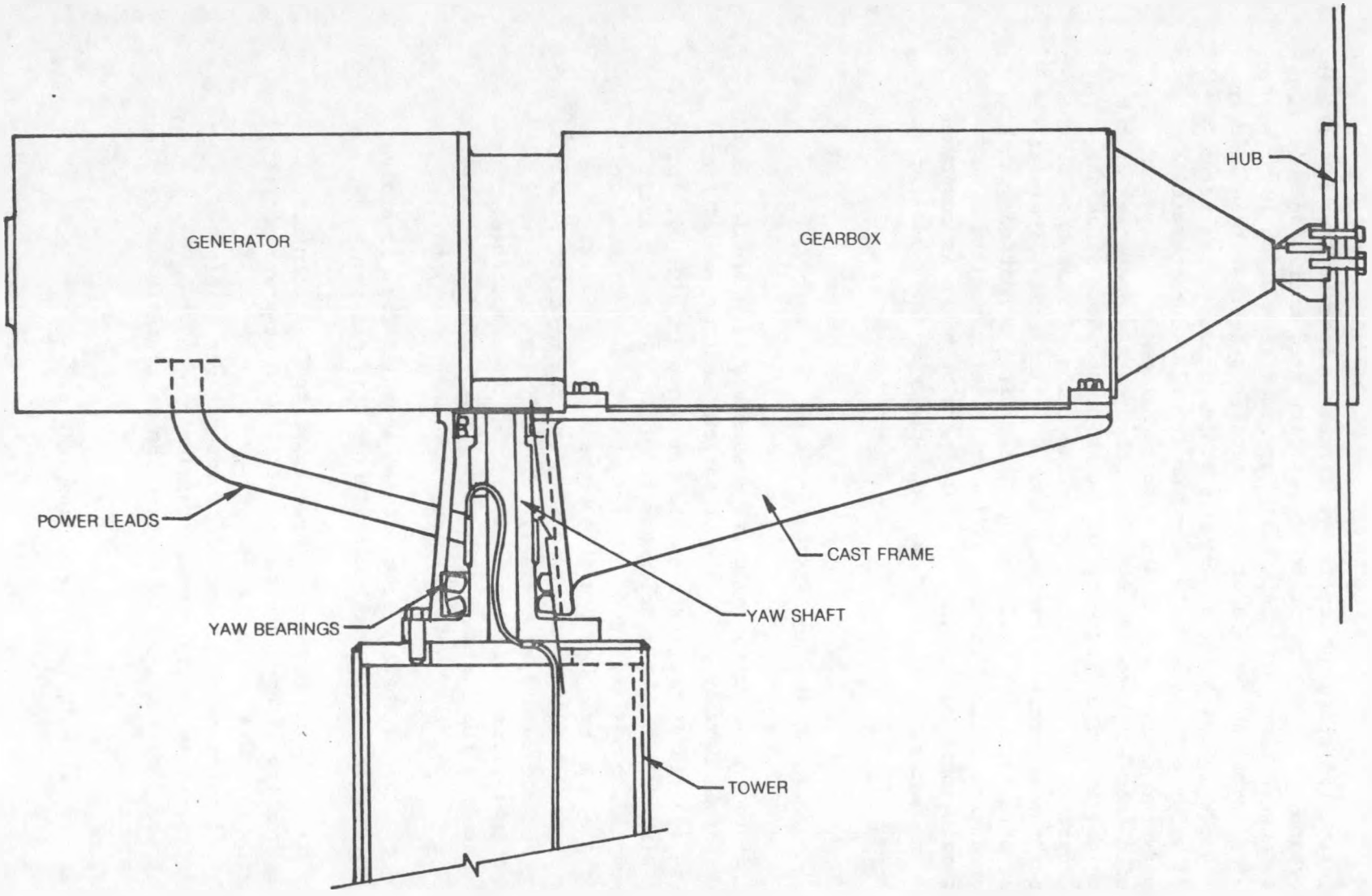

Figure 34. Platform Configuration for Head Assembly

81-6-154-59

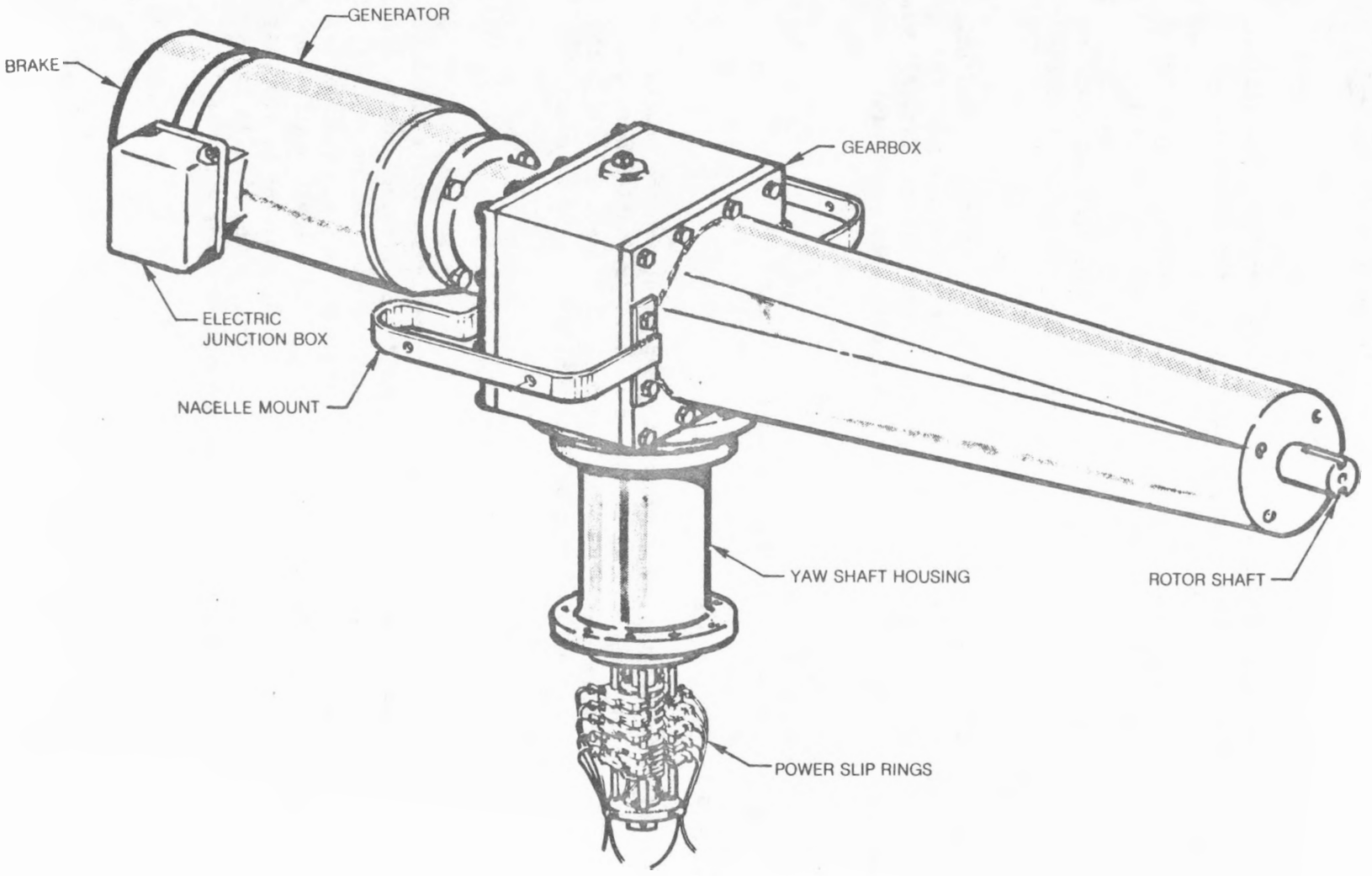

Figure 35. 15-kW Wind System Head Assembly

81-6-164-48

The gearbox shown in Fig. 35 is a special FMC design with helical gears and 1:25 ratio. The gearbox is designed to operate for 25 years at a torque of 3238 N·m (2388 lbf-ft).

Yaw Bearings

Two yaw bearing schemes have been designed for the prototype. The initial scheme (Fig. 36) consists of a vertical shaft supported by two spherical roller bearings contained within a flanged housing. Both the shaft and housing are made of cast steel. The bearings are self aligning, thus eliminating the need for rigid straightness and squareness tolerances on both the shaft and housing.

The yaw shaft is hollow, permitting wiring from the generator and brake to be routed through its center to the slipring assembly which is attached to the lower flange of the housing.

After fabrication of the above unit was initiated, a commercially available turntable bearing, whose load bearing characteristics are compatible with the 15 kW machine, was located. An alternate yaw bearing configuration (Fig. 37) was designed around this bearing. The advantages of this alternate configuration are:

1. The yaw shaft was eliminated.
2. The housing was eliminated.
3. The number of bearings was reduced from two to one.
4. Cost was reduced.
5. Weight was reduced.

For the prototype an adapter plate was fabricated to attach the bearing to the gearbox base and the tower. It is envisioned that in production both the gearbox base and tower flange bolt circle will be drilled to mate directly with the metric drilling of the bearing. This will eliminate the need to adapt the holes and thus further reduce the cost.

Nacelle

The head assembly is housed within a two-piece fiberglass nacelle shown in Fig. 38, which is split horizontally. The lower portion is attached to the head assembly with bolts and a steel bearing plate at both the yaw and rotor shaft exits. Additional support is provided by bracing between the sides and the gearbox housing. The top section is attached to the bottom with 10 quick-close lever latches and a series of bolts. Air is circulated through the nacelle by a series of openings in the bottom wall. A condensation drain is also provided. The nacelle is aerodynamically shaped and presents a smooth, clean appearance along its outside contour.

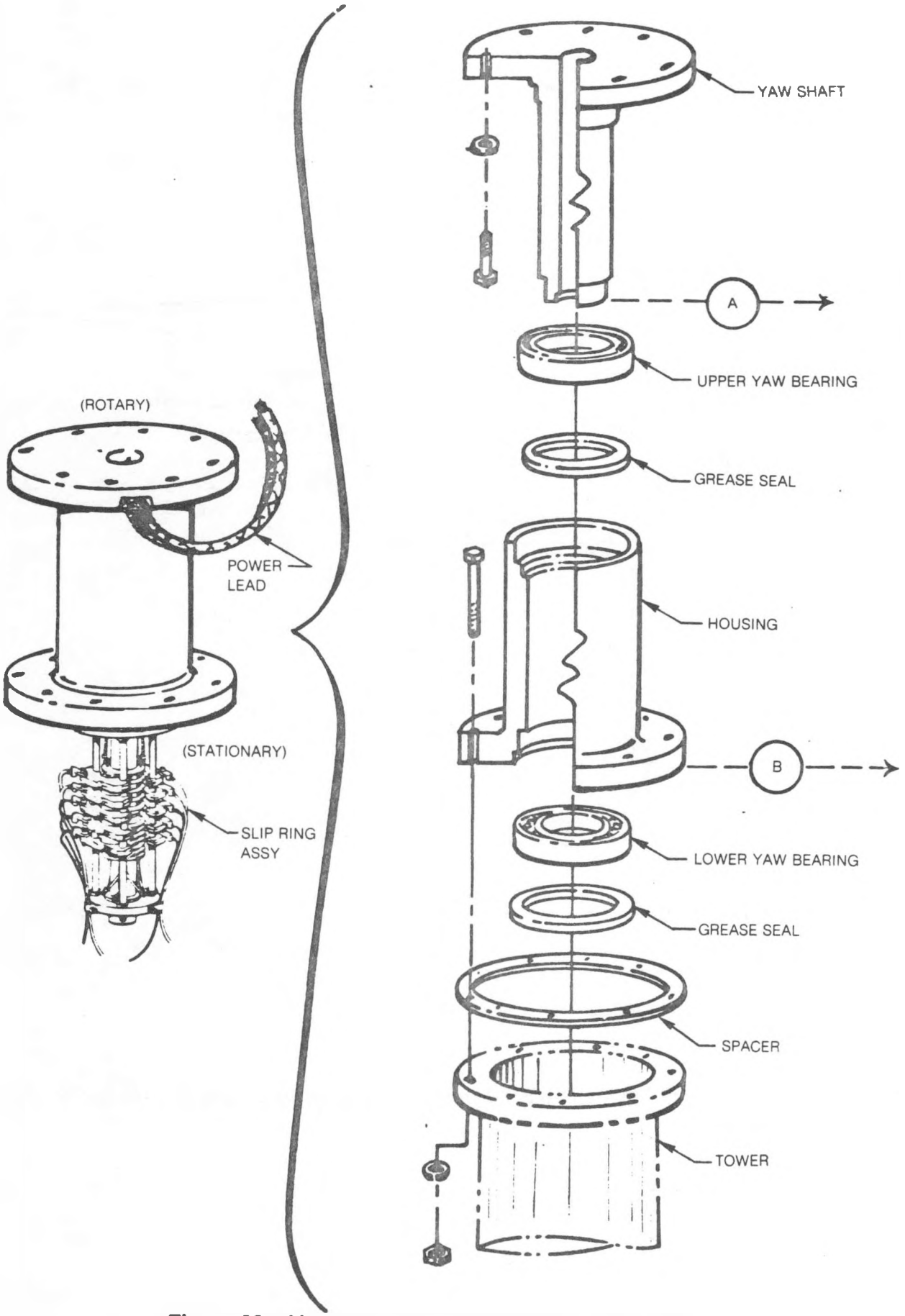

Figure 36. Alternate 15-kW Wind System Assembly

81-6-164-49

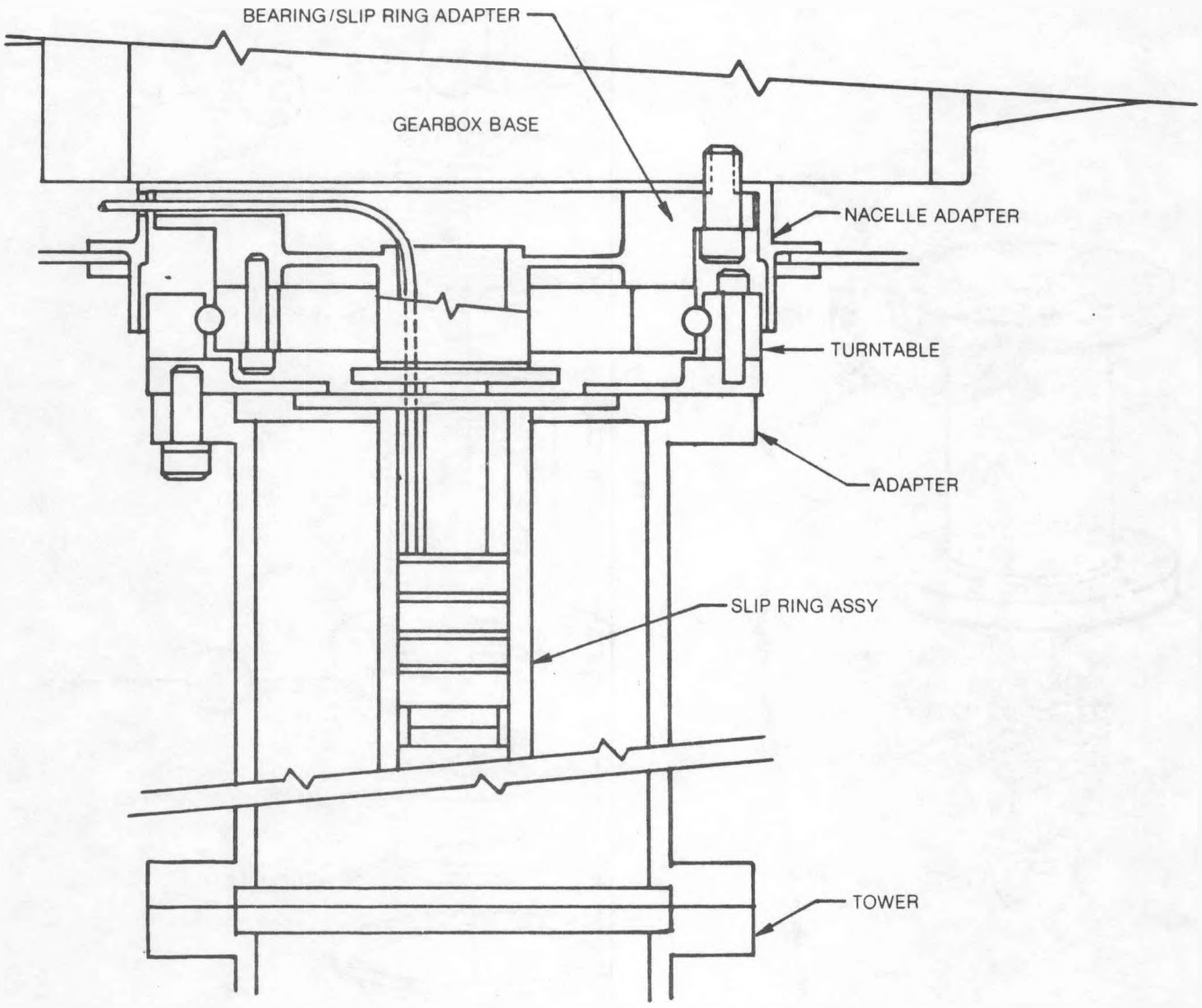

Figure 37. Section Through Tower/Gearbox Interface Showing Alternate Bearing Installation

81-6-164-50

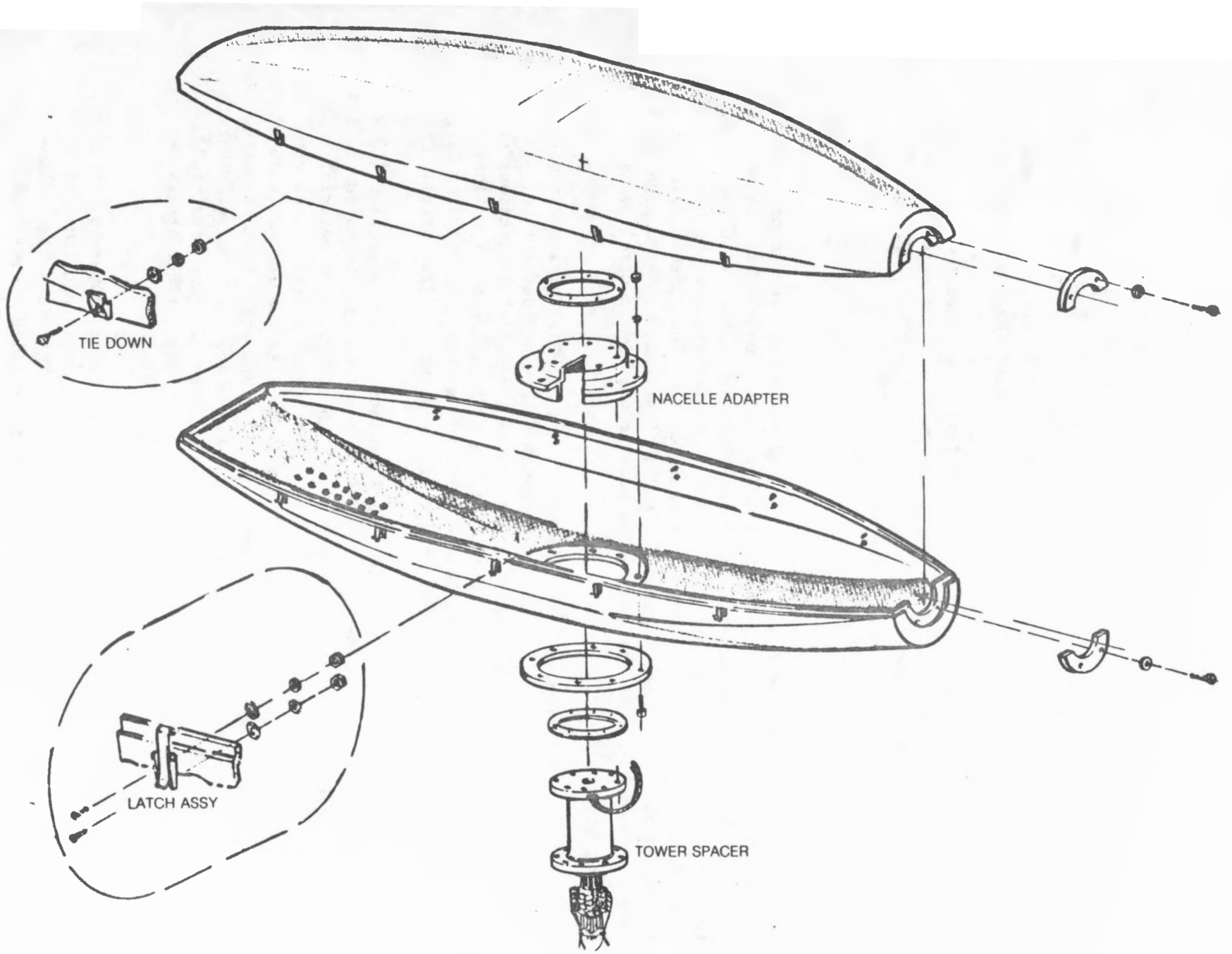

Figure 38. 15-kW Nacelle Assembly

Rotor and Control System Design

The rotor system is a scaled-up version of the UTRC Model 108 8-kW design developed initially under a DOE/Rockwell contract in 1977-79. It is a two-bladed down-wind design employing the Bearingless Rotor concept. Figure 39 is a sketch of the rotor geometry. The Composite Bearingless Rotor (CBR) concept has been used, as for the 8-kW WTG documented in Refs. 1 and 2, to simplify the design and lower manufacturing costs. The 15-kW CBR design consists of a blade with a 457-mm (18-in.) chord using a NACA 23112 airfoil. The airfoil blade position is connected to the rotor hub by a flexbeam. The four major components of the rotor system are the flexbeam, blade, flexbeam-blade attachment joint and the hub. A discussion of the design of each of these components follows.

Flexbeam

The flexbeam is made of composite materials and serves two fundamental purposes. First, the flexbeam is quite flexible in torsion by design, so that it can be readily twisted by an applied torsional moment. When the flexbeam twists, with the inner-end restrained by the hub, the pitch angle of the outer position of the blade (the aerodynamic lifting surface) changes. Therefore, the blade pitch angle, which determines aerodynamic efficiency through the angle of attack, can be controlled by twisting the flexbeam. This is performed by a passive pendulum control system, which will be discussed later.

The second function performed by the flexbeam is the relief of aerodynamic, centrifugal and inertial forces through out-of-plane (flatwise) deflection. Nearly all of the flatwise (out-of-plane) and edgewise (in-plane) deflections of the rotor blade occur in the flexbeam except for higher frequencies of motion. The freedom of the flexbeam to deflect lowers the blade stresses by allowing large forces to balance each other (e.g., aerodynamic lift and centrifugal force).

The flexbeam is made of fiberglass and has a rectangular cross section 213 x 21.3 mm (8.4 x 0.84 in.). The material used is S-2 glass and was chosen due to its moderate cost and high strength. Graphite/epoxy was considered as a material because of its high modulus and strength, but the much higher material cost compared to S-2 glass did not justify its use. E glass was also considered because of its low cost, but the lower modulus compared to S-2 glass would have resulted in a significantly larger size flexbeam. S-2 glass was a good compromise from both a strength and cost viewpoint. It will be shown later that, for the predicted loads, the S-2 glass flexbeam adequately meets the static and fatigue stress criteria previously discussed.

The flexbeam is a straight, rectangular bar with no twist, taper, or precone. This design facilitates the use of the pultrusion process for production. A schematic of the pultrusion process is shown in Fig. 40. This is a high volume manufacturing process which utilizes a heated die and a pulling system to form composite parts. This process has been successfully used to fabricate the 381-mm

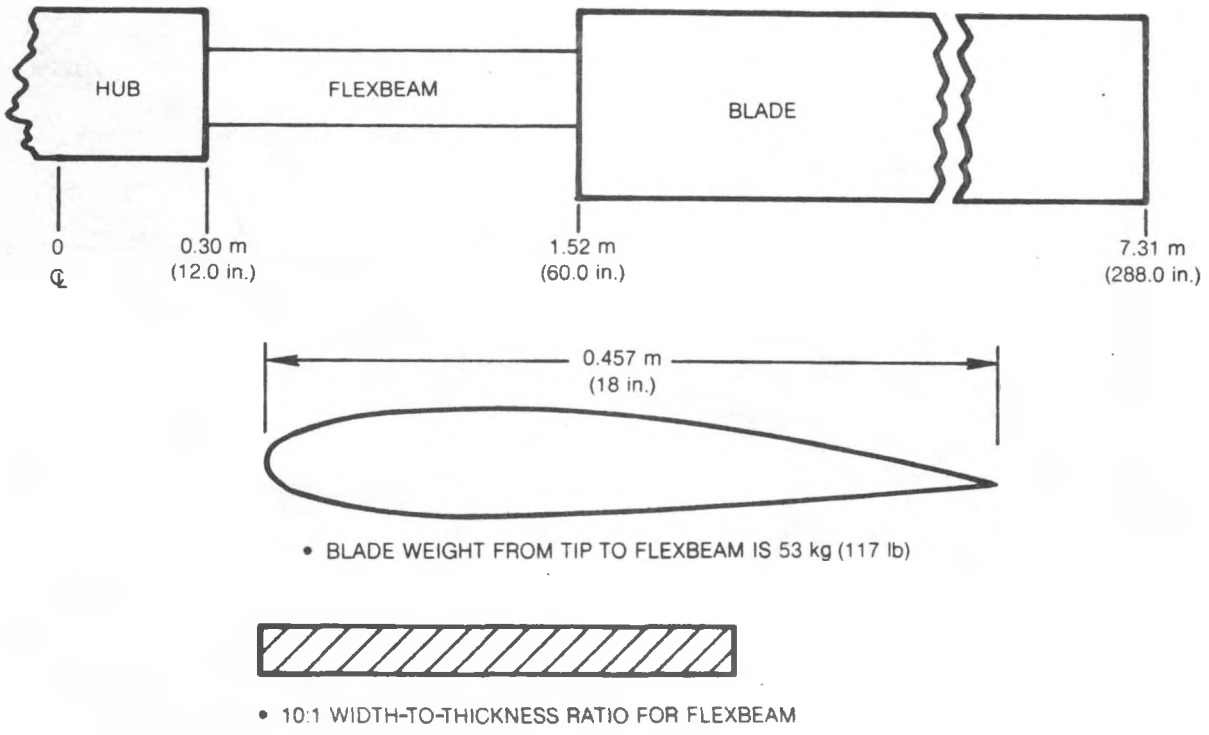

Figure 39. Schematic of 15-kW WTG Rotor System

81-6-164-52

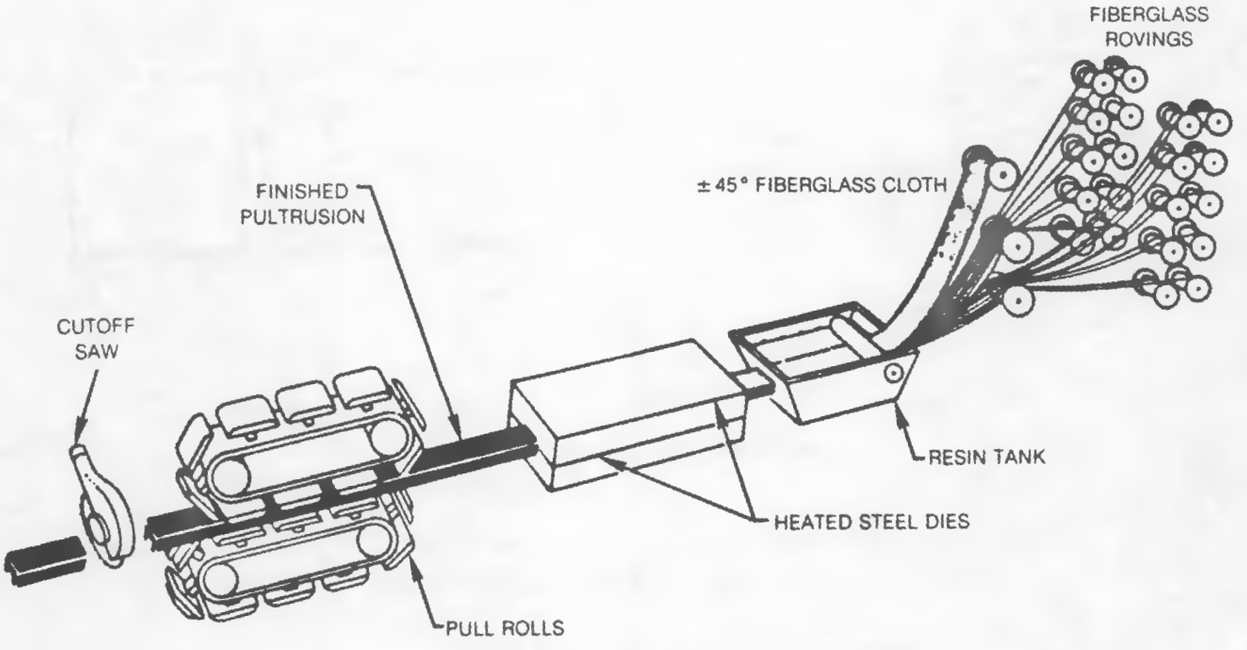

Figure 40. Schematic of Composite Material Pultrusion Process

81-6-164-53

(15-in.)-chord blades for the 8-kW wind turbine documented in Refs. 1 and 2. Because the flexbeam is not twisted, the negative blade pitch angle (nose down so that the leading edge is upwind) required for start-up (-10°) is built into the joint that attaches the blade to the flexbeam.

Blade-Flexbeam Attachment Joint

Much consideration was given to the joint between blade and flexbeam in an effort to keep the cost down. Because of the large 457-mm (18-in.) blade chord, variations in the blade cross-section were anticipated. This required that any fitting of an internal contoured metal spar would be on an individual basis to meet the required minimal clearance between blade and spar contour. The necessity for providing a hollow (foam free) cavity within the blade to accept the spar added considerable cost to blade preparation.

The attachment joint that evolved from these considerations is shown in Fig. 41. The design consists of a built-up blade cuff which provides two parallel flat surfaces on which splice plates are attached. The mating end of the flexbeam is built-up to the same thickness dimension as the blade cuff. The flexbeam buildup incorporates the -10° blade pitch angle needed for start-up. Four 25-mm (1-in.)-threaded rods hold each attachment interface in position. The design is further simplified by bending one side of the upstream splice plate 90° to act as the flexstrap attachment lug.

A mock-up of the joint was fabricated and tested in a tensile tester. The results of the test will be discussed later. This design is low in cost and allows the blade to be easily dismantled from the rotor.

Blade

The rotor blade is a 457-mm (18-in.)-chord airfoil that is untwisted and untapered. Since the blade has no twist or taper, the pultrusion process previously described to manufacture the flexbeam can also be used to manufacture the blade. Figure 42 shows a cross section of the blade airfoil with detail of the blade skin. The NACA 23112 airfoil section was selected to provide good start-up characteristics, high efficiency, and little or no pitching moment during normal operation. The blade skin is composed of longitudinal E glass fiberglass rovings for bending stiffness and $\pm$ 45° E glass woven cloth for torsional stiffness. The airfoil aft-section is filled with urethane foam which serves two functions. First, during the manufacturing process, the precured foam serves as a mandrel for the airfoil section as the composite material is pulled through the die. Secondly, the foam provides buckling support to the blade skin under the aerodynamic suction and pressure loading.

The leading edge of the airfoil section is a solid precured block of unidirectional fiberglass/resin which is pultruded in a separate operation and manually fed, along with the foam insert, into the blade pultrusion operation. This nose block provides erosion and impact protection and helps to mass-balance the airfoil section

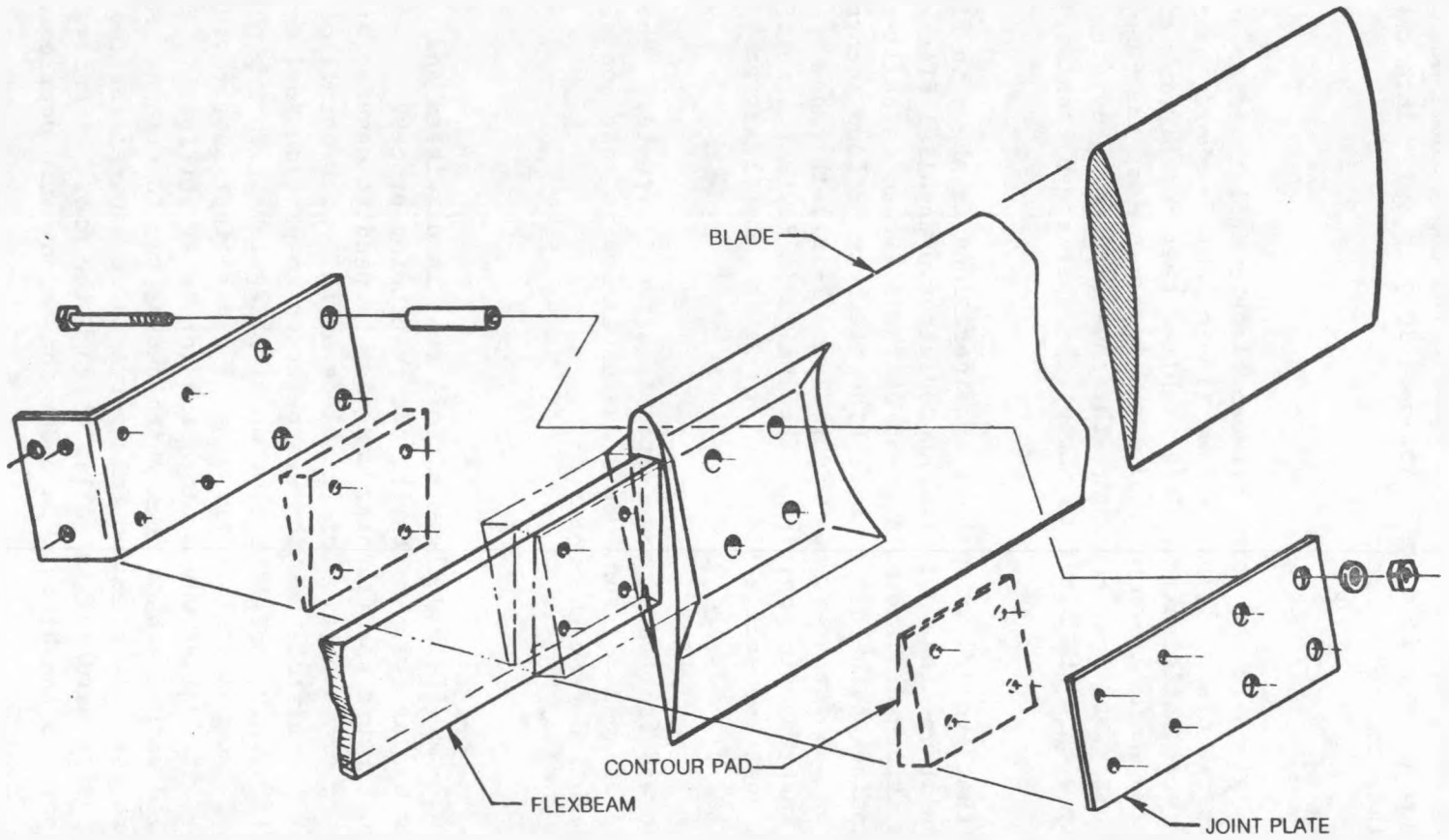

Figure 41. Schematic of Blade-Flexbeam Attachment Joint

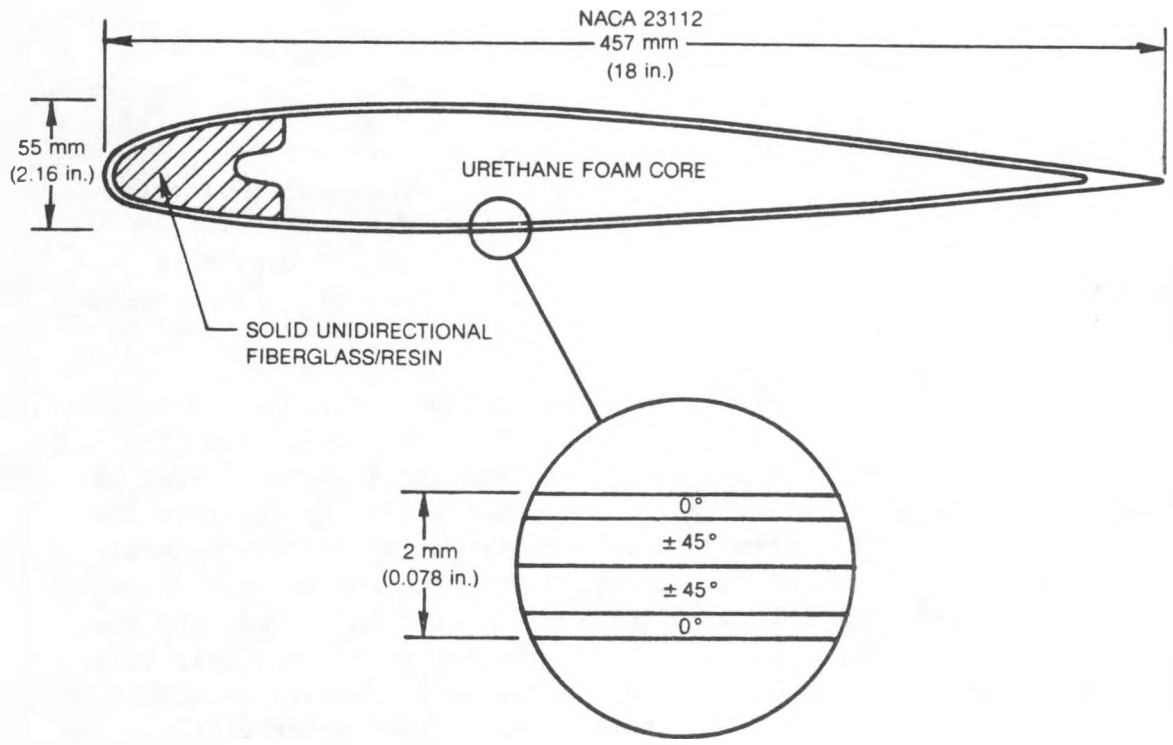

Figure 42. Airfoil Section Showing Fiberglass Layup of Blade Skin

81-6-164-55

near the quarter chord point, as well as providing bending stiffness in both flatwise and edgewise directions. The rotor blade spanwise physical properties are shown in Fig. 43.

A summary of the general rotor design parameters is shown in Table XIV.

TABLE XIV

ROTOR DESIGN PARAMETERS

Rotor Diameter	14.6 m (48 ft)
No. of Blades	2
Blade Chord	457 mm (18 in.)
Twist	0
Taper	0
Airfoil	NACA 23112
Blade Material	E glass/vinyl ester
Flexbeam Size	213 x 21.3 x 1218 mm (8.4 x 0.84 x 48 in.)
Flexbeam Material	S-2 glass/vinyl ester
Precone	0

Using the structural properties of the blade-flexbeam, the natural frequencies and mode shapes of the rotor were predicted with UTRC computer program E159. The predicted frequency diagram for the blade-flexbeam design is shown in Fig. 44. As discussed previously, the first out-of-plane mode, denoted 1F to indicate the flatwise direction of modal deflection, is relatively "soft" and the natural frequency of this mode is nearly 1P (one-per-rev) over the rotor speed range. Another important mode is the first in-plane mode, denoted 1E to indicate the edgewise direction of modal deflection. Because the motion of this mode is in the chord-wise direction, there is very little aerodynamic damping available to attenuate response of this mode. For comparison, the out-of-plane flatwise responses induce angle of attack changes and are moderately damped. Because of the low damping in the first in-plane mode, design of the flexbeam to properly place this frequency is important to minimize edgewise dynamic stresses and also to ensure rotor stability. The largest source of forcing for the edgewise mode is a once-per-rev gravity excitation since the rotor rotates in a vertical plane. Therefore, a primary consideration in the flexbeam design is to ensure that the first in-plane blade frequency (1E) is removed from one-per-rev (1P) over the rotor operating range. The operating range of the rotor, from grid connection to off-line high speed windmilling, is shown in Fig. 44 by the two vertical lines. For the high speed condition with a rotor tip speed of 107 m/s (350 ft/s), the first in-plane frequency (1E) is 1.78 per rev (4.1 Hz), well removed from the (1P) which is at about 2.3 Hz. There are other in-plane frequency placement criteria with respect to coupling with tower vibrational modes, and these aspects will be discussed later.

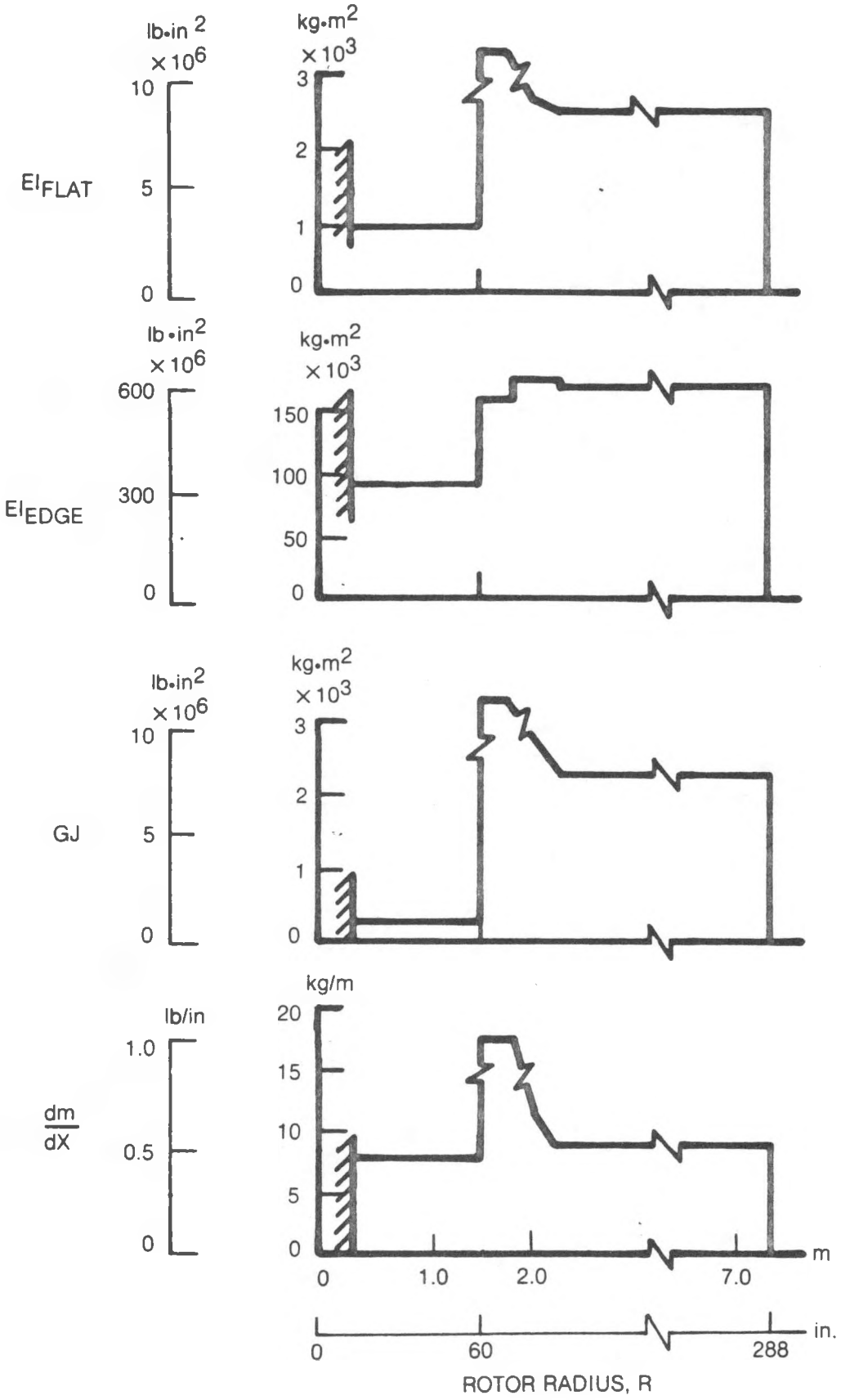

Figure 43. Rotor Blade Physical Properties

81–6–164–67

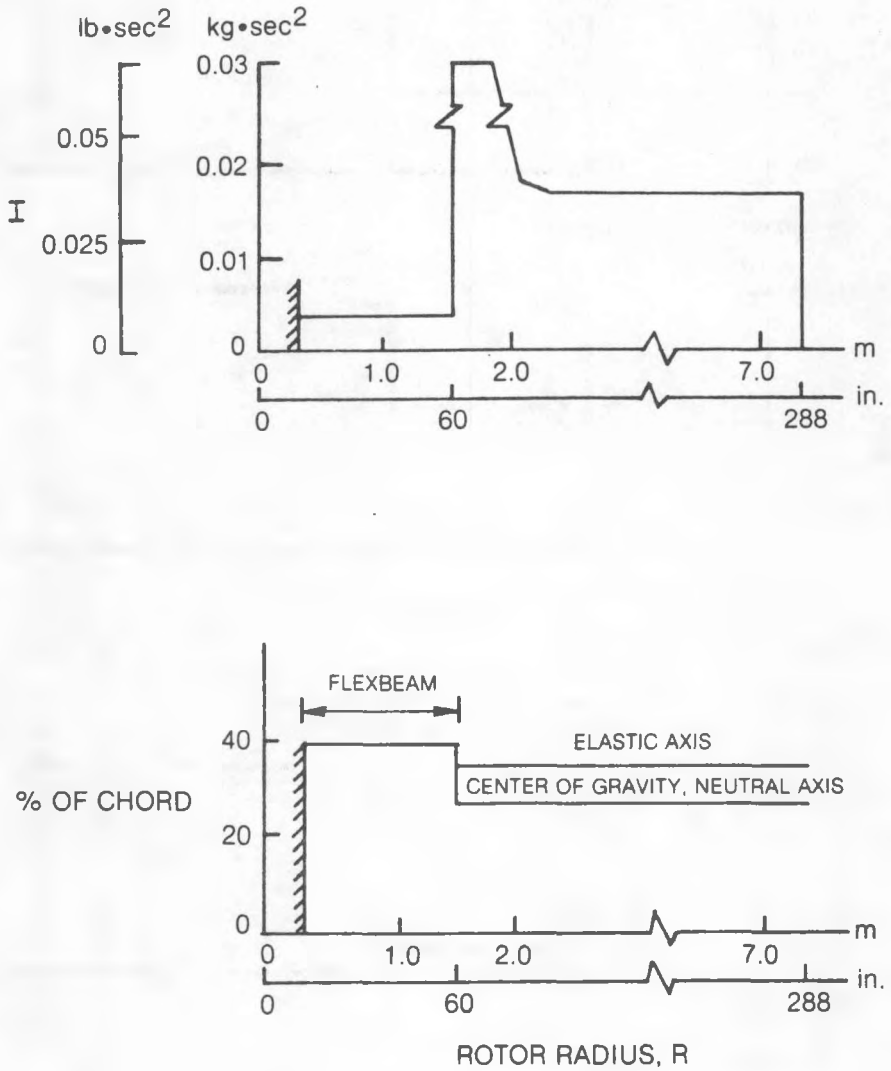

Figure 43. Continued

81-6-164-78

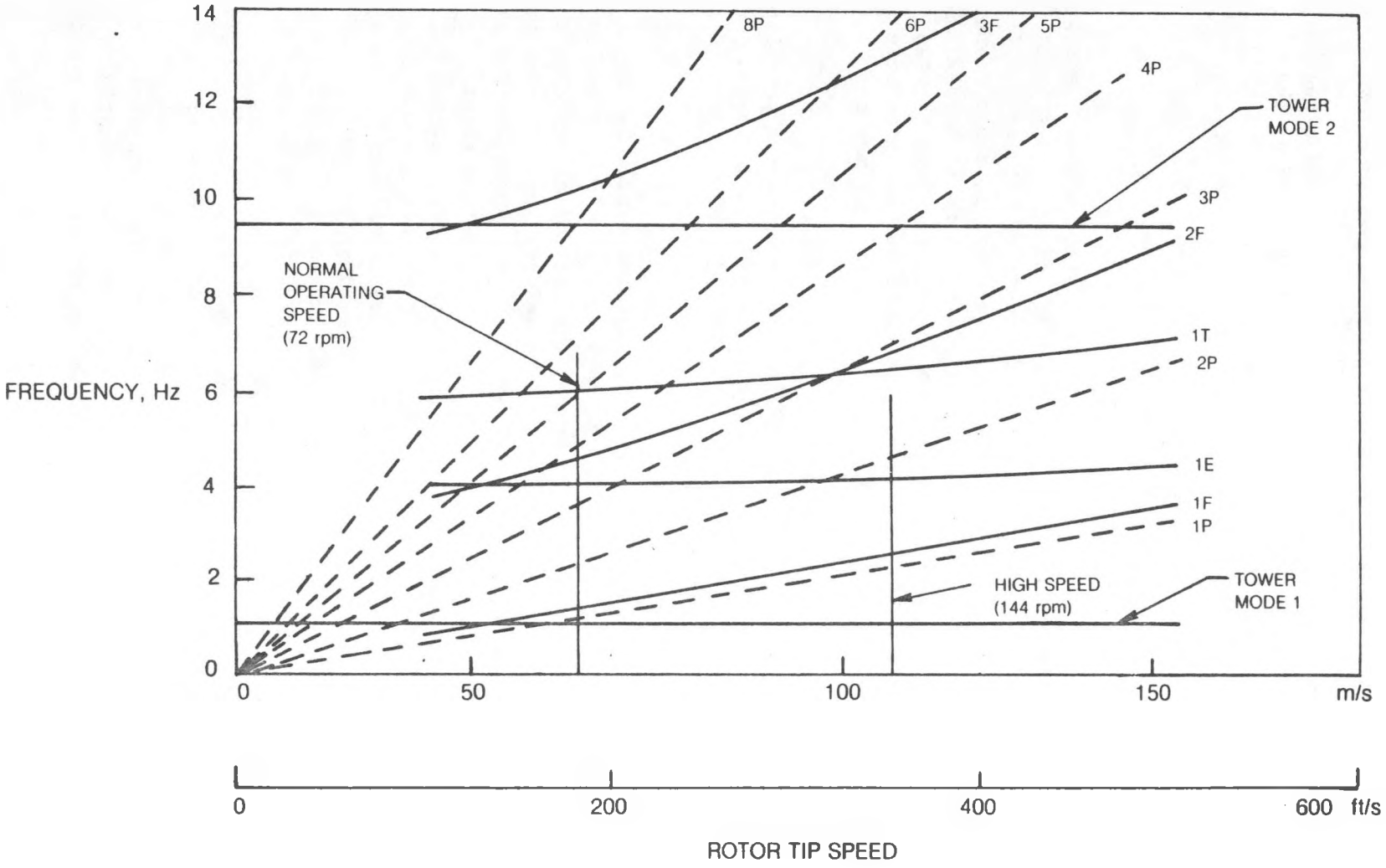

Figure 44. 15-kW Wind Turbine System Natural Frequency Spectrum

81-6-164-72

In Fig. 44, the first torsion mode frequency (1T) is also shown. This torsional frequency is relatively low compared to that for helicopter blades. This is a common characteristic of the bearingless rotor since high torsional flexibility is needed to set the blade pitch by twisting the flexbeam. This twisting is evident in Fig. 45 which shows the blade torsion mode shape along with the in-plane and out-of-plane bending mode shapes. Note that 85% of the torsional mode deflection takes place over the length of the flexbeam which indicates how much "softer" the flexbeam is in torsion than the blade airfoil section.

Rotor Hub

The rotor hub shown in Fig. 46 is comprised of two cast steel members separated by spacers to accommodate the flexbeam and is bolted together to provide a tight assembly. A thin ply of 3.2-mm (1/8-in.) polyurethane is inserted between the flexbeam and the hub castings and spacers to minimize stress concentrations and fretting. The hub is attached to the gearbox rotor shaft by means of one 25-mm (1-in.)-diam hex head bolt. Two 16-mm (5/8-in.)-square keys provide the driving lugs between the hub and rotor shaft. One drive key is marginally adequate but two have been provided in an effort to allow for unforeseen shock or overloads that may be encountered.

The downstream casting incorporates two arms 180° apart to which the pendulums are attached. Bronze bushings are installed at the pendulum rod pivot joints.

Control System

One of the distinguishing features of the UTRC wind turbine design is the passive pendulum system used to control blade pitch. A schematic of the pendulum control system is shown in Fig. 47. The control system consists of a) pendulum support arms, b) pendulum rods with, c) attached pendulum weights, and d) flexstraps which connect the end of the pendulums to the flexbeam at the attachment points of the blade airfoil section. The pendulum rod has the freedom to rotate about a bushing located at the end of the support arm. As rotor speed increases, the centrifugal force acting on the pendulum also increases, which induces a moment about the pendulum arm hinge point so that the pendulum moves towards an in-plane position. Since the end of the pendulum is attached by the flexstrap to the rotor blade-flexbeam, the flexbeam will twist as the pendulum moves. Twisting of the flexbeam creates an elastic restoring force which equilibrates the force imposed by the pendulum. Therefore, the final position of the flexbeam (in twist) and the pendulum (in angle from the plane of rotation) depends upon 1) the torsional stiffness of the flexbeam, 2) weight of the pendulum, 3) geometry of the pendulum configuration and 4) speed of rotation. If the flexbeam torsional stiffness is too high the flexbeam will twist less for a given pendulum weight and geometry. Conversely, if pendulum weight is too low, the pendulum will not sufficiently rotate to twist the flexbeam. Therefore, it is obvious that design of the control system

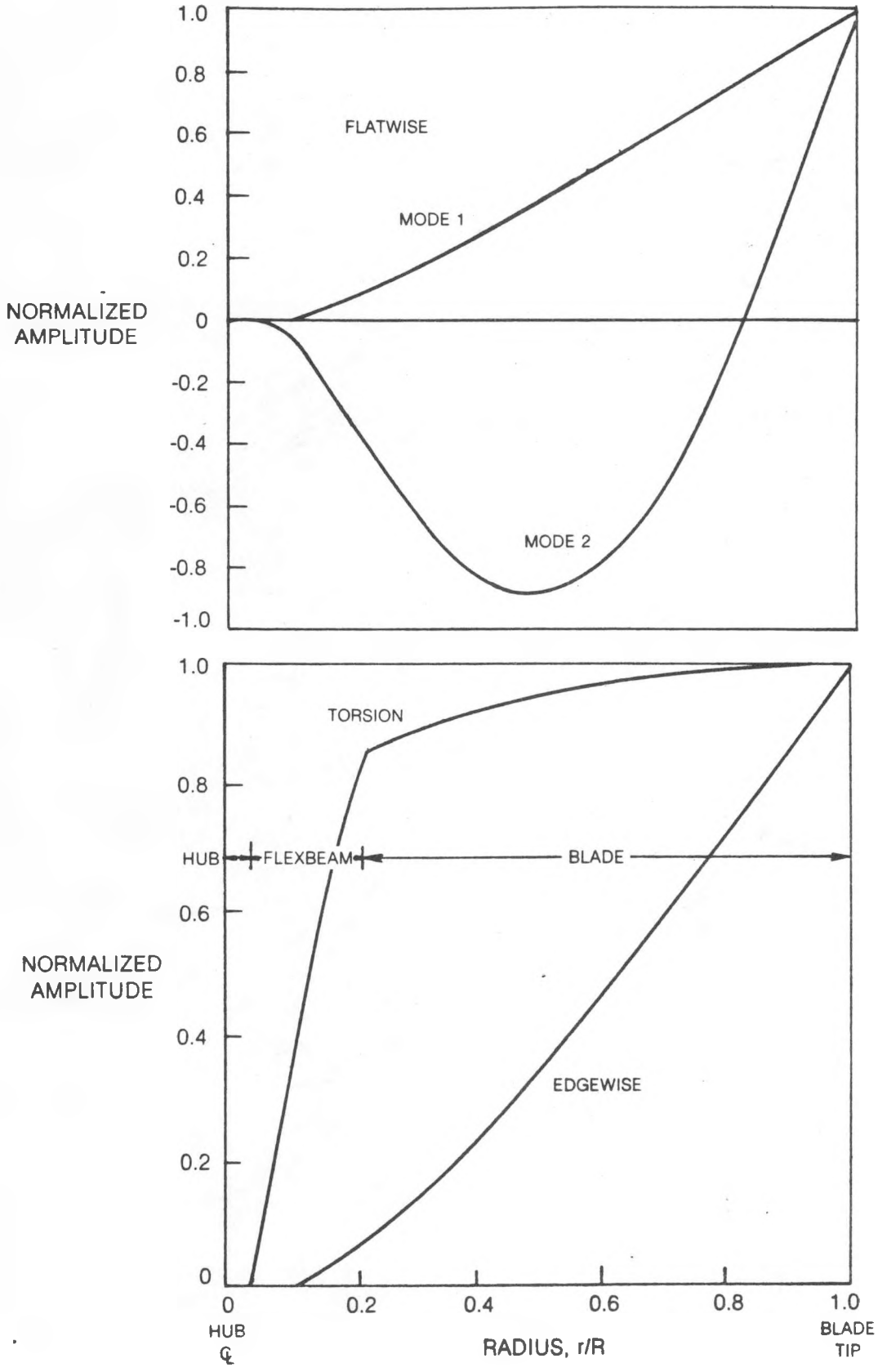

Figure 45. Blade Mode Shapes

81-6-164-73

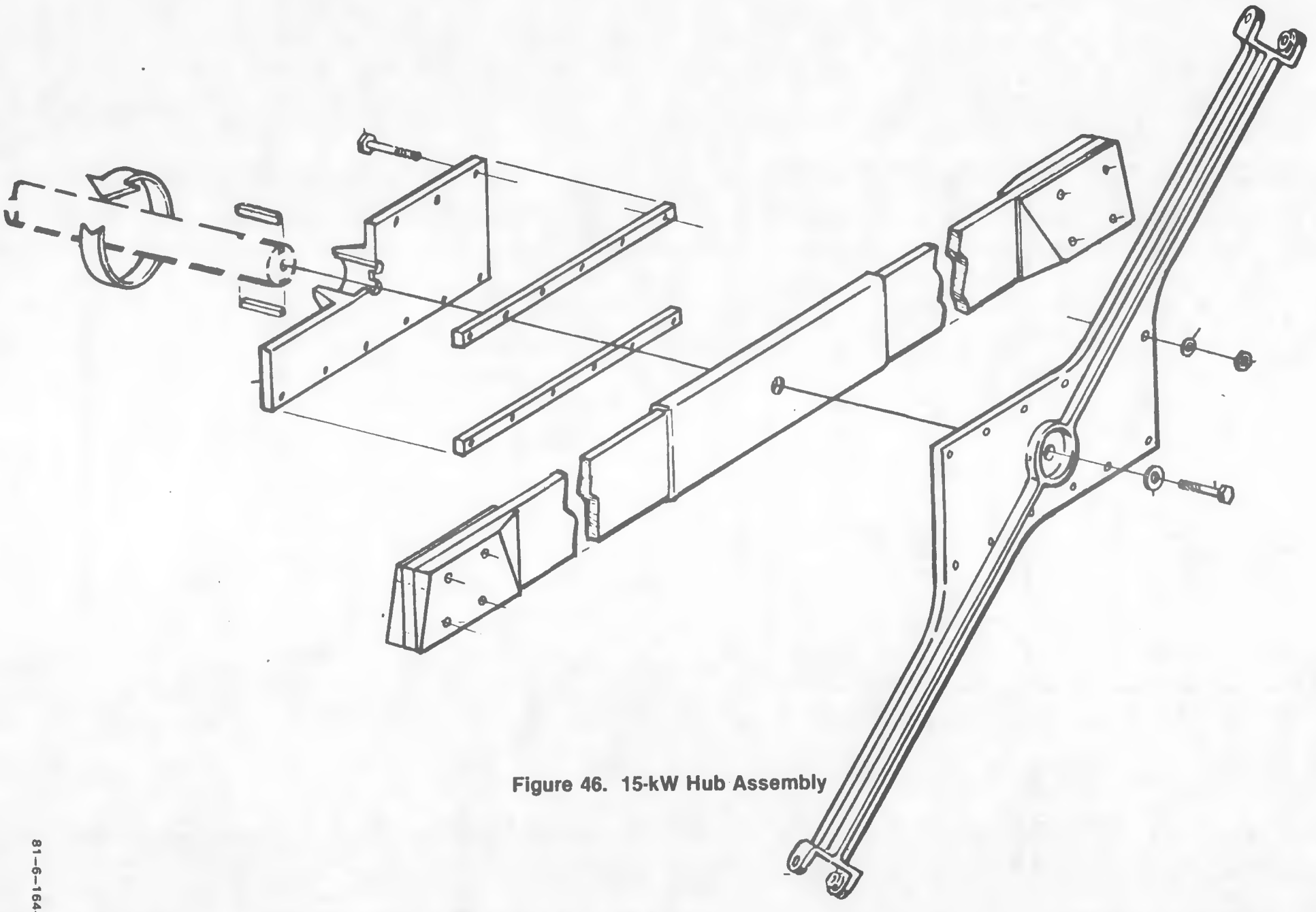

Figure 46. 15-kW Hub Assembly

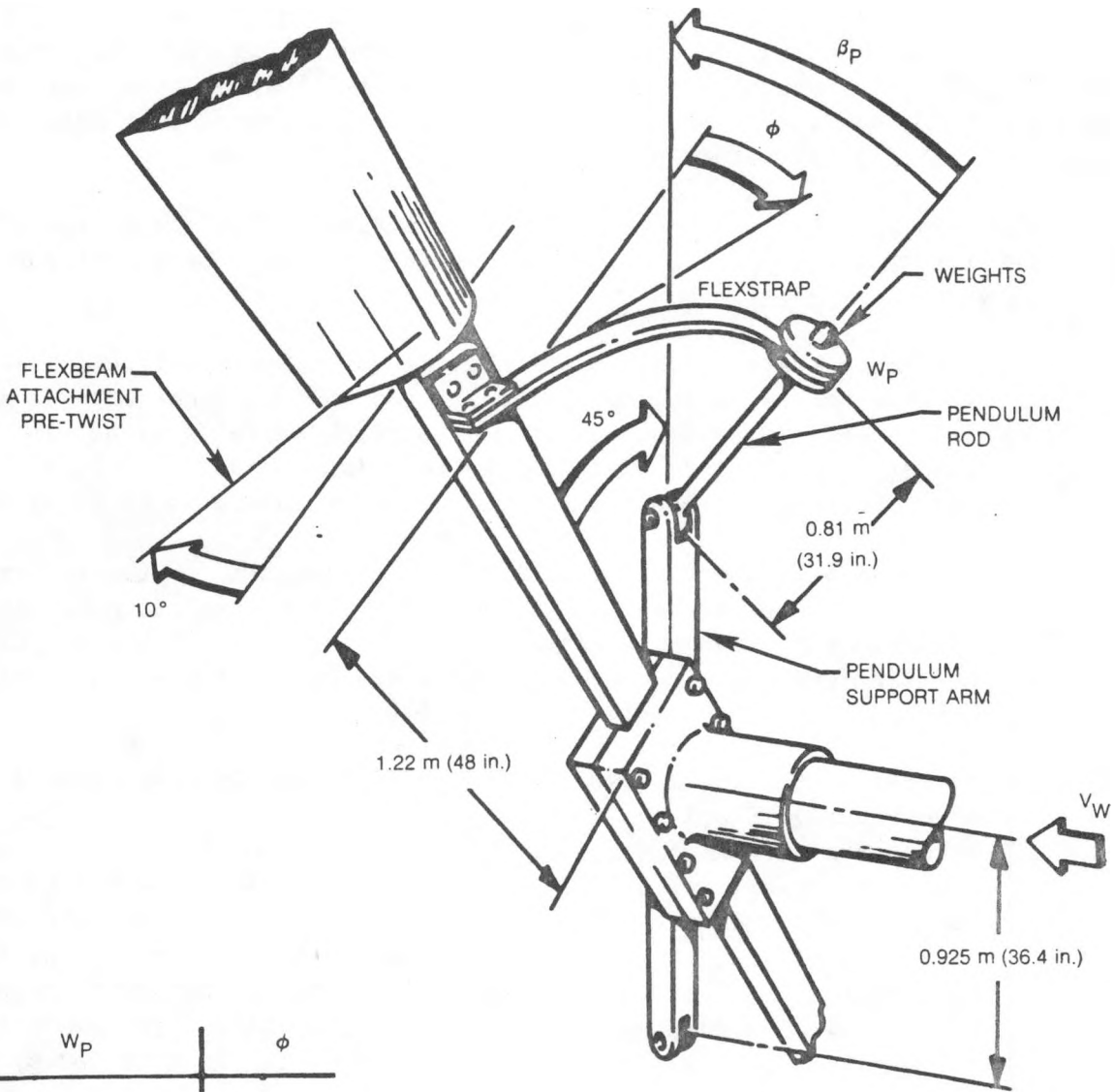

β_P	W_P	ϕ
45°	48.5 kg (22 lb)	27°
40°	63.9 kg (29 lb)	24°
35°	79.4 kg (36 lb)	21°
30°	94.8 kg (43 lb)	18°

Figure 47. Candidate Pendulum Geometries

81-6-164-76

and flexbeam torsional stiffness requires judicious selection and tailoring of parameters. Many design iterations were performed in the pendulum control system for the 8-kW wind turbine documented in Refs. 1 and 2 to achieve a satisfactory configuration, and this experience, as well as experimental test data (Ref. 2), proved valuable in formulating the design shown in Fig. 47.

The need for control of blade pitch is fundamental to the design of the UTRC wind turbine concept. Basically, three requirements must be met by the blade pitch control system.

1. For rotor start-up, the blade must be sufficiently pitched into the wind so that the net aerodynamic force tends to "pull" the rotor and accelerate it to operating speed. The required pitch angle is about -10° with the leading edge upwind. This is the position of the blade pitch, as built into the blade/flexbeam attachment joint when the rotor is at rest.

2. For operational speed when the rotor is connected to the electrical grid, a zero or slightly negative (-1°) blade pitch angle is necessary to optimize aerodynamic performance of the rotor. Hence, from the non-rotating position, the pendulum must provide sufficient control to change the blade pitch by 9°-10° for normal operation.

3. For high rotor speed operation, when the rotor is disconnected from the electrical grid and the wind speed is high, the rotor will continue to autorotate with zero net torque. Rotor speed will increase as the wind speed increases, unless the blade pitch angle is increased further so that the blade becomes stalled. With the occurrence of stall, aerodynamic drag rises sharply, which tends to slow the rotor. When the rotor is sufficiently stalled, rotor speed will be nearly constant, regardless of increases in wind speed. To achieve this stall point, a positive blade pitch angle of about 5° is required which is produced by the pendulum as rpm increases.

Many different pendulum configurations were considered to achieve these three requirements of blade pitch angle. The two main parameters are the pendulum weight and the initial pendulum angle with respect to the vertical plane when the rotor is at rest. Figure 48 shows a range of pendulum configurations involving changes in these two parameters which meet the three design points. Note that increasing the initial pendulum angle has the same effect as increasing pendulum weight since the net force imparted to the flexbeam by the pendulum through the flexstrap is a function of the sine of the pendulum angle. The pendulum configuration that was chosen for the design is in the middle of the range shown in Fig. 48 (35° pendulum angle, 16.3-kg (36-lb) pendulum weight). The resulting predicted pendulum schedule with rotor speed is shown in Fig. 49.

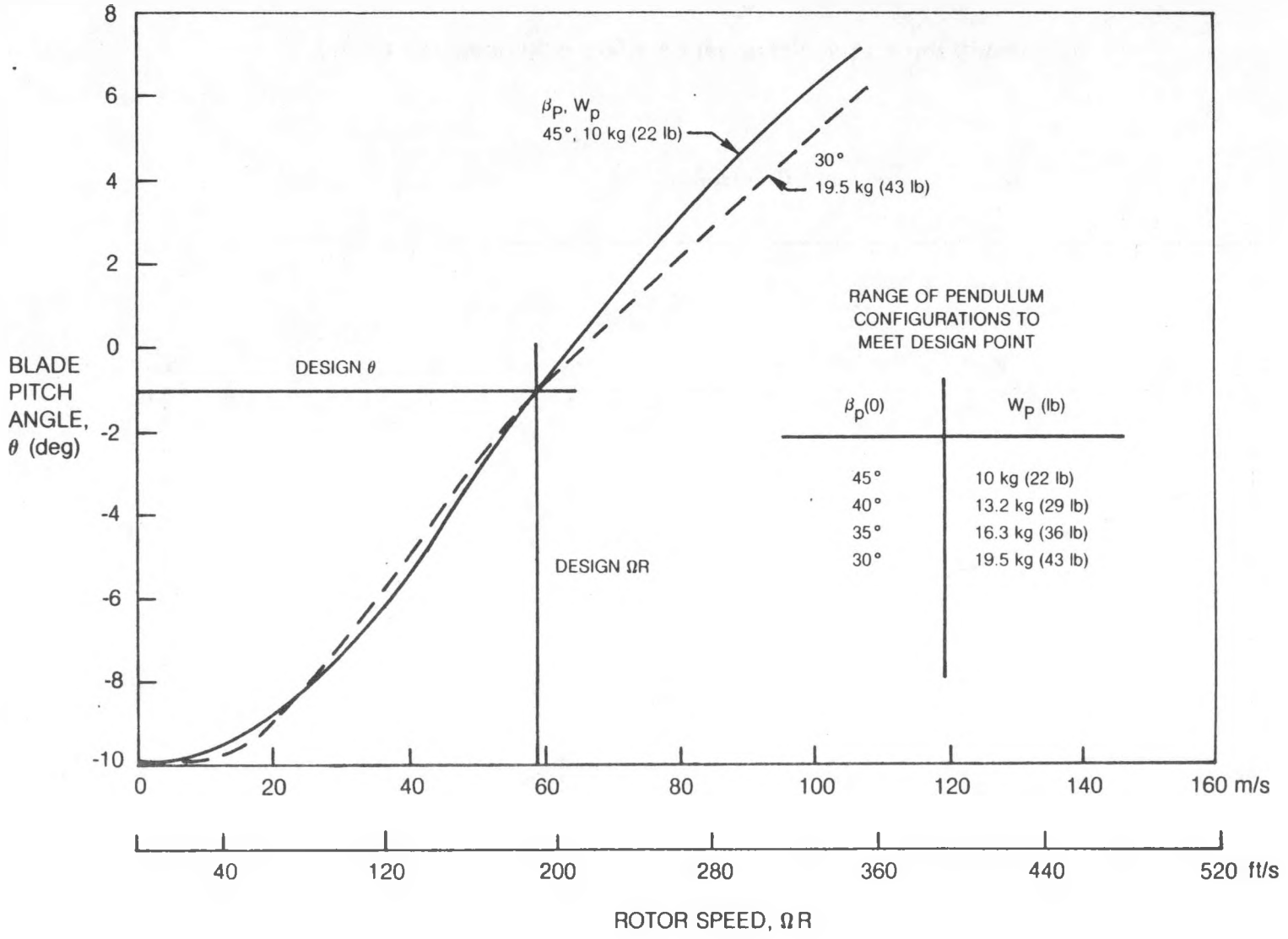

Figure 48. Blade Pitch Angle Variation (θ) with Rotor Speed (Ω R)

81-6-164-74

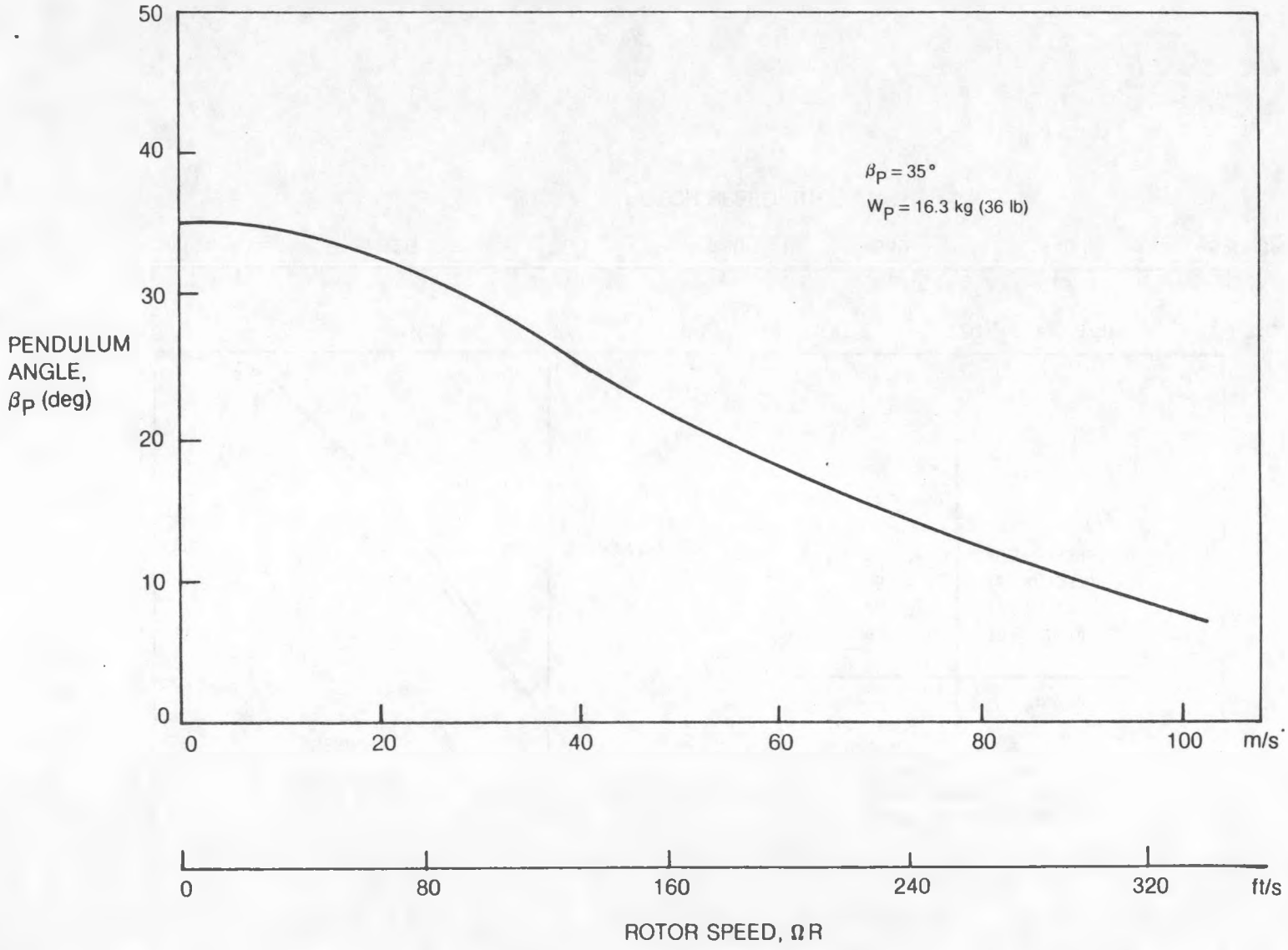

Figure 49. Pendulum Angle Variation (β_P) with Rotor Speed (ΩR)

81-6-16-75

It should be noted that changes in both of these parameters can be easily implemented on the prototype if test results prove that changes are required. Pendulum weight can be added or deleted and the initial pendulum angle can be changed by altering the angle of attachment to the flexbeam.

Tower Design and Erection

The primary objectives of the tower design were to minimize cost and improve appearance. To best achieve these objectives, a tapered stand-alone tower was selected. The principal design-limiting parameter for the stand-alone tower proved to be vibration frequency constraints imposed by rotor speed and blade characteristics. The first and second tower bending frequencies had to meet the requirements that the first mode frequency be less than 1.05 Hz and the second mode above 6.0 Hz in order to ensure a dynamically stable system and also to minimize dynamic response. Restriction of the first tower frequency to less than 1.05 Hz avoids the resonant condition at one-per-rev over the operating range as shown previously in Fig. 44. Also, restricting the second tower mode frequency to greater than 6 Hz avoids a potential coalescence with a coupled tower/blade in-plane mode. Such a coalescence may induce the transfer of a high level of energy from the rotating rotor system into the fixed tower and thus cause high tower motions. This is discussed in more detail in Ref. 2. These tower frequency requirements, in conjunction with the need to meet design loads, placed severe restrictions on tower configurations. The effective tower bending stiffness required for proper frequency placement had to be correlated with the section modulus, I/C, required to withstand the combined tower loading for a viable tower configuration. Figure 50 summarizes the design loads for the tower. These loads are taken from the results presented in the critical load section previously discussed. In addition, the effect of icing (up to 25-mm (1-in.) thickness) and the effects of relative humidity and rain on tower aerodynamic drag are also included.

Based on the tower tradeoff studies previously discussed, the final tower design is a tapered, 10-sided, aluminum pole. Figure 51 is a schematic of this design and Fig. 52 shows the distribution of EI and mass for the tower. Figure 53 shows the stress and deflection of the selected tower configuration for the 56 m/s (125 mph) design condition.

The base of the tower consists of an aluminum plate 1.22 m x 1.09 x 76 mm (48 in. x 43 in. x 3 in.) which is welded to the base of the tapered tower pole. As shown in Fig. 54, the tower base plate has two hinge pins 63-mm (2.5-in.) diam so that the tower can be rotated to the vertical position during erection. This procedure will be discussed more fully in the next section.

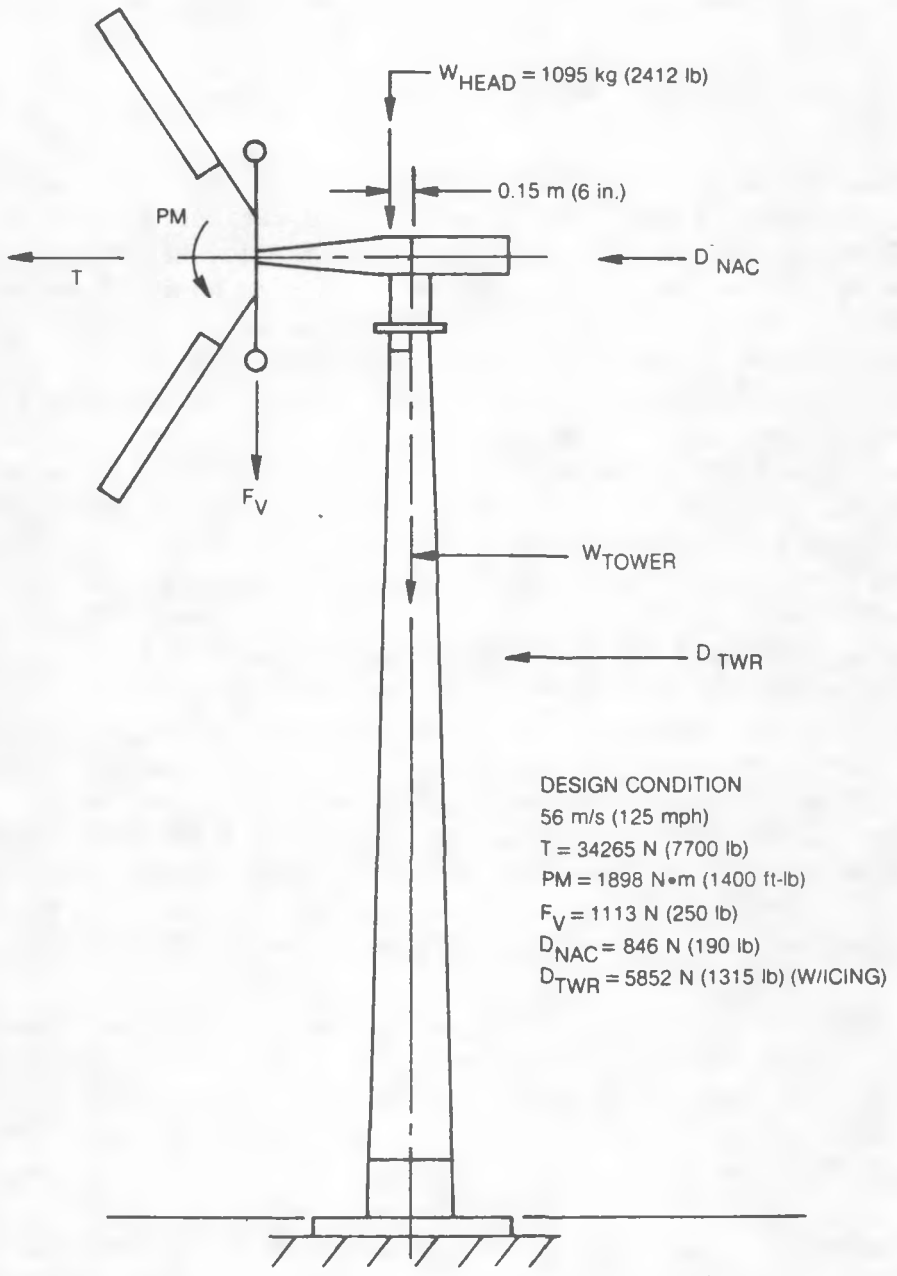

Figure 50. Tower Design Load

81-6-164-66

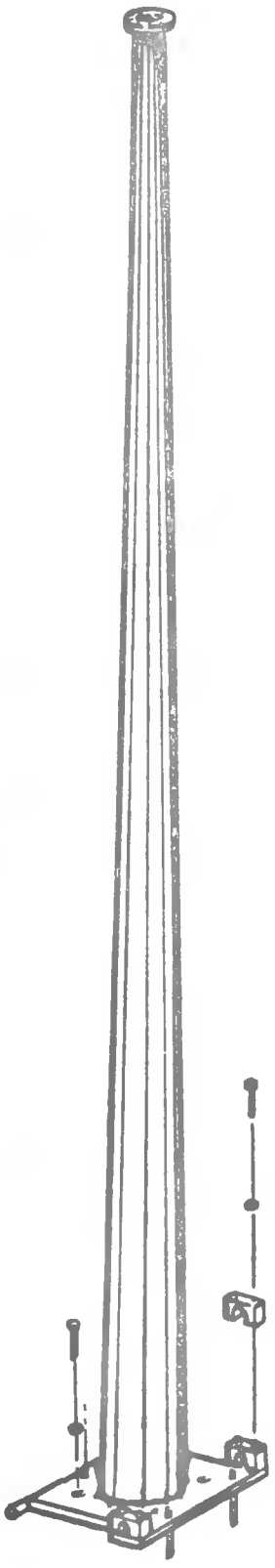

Figure 51. 15-kW Tower Assembly

81–6–164–71

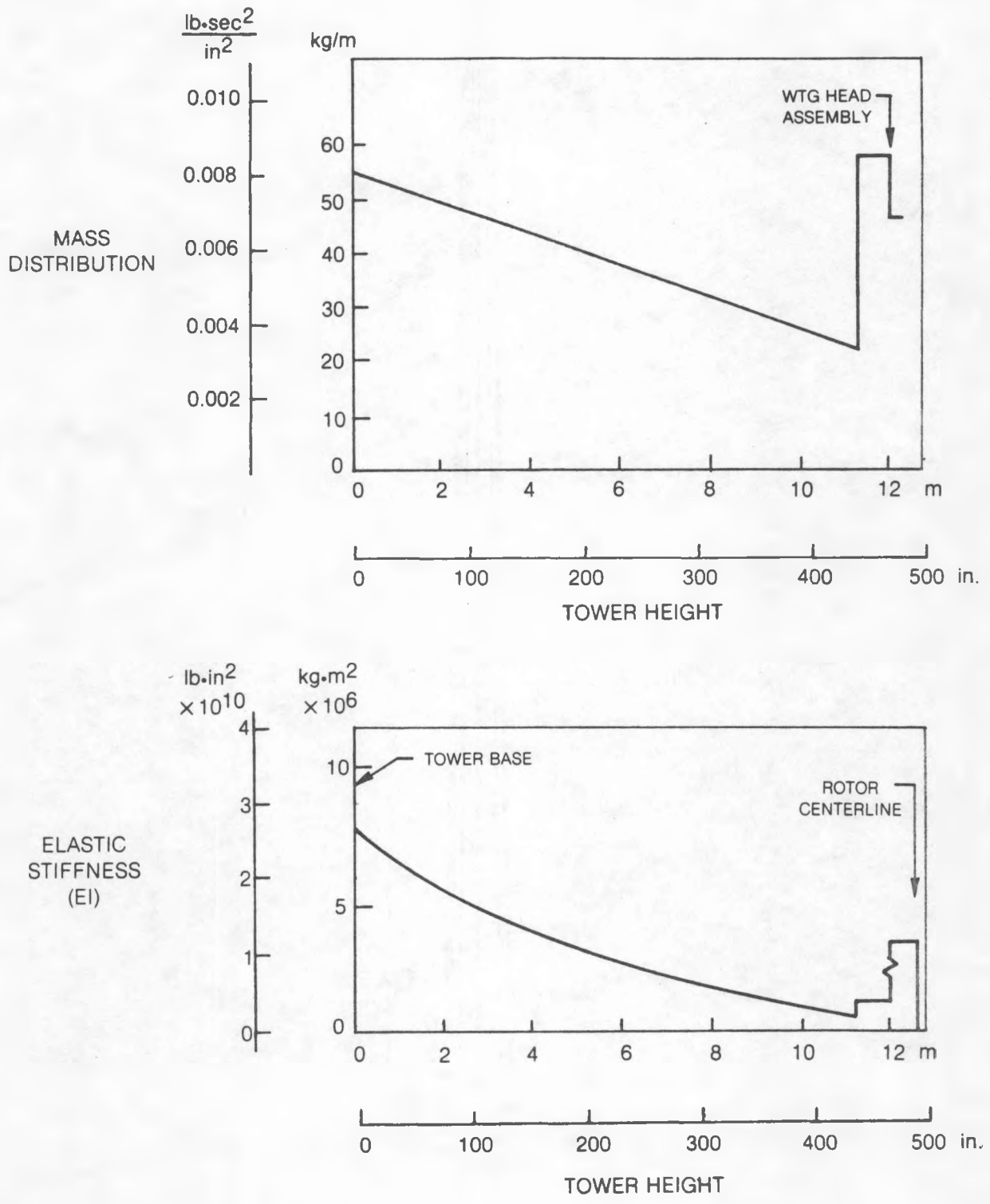

Figure 52. Tower Elastic Stiffness and Mass Distribution

81-6-164-77

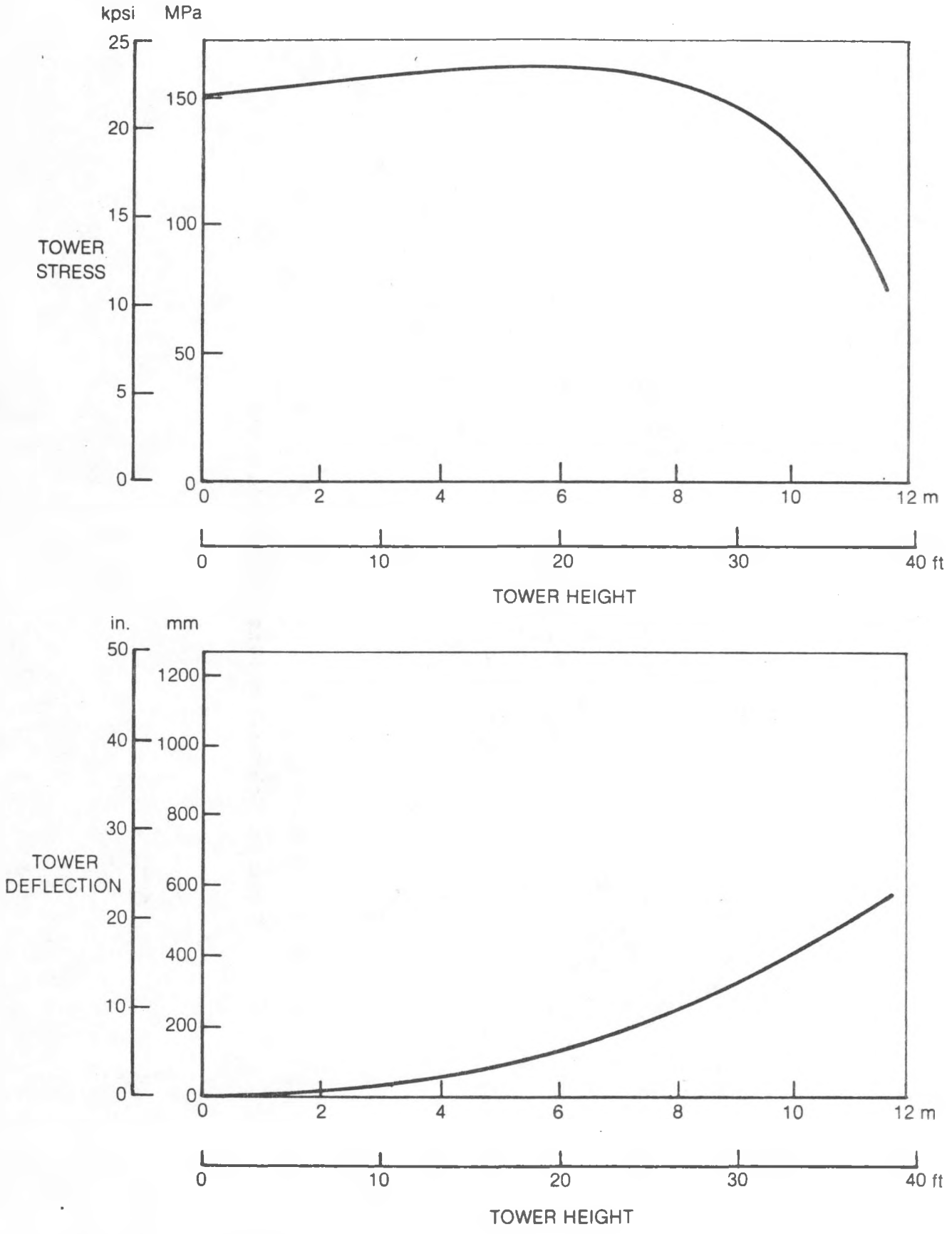

Figure 53. Tower Stress and Deflection for 56 m/s (125 mph) Design Condition

81-6-164-57

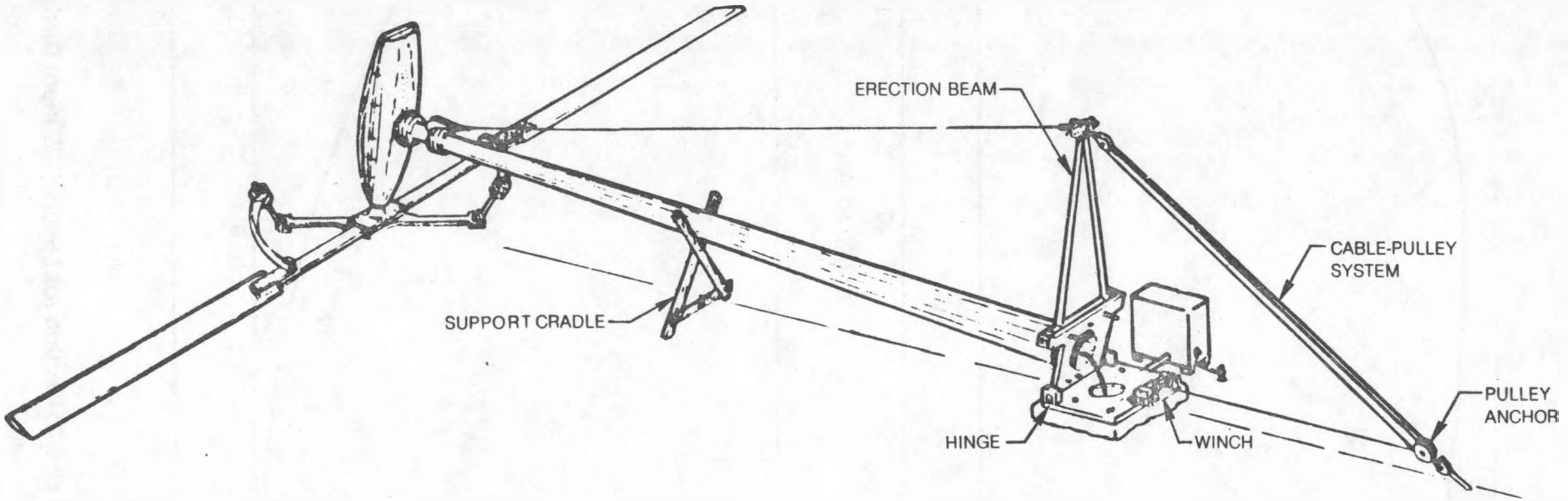

Figure 54. Schematic of Tower and Erection Device

81-6-164-39

Tower Erection System

The tower erection system consists of an erection boom, cable-pulley system, and winch. The system is designed to raise the tower from a horizontal position to a vertical operational condition within 30 min with a two-man crew. Figure 54 is a schematic of the tower and erection system. The tower is supported by a cradle before the erection operation begins and is configured to pivot about 63-mm (2 1/2-in.)-diam hinge pins on the tower base plate. The hinge pins are held in yokes attached to the foundation top plate which in turn is secured to the tower foundation. A boom and cable are used to rotate the tower to the vertical position. The boom is a triangular frame 3-m (10-ft) high and 1.2-m (4-ft) wide at the base and is made of aluminum pipe 89-mm (3.5-in.) OD x 5.5-mm (0.216-in.) wall. The base of the erection boom is secured by yokes to the base of the tower, as shown in Fig. 55. A lifting cable made of 16-mm (0.625-in.)-diam steel wire rope is attached to the top of the tower with a cable bracket, thimble and clamp, and is also attached to the top of the erection boom. A double-pulley system using 10-mm (0.375-in.)-diam steel wire rope connects the top of the erection boom to a pulley anchor, as shown in Fig. 55. The end of the wire rope is drawn up by a 12-V winch, which is secured to the foundation top plate. As the wire rope is drawn in by the winch, the tower rotates to the vertical position. The tower base is shimmed in order to level the WTG before the main tower bolts are threaded into the foundation and tightened.

Test Site Design

The test site consists of a foundation for the wind turbine tower and the pulley anchor needed for erection of the tower. This section discusses the design of each of these items.

Foundation

The design of the foundation is primarily based upon the requirement of the rotor to operate without an electrical load at high wind speeds, resulting in high rotor speeds. For these high wind conditions, the rotor creates large aerodynamic lifting forces in the horizontal plane, since the rotor disc is vertical. With the tower effectively cantilevered as previously described, a large moment and horizontal shear force act on the base of the foundation. This is shown in Fig. 56. Other forces act on the wind system, but the aerodynamic lifting force on the blades and resulting moment about the base of the foundation are dominant.

The foundation design consists of a steel-reinforced concrete pad with a pattern of bolts imbedded in the foundation surface to secure the tower to the foundation. The top of the foundation is square and the depth is greater than the top width dimension by more than a factor of two. The size of the foundation will vary with soil conditions, but for an assumed soil condition (in this case mediocre soil

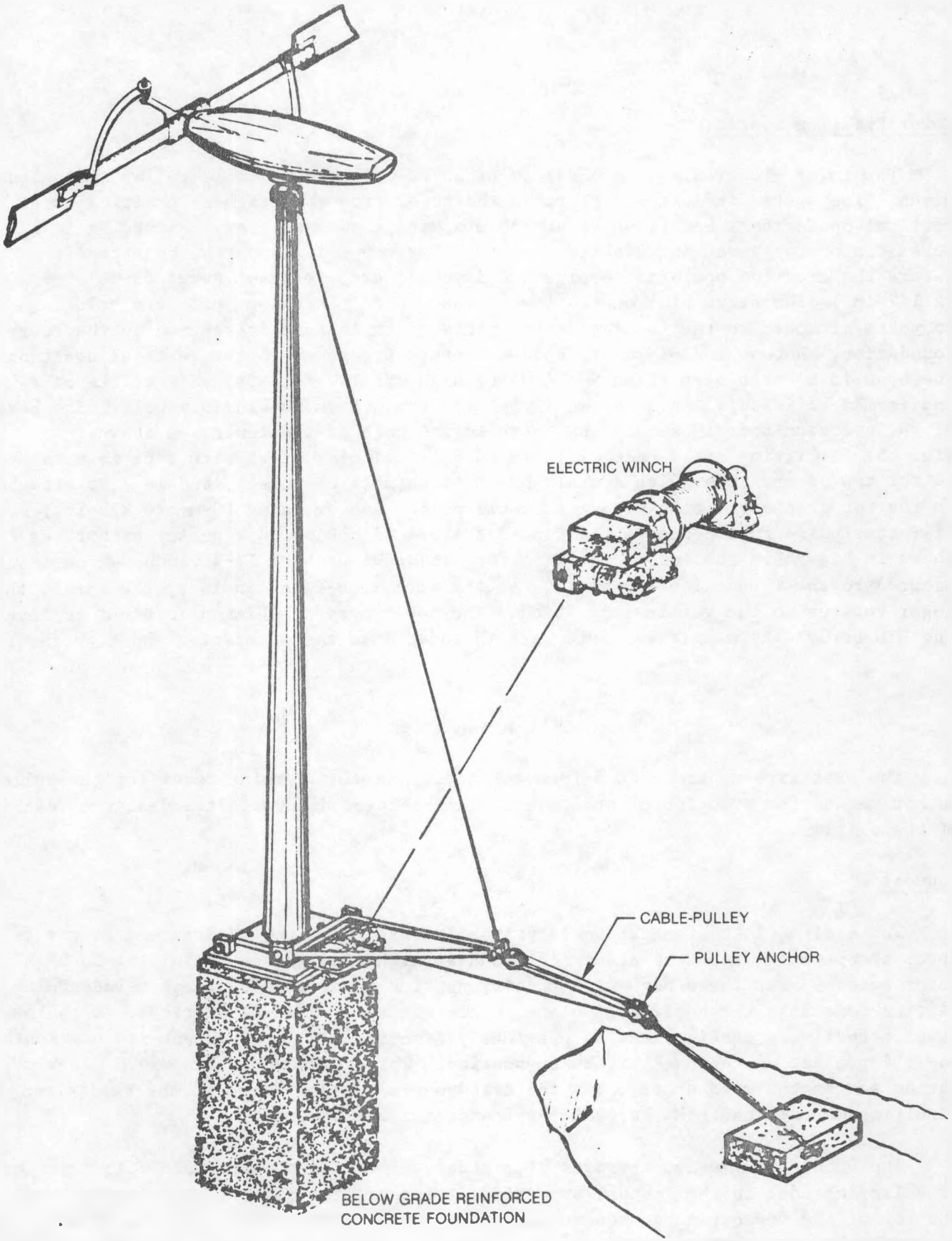

Figure 55. Foundation and Tower in Erected Position

81-6-164-64

	56 m/s 125 mph	74 m/s 165 mph	ERECTION
F_X	44,500 N 10,000 lbf	68,975 N 15,500 lbf	29,815 N 6,700 lbf
F_Z	14,240 N 3,200 lbf	14,685 N 3,300 lbf	29,815 N 6,700 lbf
M	490,800 N-M 362,000 lbf-ft	741,700 N-M 547,000 lbf-ft	—

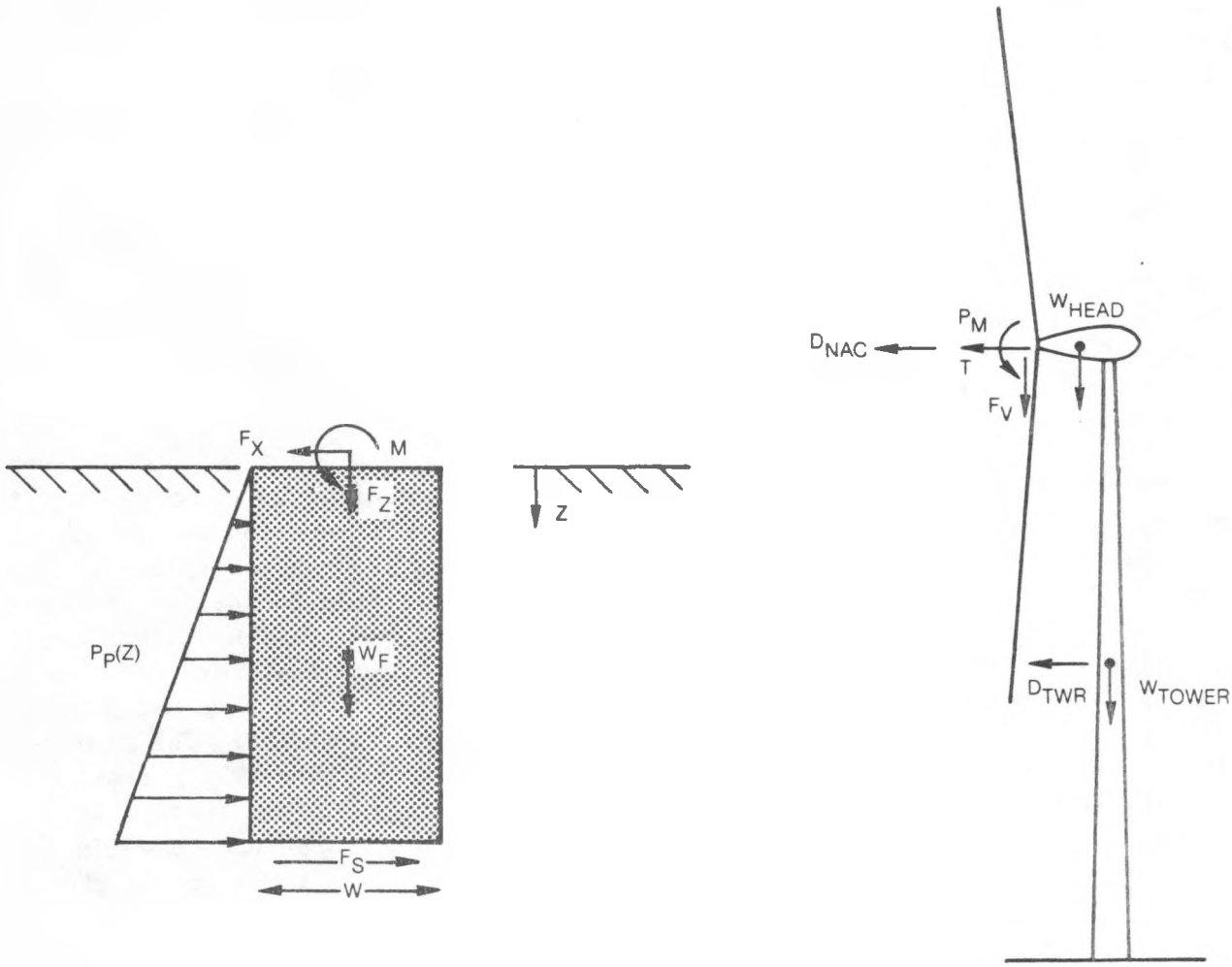

ASSUMED SOIL CHARACTERISTICS
BEARING CAPACITY — 1,916,000 Pa (40,000 lb/ft^2)
PASSIVE PRESSURE P_P — 19,160 Pa (400 lb/ft^2/ft depth)
DENSITY γ — 1602 kg/m^3 (100 lb/ft^3)
FRICTION COEFFICIENT — 0.3

Figure 56. Foundation Design

81-6-164-69

strength), a foundation design can be developed for the applied loads. As shown in Fig. 57, the loads for two high speed wind conditions were considered since they are greater than the loads incurred during erection of the system. These loads were taken from the theoretical predictions presented previously.

To maintain foundation stability, the foundation presses against the base soil for vertical loading and maintains shear resistance (plowing the soil) and moment resistance (tilting of the foundation about a corner). Therefore, the frontal area and bottom surface area of the foundation are the primary parameters, since the soil provides a resisting force proportional to surface area. The soil resistance force is also a linear function of depth, so depth of the foundation is also important.

The assumed soil characteristics are shown in Fig. 56. Based on these characteristics, the size of the foundation can be calculated for both high speed wind conditions, as shown in Fig. 57. A foundation width of 1.5 m (5 ft) was selected as suitable for tower placement and erection. A smaller width would be adequate but this increases the depth of the foundation. Based upon the 1.5-m (5-ft) width, the foundation depth is 3.7 m (12 ft) for the 56-m/s (125-mph) condition and about 4.3 m (14 ft) for the 74-m/s (165-mph) condition.

The design of the steel reinforcement for the foundation is shown in Fig. 58. The reinforcement is composed of a) a columnar steel grid centered on the top of the foundation to transfer the loading from the tower into the foundation and b) three horizontal grids, at the top, middle and bottom of the foundation, to react to the applied moment. The reinforced steel surface area and cross-sectional area requirements have been calculated per the American Concrete Institute (ACI) code. Table XV summarizes the steel and concrete requirements. The design and placement of the tower anchor bolts and couplings are shown in Fig. 59. The size requirements of these bolts and couplings are also shown in Table XV. A steel plate is placed on top of the foundation and serves two purposes. First, it provides a surface upon which to place yokes for the tower base pins used in erection. Second, the plate spreads the gravity load of the tower across the top of the reinforced concrete foundation.

Pulley Anchor

The previous section on tower erection showed that a pulley/winch system is used to erect the tower. As shown previously in Fig. 54, the pulley is placed in-line with the plane of rotation of the tower. A ground anchor is used to support the pulley. The design of the anchor is shown in Fig. 60. The anchor is a reinforced concrete block with an imbedded steel anchor rod. The anchor rod design is a standard Rohn product used specifically for anchor applications (e.g., guy wires for towers). The angle of the anchor rod with the horizontal (58°) is placed along the line of action from the top of the erection boom to the ground pulley location.

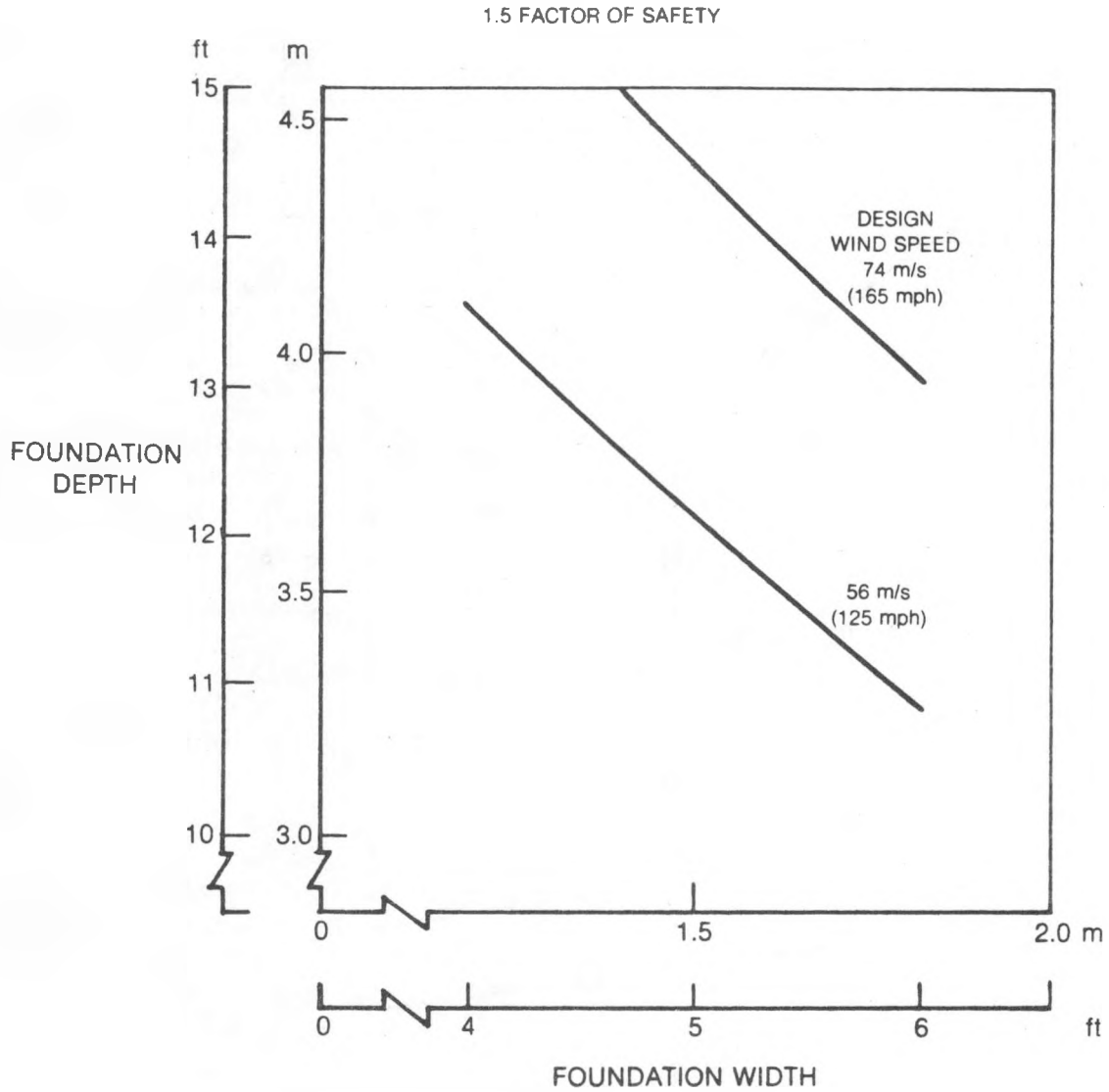

Figure 57. Size of Tower Foundation

81-6-164-36

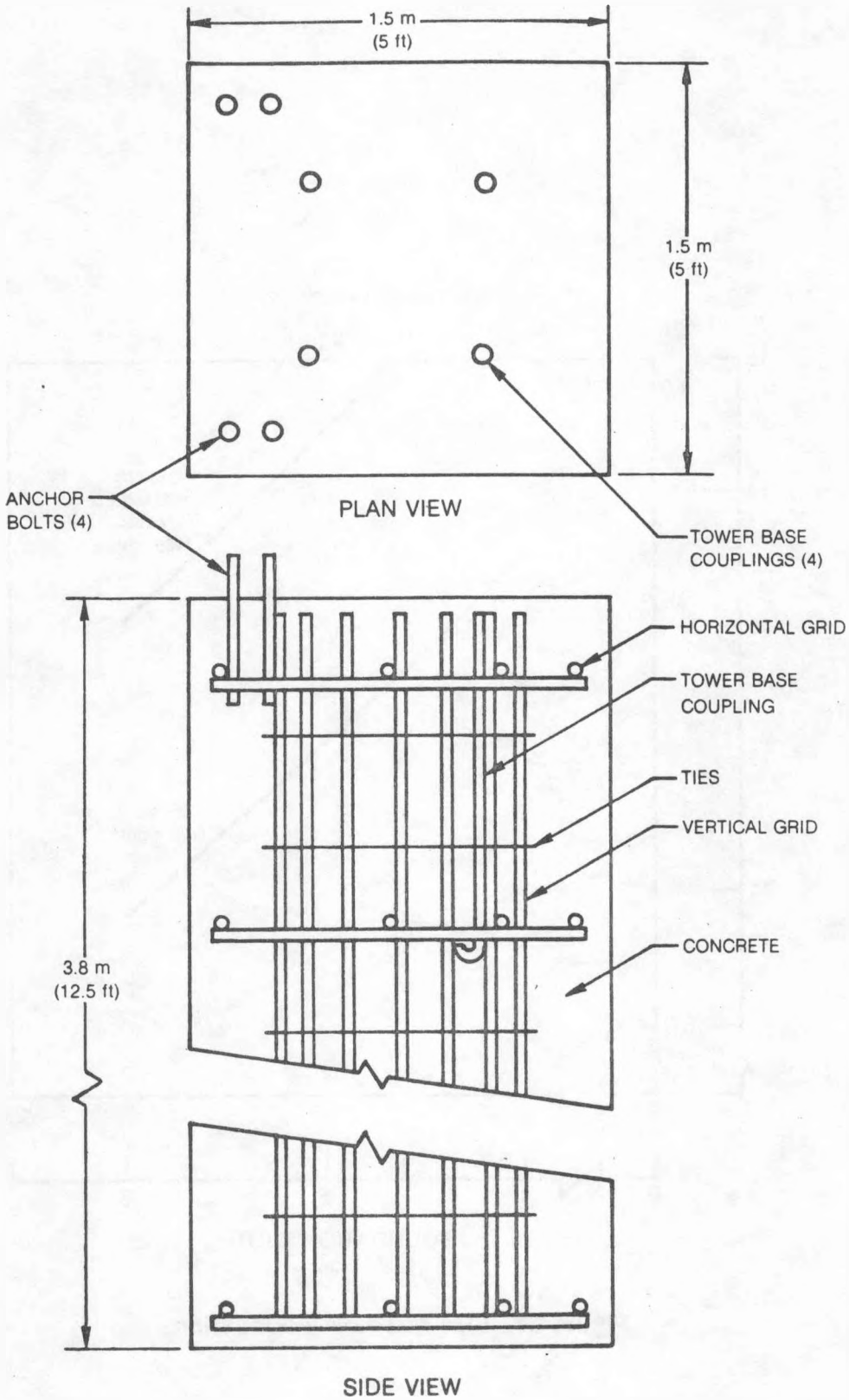

NOTE: REQUIREMENTS MAY VARY ACCORDING TO SPECIFIC SITE CONDITIONS AND LOCAL CODES

Figure 58. Schematic of Typical Tower Foundation Showing Steel Reinforcement

81-6-164-37

TABLE XV

TYPICAL FOUNDATION AND ANCHOR MATERIAL REQUIREMENTS

56-m/s (125-mph) Wind Condition

	Foundation
Concrete 17.2 MPa (2500 psi):	8.5 m^3 (11.1 yd^3)
Horizontal Steel Bar:	20 No. 7 Bar Each 1.37-m (54-in.) long
Vertical Steel Bar:	24 No. 10 Bar Each 2.67-m (105-in.) long
Steel Tie Bar:	7 No. 2 Bar Each 3.81-m (150-in.) long
Anchor Bolts:	4 38-mm (1.5-in.) diameter 558-mm (22-in.) long
Couplings:	4 38-mm (1.5-in.) diameter 1.22-m (4-ft) long
Top Plate:	1.22 m x 1.09 m x 76 mm (48x43x3in.)

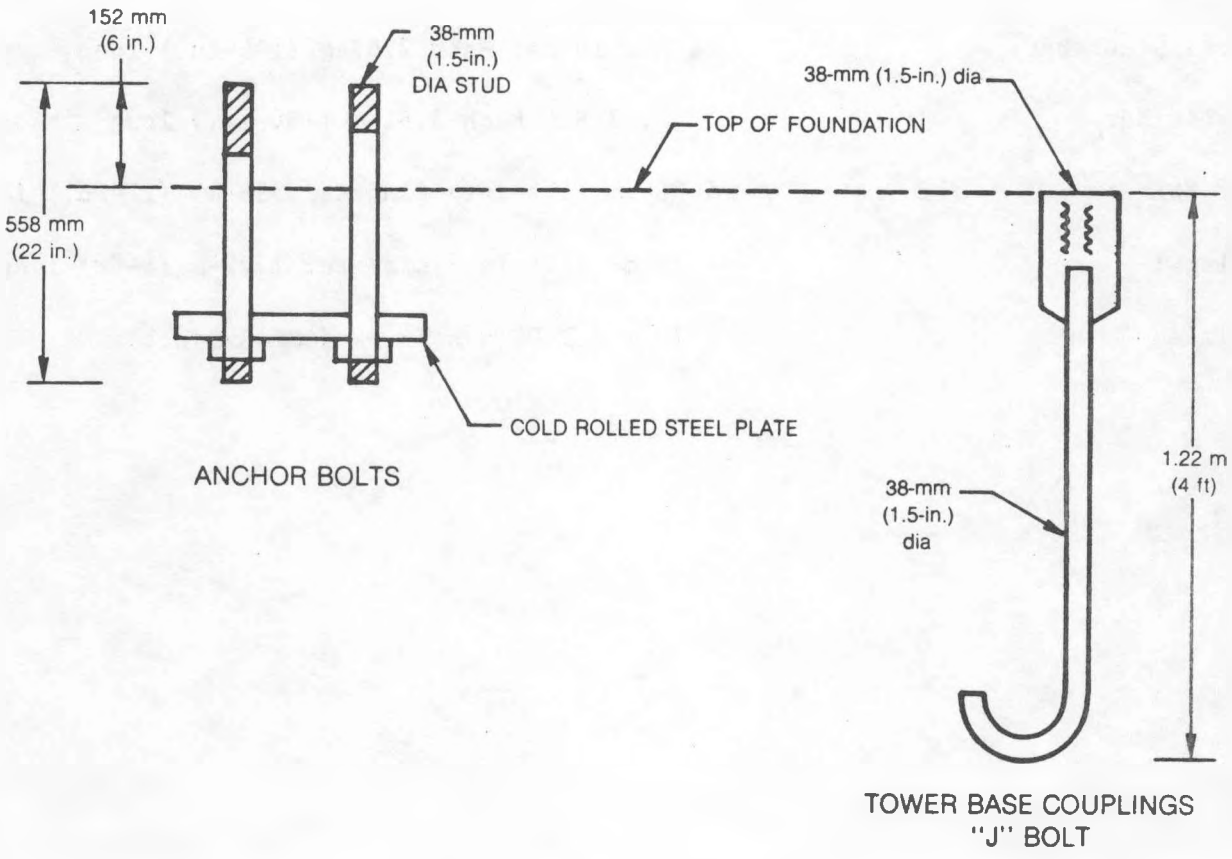

Figure 59. Schematic of Anchor Bolts and Couplings in Top of Foundation Used to Install and Secure Tower

81-6-164-38

PULLEY ANCHOR ASSEMBLY

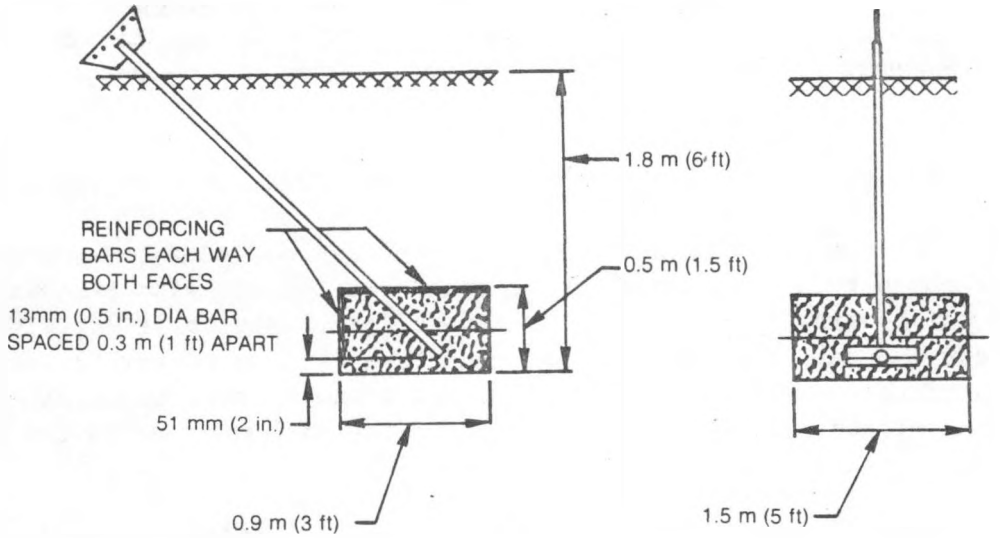

NOTE: ASSUMED SOIL PRESURE OF 595 kg/m^2 depth (400 lb/ft^2/depth)

ANCHOR ROD DETAIL

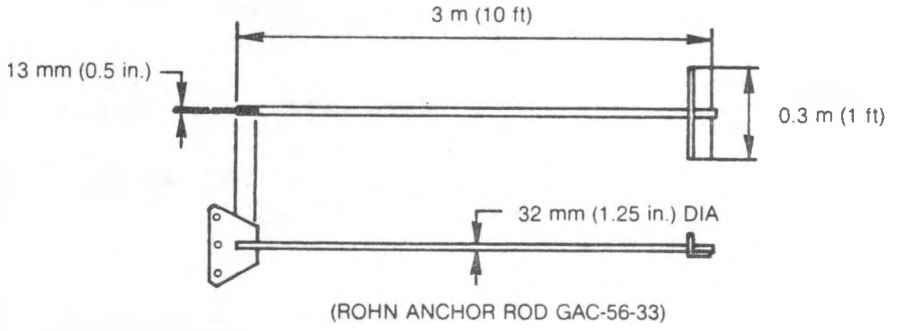

Figure 60. Schematic of Typical Pulley Anchor

81-6-164-68

AEROELASTIC ANALYSIS

In addition to the calculation of predicted loads and stresses for the design of the WTG, analyses of the other pertinent areas of rotor aeroelastics were performed to support the design.

The Effect of Flexbeam Twist on Blade Edgewise Frequency

The UTRC E159 uncoupled blade frequency analysis was used to ascertain the effect of flexbeam twisting at high rotor speeds on the edgewise frequency. This is an important consideration since reduction of the first rotor edgewise frequency may cause a catastrophic resonant condition at one-per-rev frequency. From calculations of the pendulum schedule the maximum amount that the flexbeam can twist between the untwisted condition at start-up and the high wind condition at 102-m/s (350-ft/s) tip speed is 16°.

To model the effect of the twisting, the edgewise stiffness was multiplied by the cosine of 16° (0.961) for the entire length of the flexbeam. This is a conservative estimate since the flexbeam twists linearly from the hub to the end of the flexbeam. The edgewise frequency of the twisted flexbeam configuration is compared to the untwisted frequency in Table XVI.

TABLE XVI

EFFECT OF 16° OF FLEXBEAM TWIST ON FIRST EDGEWISE FREQUENCY AT 350-ft/s TIP SPEED

Flexbeam Twist	First Blade Edgewise Frequency	
0°	4.15Hz	1.788 per rev
16°	4.10	1.723

These results demonstrate that flexbeam twisting of 16° has only a small effect on edgewise frequency at high tip speeds.

Effect of Air Density on Wind Turbine Performance

A brief analytical study was conducted to determine the effect of air density on the aerodynamic performance of the 15-kW wind turbine. The objective was to see how performance varied between near-sea-level conditions at East Hartford and 1829-m (6000-ft) elevation at the Rocky Flats, CO, site.

The UTRC F762 analysis was used to simulate the 15-kW wind turbine at the 12-m/s (26-mph) wind condition. The simulation includes a flexible tower and free pendulum. Variations in air density were made by changing air temperature and altitude.

Figure 61 summarizes the effect of air density on rotor thrust, torque, and coning. The change in all three parameters is nearly linear and in direct proportion to the change in air density. On a cool day, 15°C (59°F), or a hot day, 35°C (95°F), the loss in wind turbine power input between sea level and 1829-m (6000-ft) altitude at Rocky Flats is about 17%. The corresponding decrease in air density is about 19-20%.

The fact that rotor thrust and torque vary in direct proportion to air density is important because this implies that the blade pitch angle is essentially independent of changes in coning with air density. The low sensitivity of blade pitch angle to coning is shown in Fig. 62. Referring to the upper dashed line, the change in blade pitch angle is only 0.26° for a change in density ratio of 0.25, and the gradient with coning ($d\theta/d\beta c$) is +0.085.

The low gradient is due to the interaction of two parameters: delta-3 coupling and lift offset moment. The isolated effect of delta-3 coupling is shown by the solid line in Fig. 62. When the pendulum is fixed and the air density is varied, the new gradient with coning is -0.41. This is the true delta-3 effect since the pendulum is restrained. In reality the pendulum rotates about its hinge to equilibrate centrifugal force applied moments. The freedom to move considerably softens the delta-3 effect, as shown by the lower dot-dashed line. With no lift offset (blade chordwise aerodynamic center on the shear center axis) and a free pendulum, the gradient of pitch angle with coning (softened delta-3) is now -0.167.

The effect of the lift offset moment is to negate the delta-3 effect. With the aerodynamic center ahead of the shear center, increased lift, as evidenced by increased coning, produces a nose-up pitch moment on the blade flexbeam which causes the pitch angle to increase. For the 15-kW blade with a +7% lift offset, the resulting lift moment more than cancels the delta-3 effect so that the final gradient, including delta-3 and lift offset, is slightly positive (+0.085).

From these results it can be concluded that, when the pendulum is free to interact with blade flapping and blade pitch, the new pitch-flap coupling is small. Because the resulting change in blade pitch angle with reduced coning is small, there is little to be gained by readjusting the pendulum configuration for high altitude conditions.

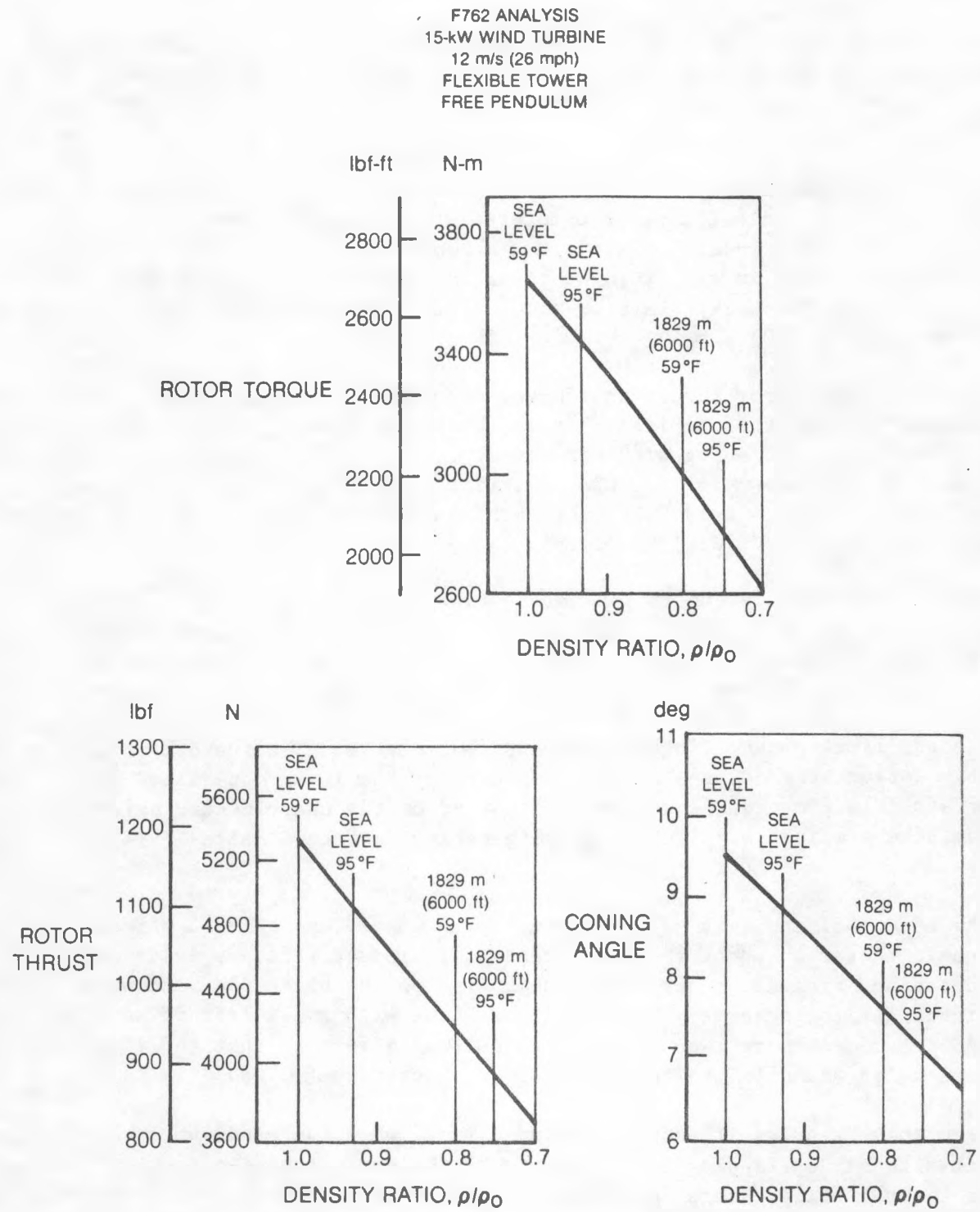

Figure 61. Effect of Air Density on Rotor Torque, Thrust and Coning

81-6-164-35

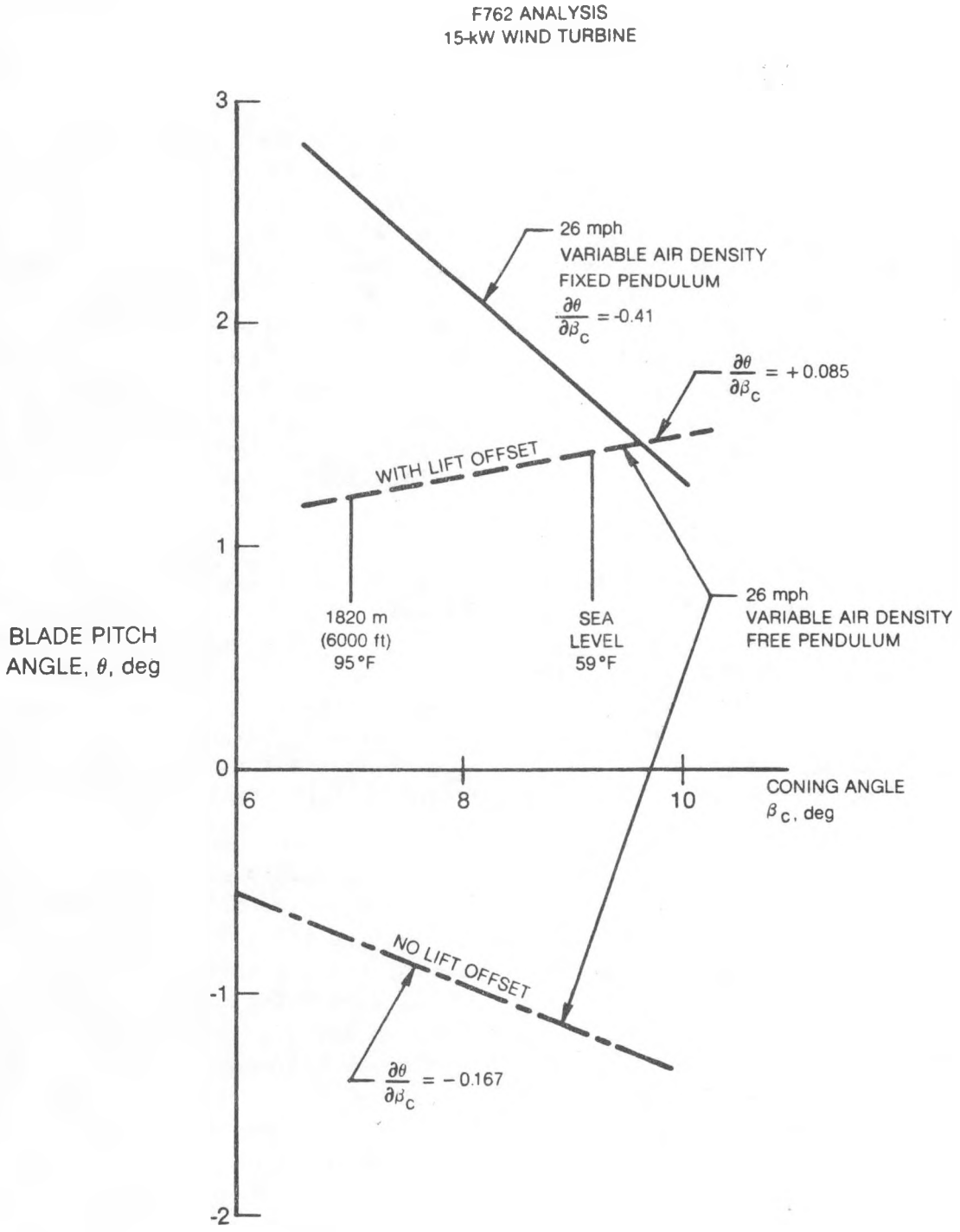

Figure 62. Predicted Pitch-Flap Coupling with Air Density

81-6-164-34

PERFORMANCE

The design characteristics of the UTRC 15-kW wind system were shown in Table I and the power output as a function of wind speed is shown in Fig. 63. The required wind speed at the hub height before the wind turbine will generate power is 4 m/s (9 mph). At wind speeds of 7 m/s (15 mph) and 9 m/s (20 mph) the power output increases to 9.5 and 17.2 kW, respectively. The peak output is 22.4 kW which occurs at a wind speed of 12.5 m/s (28 mph). At higher wind speeds the power output falls off. At wind speeds between 18 - 20 m/s (40-45 mph) it is expected that the wind turbine will produce between 8 and 10 kW. This expectation is based on the wind tunnel tests of a 3.2-m (10.5-ft)-diam model wind turbine which showed similar characteristics. Calculated rotor performance data show the power output decreasing to zero at wind speeds above 18 m/s (40 mph). Therefore, the expected power output is shown as a dashed line for wind speed above 17 m/s (38 mph).

The efficiency of the rotor, gearbox, and generator are shown, in Fig. 64, as a function of wind speed. The peak rotor efficiency of 40.8% occurs at a wind speed of about 6 m/s (14 mph) and falls off to 15.4% at the rated wind speed of 12.5 m/s (28 mph). The transmission has a peak efficiency of 96% at rated torque and wind speed. At the cut-in wind speed the transmission efficiency is about 70%. The generator peak efficiency is 84% which occurs at a wind speed of about 7 m/s (15 mph). Combining the efficiencies of the rotor, transmission, and generator give the overall efficiency as shown. The peak overall efficiency is about 30% which occurs at a wind speed of 7 m/s (15 mph).

Combining the output power (Fig. 63) with the frequency of occurrence of wind speeds during a year gives an estimate of the UTRC wind turbine annual energy capture, as shown in Fig. 65. The wind speed distribution was assumed to follow a Rayleigh distribution function for frequency and the 1/7 power law with elevation. A tabulation of the energy capture performance as a function of the site mean wind speed is given in Table XVII. The design mean wind speed is 5.4 m/s (12.1 mph) for which condition the UTRC 15-kW system will have an annual energy capture of 52,600 kWh at an availability of 90%. The mean power output (i.e., the energy capture divided by 8760 hours in the year) would be 6 kW and the wind will be above the cut-in speed 61% of the time. At wind sites with higher mean wind speeds the energy output increases proportionately.

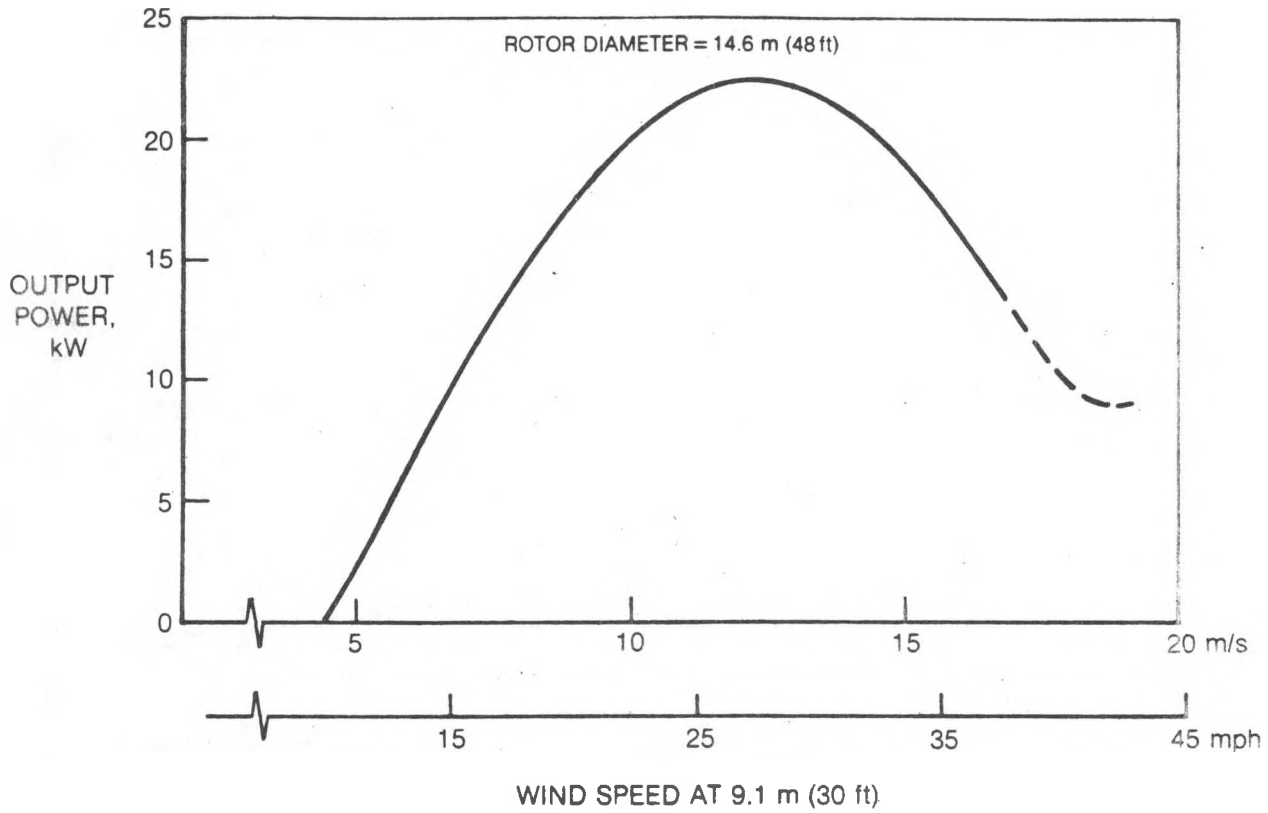

Figure 63. UTRC 15-kW Wind System Power Output

81-6-164-61

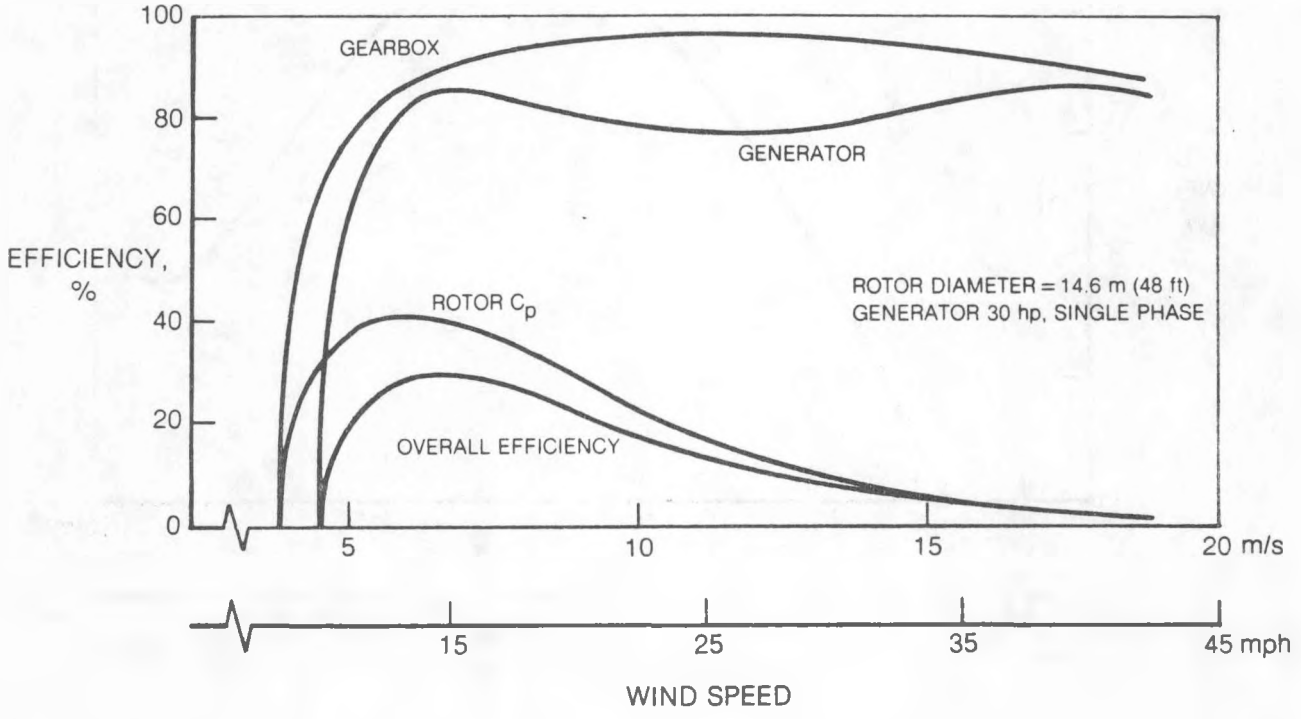

Figure 64. UTRC 15-kW Wind System Efficiencies

81-6-164-33

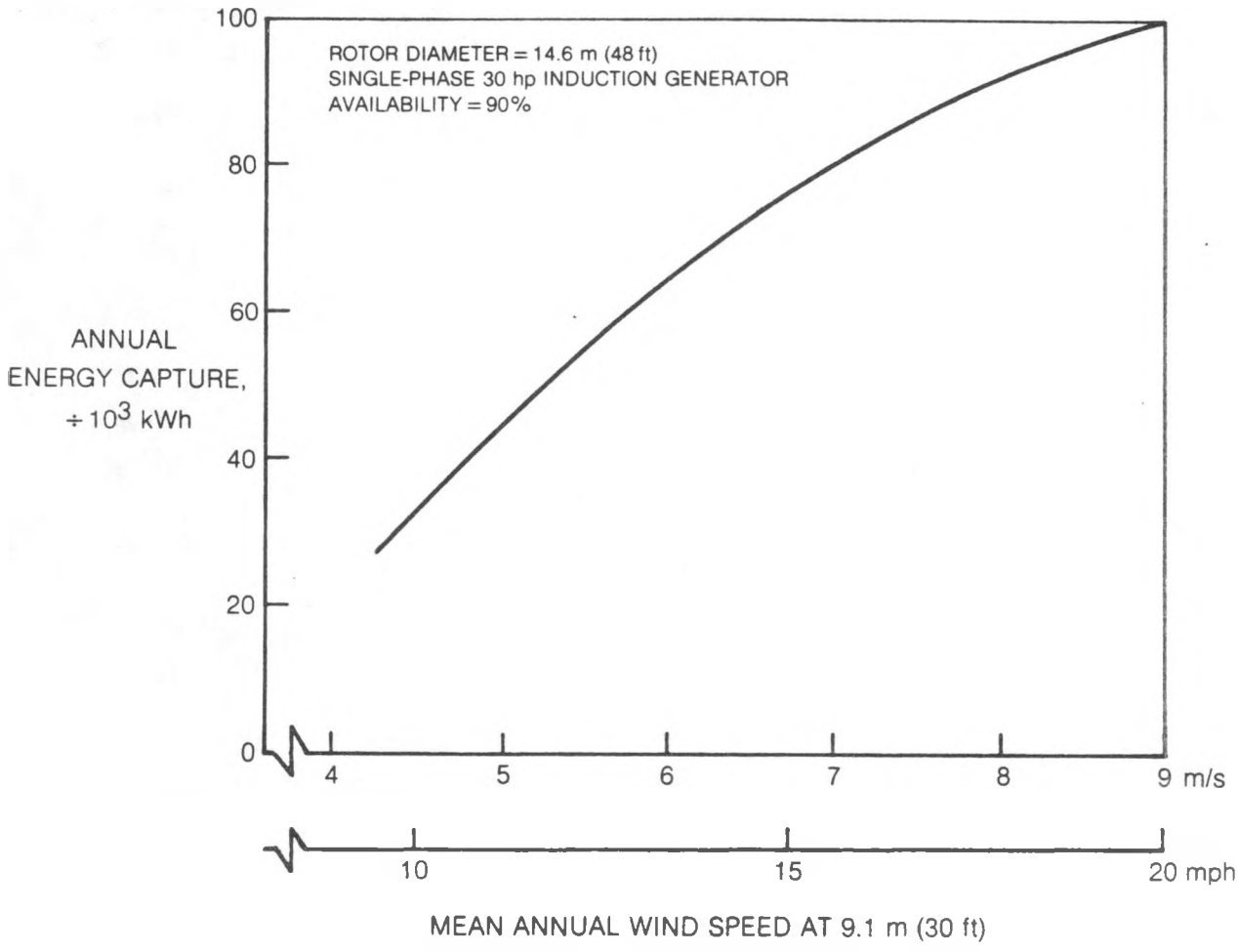

Figure 65. UTRC 15-kW Wind System Energy Capture

81-6-164-62

TABLE XVII

UTRC 15-kW WIND SYSTEM PERFORMANCE

Mean Wind Speed[1]	Annual Output[2]		
m/s (mph)	Energy kWh	Mean Power kW	Power Availability % of Time
4.5 (10.1)	34,100	3.89	49.1
5.4 (12.1)	52,600	6.00	61.0
6.3 (14.1)	69,200	7.89	69.6
7.2 (16.1)	82,700	9.43	75.7
8.1 (18.1)	92,800	10.59	80.3
9.0 (20.1)	99,900	11.40	83.6

(1) Mean wind speed as measured at the standard elevation of 9.1 m (30 ft). The wind frequency distribution profile is assumed to follow a Rayleigh distribution.

(2) Annual output assumes a 90% availability of the system when the wind speed is above cut-in speed.

COST OF ENERGY

The successful commercialization of wind systems depends not only on the development of an efficient prototype design but also on the establishment of an efficient manufacturing and distribution system to produce the system at the lowest possible cost to meet the competition of utility power. As the first step in this process, the hardware weight, material cost and manufacturing labor hours were estimated for the UTRC 15-kW system described earlier in Table I. Table XVIII shows a summary of the weight, material cost and labor hours for annual production rates of 1, 100, 1000, and 10,000 units.

The estimated weight of the production 15-kW system is 1500 kg (3300 lb) of which about 14% is in the rotor and hub assembly, 47% in the head assembly (i.e., transmission, generator and yaw package) and the remaining 39% in the tower and utility interconnect equipment.

Manufacturing Cost Estimate

The rotor blades and flexbeam each have uniform cross sections without twist or taper. As such, they are eminently suited to high-production manufacturing techniques such as fiberglass pultrusions. The blade and flexbeam cost estimates shown in Fig. 66 are based on quotes from Morrison Molded Fiberglass Company. The rotor blades are made of E glass with a prototype cost of $24,600 which includes the die and machine modification costs. The cost of additional blades as a function of annual production rate is listed in Table XVIII. For production rates greater than 1000 units, Morrison estimates that a change in the manufacturing process requiring the modification of the special leading edge and core section will reduce the cost by about 40% as shown by the cross-hatched area in Fig. 66. At these rates, the cost of the blades for the 10,000/yr production rate is $17.00/ft or $2.31/lb.

The flexbeam, because of the high start-up cost associated with the use of S-2 glass, will initially be made of a mixture of graphite and E glass to reduce the cost. But at annual production rates greater than 200 units the cost of the S-2 glass flexbeam is less because of the high cost of the graphite. Table XVIII reflects this change in materials and at the 10,000 unit production rate the flexbeam would cost $27.50/ft or $4.65/lb.

The transmission, designed by FMC, consists of two stages with helical gearing, and also houses the rotor shaft and bearings. In large volume production it is estimated to cost $1,200 or $1.60/lb.

The Baldor induction generator, rated at 22.4 kW, is a single-phase permanent split capacitor design with 120-μF capacitor in series with the auxiliary winding. The price for the generator includes the capacitor and the Stearns brake.

TABLE XVIII

UTRC 15-kW WIND SYSTEM MATERIAL COST AND LABOR SUMMARY*

Annual Production Rate		1st Production		100		1000		10,000	
Component	WT LB	MATERIAL $	LABOR HR	MATERIAL $	LABOR HR	MATERIAL $	LABOR HR	MATERIAL $	LABOR HR
Rotor Assembly									
Blades	246	4620		1290		1000		625	
Flexbeam	60	5400		585		420		330	
Hub Assembly	144	1070	240	760	96	640	60	535	38
Sub Total	450	11090	240	2635	96	2060	60	1590	38
Head Assembly									
Transmission	750	3000		1815		1530		1200	
Generator/Brake	490	1670		1470		1390		1350	
Yaw Assembly	310	1400	160	995	64	840	40	700	26
Sub Total	1550	6070	160	4280	64	3760	40	3250	26
Tower	1200	9000	15	5800	6	4700	4	3800	3
Utility Interconnect									
Cable		175		175		175		175	
Circuit Breaker		150		140		130		125	
Contactor/ Tachometer		500		255		180		125	
Weather Proof Enclosure		225		200		185		175	
Assembly			15		6		4		3
Sub Total	100	1050	15	770	6	670	4	600	3
Assembly & Test			40		16		10		6
TOTAL	3300	27210	470	13485	188	11190	118	9240	76

*1980 dollars

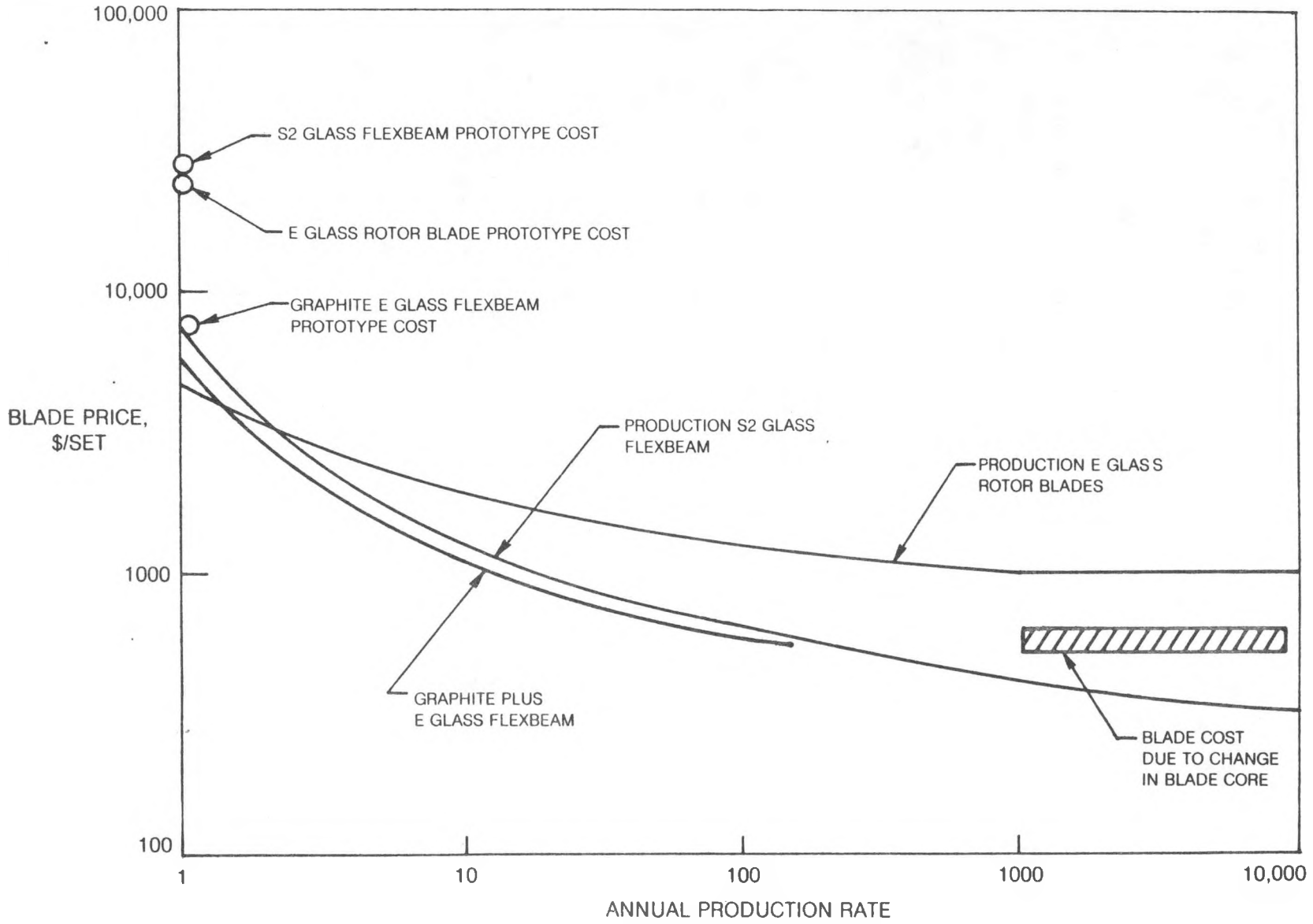

Figure 66. Blade and Flexbeam Unit Cost

81-6-164-70

The tower is a free-standing, 10-sided, tapered aluminum pole, 12-m (39-ft) long with a base diameter of 0.6 m (24 in.) and top diameter of 0.25 m (10 in.). In large volume production it is estimated to cost $3,800, which is 41% of the total system material cost.

Selling Price

The FOB price of the UTRC 15-kW system, shown in Table XIX, is based on increasing the material cost by 17% due to G&A, a fully burdened labor rate of $16/h and a profit of 10%. The selling price of the unit, which includes cost of sales, transportation and distribution system costs, has been estimated at 1.5 times the FOB price. Based on this scenario the selling price for an annual production rate of 10,000 units is $19,800, or about one-third of the single unit production rate price.

Initial Investment

In addition to the direct costs associated with the actual wind system, the total investment includes the installation and foundation costs plus indirect and contingency/spare cost. The installation, including the foundation, is estimated to require three men four days for a total cost of $3,000. Of this cost, $1,535 is for labor and $1,465 is for equipment and materials. The total investment for the 10,000/yr production rate, including installation and indirect cost, is $25,080 as shown in Table XX.

COE

The cost of energy (COE), as given by the equation below, is the ratio of the annualized costs of the wind system divided by the annual energy capture.

$$COE = IC \cdot \left[FCR+AOM\right]/AKWH$$

where
- COE = energy cost, ¢/kWh
- IC = initial investment cost
- FCR = annual fixed charge rate
- AOM = annualized operation and maintenance cost
- AKWH = annual energy capture - kWh/yr

TABLE XIX

UTRC 15-kW SYSTEM PRODUCTION COSTS (1980 Dollars)

Annual Production Rate	FOB Price	Selling Price
1	$43,300	$64,950
100	21,200	31,800
1,000	16,500	24,750
10,000	13,200	19,800

TABLE XX

UTRC 15-kW WIND SYSTEM INVESTMENT

	1980 Dollars	%
Selling Price	19,800	79.0
Installation	3,000	11.9
Direct Costs	22,800	90.9
Indirect Cost (Contingency)	2,280	9.1
Investment	25,080	100.0

The initial investment cost includes all hardware, foundations, site preparation and indirect costs as discussed earlier. For the 10,000/yr production rate the COE of the 15-kW system is estimated to be 4.63¢/kWh (1980 dollars) as shown in Table XXI. This estimate is based on a fixed charge rate of 8.7%, an annualized maintenance cost of 1% of the investment and a site mean wind speed of 5.4 m/s (12 mph). In 1978 dollars the UTRC design has a COE of 3.7 ¢/kWh which is 23% higher than the COE goal of 3 ¢/kWh.

To reach the 3 ¢/kWh COE, the UTRC system would have to be installed at a wind site with a mean speed of 6.0 m/s (13.5 mph) as shown in Fig. 67. Over the mean wind speed range of 4.5-8.2 m/s (10-18 mph) the COE in 1978 dollars varies between 5.7 and 2.1 ¢/kWh respectively.

Efforts to reduce the COE will be focused on improving the energy capture and reducing the first cost. The energy capture can be improved by continuing the search for a more efficient single-phase generator, the incorporation of twist in the rotor blade, and the reduction of mechanical losses in the system. Through these efforts, it is expected that the energy capture would increase about 5%.

During the prototype development, testing is planned to determine if the power sliprings can be eliminated from the system, which would reduce the installed cost by about 2%. The tower represents the largest single cost assembly in the system and therefore offers the best opportunity to reduce the system cost significantly. With an aggressive cost reduction program it is estimated that the COE could eventually be reduced to 3.2¢/kWh.

TABLE XXI

UTRC 15-kW WIND SYSTEM COE

Investment	$25,080
Annual Costs (1980 Dollars)	2,433
Energy Capture, kWh/yr	52,600
COE (1980 Dollars)	4.63
COE (1978 Dollars)	3.70
COE Relative to Goal	1.23

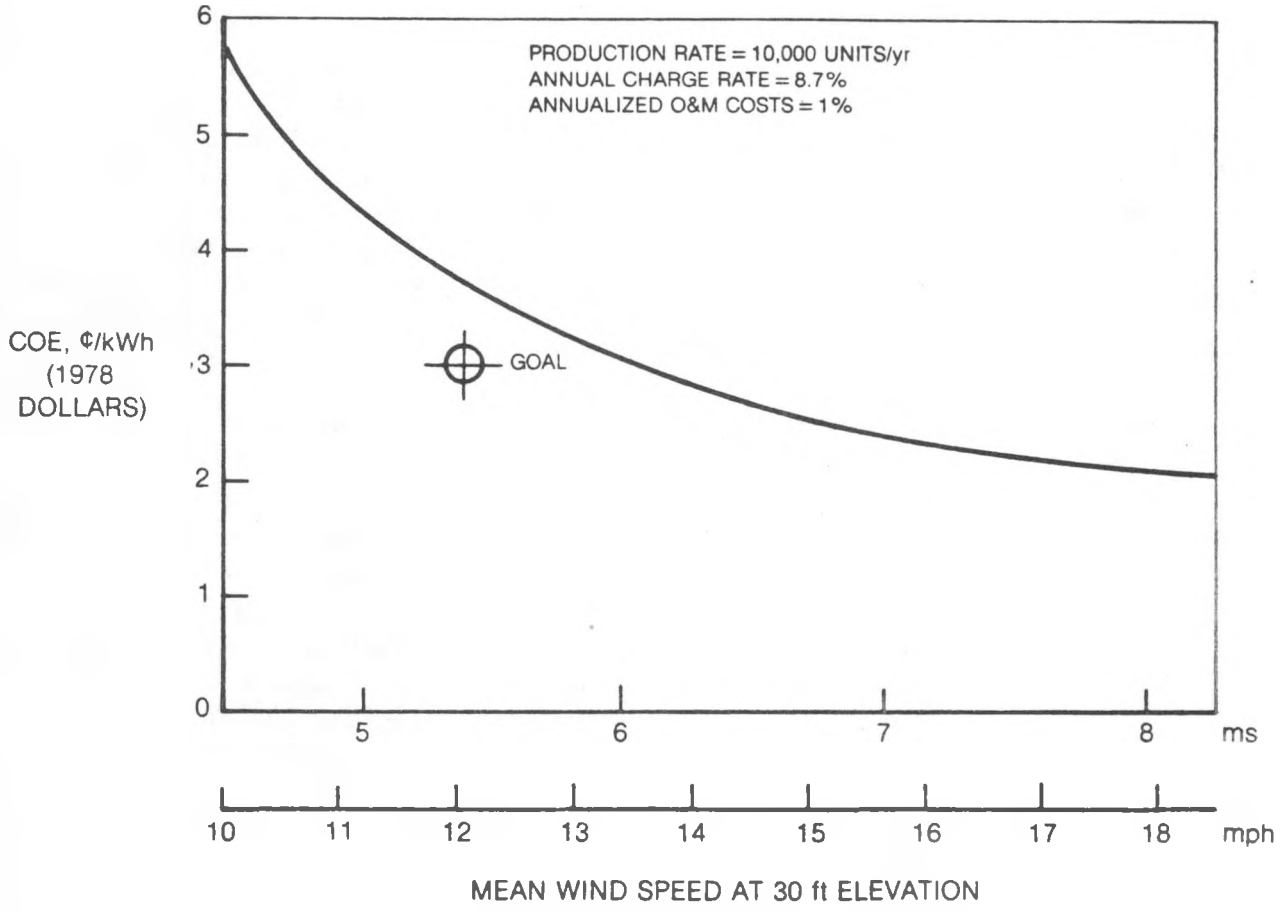

Figure 67. COE of UTRC 15-kW Wind System

81-6-164-63

SUPPORTING EXPERIMENTS

Experimental tests were performed in support of the 15-kW WTG design in the area of materials evaluation and for component testing. Following is a discussion of these results.

Material Tests

The objective of this task was to evaluate materials development efforts which could be used as a means of improving the baseline design in an effort to meet cost goals. Toward this end, the mechanical properties of S-2 glass reinforced resins were evaluated to determine if this composite could replace graphite reinforced resin as the flexbeam material. In addition, composites fabricated by the pultrusion process were evaluated since it was considered that pultrusion would be the most cost effective process for fabricating the unidirectionally reinforced composite flexbeams.

In an effort to evaluate both the composite system and the pultrusion process, S-2 glass reinforced epoxy fabricated by hot pressing, and S-2 glass reinforced vinyl ester fabricated by pultrusion,were selected as the candidate materials for the program. However, discussions with Morrison Molded Fiberglass Company revealed that only pultruded E glass reinforced vinyl ester was available in the time frame of the program. It was decided to assess the E glass vinyl ester as a representative pultruded composite since a simple extrapolation of composite mechanical properties is expected in substituting S-2 glass for E glass as the reinforcement. This would allow any potential shortcomings of fabrication by the pultrusion process to be determined. Following is a summary of the results.

Materials and Composites Fabrication

S-2 glass reinforced CE321R prepreg tape of 300-mm (12-in.) width was received from Ferro Corporation. Seven ply composites of dimensions 114 x 254 mm (4.5 x 10 in.) were fabricated from the tape by hot pressing for 2 h at 121 °C (250 °F) under 0.69 MPa (100 psi). The composite density was 1950 kg/m^3 (0.07 lb/in.^{3}).

The pultruded E glass reinforced vinyl ester composite was received from Morrison Molded Fiberglass as a continuous strip nominally 114-mm (4.5-in.) wide and 2-mm (0.08-in.) thick. The composite density was 1850 kg/m^3 (0.067 lb/in.^{3}).

Tensile Properties

Tensile specimens of dimensions 10 x 203 mm (0.4 x 8.0 in.) and 10 x 114 mm (0.4 x 4.5 in.) were cut from the composite panels in the longitudinal and transverse orientations respectively. Fiberglass doublers were bonded to the specimens providing a gage length of 102 mm (4.0 in.) for the longitudinal tensile specimens, and 75 mm (3.0 in.) for the transverse tensile specimens. Standard resistance strain gages were bonded to both sides of the gage sections, and the specimens were tested at a crosshead speed of 1.3 mm/min (0.05 in./min).

Longitudinal Tensile Properties

The data listed in Table XXII indicate that the S-2 glass reinforced resin system exhibits a tensile strength of 1490 MPa (216 ksi), an elastic modulus of 48.1 GPa (6980 ksi), and a failure strain in excess of 3.0% at room temperature. Only a minor decrease in properties is observed at 60°C (140°F). The pultruded E glass reinforced vinyl ester exhibits properties typical of E glass reinforced resins. Note that the doublers debonded during the room temperature test due to the slippery surface characteristics of the vinyl ester. Assuming the same level of property degradation at 60°C (140°F), as was observed for the S-2 glass reinforced resin, the room temperature tensile strength is approximated as 896 MPa (130 ksi).

The tensile stress-strain curves were linear elastic to failure for both composite systems at room temperature and 60°C (140°F). Some fiber breakage was observed prior to a catastrophic brooming type failure which is characteristic of glass reinforced resins.

Transverse Tensile Properties

The transverse tensile properties are listed in Table XXIII. The S-2 glass reinforced epoxy exhibited a tensile strength of 48.1 MPa (6.98 ksi), an elastic modulus of 17.2 GPa (2500 ksi), and failure strain of 0.28% at room temperature. The modulus was slightly degraded at 60°C (140°F) while the tensile strength and failure strain increased.

The data listed in Table XXIII show that transverse tensile strength and failure strain of the pultruded E glass reinforced vinyl ester are considerably reduced in comparison with S-2 glass reinforced epoxy. The level of transverse tensile strength achieved in the pultruded E glass/vinyl ester composite is relatively low in comparison with fiber reinforced epoxies and indicates low fiber/resin bond strength.

The transverse tensile stress-strain curves were linear elastic at room temperature, but exhibited nonlinear behavior at 60°C (140°F) at strains greater than 0.28%.

TABLE XXII

LONGITUDINAL TENSILE PROPERTIES OF S-2 AND E GLASS

Specimen No.	Composite	Test Temp. °C	Test Temp. (°F)	UTS, σ_{11} MPa	UTS, σ_{11} (10^3psi)	Elastic Modulus, E_{11} GPa	Elastic Modulus, E_{11} (10^6psi)	Poisson's Ratio	Failure Strain %
3558-5	S-2/CE321R	21	(70)	1380	(201)	47.4	(6.87)	0.27	3.12
-6	↓	21	(70)	1600	(232)	48.8	(7.07)	0.25	3.44
-7		60	(140)	1310	(190)	42.6	(6.18)	-	3.11
-8		60	(140)	1420	(205)	47.4	(6.87)	-	3.00
E/VR-27	E/vinyl ester	21	(70)	>673	(97.6)*	35.4	(5.13)	0.32	>1.88*
-28	↓	21	(70)	>664	(96.3)*	35.3	(5.12)	0.28	>1.85*
-29		60	(140)	874	(127)	33.5	(4.86)	-	2.64
-30		60	(140)	834	(121)	33.8	(4.90)	-	2.48

*doublers debonded

TABLE XXIII

TRANSVERSE TENSILE PROPERTIES OF S-2 AND E GLASS

Specimen No.	Composite	Test Temp. °C	Test Temp. (°F)	UTS, σ_{22} MPa	UTS, σ_{22} (10^3 psi)	Modulus, E_{22} GPa	Modulus, E_{22} (10^6 psi)	Failure Strain %
3558-1	S-2/CE321R	21	(70)	49.2	(7.14)	17.3	(2.51)	0.28
-2	↓	21	(70)	47.0	(6.82)	17.1	(2.48)	0.27
-3		60	(140)	53.4	(7.75)	14.5	(2.10)	0.38
-4		60	(140)	54.3	(7.88)	14.5	(2.11)	0.41
E/VR-32	E/vinyl ester	21	(70)	20.3	(2.95)	10.0	(1.46)	0.20
-33	↓	21	(70)	19.9	(2.88)	10.2	(1.48)	0.19
-34		60	(140)	16.3	(2.36)	6.71	(0.97)	0.32

Flexural Properties

The composite flexural strength and interlaminar shear strength were determined utilizing the three point bend test. It can be shown from simple beam theory that in three point bending the maximum applied flexural stress occurs at the specimen tensile surface and is given by $\sigma_{max} = 1.5\ PS/bh^2$. Simultaneously the maximum shear stress occurs at the specimen midplane and is given by $\tau_{max} = 0.75\ P/bh$. In these expressions, P is the load applied to the specimen midspan, S is the span width, b and h are the specimen width and depth respectively. Thus, during any given test, the ratio of maximum applied shear and flexural stresses depends on the span-to-depth ratio, S/h. Since a given material can fail by either shear or tension, one of these failure modes occurs first depending on test configuration. In general, for high longitudinal strength composites, tensile failures are observed for high values of S/h while shear failures are observed for low values of S/h.

S-2/CE321R Epoxy

To determine the flexural properties of the S-2 glass reinforced epoxy, specimens of dimensions 50 x 10 x 1.3 mm (2.0 x 0.4 x 0.050 in.) were cut from composite panels and tested at S/h = 24 and S/h = 30. For determination of the interlaminar shear strength, a separate panel was fabricated 6.4 mm (0.25 in.) in thickness. Specimens of dimensions 38.1 x 6.4 x 6.4 mm (1.5 x 0.25 x 0.25 in.) were cut from this panel and tested at S/h = 4.

The flexural strength, σ_{max}, and modulus, E_b, determined at -50°C (-58°F), room temperature, and 60°C (140°F) are listed in Table XXIV. The average room temperature flexural strength determined at S/h = 24 is slightly greater than that determined at S/h = 30 due to excessive bending at the greater span width. For this reason, the flexural strength determined at S/h = 24 is more valid. The average values of flexural strength and modulus determined at S/h = 24 are summarized in Table XXV as a function of test temperature. The flexural strength is relatively constant over the range of test temperatures, increasing only slightly at -50°C (-58°F). Observation of the fracture surfaces showed that tensile failure had occurred on the outer fiber surface as desired, although there was evidence of compressive failure at the center loading point in addition. The bending modulus at -50°C (-58°F) is not included for comparison since a different test fixture and loading machine were utilized for testing at -50°C (-58°F). Tensile modulus data supplied by Ferro Corporation for the S-2/CE321R system indicate an equivalent tensile modulus of 53.1 GPa (7700 ksi) at -55°C (-67°F) and room temperature.

The interlaminar shear strength, τ_{max}, determined at room temperature and 60°C (140°F) is listed in Table XXVI. The average interlaminar shear strength at room temperature was 57.1 MPa (8.29 ksi). Approximately a 10% reduction in interlaminar shear strength to 51.3 MPa (7.49 ksi) was determined at 60°C (140°F). Examination of the test specimens showed that all specimens failed by delamination along the specimen midplane.

TABLE XXIV

FLEXURAL PROPERTIES OF S-2 GLASS REINFORCED CE321R EPOXY

Specimen No.	S/h	Test Temp.		Strength σ_{max}		Modulus E_h	
		°C	(°F)	MPa	(10^3 psi)	GPa	(10^6 psi)
3586-6	24	-50	(-58)	1700	(247)		
-7				1730	(251)		
-8				1760	(256)		
-9				1820	(263)		
-10				1900	(275)		
				1780	(258) Avg.		
3557-11	24	21	(70)	1660	(241)	52.5	(7.62)
-12				1800	(261)	53.9	(7.82)
-13				1660	(240)	49.4	(7.17)
-14				1720	(250)	51.7	(7.49)
-15				1800	(260)	54.3	(7.87)
				1730	(250) Avg.	52.4	(7.59) Avg.
3586-1	24	60	(140)	1660	(241)	49.9	(7.23)
-2				1820	(263)	58.6	(8.50)
-3				1770	(257)	58.0	(8.41)
-4				1700	(246)	54.0	(7.83)
-5				1710	(248)	54.3	(7.87)
				1730	(251) Avg.	54.9	(7.97) Avg.
3557-1	30	21	(70)	1740	(253)	55.5	(8.05)
-2				1530	(221)	49.7	(7.21)
-3				1500	(217)	49.0	(7.11)
-4				1690	(245)	52.8	(7.66)
-5				1770	(256)	55.9	(8.11)
				1640	(238) Avg.	52.6	(7.63) Avg.
3557-6	30	60	(140)	1600	(231)	56.5	(8.19)
-7				1490	(216)	52.3	(7.59)
-8				1420	(205)	49.5	(7.18)
-9				1470	(214)	53.2	(7.72)
-10				1580	(229)	54.9	(7.97)
				1510	(219) Avg.	53.3	(7.73) Avg.

TABLE XXV

FLEXURAL PROPERTIES AS A FUNCTION OF TEMPERATURE
DETERMINED IN THREE POINT BEND AT S/h = 24
(LONGITUDINAL FIBER ORIENTATION)

Composite	Test Temperature		Strength σ_{max}		Modulus E_b	
	°C	(°F)	MPa	(10^3 psi)	GPa	(10^6 psi)
S-2/CE 321R	-50	(-58)	1780	(258)		
	21	(70)	1730	(250)	52.4	(7.59)
	60	(140)	1730	(251)	54.9	(7.97)

TABLE XXVI

INTERLAMINAR SHEAR STRENGTH OF S-2 GLASS REINFORCED CE321R EPOXY

Specimen #	S/h	Test Temp. °C	Test Temp. (°F)	τ_{max} MPa	τ_{max} (ksi)	
3585-1	4	21	(70)	57.5	(8.33)	
-2				59.7	(8.66)	
-3				55.5	(8.05)	
-4				55.8	(8.10)	
				57.1	(8.29)	Avg.
-5	4	60	(140)	51.5	(7.46)	
-6				51.3	(7.44)	
-7				51.2	(7.57)	
				51.3	(7.49)	Avg.

Pultruded E Glass/Vinyl Ester

Since the pultruded composite was only available in one thickness, three point bend tests were performed at S/h = 8, 16, 24, and 32 in an effort to define both the interlaminar shear strength and the flexural strength. At room temperature, the specimen dimensions were 76 x 10 x 2 mm (3.0 x 0.4 x 0.079 in.). The results of these tests are listed in Table XXVII. Included are the maximum flexural stress, σ_{max}, and maximum midplane shear stress, τ_{max}, as well as the bending modulus, E_b. These data are also plotted in the form of flexural and shear interaction diagrams in Figs. 68 and 69 respectively.

It is apparent from the flexural interaction diagram, Fig. 68, that excessive bending at S/h = 32 reduced the flexural strength with respect to that observed at S/h = 16 and 24. The true flexural strength is defined by the plateau observed for these two points and is 1140 MPa (165 ksi). The specimens exhibited typical outer fiber tensile failures with some compression failure under the loading nose also evident.

The shear interaction diagram, Fig. 69, shows that the midplane shear stress, τ, increases as S/h decreases. At some value of S/h, the midplane shear stress becomes high enough to cause interlaminar failure before flexural failure can occur. Note that a significant deviation from the calculated curve is observed when testing at S/h = 8. Examination of these specimens showed that interlaminar failure occurred at S/h = 8. Thus, the interlaminar shear strength is defined by testing at S/h = 8. The average value was 49.6 MPa (7.19 ksi).

Testing was subsequently performed at -50°C (-58°F) and 60°C (140°F) to determine the effect of test temperature on the flexural properties. These data are listed in Table XXVIII. It can be seen that the flexural strength exhibits some dependence on test temperature, increasing to 1260 MPa (183 ksi) at -50°C (-58°F) and decreasing to 1010 MPa (146 ksi) at 60°C (140°F), with respect to the room temperature value of 1140 MPa (166 ksi). The interlaminar shear strength determined for the test parameters of S/h = 8 decreased at 60°C (140°F) to a value of 37.3 MPa (5.41 ksi) in comparison with the room temperature value of 49.6 MPa (7.19 ksi).

Flexural Fatigue

Specimens of the same dimensions as those used for the static flexural testing were tested in three point flexural fatigue at S/h = 24. To establish reasonable starting stress conditions, tension-tension data for the S-2/CE321R system supplied by the manufacturer were reviewed (Table XXIX). It is evident from these data that a maximum stress of 428 MPa (62 ksi) is associated with a 10^6 cycle life. The results also indicate a precipitous falloff in fatigue life with increased stress level. Based on these results, it was assumed that a reasonable estimate of the fatigue limit in three point bending could be defined by the stress level at which no cracking or strength degradation occurred for a 2×10^5 cycle life.

TABLE XXVII

FLEXURAL PROPERTIES OF PULTRUDED E GLASS REINFORCED VINYL ESTER AT ROOM TEMPERATURE

Specimen #	S/h	σ_{max} MPa	σ_{max} (10^3 psi)	τ_{max} MPa	τ_{max} (10^3 psi)	E_b GPa	E_b (10^6 psi)
E/VR-17	8	782	(113)	48.7	(7.07)	28.1	(4.08)
-18		724	(105)	44.5	(6.46)	29.0	(4.20)
-19		883	(128)	54.7	(7.93)	29.5	(4.28)
-20		812	(118)	50.3	(7.29)	30.5	(4.42)
		800	(116) Avg.	49.6	(7.19) Avg.	29.3	(4.25)
-14	16	1140	(166)	35.7	(5.18)	36.7	(5.32)
-15		1160	(168)	35.9	(5.21)	36.9	(5.35)
-16		1110	(161)	35.1	(5.09)	35.8	(5.20)
		1140	(165) Avg.	35.6	(5.16) Avg.	36.5	(5.29) Avg.
-11	24	1150	(166)	23.7	(3.44)	37.4	(5.43)
-12		1120	(163)	23.2	(3.36)	37.3	(5.41)
-13		1160	(168)	23.8	(3.45)	39.3	(5.70)
		1140	(166) Avg.	23.6	(3.42) Avg.	38.0	(5.51) Avg.
-1	32	1020	(148)	16.1	(2.34)	36.4	(5.27)
-2		1040	(151)	16.4	(2.38)	36.0	(5.22)
-3		1030	(149)	16.2	(2.34)	36.6	(5.31)
-4		1060	(153)	16.6	(2.40)	37.0	(5.37)
-5		1040	(151)	16.5	(2.39)	36.2	(5.25)
		1040	(150) Avg.	16.3	(2.37) Avg.	36.4	(5.28) Avg.

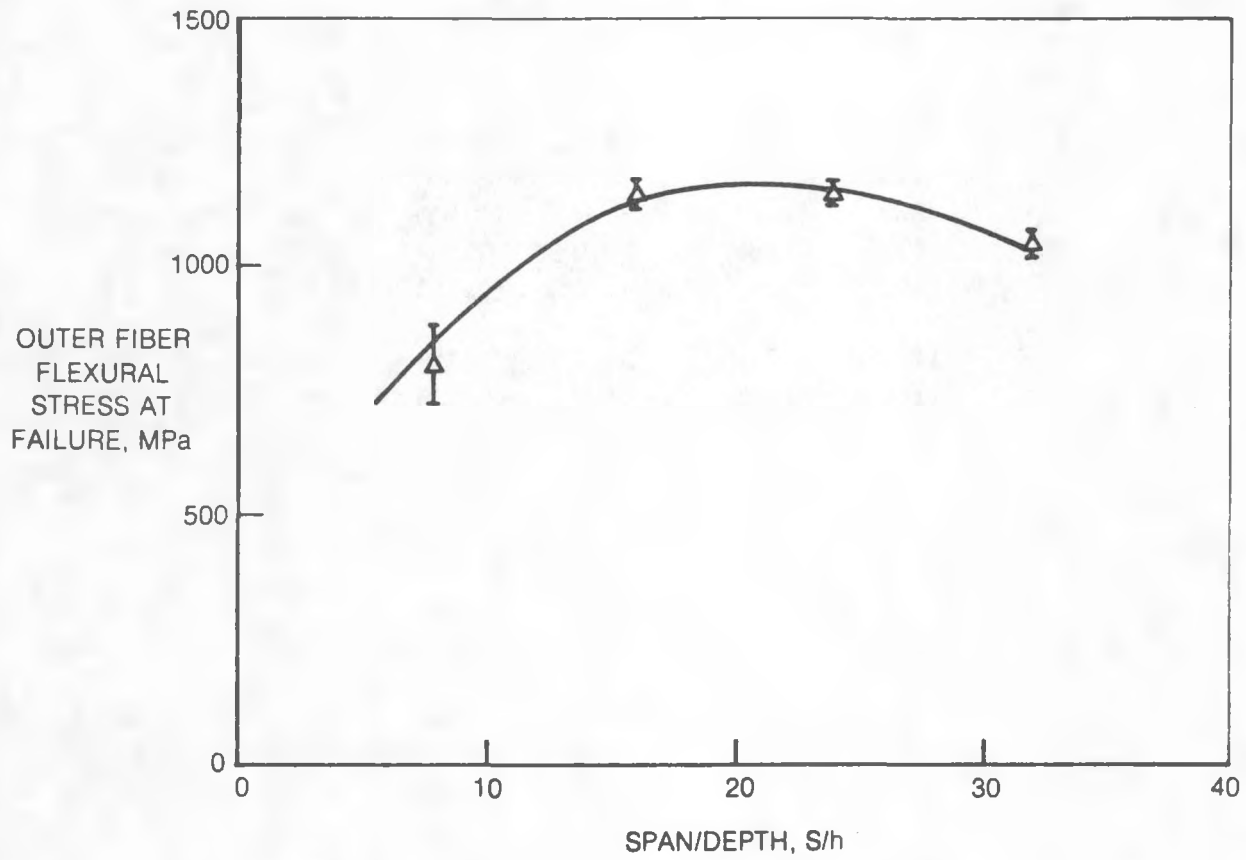

Figure 68. Flexural Interaction Diagram for Pultruded E Glass Reinforced Vinyl Ester (Room Temperature)

81-6-164-46

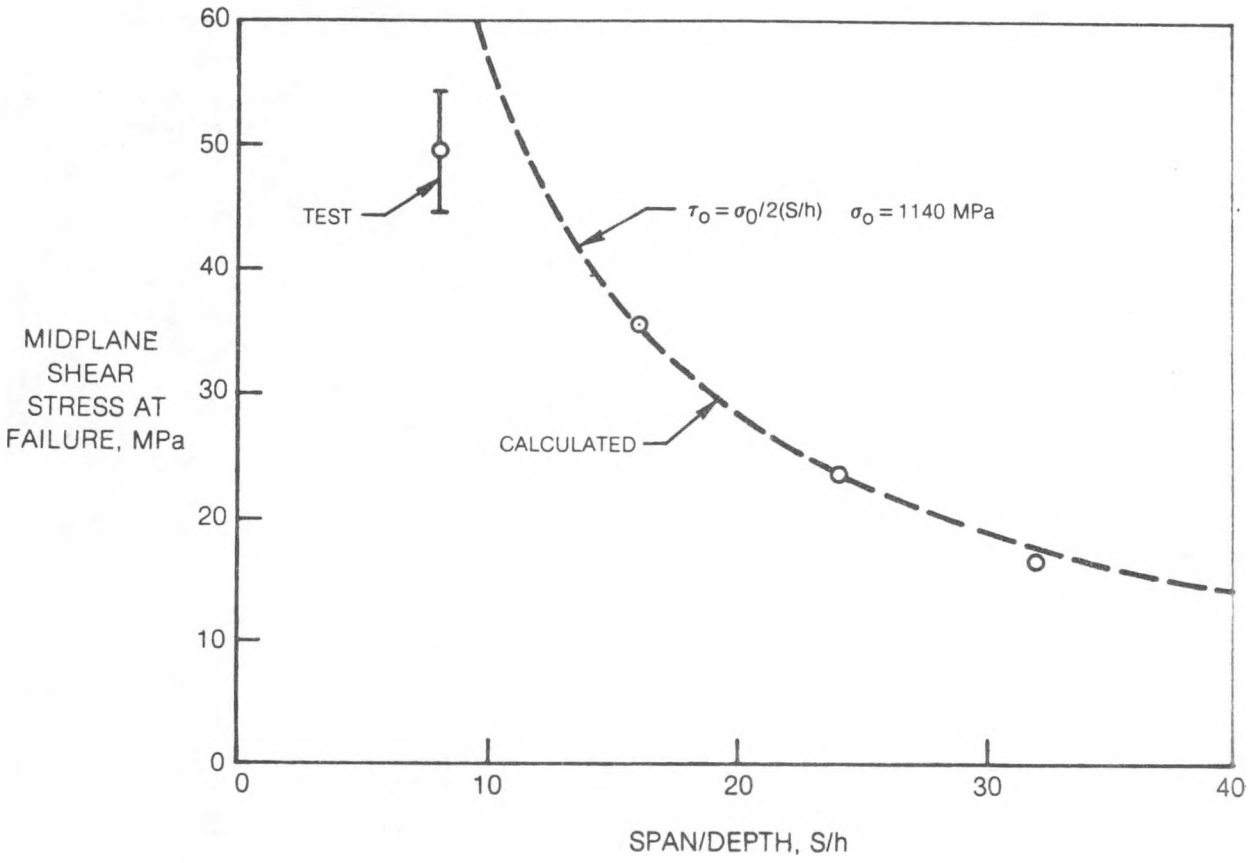

Figure 69. Shear Interaction Diagram for Pultruded E Glass Reinforced Vinyl Ester (Room Temperature)

81-6-164-47

TABLE XXVIII

FLEXURAL PROPERTIES OF PULTRUDED E GLASS REINFORCED VINYL ESTER AS A FUNCTION OF TEST TEMPERATURE

Specimen No.	S/h	Test Temp. °C	Test Temp. (°F)	Flexural Strength MPa	Flexural Strength (10^3 psi)	Flexural Modulus GPa	Flexural Modulus (10^6 psi)	Interlaminar Shear Strength MPa	Interlaminar Shear Strength (10^3 psi)
E/VR-40	24	-50	(-58)	1270	(185)				
-41				1260	(183)				
-42				1260	(182)				
				1260	(183) Avg.				
-11	24	21	(70)	1150	(166)	37.4	(5.43)		
-12				1120	(163)	37.3	(5.41)		
-13				1160	(168)	39.3	(5.70)		
				1140	(166) Avg.	38.0	(5.51) Avg.		
-35	24	60	(140)	973	(141)	36.2	(5.25)		
-36				1020	(148)	38.7	(5.61)		
-37				1050	(152)	39.2	(5.69)		
-38				978	(142)	38.7	(5.62)		
-39				1030	(149)	39.3	(5.70)		
				1010	(146) Avg.	38.4	(5.57) Avg.		
-17	8	21	(70)					48.7	(7.07)
-18								44.5	(6.46)
-19								54.7	(7.93)
-20								50.3	(7.29)
								49.6	7.19 Avg.
-45	8	60	(140)					37.9	(5.49)
-46								37.2	(5.40)
-47								36.9	(5.35)
								37.3	(5.41) Avg.

TABLE XXIX

TENSION-TENSION FATIGUE DATA FOR S-2/CE321R
SUPPLIED BY FERRO CORPORATION

Single Amplitude Alternating Stress		Max. Stress		Min. Stress		Cycles to Failure
MPa	(ksi)	MPa	(ksi)	MPa	(ksi)	
152	22	338	48.9	33.8	4.89	10,000,000 -
152	22	338	48.9	33.8	4.89	no failure
193	28	429	62.2	42.9	6.22	6,798,400
193	28	429	62.2	42.9	6.22	1,277,500
221	32	491	71.1	49.1	7.11	929,500
221	32	491	71.1	49.1	7.11	70,300
249	36	552	80.0	55.2	8.0	115,700
249	36	552	80.0	55.2	8.0	22,800

A series of specimens of the S-2 glass reinforced epoxy were run at different maximum stress levels at a stress ratio R_1 of 0.1 and a cycle rate of 1 Hz. The specimens were run under load control with limits set so that excessive softening of the specimen due to fatigue crack growth would result in test termination. The residual flexural strength and modulus were determined when the 2×10^5 cycle life was exceeded or after detection of a crack. The data obtained are listed in Table XXX. For maximum stress levels of 552 and 690 MPa (80 and 100 ksi) no degradation in specimen flexural strength or modulus was observed in excess of 2.5×10^5 fatigue cycles. However, at a maximum stress level of 862 MPa (125 ksi) longitudinal cracking was detected which resulted in a decrease in residual specimen strength and modulus. These results indicate that the fatigue limit in three point bending is significantly greater than that in tension-tension for R = 0.1 conditions (where R is the ratio of minimum/maximum stress).

Several samples of the E glass reinforced vinyl ester were also tested and the data are listed in Table XXX. For ratios of maximum stress to zero cycle flexural stress equivalent to those used in the S-2 glass reinforced epoxy, fatigue crack growth was also observed. Small decreases in flexural strength and modulus were associated with the initiation of cracking. Sample E/VR-43 was cycled to failure to observe fatigue crack growth. Longitudinal cracks initiated in the beam center and then spread transversely so that the majority of the cross section exhibited material degradation at failure.

Shear Modulus Measurement

The composite shear modulus was determined using a torsional loading apparatus. Torque-twist diagrams were generated using composite beams of dimensions 152 x 12.7 x h mm (6.0 x 0.5 xh in.). Typical torque-twist diagrams are shown in Fig. 70. The shear modulus was calculated from the linear portion of these curves using the relationship $G = TS/\theta\beta bh^3$ where G is the shear modulus, T is the applied torque, S is the specimen gage length, θ is the corresponding twist, $\beta = 1/3\ (1-0.63\ h/b)$, b and h are the specimen width and thickness. The values of shear modulus calculated in this manner are listed in Table XXXI. Also included in the table is the shear modulus of AS graphite/epoxy determined in the same manner. The average shear modulus of the S-2 glass reinforced epoxy was 5446 MPa (790 ksi) while that for the E glass reinforced vinyl ester was 3290 MPa (477 ksi). Note that the S-2 glass reinforced epoxy is similar in shear modulus to AS graphite reinforced epoxy. As a final note, both glass reinforced composites were twisted beyond 90° without failure.

Torsional Creep Behavior

The torsional creep behavior of the S-2 glass reinforced CE321R epoxy was monitored under constant deflection conditions. The specimen dimensions and gage length were scaled to simulate the design condition for an S-2 glass reinforced epoxy flexbeam. The appropriate angle of twist was transmitted to the specimen

TABLE XXX

THREE POINT FLEXURAL FATIGUE RESULTS -
ROOM TEMPERATURE TESTING AT R = 0.1 (See Note)

Specimen No.	Composite	Maximum Stress MPa (10^3 psi)		Cycles	Residual Strength MPa (10^3 psi)		Bending Modulus GPa	(10^6 psi)
3558-13	S-2/CE321R	1520	(221)	1	-		44.8	(6.50)
-14		1610	(223)	1	-		45.5	(6.60)
-16		1570	(227)	1	-		44.5	(6.40)
-12		552	(80)	272610	1560	(226)	46.5	(6.75)
-15		690	(100)	254000	1560	(226)	48.2	(6.98)
-17		862	(125)	164154*	1430	(208)	44.0	(6.38)
E/VR**	E/vinyl ester	1140	(165)	1	-			
E/VR-44		552	(80)	158000*	1090	(158)	38.0	(5.51)
-43		690	(100)	58000*	***		35.7	(5.18)

Note: The stress ratio (R) is the ratio of minimum to maximum stress.

* crack detected
** average flexural properties, Table VI
*** continued fatigue cycling, failed at 226000 cycles

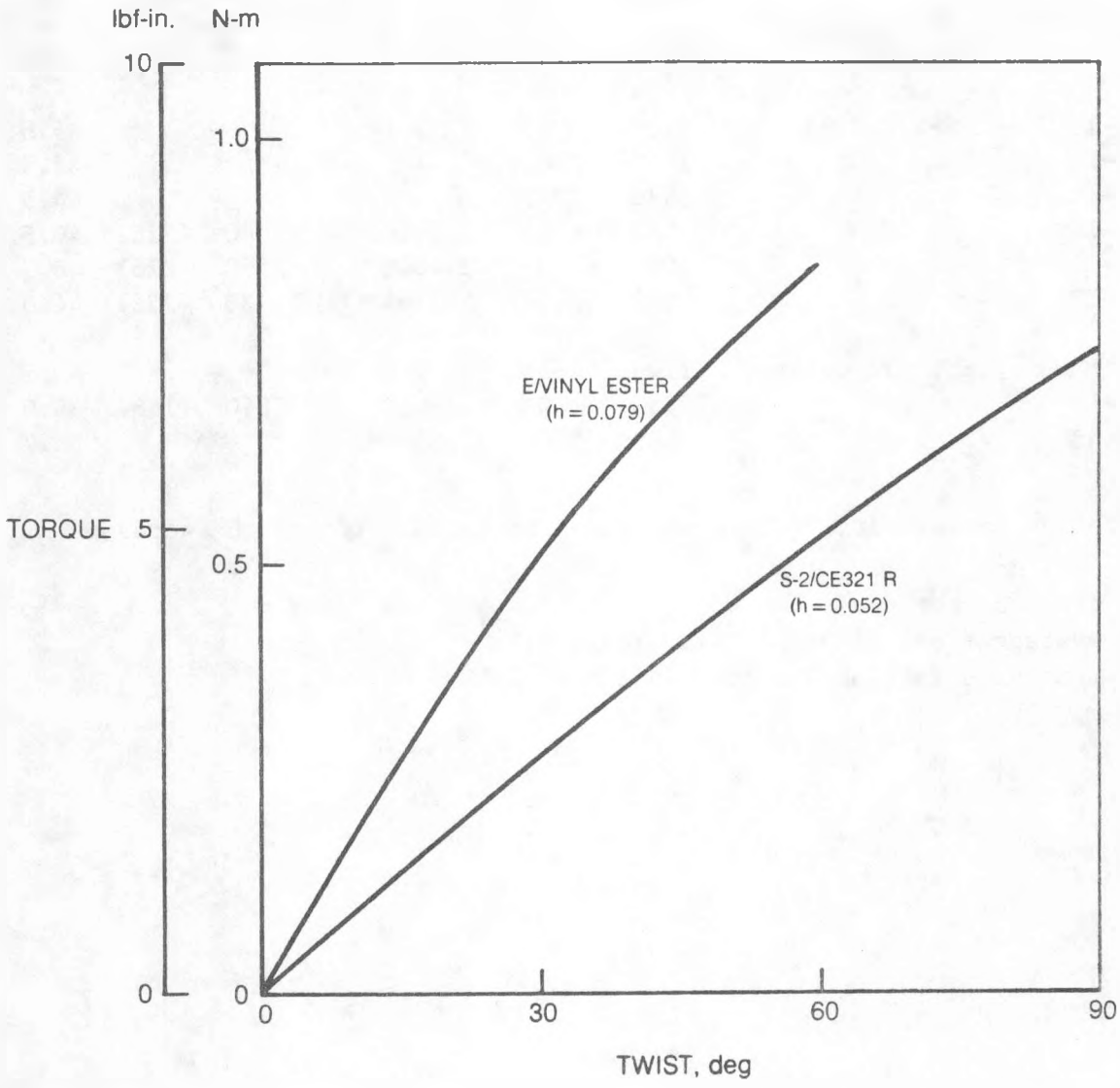

Figure 70. Typical Torque-Twist Curves (Room Temperature)

81-6-164-45

TABLE XXXI

SHEAR MODULUS COMPARISON

Specimen No.	Composite	Shear Modulus MPa	(10^3 psi)	
3557-16	S-2/CE321R	5560	(807)	
-17		5240	(760)	
-18		5540	(804)	
		5446	(790)	Avg.
E/VR-21	E/vinyl ester	3280	(476)	
-22		3310	(480)	
-23		3280	(476)	
		3290	(477)	Avg
	AS graphite/epoxy	5170	(750)	

via a motor driven gear whose axle was connected to one grip. A lever arm connected to a load cell from the other grip maintained the zero position for the other end of the specimen and allowed the load associated with a particular angle of twist to be determined. In this manner, a twist angle of 21° was set and the resultant load, P, was monitored as a function of time. The data determined at test temperatures of 21°C (70°F) and 60°C (140°F) are listed in Table XXXII in terms of the ratio of load measured to the initial load, P/Po, as a function of time. At elevated temperature, the specimens were allowed to soak one hour at temperature prior to testing. For a test temperature of 21°C (70°F), the primary load relaxation occurs in the first two hours of testing with subsequent relaxation occurring at a very slow rate. After unloading the specimen a permanent set of approximately 1° was observed. For a test temperature of 60°C (140°F), load relaxation occurred at an accelerated rate and continued throughout testing. Approximately twice as much load relaxation occurred at 60°C (140°F) as at 21°C (70°F). The permanent set observed on unloading was approximately 5-6°. These results indicate that this composite system may be susceptible to a considerable amount of torsional creep at 60°C (140°F).

Testing of Pultruded S-2 Reinforced 6.35-mm (0.25-in.)-Diam Rod

Samples of the 6.35-mm (0.25-in.)-diam S-2 glass reinforced rods were pultruded at Morrison Molded Fiberglass (MMFG). Morrison indicated in subsequent discussions that parameters utilized in fabricating rod #10 were the most likely to be utilized for the beam fabrication. For this reason, samples from the other rods were used for preliminary testing while rod #10 samples were utilized once the testing technique was established.

Several specimens were tested in both three point and four point loading at various span/depth ratios. The fixtures were equipped with 6.35-mm (0.25-in.)-diam loading pins. The results of these tests are summarized in Table XXXIII. It is evident from these data that the flexural strength and modulus measured are a strong function of the test span-to-depth ratio (S/h). This is not atypical of similar composite materials although this material in rod form seems particularly sensitive to this test parameter. These results dictated the use of the highest S/h practical to obtain most accurate material properties. It was also noted that compressive failures were occurring under the loading pins, thus causing premature failure and lower than actual strength values.

In view of these findings, further discussions were held with MMFG concerning test method so that identical approaches would be utilized at UTRC and MMFG. The test procedure followed at MMFG is outlined as follows:

a. 3 point bend test - S/h = 40
b. 25.4-mm (1.0-in.)-diam support pins
c. 19-mm (0.75-in.) load nose
d. crosshead speed 0.28 mm/s (0.67 in./min)

TABLE XXXII

TORSIONAL CREEP BEHAVIOR OF S-2 GLASS REINFORCED CE321R EPOXY

	P/Po* for twist angle, $\theta = 21^\circ$			
Time (hr)	3557-16 21°C (70°F)	3593-1 21°C (70°F)	3593-2 60°C (140°F)	3593-4 60°C (140°F)
0.5	0.93	0.94	0.93	0.88
1.0	0.92	0.94	0.91	0.86
2.0	0.91	0.93	0.88	0.85
4.0	0.91	0.92	0.86	0.82
24.0	0.90	0.90	0.82	0.77
48.0	0.90	0.89	0.78	0.76
66.0	0.89	--	--	0.74
96.0	--	--	0.76	--

*P/Po is the ratio of the load at any time to the initial load.

TABLE XXXIII

PRELIMINARY BEND TEST RESULTS - S-2 GLASS REINFORCED VINYL ESTER

Rod No.	Loading	S/h**	Flexural Strength		Flexural Modulus	
			MPa	10^3 psi	GPa	10^6 psi
2	3 pt	10	645	93.6	40.9	5.93
2	3 pt	20	724	105	44.6	6.47
2	4 pt*	20	622	90.2	45.3	6.57
4	4 pt*	30	820	119	48.3	7.0
4	3 pt	40	993	144	47.6	6.90

* Load span/support span = 1/3
** Span-to-depth ratio

Several specimens from rod #10 were tested using these parameters. In addition, 6.35-mm (0.25-in.)-diam aluminum alloy rod was tested as a modulus standard. The results obtained are listed in Table XXXIV. The average flexural strength and modulus determined from the pultruded composite rod were 1024 MPa (149 x 10^3 psi) and 49 GPa (7.1 x 10^6 psi) respectively. The modulus determined for the aluminum alloy rod was 70.3 GPa (10.2 x 10^6 psi) which is in agreement with handbook values. The flexural failures were again compressive so that the true flexural strength is in excess of the value determined.

TABLE XXXIV

THREE POINT BEND TEST RESULTS FOR S-2 GLASS AND ALUMINUM ALLOY RODS

Sample No.	S/h	Flexural Strength		Flexural Modulus	
		MPa	10^3 psi	GPa	10^6 psi
10-1	40	1014	147	47.3	6.86
10-2		1027	149	47.9	6.95
10-3		1041	151	50.3	7.29
10-4		1014	147	50.3	7.29
Al-1 (Aluminum)		-	-	70.3	10.2
Al-2		-	-	70.3	10.2
Al-3		-	-	70.3	10.2

Component Tests

Bending Test of 152-mm (6-in.)-O.D. Pultruded Fiberglass Pole

An experimental test was performed on a 152-mm (6-in.)-O.D. pultruded fiberglass tubular pole as part of the study of using a free standing fiberglass tower as a supporting structure for wind systems. The test configuration shown in Fig. 71 simulated the tubular pole being end-loaded as a cantilever beam. The purpose of the test was to determine the strength characteristics of the pultruded tube and the mode of failure under the applied load.

Figure 72 shows the deflection-versus-load result when the end-load was applied to the pole. Two loadings were performed; the first loading peaked at 2981 N (650 lbf) and the second loading peaked at 3648 N (820 lbf). This was the point of failure.

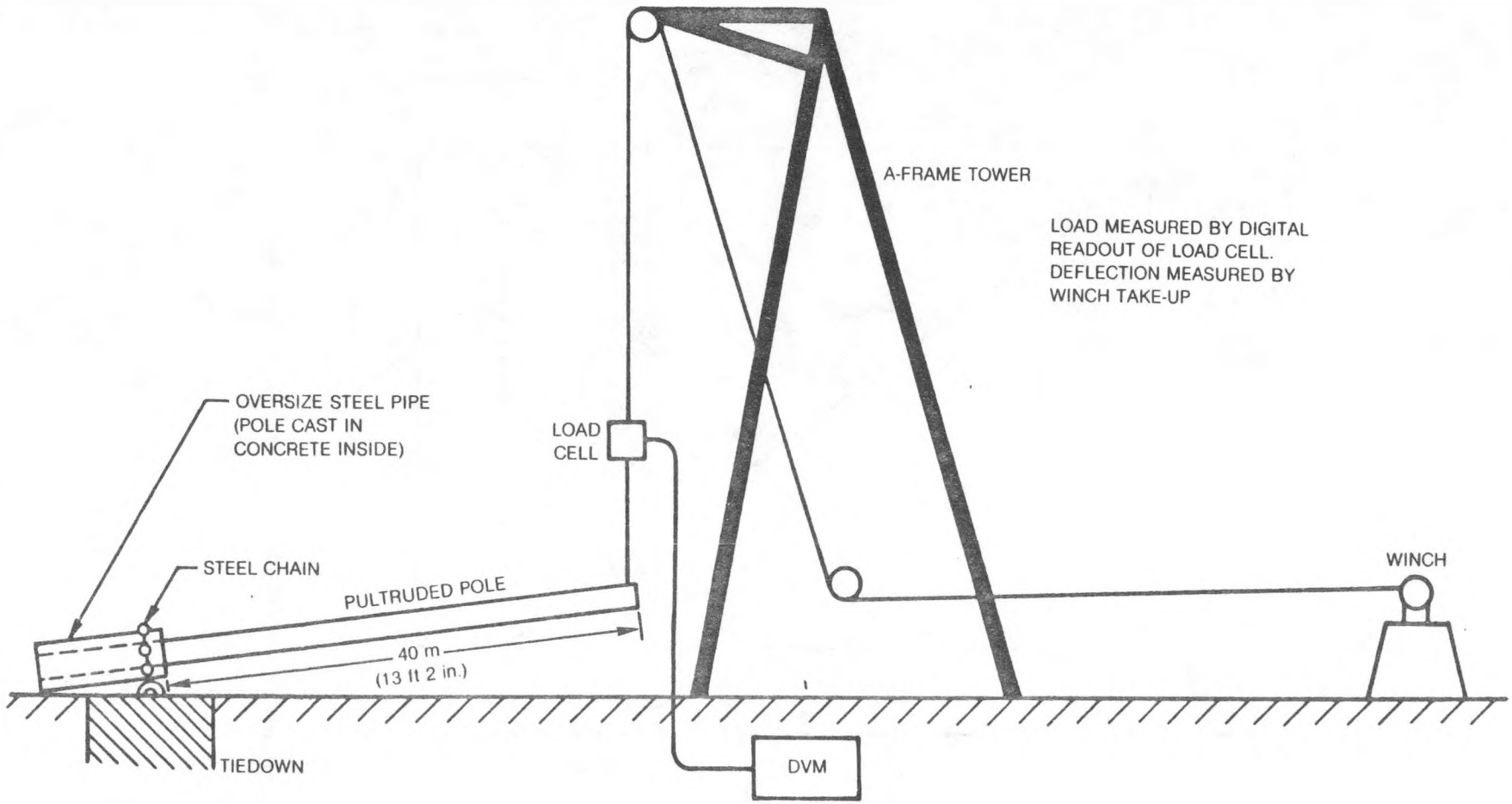

Figure 71. Bend Test Set-Up for Pultruded Tubular Pole

81-6-164-40

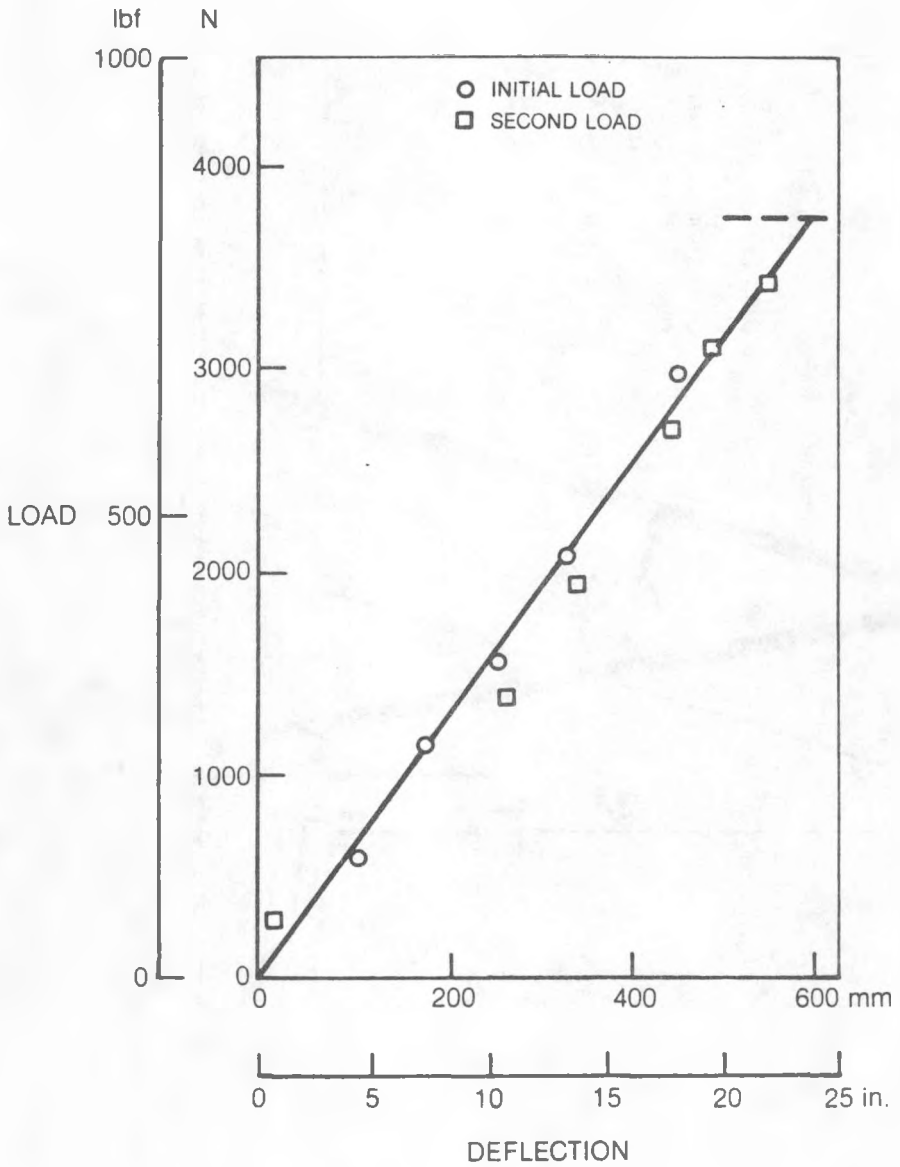

Figure 72. Pultruded Tube Bending Test Results

81-6-164-65

From the results in Fig. 72, some strength characteristics of the pultruded pole have been calculated and are compared to theoretical predictions in Table XXXV.

TABLE XXXV

STRENGTH CHARACTERISTICS OBTAINED FROM
6-IN. DIAM PULTRUDED POLE TEST

			Theory		Test	
Max Moment	N·m	(lbf·in.)	31860	(293000)	12485	(114800)
Flex Strength	MPa	(10^3 psi)	324	(47)	127	(18.4)
Bending Modulus	GPa	(10^6 psi)	38	(5.5)	17	(2.45)
Ultimate Strain	mm/mm	(in./in.)	0.0085	(0.0085)	0.0075	(0.0075)

The mode of failure was a standard compressive failure in bending. The failure was sudden with no apparent audio or deflection warning.

Tension Test of Blade-Flexbeam Attachment Joint

An experimental test was performed in the Materials Laboratory on the attachment fixture that joins the pultruded blade proper with the flexbeam. The purpose of the test was to evaluate the blade attachment fixture for strength characteristics under simulated centrifugal force loading and to determine the mode of failure.

The test configuration is shown in Fig. 73. A section of 381-mm (15-in.)-chord pultruded blade approximately 0.61-m (2-ft) long was used as part of the test setup. A pad of G-10, a commercially available composite material, was built up at the end of the blade section on both the upper and lower airfoil surfaces to provide a flat surface for joining to the blade attachment fixture. The attachment fixture is composed of two steel plates, secured to the upper and lower surfaces of the blade and flexbeam by bolts. In the test setup the flexbeam was replaced by a steel block threaded on the outer end to provide a connection point to the tensile testing machine. An identical attachment fixture was also mounted to the other end of the pultruded blade section. During testing, the deflection between the upper and lower attachment fixtures was measured by a deflectometer and monitored during the loading sequence. The applied tensile loading was also measured.

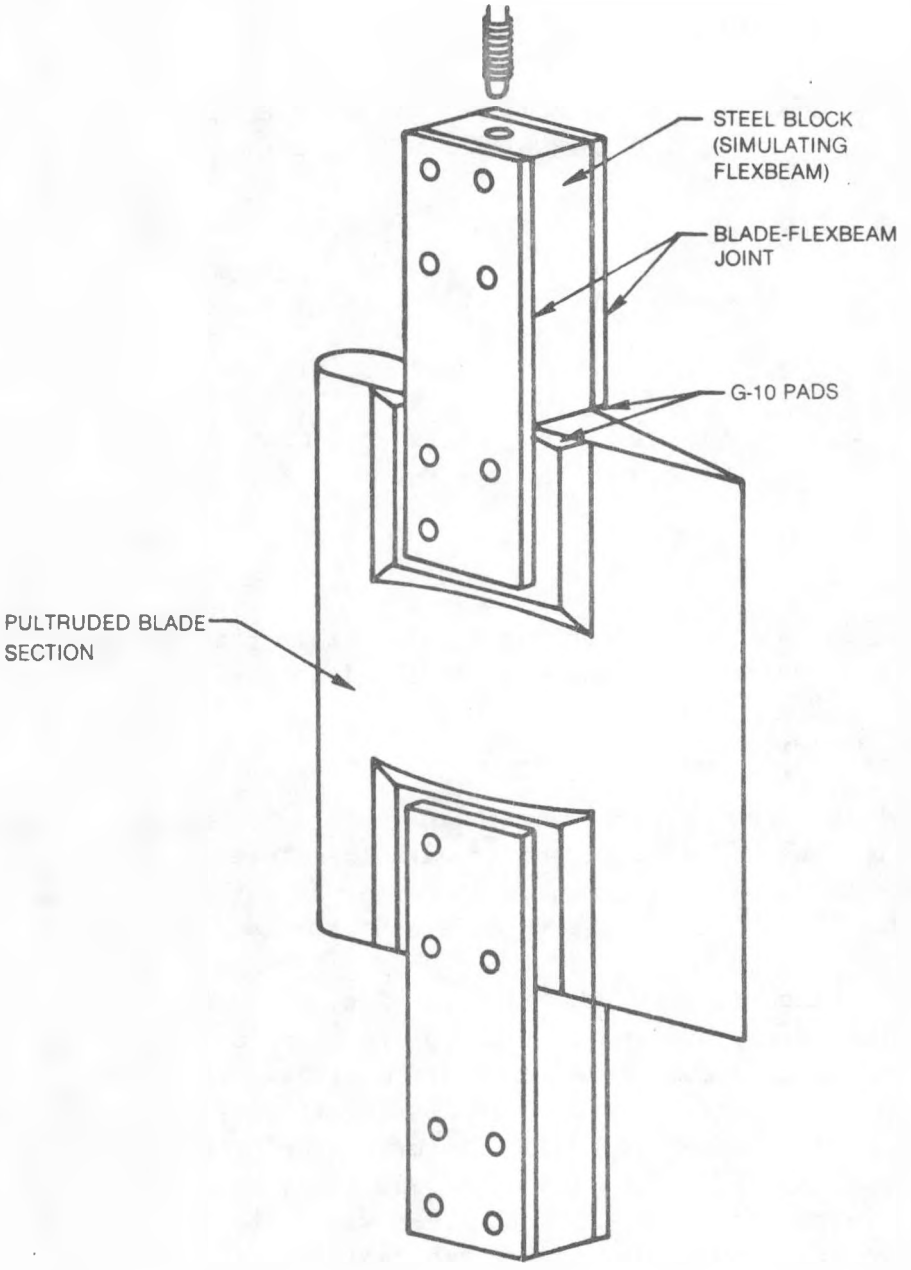

Figure 73. Blade-Flexbeam Joint Test Set-Up

81-6-164-43

Figure 74 shows the deflection versus load result when the tensile load was applied. Two loadings were performed; the first loading peaked at 53,000 N (12,000 lbf), the second loading peaked at 116,000 N (26,000 lbf). This was the point of failure for the upper attachment fixture shown in Fig. 73. The lower fixture remained intact.

The mode of failure was loss of the shear bond between the pads and the pultruded blade. The G-10 pads completely separated from the blade, and the bolts securing the pads to the blade then pulled through the fiberglass blade skin which was 2.34 mm (0.100 in.) thick. The mode of failure was evident during testing by separation of the pad from the blade along the edges. Polyester resin was used to bond the pad to the blade. Based on the peak load and the surface area of the pad, the estimated shear strength of the polyester resin is about 1.38 MPa (200 psi). The blade and pad were thoroughly cleaned before bonding, so loss of shear strength was not attributed to a poor bond. Therefore, the shear failure is attributed to the low shear strength of the resin itself.

The parts were disassembled and inspected after the test. No significant deformation of the bolt holes in the G-10 material was observed. This indicates that the blade attachment fixture tested is a good approach to joining the flexbeam to the blade, provided an acceptable shear bond is achieved between the pads and the pultruded blade.

Bending Test of Pultruded Wind Turbine Blade Specimen

An experimental test was performed on a 380-mm (15-in.)-chord pultruded wind turbine blade specimen. The test configuration simulated a flatwise moment being applied to the cantilevered blade. The purpose of the test was to determine the strength characteristics of the pultruded blade and the mode of failure under the applied load.

Test Setup

As shown in Fig. 75 a 2.44-m (8-ft)-long pultruded blade specimen was effectively cantilevered horizontally and then shear loaded in the flatwise direction. A blade-flexbeam joint comprised of two steel plates connected the pultruded blade to a steel block that simulated the flexbeam. The steel block was then bolted to a 203-mm (8-in.)-steel I-beam and the I-beam was restrained to the ground by a chain connected to a tie-down point. A wooden block under the end of the I-beam held the assembly in a horizontal position when the blade was vertically deflected. The load was applied by pulling up on a wooden fixture contoured to match the blade lower surface. This fixture was used to distribute the shear load over the blade chord and was located under the blade approximately 1.016 m (40 in.) from the flexbeam joint. As the winch drew in cable, the blade deflected in the flatwise direction and an effective load was applied as the blade stiffness resisted the deflection. An A-frame tower was used to support the cable attached to the contoured wood fixture, and a load cell in series with the cable measured the applied load. Vertical

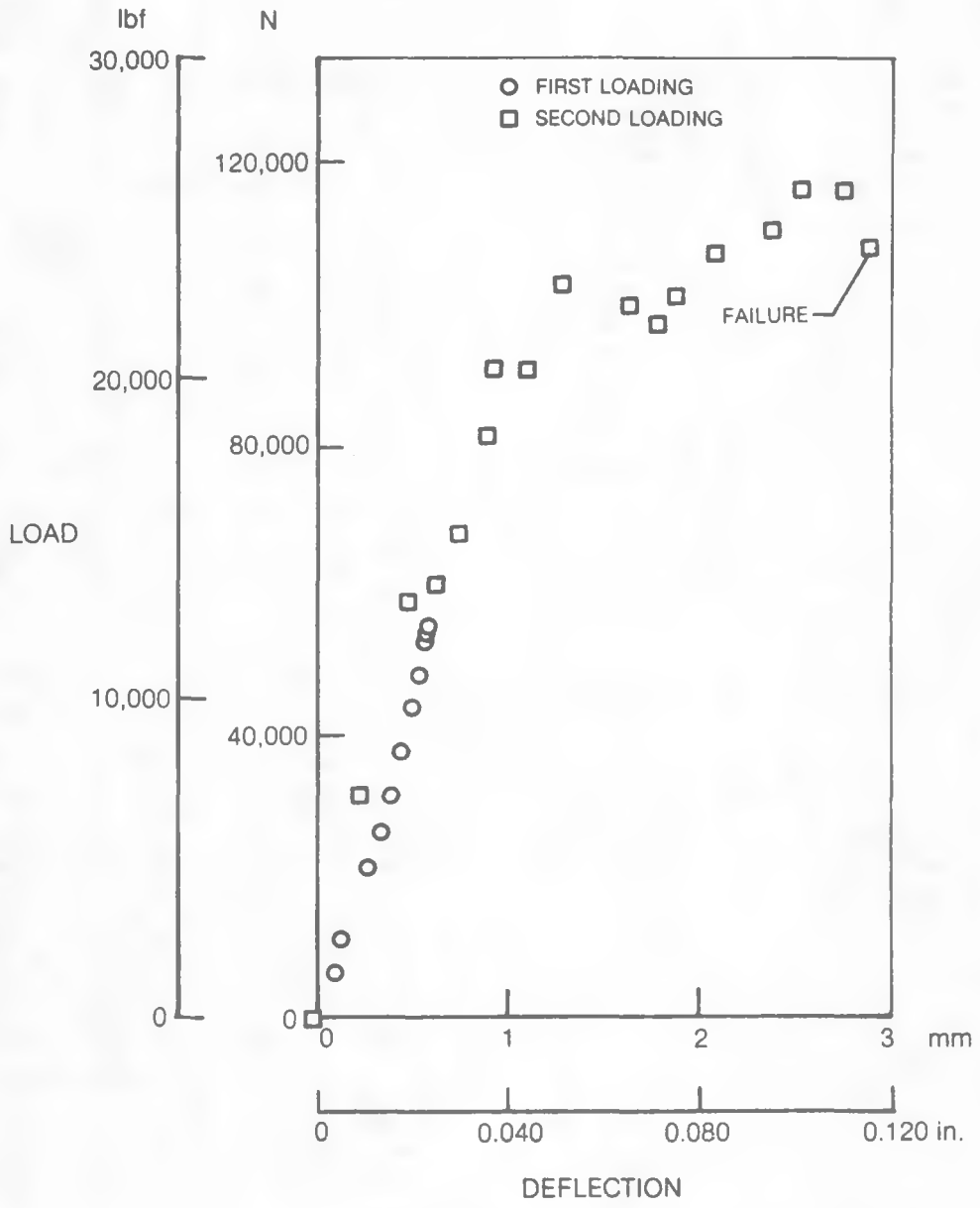

Figure 74. Blade-Flexbeam Joint Tension Test Results

81-6-164-44

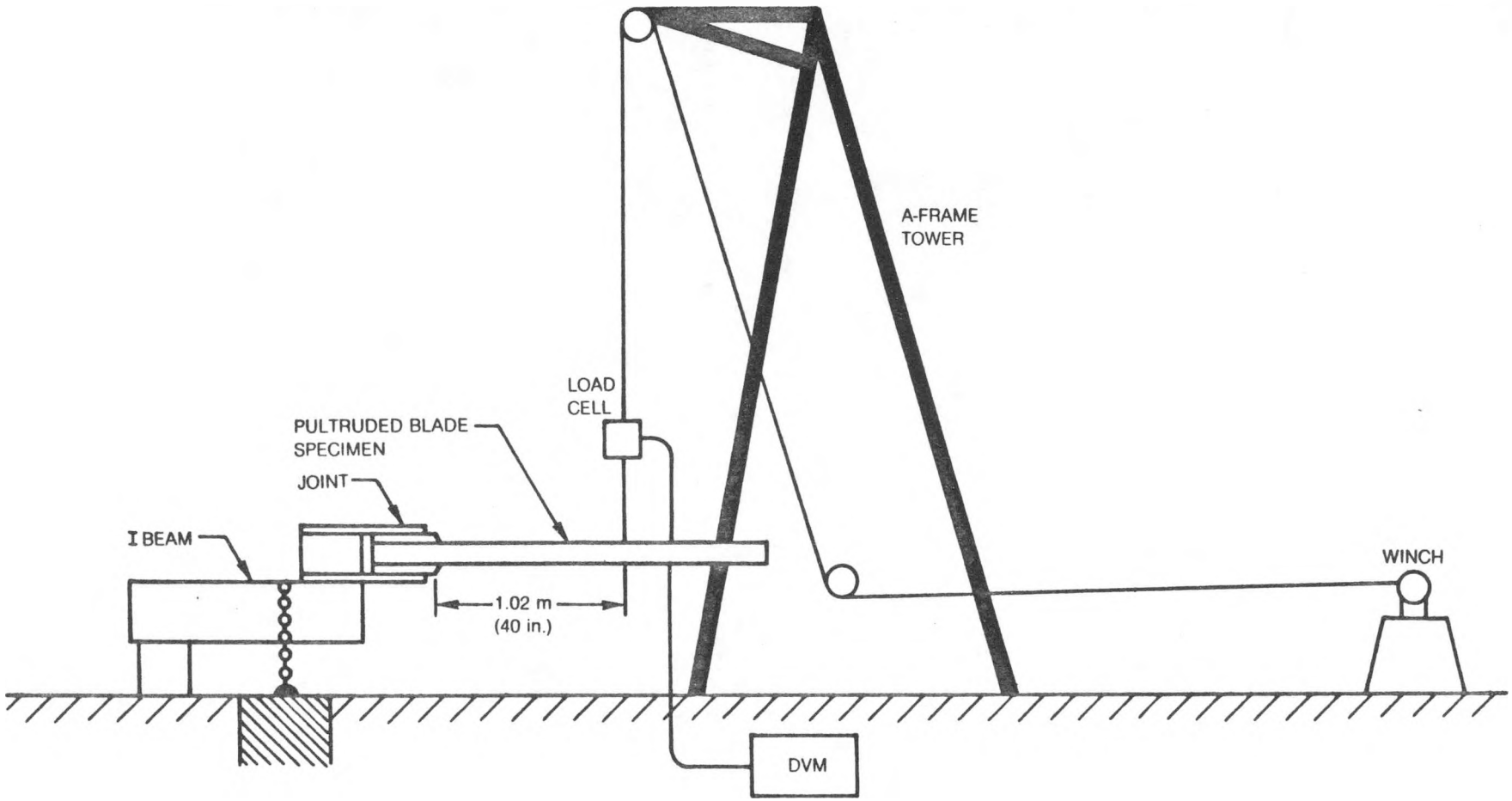

Figure 75. Blade Bending Test Set-Up

81-6-164-41

deflection of the blade was measured at the free end of the blade specimen, approximately 0.87 m (34.25 in.) outboard of the loading point. Deflection at the point of load application was later calculated from the known geometry of the setup. The blade area near the blade-flexbeam joint was shaded to maintain a skin temperature of approximately 32°C (90°F).

Test Results

The pultruded blade specimen was loaded vertically until ultimate failure occurred. The load-deflection test results are shown in Fig. 76. Several loading sequences occurred during the test, and each loading sequence is shown by a solid line connecting data points. The sequences resulted from pauses in the loading, during which time elapsed with no additional increase in the load. Because the load is applied by shortening the cable in Fig. 75, a discontinuity in the load-deflection relationship results between loading sequences as the blade fibers relax and the effective load decreases for a constant strain. The best example of relaxation occurs at the high loading condition where an elapsed time of approximately 5 min between loading sequences resulted in a load discontinuity of about 445 N (100 lb).

The blade failure occurred at a loading of 2870 N (645 lb). At the peak loading condition, the slope of the blade specimen at the free end is 16°. This is the angle formed between the blade and the horizontal plane due to the blade vertical deflection. The point of failure was just outboard of the pads on the blade used to attach the blade-flexbeam joint. This point is about 1.016 m (40 in.) from the loading point, so the bending moment at failure is 2820 N·m (25,000 lbf·in.).

Based upon the results of Fig. 76, the blade stiffness, elastic modulus, and ultimate flex strength were calculated. These characteristics are summarized below.

Elastic Stiffness (EI)	56.5 $kg \cdot m^2$	(0.193×10^6 $lb \cdot in.^2$)
Elastic Modulus (E)	10 GPa	(1.45×10^6 psi)
Ultimate Flex Strength	120 MPa	(17460 psi)

The mode of failure was compressive-bending on the upper blade surface. Slight separation of the edge of the pads from the blade was also noted on the lower blade surface.

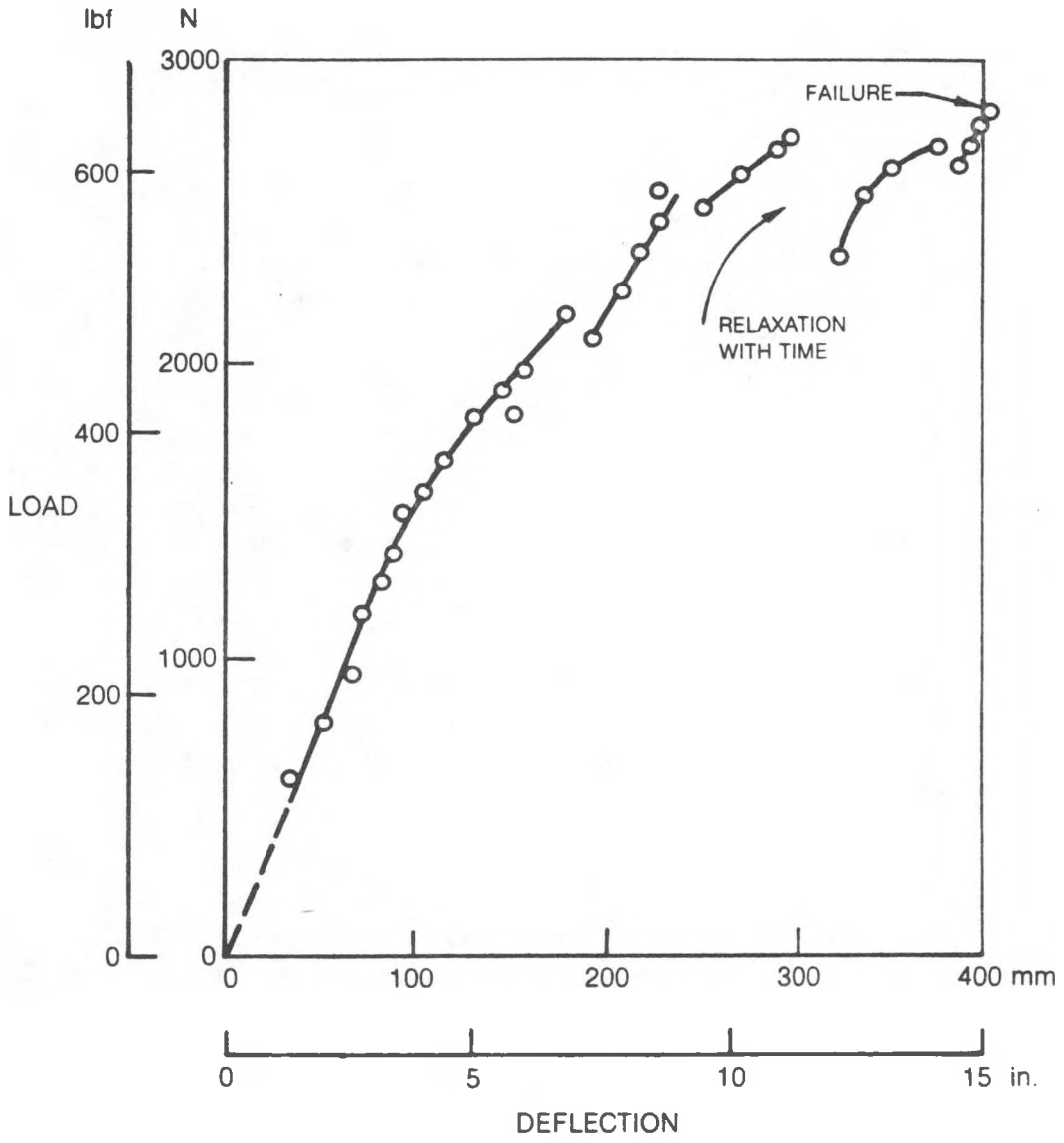

Figure 76. Blade Bending Test Results

81-6-164-42

AVAILABILITY ANALYSIS

An availability analysis of the 15-kW wind system was performed and updated. The calculations presented in Table XXXVI show that availability for the ideal case is predicted to be 99.96% while for the site specific case it would be 99.83%.

The availability analysis was performed utilizing annual downtime estimates derived as shown in the sample calculation sheet presented in Table XXXVII. The input to the total annual downtime analysis was, in turn, derived from the reliability and maintainability analyses shown in the sample calculation sheets presented in Tables XXXVIII, XXXIX, and XL.

The availability, as shown in Table XXXVI, was calculated as a function of uptime over the total number of hours in the calendar year, where uptime (total hours in a year minus downtime) is the number of hours in a year that the machine is available, and disregards whether the wind velocity is within operational range. The downtime (total hours in a year minus uptime) was calculated by estimating the scheduled downtime for routine maintenance during the year, plus the time required to effect repairs due to failures during the same period.

The ideal case noted above considers that the operator of the machine is on-site and failure detection time is nil. It assumes that spare/repair parts are on hand at the site. Total downtime for repairs is the sum of subsystem failure rate (reliability) multiplied by the estimated repair time.

The site specific case considers that the operator is off-site and failure detection times must be taken into account. It assumes that failure-prone parts are on hand, but other parts must be obtained from a parts house 150 miles distant. Total downtime for repairs in this case is calculated the same as for the ideal case except for the foregoing differences.

Failure Mode and Effects Analysis (FMEA)

An FMEA to the subsystem and component level was prepared and updated as required by Appendix A to the Contract Statement of Work. Hazard severity categories and hazard probability levels utilized in the FMEA are defined in Tables XLI and XLII respectively. The FMEA, presented in Tables XLIII through XLVIII, considers only single failure cases.

TABLE XXXVI

AVAILABILITY ANALYSIS

$$\text{Availability} = \frac{\text{Total time} - [\text{repair downtime} + \text{maintenance downtime}]}{\text{Total time}}$$

$$= \frac{8760 - [2.152 + 1.570]}{8760}$$

$$= \frac{8760 - 3.722}{8760}$$

$$= 0.9996 \text{ or } 99.96\% \text{ ideal case}$$

$$= \frac{8760 - [13.280 + 1.570]}{8760}$$

$$= \frac{8760 - 14.850}{8760}$$

$$= 0.9983 \text{ or } 99.83\% \text{ site specific case}$$

TABLE XXXVII

ANNUAL DOWNTIME - SAMPLE CALCULATIONS

Item	Failure/yr	Repair Downtime (hrs) Ideal	Repair Downtime (hrs) Site Specific	Annual Repair Downtime (hrs) Ideal	Annual Repair Downtime (hrs) Site Specific	Annual Routine Maintenance (hrs)	Total Annual Downtime (hrs) Ideal	Total Annual Downtime (hrs) Site Specific
Pendulum subsystem								
Flexstrap								
Fault detect		0.05	12.00					
Fault isolate		0.10	0.10					
Lower wind turbine		0.40	0.40					
Obtain parts		0.25	12.00					
Repair/replace parts		0.50	0.50					
Raise wind turbine		0.40	0.40					
Checkout		0.60	0.60					
	0.0046	2.30	26.00	0.011	0.120	-	0.011	0.120
Mechanical subsystem								
Speed increaser gearbox								
Fault detect		0.05	12.00					
Fault isolate		0.15	0.15					
Lower wind turbine		0.40	0.40					
Obtain parts		1.00	12.00					
Repair/replace parts		2.50	2.50					
Raise wind turbine		0.40	0.40					
Checkout		0.60	0.60					
	0.22	5.10	28.05	1.122	6.171	-	1.122	6.171

TABLE XXXVIII

EXAMPLE OF RELIABILITY ANALYSIS
Speed Increaser Gearbox

Part Name	Data Source	Qty n	λ*	nλ
Bearing, rotor shaft, outboard	FMC**	1	0.500	0.500
Bearing, rotor shaft, inboard	FMC	1	2.381	2.381
Bearing, intermediate shaft	FMC	1	3.125	3.125
Bearing, intermediate shaft	FMC	1	3.333	3.333
Bearing, high speed shaft	FMC	2	1.250	2.500
Seal, shaft, high speed (oil)	P-3 gearbox	1	11.490	11.490
Seal, shaft, low speed (grease)	P-3 gearbox	1	11.190	11.190
Shaft, low speed (rotor)	JFC***	1	0.013	0.013
Shaft, intermediate speed	JFC	1	0.013	0.013
Shaft, high speed (generator)	JFC	1	0.013	0.013
Gears	JFC	4	0.372	1.488
				36.046
				or
				0.316 failures per year

* λ = Failures per million operating hours

** Gearbox Manufacturer

*** Hamilton Standard jet engine fuel control data

TABLE XXXIX

EXAMPLE OF MAINTAINABILITY ANALYSIS

Induction Generator

Task Description	Elapsed Minutes	No. Men	Man Minutes	No./Type Fasteners	Type of Tool
Remove					
a. Remove cover, then (3) nuts, washers and power cables from generator	2.0	1	2.0	3 N, W	SW
b. Attach overhead hoist to generator, take up tension on cable	1.0	1	1.0	-	-
c. Loosen and remove (4) bolts that attach generator to gearbox	2.0	2	4.0	4 B, W	OEW
d. Remove generator from gear reduction case and lower to ground/cart/shipping container	5.0	2	10.0	-	-
e. Disengage hoist hook	1.0	1	1.0	-	-
	11.0		18.0		

TABLE XL

ANNUAL ROUTINE MAINTENANCE

Action	Required Parts/Items	Materials Dollars (1980$)	Manhours	Labor Dollars @15.00 per hour	Total Dollars	Scheduled Downtime (Elapsed Hours)
1. Lower WTG assembly to ground level.	Two men with required support equipment to lower WTG	----	0.800	12.00	12.00	0.400
2. Grease low speed shaft bearing(s).	One man with grease gun	0.25	0.050	0.75	1.00	0.050
3. Check/replenish lubricant in gearbox annually, as required.	One man with oil in one quart containers	2.00	0.100	2.25	4.25	0.100
4. Drain/replace lubricant in gearbox every five (5) years.	One man with four quarts of oil	1.60/year	0.100/year	1.50	3.10	0.100
5. Grease electric generator bearings.	One man with grease gun	0.25	0.050	0.75	1.00	0.050
6. Grease yaw shaft bearings.	One man with grease gun	0.25	0.050	0.75	1.00	0.050
7. Remove cover - inspect electrical brushes, and replace cover.	One man with standard tools	----	0.100	1.50	1.50	0.100
8. Replace worn or burned brushes as necessary.	One man with standard tools and a set of replacement brushes	4.00/set	0.150	2.25	6.25	0.150
9. Inspect/replace/lubricate pendulum arm and pendulum weight bushings, as necessary.	One man with puller tool, replacement bushings, and an oil can.	18.00/set (3.00/bushing)	0.833	12.45	30.45	0.667
10. Inspect blades, flexbeam, pendulum system for cracks or other damage.	Two men with standard tools	----	0.500	7.50	7.50	0.333
11. Raise WTG assembly to operating position.	Two men with required support equipment to raise WTG to operating position.	----	0.800	12.00	12.00	0.400
	TOTALS	$26.35	3.14 for Time Line(hr)	$33.70	$80.05	1.57 for Time Line(hr)

TABLE XLI

HAZARD SEVERITY

Hazard severity categories are defined to provide a qualitative measure of the worst potential consequences resulting from personnel error, environmental conditions, design inadequacies, procedural deficiencies, system, subsystem or component failure or malfunction as follows:

a. Category I - Catastrophic. May cause death or system loss.
b. Category II - Critical. May cause severe injury, severe occupational illness, or major system damage.
c. Category III - Marginal. May cause minor injury, minor occupational illness, or minor system damage.
d. Category IV - Negligible. Will not result in injury, occupational illness, or system damage.

Hazard Probability

The probability that a hazard will occur during the planned life expectancy of the system is described in potential occurrences for each item. Assigning a quantitative hazard probability to a potential design or procedural hazard is generally difficult early in the design process. The probabilities assigned in this FMEA are, therefore, subject to change as the design progresses. The quantitative hazard probability ranking is defined in Table XLII.

TABLE XLII

HAZARD PROBABILITY RANKING LEVELS

Descriptive Word	Level*	Specific Individual Item
Frequent	A	Likely to occur frequently
Reasonably Probable	B	Will occur several times in life of an item
Occasional	C	Likely to occur sometime in life of an item
Remote	D	So unlikely, it can be assumed that this hazard will not be experienced
Extremely Improbable	E	Probability of occurrence cannot be distinguished from zero
Impossible	F	Physically impossible to occur

* Note: The assigned probability of hazard occurrence (as designated by alphabetic level) will be listed adjacent to the Hazard Severity Category in the FMEA.

The opinions contained in the FMEA represent best estimates based on information presently known, and the current development of the equipment at the date of this analysis. Revised estimates should be made as additional information and operating experience become available.

Column (f) of the FMEA contains information relative to Design Criteria or Design Margins. Column (f) for the Blade Assembly in Table XLIII presents the safety factor for three design conditions: Maximum Torque (highest power) Condition - Wind Velocity (V) = 26 mph; Survival Design Conditions - Wind Velocity (V) = 125 mph; and Special Design Condition - Wind Velocity (V) = 165 mph. On subsequent pages, the titles are dropped for reasons of brevity and only the wind velocities and safety factors are listed.

Failure Rate Prediction

Failure rate predictions were made for the components and subsystems which comprise the wind turbine. Table XXXVIII presents a sample set of predictions for the speed increaser gearbox. The table is self-explanatory with the exception of the data sources, which are defined as follows, and which are typical of the entire analysis:

1. Bearing failure rates are based on B_{10} lives supplied by the gearbox manufacturer, FMC Corp.

2. Shaft seal failure rates have been calculated based on field experience from the gearbox supplied by Hamilton Standard for the propeller system on the Lockheed P-3 Arion aircraft.

3. Shaft and gear failure rates are based on field experience with Hamilton Standard jet engine fuel controls on a variety of aircraft engines.

Table XLIX lists the predicted failure rates for the wind turbine subsystems by subsystem component. The failure rates are summed at the bottom of the table for the complete system total of 105.94 failures per million operating hours, which is equivalent to a Mean-Time Between Failure (MTBF) of 9,439 operating hours, or approximately 1.57 years, based on an estimated 6000 hours of operation per year. The failure rate predictions made for these analyses are considered to be those for a mature wind system.

TABLE XLIII

FAILURE MODE AND EFFECT ANALYSIS

SYSTEM 15 kW Small Wind Energy Conversion System (SWECS)

COMPONENT Rotor Assembly

Item No. and Component or Part Description and Function (a)	Assumed Failure Mode (b)	Probable Failure Cause (c)	Failure Effect and Consequence on Sub-System and System (d)	Design Philosophy or Inherent Compensating Provisions (e)	Design Criteria or Design Margins (f)	Method of Detection (g)	Matched Category	Remarks (h)
15 kW SWECS								
ROTOR ASSEMBLY	Rotor blade strikes tower	Excessive blade flexing as a result of aero-elastic phenomena due to nacelle not properly weathervaned into the wind.	Loss of blade with resulting rotor unbalance. Resulting unbalanced loads will most likely cause opposite blade to break free as well.	Nacelle/rotor design provides for adequate and stable weathervaning of system.		Visual	1D	Extensive wind tunnel and prototype development tests have been conducted to show that the design is adequate and that this failure mode has a remote probability of occurrence.
Blade Assembly Blade Shell: The blades are formed from layers of fiber-glass cloth and rovings with a surface skin of nexus cloth bonded with vinyl ester resin. The layers of cloth and rovings are initially laid over a foam core* which is configured to form the inside shape of the blade. The laid up cloth is then impregnated with the vinyl ester resin and the foam core with the impregnated cloth is drawn through a heated female die configured to the outside airfoil shape of the blade. The end result is a blade of constant cross-section over the entire length, which has controlled thickness and integral foam core.	1. Shell fractures across its width.	Inherent defect in shell structure or damage by foreign object.	Loss of blade with resulting rotor unblance. Resulting unbalanced loads will most likely cause opposite blade to break free as well.	Three way layup of glass cloth in the laminated shell provides a redundant type of structure which will resist fracture and/or propagation thereof.	Designed for safety factors as shown based on stress analyses & wind tunnel test. Max Torque Design Cond. V = 26 mph — Safety Factor > 20 Survival Design Cond. V = 125 mph > 10 Special Design Cond. V = 165 mph > 10	Visual	1D	Extensive fiberglass fatigue tests and available foreign object damage (FOD) data for fiberglass show that blade fracture from fatigue or FOD has a remote probability of occurrence.
	2. Radial delamination of shell.	Inherent defect in shell lamination, e.g., poor impregnation of vinyl ester resin into cloth layers.	Same as above	Same as above	Same as above	Visual	1D	a. Depending on degree of delamination, the blade may hold together until annual inspection at which time appropriate corrective action can be taken.. b. Manufacturing processes and inspection techniques will be employed to reduce this type of malfunction to a remote probability of occurrence.

* Extruded Foam Core (Production)
Cut Foam Core (Prototype)

TABLE XLIV

FAILURE MODE AND EFFECT ANALYSIS

SYSTEM 15 kW Small Wind Energy Conversion System (SWECS)

COMPONENT Rotor Assembly

Item No. and Component or Part Description and Function (a)	Assumed Failure Mode (b)	Probable Failure Cause (c)	Failure Effect and Consequence on Sub-System and System (d)	Design Philosophy or Inherent Compensating Provisions (e)	Design Criteria or Design Margins (f)	Method of Detection (g)	Class (h)	Remarks (i)
ROTOR ASSEMBLY (Cont'd)								
Blade Joint Plates:	Fractures	Fatigue	Same as above.	Prime Structure, designed to not fail	V=26 mph > 2.8 V=125 mph 2.8 V=165 mph 2.8	Visual	ID	
Hub Assembly								
Hub Flange: (Cast Steel)	Fracture	Fatigue or corrosion	Loss of rotor.		TBD	Visual	ID	
Shaft key:	Shears	Fatigue or Corrosion	Rotor will rotate independently of the low speed shaft and will spin freely, possibly at high rpm. Rotor will go into stall mode, as designed for high speed survivability.	Key is of a standard design and is proven off-the-shelf hardware.	V=26 mph, V=125 mph, V=165 mph } 2.8 high since torque levels are very low.	Visual	IIID	Specified manufacturing tolerances for shaft keys must be strictly adhered to and shaft keys must not be abused by owner/operators. Recommend left hand thread on rotor retention bolt to prevent the free spinning rotor from unscrewing the bolt.
Rub Strip(s): (Polyurethane)	Worn	Relative motion of parts due to improper torque or loss of torque between hub and flange and pendulum support flange.	Retention of flexbeam between hub flange and pendulum support becomes progressively less secure until rub strips are worn completely through. Relative motion of flexbeam within the flanges could possibly result in loss of the rotor subassembly.	Bolt torque requirements for clamping are specified at assembly. Rub strip is compressed 25 percent, thus preventing relative motion between it and flexbeam.		Visual	ID	
Flexbeam: The flexbeam is made from unidirectional S-glass and is a simple rectangular cross section running from one blade through the hub out to the other blade.	1. Flexbeam fractures across its width.	Fatigue	Loss of blade with resulting rotor unbalance, and most likely loss of opposite blade.	Material layup inherently precludes propagation. Prime structure designed not to fail.	V=26 mph 4.5 V=125 mph 2.3 V=165 mph 1.8		ID	Extensive flexbeam fatigue tests have been conducted to show that fracture from fatigue has a remote probability of occurrence.
Rotor Retention Bolt	Shears	Fatigue or corrosion	Loss of rotor	Bolt is of a standard design and is proven off-the-shelf hardware.	V=26 mph 20 V=125 mph 2.8 V=165 mph 1.9		ID	

TABLE XLV

FAILURE MODE AND EFFECT ANALYSIS

SYSTEM 15 kW Small Wind Energy Conversion System (SWECS)

COMPONENT Rotor Assembly

Item No. and Component or Part Description and Function (a)	Assumed Failure Mode (b)	Probable Failure Cause (c)	Failure Effect and Consequence on Sub-System and System (d)	Design Philosophy or Inherent Compensating Provisions (e)	Design Criteria or Design Margins (f)	Method of Detection (g)	Matched Category	Remarks (h)
ROTOR ASSEMBLY (Cont'd)								
Flexbeam:	2. Radial delamination of flexbeam.	Inherent defect in lamination.	Chafing of fibers will occur leading to fiber fracture and loss of blade with resulting rotor unbalance, and most likely loss of opposite blade.	Structural strength of the S-2 fibers is sufficient to prevent loss of blade even if the vinyl ester binder should deteriorate.	V=26 mph 4.5 V=125 mph 2.3 V=165 mph 1.8	Visual	1D	a. Depending on degree of delamination, the flexbeam may hold together until annual inspection at which time appropriate corrective action can be taken. b. Manufacturing processes and inspection techniques will be employed to reduce this type of malfunction to a remote probability of occurrence.
Pitch Change Assy								
Pendulum Support Arm: (Cast Steel)	Fractures	Fatigue	Blade pitch control will be lost to one or both blades. Blade (s) will go to preset nonrotating -12 degree blade angle.		V=26 mph 11 V=125 mph 9.6 V=165 mph 9.6	Visual	IIID	
Pendulum Arm: (Steel)	Fractures	Fatigue	Same as above except that only one blade will go to the preset angle.		V=26 mph 24 V=125 mph 18 V=165 mph 18	Visual	IIIC	
Pendulum Weights: (Steel)	Fly-off	Loss of retention nut.	Same as for pendulum arm.	Weights are held in place by self-locking Elastic Stop Nuts.	N/A	Visual	IIIC	
Flexstrap: (Spring Steel)	Fractures	Fatigue	Same as for pendulum arm		V=26 mph 5 est V=125 mph 4 est V=165 mph 4 est	Visual	IIIC	

TABLE XLVI

FAILURE MODE AND EFFECT ANALYSIS

SYSTEM 15 kW Small Wind Energy Conversion System (SWECS)

COMPONENT Head Assembly

Item No. and Component or Part Description and Function (a)	Assumed Failure Mode (b)	Probable Failure Cause (c)	Failure Effect and Consequence on Sub-System and System (d)	Design Philosophy or Inherent Compensating Provisions (e)	Design Criteria or Design Margins (f)	Method of Detection (g)	Matched Category	Remarks (h)
HEAD ASSEMBLY					Designed for safety factors as shown based on stress analyses.			
Gearbox Assembly								
Rotor Shaft: (Steel)	Shears	Fatigue	Rotor assembly may fly free. Blades may strike tower.		V=26 mph 2 V=125 mph 3 V=165 mph 3	Visual	ID	
Rotor Bearings:	Disintegrate	Bearings seize initially due to fatigue or from lack of lubrication.	Loss of proper support for rotor shaft. Shaft will wobble loosely within bearing support tube, resulting in possible shearing of the rotor shaft/gearbox input drive coupling. Rotor shaft may eventually wear through and rotor assembly will fly free.		Same as above	Visual/ Audible	ID	Maintenance manual will specify lubrication intervals and inspection requirements.
Bearing Support Tube: (Cast Steel)	Does not provide support for rotor shaft bearings.	Fracture due to casting defect.	Same as for rotor bearings above	Low loads are imparted into the support tube because of the self-aligning rotor bearings.	Same as above	Visual	ID	
Speed Increaser Drive	Disintegrates	Bearings seize initially due to fatigue or from lack of lubrication.	No power output from generator to power grid.	Off the shelf gears and bearings, parallel shaft, double step unit.	Same as above	Visual/ audible	IID	
Yaw Assembly:								
Yaw Shaft: (Steel)	Fractures	Fatigue	Possible loss of head assembly.		V=26 mph 5.6 V=125 mph 1.5 V=165 mph 1.1	Visual	ID	

TABLE XLVII

FAILURE MODE AND EFFECT ANALYSIS

SYSTEM 15 kW Small Wind Energy Conversion System (SWECS)

COMPONENT Head Assembly

Item No. and Component or Part Description and Function (a)	Assumed Failure Mode (b)	Probable Failure Cause (c)	Failure Effect and Consequence on Sub-System and System (d)	Design Philosophy or Inherent Compensating Provisions (e)	Design Criteria or Design Margins (f)	Method of Detection (g)	Matched Category	Remarks (h)
HEAD ASSEMBLY (Cont'd)								
Yaw Assembly (Cont'd)								
Yaw Shaft Housing: (Steel)	Fractures	Fatigue	Possible loss of head asembly		V=26 mph 13 V=125 mph 4.7 V=165 mph 3.8	Visual	ID	
Bearing Grease Seals:	Leak	Wear/ Contamination	Loss of lubricant to bearings, possible contamination of electrical slip rings.	Off-the-shelf design of proven long-life non-time contolled material.		Visual	IIIB	
Slip Ring Assy:	Burned/worn	Wear/ Contamination	No power output from generator to power grid.	Protected from dirt/grease by shaft lip seals.		No power output	IIIC	
Brush Block Assy:	Burned/worn	Wear/ Contamination	No power output from generator to power grid.	Protected by cover housing and yaw shaft lip seals.		No power output	IIIC	
Yaw Bearings:	Disintegrate	Bearings seize initially due to fatigue or lack of lubrication.	Loss of support for head assembly. Head assembly will grind around in top of tower. Head rotation will be sluggish and rotor performance will decrease.	No power output from generator to power grid.		Visual/ Audible	IIIC	Maintenance manual will specify lubrication intervals and inspection requirements.
Induction Generator:	Fails to operate	Bearings seize initially due to fatigue or lack of lubrication.	No power output from generator to power grid.	Off-the-shelf proven structural units.		Visual	IVC	Maintenance manual will specify lubrication intervals and inspection requirements.
	Short/open circuit.	Improper maintenance, inherent defect, or lightning strike.	Induction generator will burn out. No power output. Possible fire.	Grounding is provided to reduce damaging effect of electrical shorts or lightning strike.		Visual	IIIB	

TABLE XLVIII

FAILURE MODE AND EFFECT ANALYSIS

SYSTEM 15 kW Small Wind Energy Conversion System (SWECS)

COMPONENT Tower Assembly

Item No. and Component or Part Description and Function (a)	Assumed Failure Mode (b)	Probable Failure Cause (c)	Failure Effect and Consequence on Sub-System and System (d)	Design Philosophy or Inherent Compensating Provisions (e)	Design Criteria or Design Margins (f)	Method of Detection (g)	Matched Category	Remarks (h)
TOWER ASSEMBLY								
Base Assembly								
Pivot Pin: (AA6061-T6/Proto.) (AA5456-H343/Prod.)	Shears during tower erection or lowering.	Corrosion or fatigue.	Complete WTG assembly will fall to ground. Total loss of WTG.	Prime structure. Designed to low stress levels.	TBD	Visual	ID	
Pivot Bracket (s): (AA6061-T6/Proto.) (AA 5456-H343/Prod.)	Weld joint fractures during tower erection or lowering.	Corrosion or fatigue.	Same as above.	Same as above.	TBD Designed for safety factors as shown based on stress analyses.	Visual	ID	
TOWER: AA6061-T6/Proto. AA5456-H343/Prod. 3/8" wall thickness 10" O.D. at top with constant taper to 24" O.D. at bottom.	Buckles during erection or while lowering.	Corrosion or fatigue.	Same as above.	Taper design has 2.7 x 10^6 lb buckling resistance.	V=12 mph TBD V=125 mph 1.57 V=165 mph TBD	Visual	ID	

TABLE XLIX

RELIABILITY SUMMARY SYSTEM

Subsystem/Component		Failures Per Million Operating Hours
Rotor		
Blade		Negligible
Blade/flexbeam joint		Negligible
Flexbeam		Negligible
Hub		Negligible
Flexbeam/flexstrap joint		Negligible
	subtotal	Negligible
Pendulum		
Flexstrap (qty = 2)		0.770
Support arm		Negligible
Pendulum arm (qty = 2)		7.800
Pendulum arm/support joint (qty = 2)		Negligible
	subtotal	8.570
Mechanical		
Gearbox		37.000
Generator		25.000
	subtotal	62.000
Tower		
Yaw shafts		2.400
Yaw shaft bearings and seals		24.320
Slip rings		5.620
Brush blocks		3.030
Tower base plate and pin		Negligible
Tower		Negligible
	subtotal	35.370
	System grand total	105.940
	System MTBF =	9,439 op. hrs.

Maintainability

Maintainability analyses were performed for the components and subsystems which comprise the wind turbine. Table XXXIX presents a sample estimate of the removal task time for the induction generator. The replace task procedure for the generator is essentially the reverse of that shown, and the remove/replace analyses for the remainder of the subsystem components were accomplished in similar fashion. Table XXXIX lists the task time required in both man-minutes and elapsed minutes, and takes into account the number and type of fasteners, plus the type of tool required, such as, socket wrench (sw) or open end wrench (oew). The task times estimated for these analyses are considered to be those for a mature wind system at the conclusion of the learning curve experience. They are "hands-on" times considered to be attainable by competent experienced persons who perform the required tasks agressively rather than passively.

The information generated in the component task analyses is fed into a second analysis for each component as shown in the sample in Table XXXVII. Table XXXVII utilizes the "failures per year" values generated from the reliability analyses, combined with the downtime per repair generated in the maintainability analyses, to arrive at the annual downtime due to corrective (repair) actions. Table XXXVII also presents a section for annual preventive (routine-scheduled) maintenance. Annual preventive downtime was then combined with annual corrective downtime to arrive at the total annual downtime. The estimated total annual routine maintenance is presented in Table XL, along with an estimate of material/labor costs in 1980 dollars. Table L shows the estimated total annual downtime by subsystem, including both preventive and corrective maintenance.

TABLE L

ESTIMATED TOTAL ANNUAL DOWNTIME BY SUBSYSTEM

	Repair Downtime (Elapsed Hours)		Total Annual Downtime (Elapsed Hours)	
	Ideal	Site Specific	Ideal	Site Specific
Preventive maintenance				
Annual routine maintenance	-	-	1.570	1.570
Corrective maintenance				
Rotor subsystem	7.55 max.	27.80 max.	Negligible	Negligible
Pendulum subsystem	4.10 max.	27.80 max.	0.119	1.337
Mechanical subsystem	5.10 max.	28.05 max.	1.662	10.153
Tower subsystem	8.05 max.	31.00 max.	0.371	1.790
		Sub totals:	2.152	13.280
		Total:	3.722	14.850

SAFETY ANALYSIS

A system safety analysis was conducted and updated. A review of the Failure Mode and Effects Analysis (FMEA) disclosed 17 Category I hazards. All 17 are classified as Hazard Probability "D", i.e., "Remote". The Hazard Severity Categories and Probability Ranking levels are defined in Tables XLI and XLII.

Maintenance and overhaul practices were considered as part of the safety analysis, and as a result, suitable "Hazard" and/or "Caution" notes will be required in the operation and maintenance manuals and on the equipment to minimize personal injury. It was determined that there are no noxious materials involved in the normal operation of the turbine. However, the usual precautions must be observed in handling the resins involved in fiberglass blade repair activity. These are, basically, to keep resins from contact with the skin and/or eyes through the use of safety glasses, rubber/plastic gloves, and adequate protective clothing. It is also recommended that instructions of the resin manufacturer be closely followed to insure sufficient air ventilation during any repair of blades indoors.

It is similarly important to observe safety precautions associated with the lifting of heavy components, movement near rotating objects, and working with or near energized electrical apparatus.

CONCLUDING REMARKS

The results of the Phase I design study demonstrate that the UTRC 15-kW wind turbine design satisfies the basic performance and structural requirements set forth in the contract statement of work. The experience gained in the design, fabrication and testing of the 8-kW WTG proved quite valuable in developing the 15-kW prototype design. Prime examples of this experience are the integrated transmission generator, the pultruded fiberglass flexbeam, and the stand-alone tower. These are some of the innovations that contribute to lower weight, lower manufacturing cost and lower installation cost, and when taken collectively, will provide a prototype design that is closer to a production unit design.

It is felt that, with the completion of the 15-kW prototype design, the UTRC bearingless wind turbine has reached a refined stage of development, to which only minor modifications will be necessary to finalize a production design. The use of a Composite Bearingless Rotor (CBR) coupled with a passive pendulum control system has proven its worth, not only from the point of aerodynamic performance and aeroelastic stability, but also from the manufacturing cost viewpoint. The use of pultrusion for both blade and flexbeam fabrication makes the CBR approach especially attractive.

Another important result of this design study is the optimization of tower configuration. The detailed investigation into different tower approaches resulted in a cantilevered, stand-alone tower which eliminates the need for guy wires.

The pertinent results of this design study extend past the description of the detailed prototype design. Extensive studies of reliability, maintainability, and availability indicate that a production version will perform efficiently with a resulting beneficial effect on life cycle costs.

Finally, the detailed studies of the cost-of-energy indicate that the 15-kW WTG design is potentially a low cost wind energy conversion system. The estimated cost of energy for a production system is well below most current utility rates. The experience gained with the 8-kW wind turbine, developed under an earlier DOE contract, and the Phase II tests scheduled under this contract will provide the Bearingless Rotor Wind Turbine concept with extensive technical background.

REFERENCES

1. Cheney, M. C., et al.: Development of an 8-kW Wind Turbine Generator for Residential Type Applications. United Technologies Research Center Final Report - Phase I, (RFP-3006/1 & 2), June 1979.

2. Taylor, R. B., and Cheney, M. C.: Development of an 8-kW Wind Turbine Generator for Residential Type Applications. United Technologies Research Center Final Report - Phase II, (RFP-3232/1 $ 2), February 1981.

3. Frost, W., Long, B. H. and Turner, R. E.: Engineering Handbook on the Atmospheric Environmental Guidelines for Use in Wind Turbine Generator Development. NASA Technical Paper 1359, December 1978.

4. Foley, J. S.: Wind Energy Conversion System Design and Analysis Program. Presented at American Wind Energy Association Conference, Pittsburgh, Pennsylvania, June 8-11, 1980.

5. Egolf, T. A.: Small Wind Energy Conversion Systems (SWECS) Rotor Performance Model Comparison Study, Task I - Topical Report of Results Obtained Using the UTRC Horizontal Axis Wind Turbine Performance Analysis (WECSPER). United Technologies Research Center R80-915106-1, June 1980.